

University of Strathclyde
Department of Civil and Environmental Engineering

**Exploring subsurface groundwater and geochemical
rock interactions during drainage of a surface water
reservoir in Switzerland**

Mark Stillings

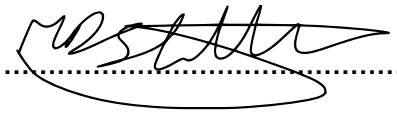
Doctor of Philosophy (PhD)

2020

Declaration of Authenticity and Author's Rights

This thesis is the result of the author's original research. It has been composed by the author and has not been previously submitted for examination which has led to the award of a degree. The copyright of this thesis belongs to the author under the terms of the United Kingdom Copyright Acts as qualified by the University of Strathclyde Regulations 3.50. Due acknowledgement must always be made of the use of any material contained in, or derived from, this thesis

Signed:

A handwritten signature in black ink, appearing to be 'M. S. H.', is written over a horizontal dotted line. The signature is enclosed within a hand-drawn oval shape.

Date:

10 / 02 / 2020

Acknowledgements

It won't come as a shock that the PhD journey is difficult, frustrating, exciting, emotional and sometimes depressing when things don't go as you had hoped. However, the people I have had the pleasure to work alongside and with over this time have generally made things better, even if at the time it didn't seem like it. I can certainly say that they have helped make myself and this thesis better while improving my mental health along the way. Everyone's kindness, patience, humour and dedication has made the PhD experience enjoyable.

Firstly, I would like to thank my Supervisors Richard and Zoe for their continued support. Their teachings, advice and discussions all lead to my thesis and its eventual completion. Additionally, Becky who is not an official supervisor, but the project group leader has helped, guided and support me in my PhD as well as my future career. As you will see, this PhD required a lot of practical learning both in the lab and in the field. I would like to acknowledge Richard for showing me the ins and outs of groundwater sampling in the field, and my two field assistants Zoe and Caitlin who helped carry water, dig holes and were excellent company for tadpole-gazing. As we moved into the lab, I can whole heartedly say that without the continued tuition and support of Mara and Tanya a lot of the data produced in my thesis would not be possible. I also have to thank Mike who was my lab buddy for a long night of measuring my experiment every hour for 24 hours. He kept me entertained, awake and made the spookily empty lab a little less spooky. My project would also not be possible without the support of RWM, Adrian Bath and the rest of the Strathclyde LASMO team (Stella and Mariana), who provided guidance discussion and support for my PhD. I would also like to thank for the support of the wider LAMO team and Uni Bern, and NAGRA for the access to the GTS and in-depth knowledge of the test site. I would also like to acknowledge and thank SUERC and Adrian Boyce who helped with the analysis of stable isotopes. Additionally, Funding for this work came from both the Engineering and Physical Sciences Research Council's Doctoral Training Awards Grant EP/M506643/1 and from Radioactive Waste Management (RWM). The research forms part of the collaborative Large-Scale Monitoring (LASMO) program at the Grimsel Test Site.

Finally, I would like to thank everyone I have worked with and met throughout the course of my PhD, and anyone who have had to deal with my incessant moaning about groundwater, equipment breaking, and general rough times. It was all worth it. If we go with the running joke that the time doing my PhD was an additional 5 years on top of the actual, then it has taken me just about 9.5 years to submit.

Abstract

This thesis examines the spatial and temporal controls on groundwater chemistry in a fractured granitic environment. The research was conducted at the Grimsel Test Site, Switzerland (GTS), where draining and refilling of a nearby surface water reservoir induced microseismicity in the surrounding rocks. The GTS is a network of closely monitored tunnels and boreholes ~300-500m below ground surface. Characterisation of background geochemical conditions over a two-year period consisted of a time series of physiochemical, major and minor dissolved ion chemistry, stable isotope analysis and dissolved organics, for boreholes spanning the length of the GTS. Results show poor fracture connectivity; physiochemical and dissolved ion chemistry are dominated by water-rock reactions between infiltrating meteoric waters and spatially varying host rock lithology. A new technique is developed that compares the differing signatures of dissolved organic compounds (2D-gas chromatographs) found within surface soils, river sediments and the lake, to those found in groundwater samples from the GTS. Results show that organic signatures are well-preserved and that different groundwater samples can be traced to different surface infiltration sites. This organic fingerprinting technique has the potential to be a powerful new tool for determining groundwater origins. Analysing the groundwater data over time, identified no changes to major or minor ion chemistry, but repeated drops in groundwater pH (1-3 units) were observed during periods of reservoir drainage. These drops were concurrent with nearby shallow (<1 km below ground surface) microearthquakes $-1.2 < ML < 1$. Experiments to crush granite from the GTS in the presence of equilibrated groundwater, and in the absence of oxygen, were able to reproduce similar pH drops with no changes to water chemistry. This is the first evidence that microseismic events cause substantial pH drops, these findings have significant implications for a wide variety of geological processes.

Table of Contents

Acknowledgements	ii
Abstract	iii
Table of Contents	iv
Table of Figures	viii
List of Tables	xiii
1. Introduction	1
1.1 Context of this Study	1
1.2 LARge Scale MONitoring Project (LASMO)	3
1.3 Research Question and Objectives	4
1.4 Structure of Thesis	5
1.5 Study Area	7
1.5.1 Why the Grimsel Test Site?	8
2. Controls on groundwater chemistry	10
2.1 Introduction	10
2.2 Water rock reactions	10
2.2.1 Hydrochemical equilibrium and saturation index	11
2.2.2 Hydrochemical Kinetics and Rate factors	12
2.2.3 Oxidation and Reduction	14
2.2.4 Hydration	15
2.2.5 Carbonation	15
2.2.6 Hydrolysis	16
2.2.7 Hydrochemical evolution in crystalline rocks	17
2.3 How is groundwater evolution affected by infiltrating water conditions?	19
2.4 What causes dynamic fluctuations in groundwater	21
2.4.1 Seasonal variability (metrological recharge and mixing)	21

2.4.2	Earthquakes groundwater flow and chemistry	22
2.4.3	Glaciers, permafrost and climate change	24
2.4.4	Reservoirs/Dam Draining and refilling	26
3.	<i>Spatial Groundwater Chemistry</i>	27
3.1	Introduction	27
3.2	Introduction	27
3.3	Methods	30
3.3.1	Ground and surface water sampling locations	30
3.3.2	Sample Collection and Preservation	32
3.3.3	Lab Analysis	33
3.3.4	Geochemical modelling PHREEQC	34
3.4	Results and Discussion	35
3.4.1	Physiochemical Properties	35
3.1.1.1.	Major Element + Spatial Changes	39
3.1.1.2.	Multivariant analysis of dissolved ion species	45
3.1.1.3.	Geochemical Modelling	54
3.2.	Discussion and Conclusions	56
4.	<i>Tracing the source of surface infiltration</i>	58
4.1.	Abstract	58
4.2.	Introduction	58
4.3.	Field Site	60
4.4.	Materials and Methods	63
4.4.1.	Surface site, and groundwater sampling	63
4.4.2.	Sample preparation for organic analysis	64
4.4.3.	Analysis by GCxGC-ToF	64
4.4.4.	Peak Alignment	66
4.5.	Results	67
4.5.1.	Groundwater pressure and physiochemistry	67
4.5.2.	Analysis of GCxGC data	68
4.5.3.	Principal Component Analysis (PCA)	69
4.6.	Discussion	71

4.6.1.	Why do different groundwaters contain different characteristic signatures - what are we detecting? _____	71
4.6.2.	How are compounds preserved over time i.e. when and where will this technique work? _____	72
4.6.3.	Are there any sub-surface sources of organic molecules? _____	73
4.6.4.	Are the findings consistent with those of other tracers at the GTS? _____	73
4.7.	Summary and Conclusions _____	74
5.	<i>Temporal Groundwater Change</i> _____	76
5.1.	Microseismic events cause significant pH drops in Groundwater _____	76
5.2.	Methods _____	83
5.2.1.	Microseismic monitoring system _____	83
5.2.2.	Microseismic event selection _____	83
5.2.3.	Selected microseismic event hypocentral determination _____	84
5.2.4.	Selected microseismic event local magnitude and source dimensions estimation _____	85
5.2.5.	Groundwater Sampling _____	85
5.2.6.	Alkalinity determination _____	86
5.2.7.	Laboratory Determinants _____	86
5.2.8.	Experiments _____	87
5.2.9.	Geochemical Modelling _____	88
5.3.	Supplementary Information _____	89
5.3.1.	Supplementary Figures _____	89
5.3.2.	Supplementary Table(s) _____	89
5.3.3.	Supplementary Equations _____	91
6.	<i>Discussion and Conclusions</i> _____	93
6.1.	Spatial Hydrogeochemical Model of the GTS _____	93
6.1.1.	Input _____	94
6.1.2.	Infiltration and Water transport processes _____	95
6.1.3.	Chemical processes: Water-rock interactions along flow paths _____	99
6.1.4.	Groundwater Hydrogeological Conceptual model for the GTS _____	100
6.1.5.	How does the GTS hydrogeology and groundwater geochemistry respond to transient stress changes from Lake Draining? _____	104
6.2.	How does the lake draining compare as an analogue for Glacial loading and unloading? _____	105

6.3. Implication for Siting a GDF in the UK	106
6.3.1. Siting method and implications	106
6.3.2. Implication of temporal groundwater acidification	109
6.4. Conclusions	111
7. Future work and Recommendations	114
7.1. Recommendations for future site investigation practice	114
7.1.1. Devising a site investigation program	114
7.1.2. Flexibility in site model evolution	115
7.1.3. Sampling and analysis methodologies	115
7.1.4. Data storage and interpretation	116
7.1.5. Conveying different data types	116
7.2. Recommendations for Future research	117
7.2.1. Geochemical evolution in fracture networks	117
7.2.2. Organic Tracing	117
7.2.3. Seismic induced mechano-chemical reactions	118
REFERENCES	120
APPENDICES	133
Appendix I	133
Appendix II	143
Appendix III	164
Appendix IV Available pressure data from NAGRA LASMO monitored boreholes during the periods of sampling in 2016.	191

Table of Figures

Figure 1.1 3D block diagram of the GTS exposure underground (Not to Scale). Satellite imagery imposed on vertically exaggerated topography. Hydropower reservoirs Räterichsbodensee and Grimsensee are highlighted.	7
Figure 1.2 (top right) outline of Switzerland with the location of the GTS highlighted. (top left) not to scale schematic diagram of the complex hydropower pumping network connecting Grimsensee and Räterichsbodensee to the reservoir systems in other water catchments. Geological map (adapted from Schneeberger et al., 2018) of the GTS (bottom), hydropower reservoirs (light blue) Grimsensee and Räterichsbodensee, lithology as mapped at the surface, surface liniments (red lines), GTS access tunnel (Grey) and GTS tunnel network highlighted in dashed box.	8
Figure 1.3 Borehole schematic of the GTS. Lithology as mapped at depth (CAGr - lilac, GrGr - Pale Red). Boreholes used through the thesis are labelled; US 85.001, US 85.002, SB 80.001, US 85.003, SB 80.003, HP 98.007 and VE88.003. Shear zones mapped at depth indicated by solid red lines. CAGr – Central Aar Granite, GrGr – Grimsel Granodiorite	9
Figure 2.1 Kinetic and equilibrium stages for the evolution of concentration of compound [A+] with time (adapted from Appelo and Postma, 2005).	13
Figure 2.2 concentration of reactants and products for the reaction of $X \rightarrow Y$. Rate of reaction derived from changing concentration over change in time.	14
Figure 2.3 Goldich weathering observational based mineral appearance of primary silicate minerals in soils (adapted from Goldich, 1938).	18
Figure 2.4 Schematic diagram of the evolution of groundwater from infiltrating meteoric water through a). soil and unsaturated zone and b). the unsaturated zone into the saturated zone. Showing important hydrochemical processes in each zone (adapted from Hiscock and Bense, 2014).	20
Figure 3.1 Map of the Grimsel Valley and the location of the GTS (red box). Top of Juchlistock to the west of the GTS.	28
Figure 3.2 Borehole plan view schematic showing access tunnels in grey, boreholes (black), Shear Zones (red line) and host rock lithology.	31
Figure 3.3 Map of the Grimsel valley. Surface water sample sites (S1) river flowing into Grimsensee, (S2) Grimsensee, (S3) Räterichsbodensee, (S4) surface runoff into Räterichsbodensee. Host rock lithology faults from liniment tracing at the surface (Schneeberger <i>et al.</i> , 2016).	32

Figure 3.4 Tunnel schematic showing the spatial distribution in size categorised red bubbles (left to right) of temperature, electrical conductivity (EC), pH and borehole flow rate (Q). CAGr (white) GrGr (light grey), boreholes (black lines), tunnels (Dark grey). ...	38
Figure 3.5 Piper diagram of groundwaters hosted in GrGr (red), CAGr (blue) and surface water (black).	39
Figure 3.6 Tunnel schematic showing the spatial distribution in size categorised red bubbles (left to right) of Na ⁺ , Ca ²⁺ , K ⁺ , Alkalinity (ppm). CAGr (white background) GrGr (light grey), boreholes (black lines), tunnels (Dark grey).	41
Figure 3.7 Tunnel schematic showing the spatial distribution in size categorised red bubbles (left to right) of F ⁻ , SO ₄ ²⁻ , Cl ⁻ , Li ⁺ (ppm). CAGr (white background) GrGr (light grey), boreholes (black lines), tunnels (Dark grey).	42
Figure 3.8 Groundwater stable isotope data (2014-15) δ ¹⁸ O vs δ ² H in comparison with local decadal meteoric water (LMWL blue line) and the global meteoric water line (GMWL yellow line). Winter lake draining 2014/15 blue, clusters with summer groundwater Aug 2015. Surface river water and lake water plot outside the groundwater cluster.	43
Figure 3.9 Average (n=7) borehole interval δ ¹⁸ O .isotope values (black squares) verses distance along a north to south transect through the GTS. Standard error isotope measurement δ ¹⁸ O ± 0.2‰.	44
Figure 3.10 Schematic diagram of part of the hydropower network. Showing lake altitude, calculated oxygen isotope values based on altitude (Schotterer, 2010) and measured oxygen isotope values for Grimsensee and Räterichsbodensee. Glaciers directly feed into Oberaar and Grimsensee.	45
Figure 3.11 PCA analysis of all borehole geochemical data from the GTS.	46
Figure 3.12 PCA plot of scaled ion groundwater chemistry data. Colours correspond to cluster analysis by k-mean, fit of 4 clusters.	47
Figure 3.13 Graph of Sodium vs Calcium ion borehole groundwater concentrations.	49
Figure 3.14 Graph of Potassium vs Sodium ion borehole groundwater concentrations.	51
Figure 3.15 Conceptual diagram showing the key reaction processes leading to the evolution of groundwater from infiltrating meteoric water along a fracture path (Brown plane). (i) Influx of organic compounds, organic acids, Sulfur/Phosphorus compounds, and CO ₂ added from the soil zone dissolving and forming bicarbonate and carbonate in groundwater. (ii) Precipitation and dissolution reactions of Mg ²⁺ and Ca ²⁺ at the start of the flow path forming (Mg/Ca)CO ₃ precipitates depending on water conditions. (iii) Pyrite oxidation and potential precipitation of iron oxyhydroxides. (iv) Fluorite dissolution from intersecting 'alpine clefts' adding F ⁻ and Ca ²⁺ into groundwater. (v) Feldspar weathering (Alb = Albite, An = Anorthite) by hydrolysis releasing cations forming Quartz and Kaolinite on fracture surface.	57

- Figure 4.1 Satellite map (Google Maps) of sample locations; groundwater a-g (red circles), Soil and sediment samples 3-6 (blue circles), and lake water sample (green circle). The footprint of the Grimsel Test Site tunnel is show in red.62
- Figure 4.2 Borehole map, groundwater sample locations (red circles), shear zones (red lines), tunnels (grey), boreholes (black lines), CAGr (pale yellow), GrGr (orange) and magmatic transition zone (pale orange).....63
- Figure 4.3 Schematic diagram of the GCxGC ToF system with thermal modulator. While displayed as separate sections; GC column 1, thermal modulator and GC column 2 are all enclosed in the Agilent 7890A. Column 2 is in a secondary oven enclosed in the primary oven. The time of flight (ToF) mass spectrometer is connected to GC column 2 via a heated transfer line.65
- Figure 4.4 GCxGC 2D chromatographs; soil '5a' (left) and groundwater 'g' (right). The x-axis represents the first dimension of separation in column one, y-axis represents the separation of compounds in the shorter second column. Colour temperature reflects the Total Ion Count (TIC) of the Mass Spectrometer. Red is a high TIC and blue is low TIC, Red to light blue dots represent individual compounds. Long coloured streaks parallel to the x-axis are artefacts from the sample matrix and the GC column stationary phases.68
- Figure 4.5 Coloured bar plot of the normalized concentration data for all 228 aligned compounds for each sample; each multi-coloured bar represents one sample (labelled right) soil samples '3'-'6', groundwater samples 'a'-'g' and lake water 'LW', the width of each coloured rectangle represents the relative concentration of the organic compound with respect to the total concentration of all 228 compounds presented in the plot. Black lines connect selected matching compounds between samples to display similarities and differences between compound presence.69
- Figure 4.6 Ratio transformed PCA scores plot of all organic sample analysis. All points are labelled with the sample id corresponding to Figure 4.1 and 4.2; soil/sediment (blue), lake (green), groundwater (red). Principal Component 1 (PC1), and Principal Component 2 (PC2).70
- Figure 4.7 Conceptual diagram updated sample location colours reflect the surface water origins as determined by organic signature comparison; green dots (c, d, f and Lake) reflect water samples with lake surface signature, yellow dots (a, b, 3, 4 and 5) are water/soil samples with a soil surface origin, light blue dots (g and 6) are samples localities containing an stream signature (ephemeral and long-lived streams at the surface are highlighted in transparent blue. Liniments are given by red lines (Schneeberger *et al.*, 2016, 2017; Schneeberger, 2017). GTS tunnel exposure is given as a red polygon outlined in black.74
- Figure 5.1 Map of the Grimsel Test Site (GTS). Solid red lines are fault traces mapped from surface lineaments (Schneeberger *et al.*, 2017) grey lines represent tunnels including

the GTS. Microseismic epicentres are chronologically numbered (yellow circles). The main map shows the lithological contact between Aar Granite (purple) and Grimsel Granodiorite (green) at the surface. The enlarged GTS map (inset left) shows the contact at 1728 m AMSL and the sampled borehole intervals B to K. Intervals with a pH change are coloured to match Fig2. The stereonet shows orientations of open fractures in the GTS (Schneeberger *et al.*, 2017) and other tunnels.77

Figure 5.2 Groundwater pH measurements during periods of increased microseismicity due to lake drainage. Lines with markers show pH in borehole intervals coloured to match locations in Figure 5.1. Dark grey lines denote boreholes with no detectible change. Graphs are separated by year and host rock lithology a. and c. come from the Aar Granite whereas b. and d. are sampled in the Grimsel granodiorite. The grey shaded area shows 95 percentiles for background pH. Located microseismic events corresponding to the numbered epicentres in figure 5.1 are denoted by vertical black lines. Unlocated events are vertical yellow lines.79

Figure 5.3 Quartz and Granodiorite grain crushing and abrading experiments. Experimental results showing evolution of pH as a result of grain crushing with different mass ratios of rock to water. a. quartz and b. pH evolution with time for granodiorite grains crushed in granodiorite-equilibrated water under an argon atmosphere.81

Figure 5.4 Effect on pH of hydrostatic grain fracturing at increasing pressures. Hydrostatic fracturing of quartz sand grains in the same synthetic groundwater solution used in Figure 3a shows increasing pH change with pressure. Measurements of pH taken 10 minutes after uniaxial cell reaches the desired pressure. Dashed grey line shows the pH evolution for ball-mill-crushed Quartz (Figure 3a) after 10 minutes for a rock to water mass ratio of 3:8.82

Figure 6.1 Flow diagram for the different factors involved in the hydrogeochemical model of the GTS.93

Figure 6.2 Schematic diagram building on figure 6.1 adding the potential water inputs into the GTS groundwater system. Including Lake water, organic poor and rich soils and infiltration with no soil zone. Water origin is meteoric in source i.e. precipitation as rain or snow.95

Figure 6.3 Schematic flow diagram building on figure 6.2 adding flow and transport pathways from the surface to the GTS groundwater system. Including Lake water, topographic stress fractures extending to ~300m and brittle overprinting to ductile shear zones.97

Figure 6.4 Schematic diagram building on figure 6.3 adding flow and transport pathways from the surface to the GTS groundwater system. Including key chemical reactions occurring in the top ~300m of the crust surrounding the GTS.99

Figure 6.5 Conceptual diagram of water flow pathways. Meteoric water source from precipitation, infiltrates from different surface environments; lake/glacial melt, river

sediment, dark soil, light stony soil, direct infiltration to shear zones. Water follows several fracture pathways; surface weathering fractures, topographic stress fractures and brittle shear zones. Fractures hosted in two main lithologies Central Aar Granite (CAGr) and Grimsel Granodiorite (GrGr). Brittle shear zones and other fractures can contain different mineralogies for water rock reaction (i.e. biotite, fault gauge, epidote, quartz, fluorite, meta-basic dyke)..... 101

Figure 6.6 Soil map of the Grimsel region, showing the groundwater (alpha numeric) and surface organic sampling sites (numeric). Sample sites are colour coded by origin; lake in green circle, soil yellow circle, river blue circle, low organic red circle. The GTS access tunnels are in red. 102

List of Tables

Table 3-1 Average groundwater values (n= 27) and measured surface water values for temperature, conductivity and pH are presented in the table along with the host rock lithology.....	35
Table 3-2 Composition of rock types in the GTS outlining the key mineralogy CAGr: Central Aar Granite, GrGr: Grimsel Granodiorite, MBD: Metabasic dyke. Taken from Schneeberger <i>et al.</i> , 2019 compiled from: Keusen <i>et al.</i> , 1989; Mäder <i>et al.</i> , 2006; Wehrens, 2015	40
Table 3-3 Table of the Principal component analysis groups displayed in figure 3.9.	48
Table 3-4 Whole rock major oxide geochemistry for the different lithologies in the GTS.	50
Table 3-5 maximum and minimum mole transfer of phases from inverse modelling of surface water to the average cluster water composition. Where 'n' is the number of potential models. Positive mole transfer record dissolution and negative mole transfer indicate precipitation.....	55
Table 4-1 Groundwater sample locations and their respective physiochemical, major ion stable isotope and tritium and age. *Tritium and stable isotope values from Schneeberger, Mäder and Waber, 2017	67
Table 5-1 Table of saturation index from groundwater modelling in PHREEQC(Parkhurst and Appelo, 2013).	90
Table 6-1 Summary of the key findings for each sample site; water input, water rock interactions and dissolved chemical ion differences. Showing if water rock interactions are consistent with the expected groundwater chemistry in that lithology	103

1. Introduction

This thesis describes a study to characterize the hydrogeochemistry of a fractured granitic rock groundwater system. Documenting spatial differences and temporal changes in response to the repeated draining and refilling of a nearby hydroelectric reservoir (Räterichsbodensee). An in-depth characterization of spatial chemistry and groundwater flow is needed in order to evaluate perturbations to the hydrochemical system associated with the draining and filling events. Knowing how groundwater systems respond to changing stresses at the surface (i.e. climate change, surface infrastructure, tectonics) is vital in assessing the suitability of potential site(s) for a geological disposal facility (GDF) and in developing appropriate designs for which a safety case could be developed. Changing surface conditions could lead to changes in groundwater flow paths and could result in changes to groundwater chemistry. Major perturbations to the groundwater system during the life of a GDF will also influence the transport of contaminants stored underground to the surface. A GDF site in the UK will only be located where the site and surrounding area can be sufficiently well-characterised, which includes recognising the effect of significant changes in the surface load and groundwater head (e.g. associated with glaciation, climate change) over the life time of the GDF, and for which a safety case can be developed to show that radionuclides will not travel to the surface environment whilst still harmful.

1.1 Context of this Study

The UK's radioactive waste has accumulated since the opening of the world's first nuclear power plant at Sellafield in the 1950's, with other waste associated with defence and medical activities. In a drive to support low carbon energy choices, nuclear provides a cleaner source of electricity generation for the UK. Increased nuclear dependence supports the UK's climate change goals, to cut greenhouse gas emissions to almost Zero by 2050 (Department for Business, 2019). While nuclear helps to attain our climate goals it introduces another waste source. Currently there is not a permanent disposal route for high and intermediate level radioactive waste (HLW / ILW) waste, with these higher activity wastes currently being stored above ground. The majority of the UK's lower activity waste (low level waste) is disposed of to the National Low Level Waste Repository (LLWR), located in the village of Drigg, Cumbria. Government Policy (GOV.UK, 2014), is that higher activity wastes are to be disposed permanently within an engineered GDF deep underground (between 200-100m below ground level), where the rock mass and engineering work in combination to contain and isolate the

radioactive waste whilst they are still harmful. The UK's radioactive inventory contains some wastes that will remain active for over 100,000 years.

International consensus is that Geological Disposal of nuclear waste is the safest option. A Geological Disposal Facility (GDF) is designed to as a multibarrier approach which prevent radioactive materials reaching the surface environment whilst they are still harmful.

In the UK, the Radioactive Waste Management (RWM) is the developer for the GDF for the nations radioactive waste. RWM (2016) describes a multibarrier approach for the GDF as follows:

1. The waste form and waste package; vitrified waste is stored in a sealed low reactive metal canister (i.e. copper)
2. The Engineered Barrier (EBS) – depending of the nature of the waste, this can be a bentonite barrier placed around the metal canister where the bentonite provides a low permeable layer that delays the transport of water to the canister and suppresses microbial communities which may otherwise promote canister corrosion, or will involve cement based backfill which will promote a high pH environment to delay migration of radionuclides
3. The geological environment; the wastes are placed in engineered vaults or deposition holes at depths between 200m and 1000m – the rock mass contains the waste, and isolates it from the surface environment

Experiments and modelling are used to understand the long-term evolution of all parts of the multibarrier system to inform concept and design decisions. Each country developing a GDF will make designs and safety cases that reflect their government policy, community drivers and the geological setting. Notably, a common requirement for a GDF is a slow return to surface travel time for radionuclides between the waste and the surface environment. This can be achieved, for example, in rocks that do not have groundwater (e.g. halite), where radionuclide migration is via diffusion (e.g. in clay rocks 'lower strength sedimentary rocks (LSSR)'), or where bedrock has low permeability with limited interconnectivity of transmissive features to the surface (e.g. certain crystalline rock environments 'Higher Strength Rocks' (HSR)).

The locating of a GDF in the UK will be consent led, with a community volunteering to host the facility. A site has not currently been identified, and RWM undertakes research to underpin concepts and designs for GDF in HSR, LSSR and halite environments.

This thesis furthers understanding of the temporal changes to water chemistry and groundwater flow paths in HSR, in response to surface water induced hydro-mechanical perturbations, and to develop tools for assessing these changes.

On the time scale of a few 100,000 years, a repository in the Northern-Hemisphere is likely to experience a glacial maximum and sea-level fluctuation. Previous large northern hemisphere

glacial periods resulted in Ice-Sheet formation. Ice Sheets are thick (1-2km) and laterally extensive across land masses, which exert stresses on the rock mass impacting a GDF. Advance and retreat of glaciers will change the groundwater flow pathways surrounding a GDF. A GDF safety case will also need to consider the effect of glacial stresses on a GDF, along with the impact of these on the hydrogeological (hydraulic and geochemical setting). A variety of tools will be used to evaluate the future evolution of potential GDF sites, including numerical simulations of glacial cycling. Use of real analogues that provide evidence to underpin these numerical models are however limited, particularly those with relevance to the UK context.

Draining and refilling of surface water bodies have the potential to generate stresses that are analogous to those exerted by glaciers. The magnitude and the rate of the stress changes during the dewatering of surface water bodies, will be different. However, draining and refilling of surface water reservoirs is possibly the closest analogue we have to studying how glaciers may affect the hydrogeochemistry and hydrogeology of the rock barrier surrounding a GDF.

To determine if dewatering has an effect on the hydrogeochemistry and hydrogeology of a system, detailed characterization and understanding of the baseline groundwater chemistry, and its expected future evolution in the timeframe of interest is required. End member groundwater conditions need to be known, as do the different sources and origins of water contributing to a groundwater system. Once background conditions are constrained, a comprehensive time series of data will show any detectable changes to the groundwater system in response to the dewatering. Finally, to relate the findings of dewatering experiments to deglaciation and glacial cycling an understanding of the limitations of using lake draining as an analogue for a glacial cycle is required i.e. would you find similar conditions under a glacier?

1.2 Large Scale Monitoring Project (LASMO)

The Large Scale Monitoring Project (LASMO) is collaborative project led by NAGRA, the developer for a GDF in Switzerland. Project partners are RWM (Radioactive Waste Management Ltd.), and SURAO (the Czech Republic waste management organisation). Experimental work is being delivered on behalf of the partners by the Universities of Strathclyde (UK) and Bern (Switzerland), along with the Institute of Geonics in Prague, Czech Republic.

The aim for the LASMO project is to perform an integrated characterisation of the geological, hydrogeological, geochemical and stress / strain around a site. This type of characterisation activity would be required to evaluate the suitability of a site for a GDF. The LASMO project site selected was the area the Grimsel Test Site (GTS), which is an underground rock laboratory (URL) operated by NAGRA, located in the Swiss Alps. GTS has been operating

for nearly 30 years, and a substantial data base of relevant characterisation information, to support LASMO exists. Consequently, LASMO gives the opportunity to evaluate and validate new tools and techniques to characterise the site, using historic information to baseline and validate the data against.

The GTS tunnel is accessed via a service tunnel associated with a hydroelectric power plan that is operated by Kraftwerke Oberhasli AG (KWO). The service tunnel supports hydroelectric power infrastructure associated with a series of hydro power reservoirs in the area. The LASMO project takes advantage of construction works related to draining of the nearby Lake Räterichsbodensee reservoir. I hypothesise that the draining and refilling of the lake will affect hydraulic and/or rock mechanical conditions around the GTS and could potentially be used as an analogue for glacial perturbations during GDF construction, operation and closure. Some radionuclides are expected to remain at harmful activities for several 100,000's years. In the next 10,000 years or so, the northern hemisphere is predicted to undergo several glaciations resulting in ice sheet formation. A safety case must therefore consider the long-term safe storage of nuclear waste over glacial time periods. During glaciation, predictions regarding how the geological barrier will respond mechanically, chemically and hydrogeologically to the changing surface conditions have limited scientific underpinning. This thesis evaluates the response of groundwater in the rock mass surrounding the GTS to associated with draining and refilling of a surface water lake. The response is considered in context of being an analogue of the effect of glacial advance and retreat on the hydrogeochemical system surrounding a GDF.

1.3 Research Question and Objectives

The research presented here focuses on how geochemical and hydraulic observations and modelling can be used to:

- (1) develop an understanding of groundwater origins, and
- (2) understand the evolution of groundwater pathways over time during a period of substantial surface unloading?

To guide the research, and to fill the gaps in knowledge, four key research questions (RQ) were defined. Each of these were broken down into specific objectives (SO) as follows:

RQ-1. How can existing hydrogeochemical investigation techniques be used to characterize the spatial groundwater chemistry at the GTS?

SO-1 Collect a time series of groundwater samples, before, during and after the draining and refilling of a surface water reservoir.

SO-2 Analyse and interpret groundwater chemistry data to characterize the background groundwater geochemistry and flow.

SO-3 Use data from groundwater analysis to develop a conceptual model of how groundwater evolves through water rock reactions, supported by geochemical modelling in PHREEQC.

RQ-2. Determine how lake draining and refilling affects the groundwater system

SO-4 Use the data set collected in SO1 to identify any changes to groundwater chemistry or flow, during draining and refilling of lake Räterichsbodensee.

SO-5 Determine the mechanisms that could lead to changes in geochemistry or flow paths.

RQ-3. Assess new environmental tracing techniques to evaluate benefit in site investigations to better characterize groundwater?

SO-6 Analyse the different dissolved organic components of groundwater and establish what they indicate about the groundwater system.

RQ-4. Investigate the coupling behaviour of lake draining on flow and groundwater chemistry to answer the question: *does lake draining effect groundwater systems in fractured crystalline rock and is this an acceptable analogues for glacial retreat?*

SO-7 Develop a combined conceptual model to show how groundwater flow and chemistry respond to lake draining at the Grimsel Test Site (GTS).

1.4 Structure of Thesis

This thesis contains four main research chapters, chapters 4 and 5 are written as individual journal papers. Instead of concluding each individual chapter and paper, the findings are synthesised and discussed in chapter 6. Chapter 6 forms, in part, the Strathclyde contribution to a final research publication to be submitted in conjunction with the LASMO partners as a peer-reviewed publication.

Chapter 2 reviews literatures attaining to the chemical and physical controls on hydrogeochemistry. Expanding on the influence and causes of dynamic fluctuations of groundwater chemistry and flow from; seasonal and long-term changes to climate, earthquakes and the effect of fault/fracture slip on groundwater chemistry and flow. This chapter also discusses the impact of operational surface water and hydropower reservoirs on the surrounding rock mass.

Chapter 3 describes the GTS field site, briefly introduces the current state of hydrogeological and geochemical knowledge of the GTS, leading on to assess the controls on spatial groundwater chemistry. It records the findings of an intensive sampling campaign. The results of chemical analyses are discussed and the geological controls on modern groundwater chemistry at the GTS are highlighted. Geochemical modelling is carried out to support interpretations of the modern hydrogeochemical system at the GTS.

Chapter 4 develops a new method for tracing the infiltration site of meteoric water into a groundwater system. This is the first time analysis of this type has been used to detail the organic compounds present in groundwater. 2D-Gas Chromatography is used to compare a comprehensive suite of organic compounds present at the surface to those within groundwater at depth. This forms a paper in submission.

In **Chapter 5**, we present data and experiments showing that reservoir drainage induces microseismicity, and that this triggers mechanochemical reactions leading to short lived temporal drops in the pH of groundwater. Chapter 5 is in submission to Geology.

Chapter 6 defined the hydrogeochemical system at the GTS. It analyses the geological controls on spatial chemistry, flow (Chapter 3) and infiltration sources (Chapter 4), as well as considering the temporal changes associated with microseismic events (Chapter 5). A 3D conceptual model of hydrogeochemistry at the GTS is presented. This chapter discusses how the conceptual model responds to lake drainage, assessing whether lake drainage provides a useful analogue to study the effects of future glaciation and ice-sheet formation. It then goes on to discuss how the information gathered previously in the thesis is relevant and useful in characterising a potential site for a GDF. Finally concludes the key findings of the thesis. This chapter forms part of the RWM contribution to the final LASMO report, in preparation.

Finally, **Chapter 7** includes recommendations for future practice and an outlook for future work and potential new avenues of research that have arisen from the findings in this thesis.

1.5 Study Area

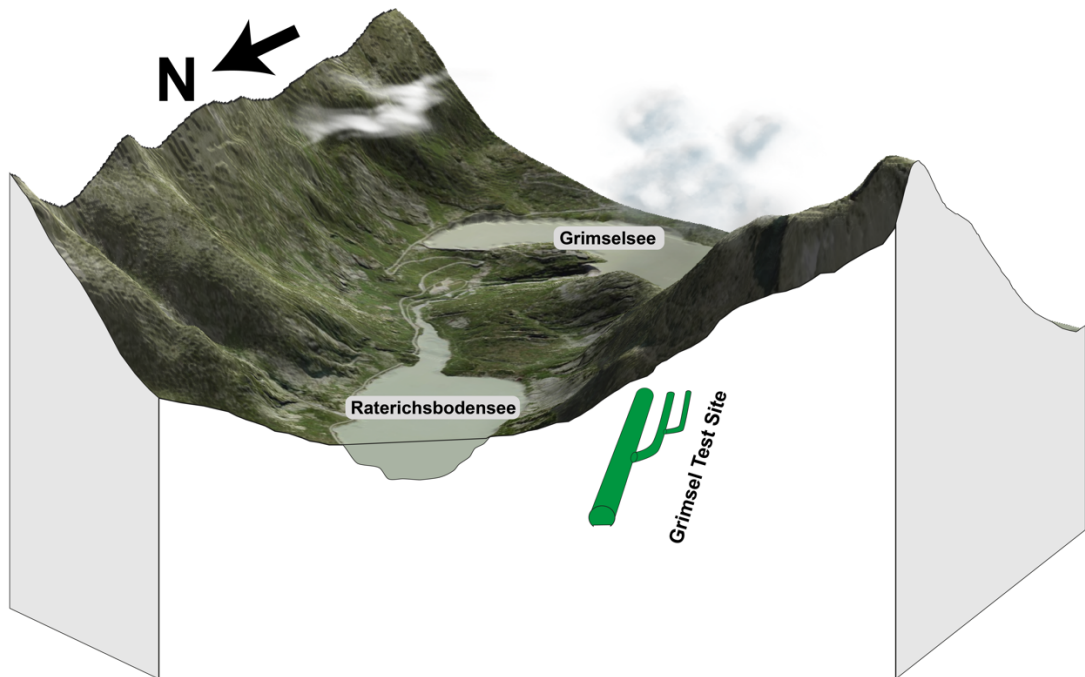


Figure 1.1 3D block diagram of the GTS exposure underground (Not to Scale). Satellite imagery imposed on vertically exaggerated topography. Hydropower reservoirs Räterichsbodensee and Grimselsee are highlighted.

The field area at the core of this thesis (Figure 1.1) is the Grimsel Test Site (GTS) Switzerland an Underground Rock Laboratory (URL) operated by NAGRA. The GTS (Figure 1.2) is located in the Upper Hasli valley, north of the Grimsel Pass. The entrance tunnel to access the site is located just to the west of the Räterichsbodensee dam wall. The GTS is reached by a network of access tunnels owned and operated by KWO (Kraftwerke Oberhasli hydroelectric power company) hydroelectric power company. Underground accessible tunnel systems are extensive as are the network of pipes and spillways connecting thirteen different water bodies, eight of which are purpose built storage lakes for the generation of hydroelectric power. This complex pump storage network operated by KWO covers an entire alpine water catchment. Two hydropower reservoirs Räterichsbodensee and Grimselsee are to the east and directly south of the GTS respectively. The GTS system mainly encompasses water from Grimselsee, Oberaar (fed by glacial melt) and Räterichsbodensee.

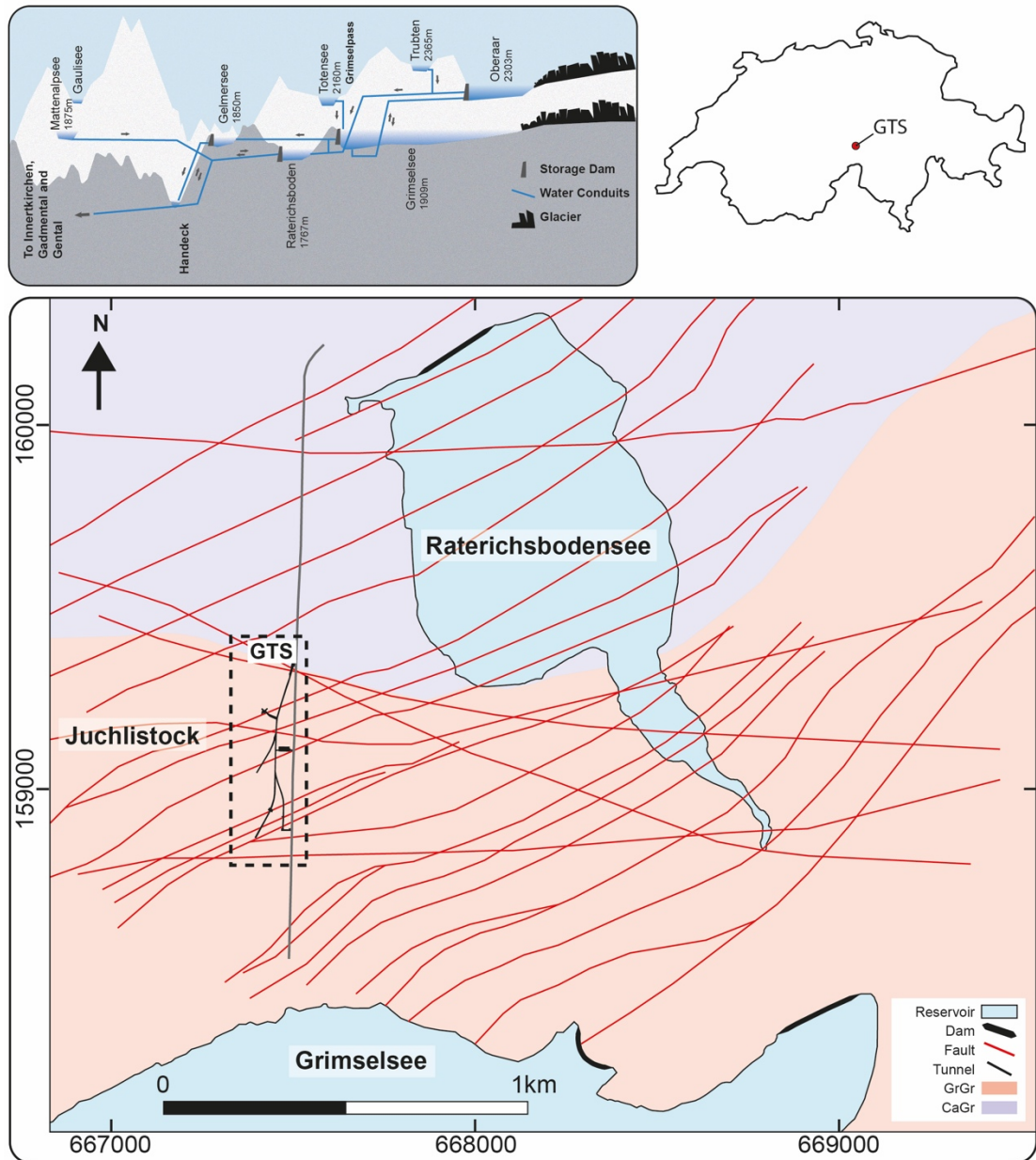


Figure 1.2 (top right) outline of Switzerland with the location of the GTS highlighted. (top left) not to scale schematic diagram of the complex hydropower pumping network connecting Grimselsee and Räterichsbodensee to the reservoir systems in other water catchments. Geological map (adapted from Schneeberger et al., 2018) of the GTS (bottom), hydropower reservoirs (light blue) Grimselsee and Räterichsbodensee, lithology as mapped at the surface, surface liniments (red lines), GTS access tunnel (Grey) and GTS tunnel network highlighted in dashed box.

1.5.1 Why the Grimsel Test Site?

The GTS offers the ideal opportunity to study the effects of lake draining and refilling on groundwater systems. This thesis takes advantage of planned maintenance works carried out on Räterichsbodensee. Maintenance requires the complete draining and subsequent refilling of the lake. This occurred once from Nov-2014 to Feb-2015 and a second time from Feb-2016 to Mar-2016. The GTS is located within the adjacent mountainside, at an altitude beneath the

base of the lake, and contains an already well-established network of groundwater sampling boreholes. The borehole network in the GTS covers an area of rock 1.8km by 0.4km of well characterized host rock. Boreholes at the GTS are individually packed (Figure 1.3) to isolate different geological features such as, faults, shear zones, dykes, and lithological changes. Groundwater at the GTS is dilute, and as such provides the opportunity to detect changes to physiochemical parameters or major or minor dissolved ion chemistry. It is possibly one of only a few locations in the world suited to investigating the dynamic response of a groundwater system to lake draining.

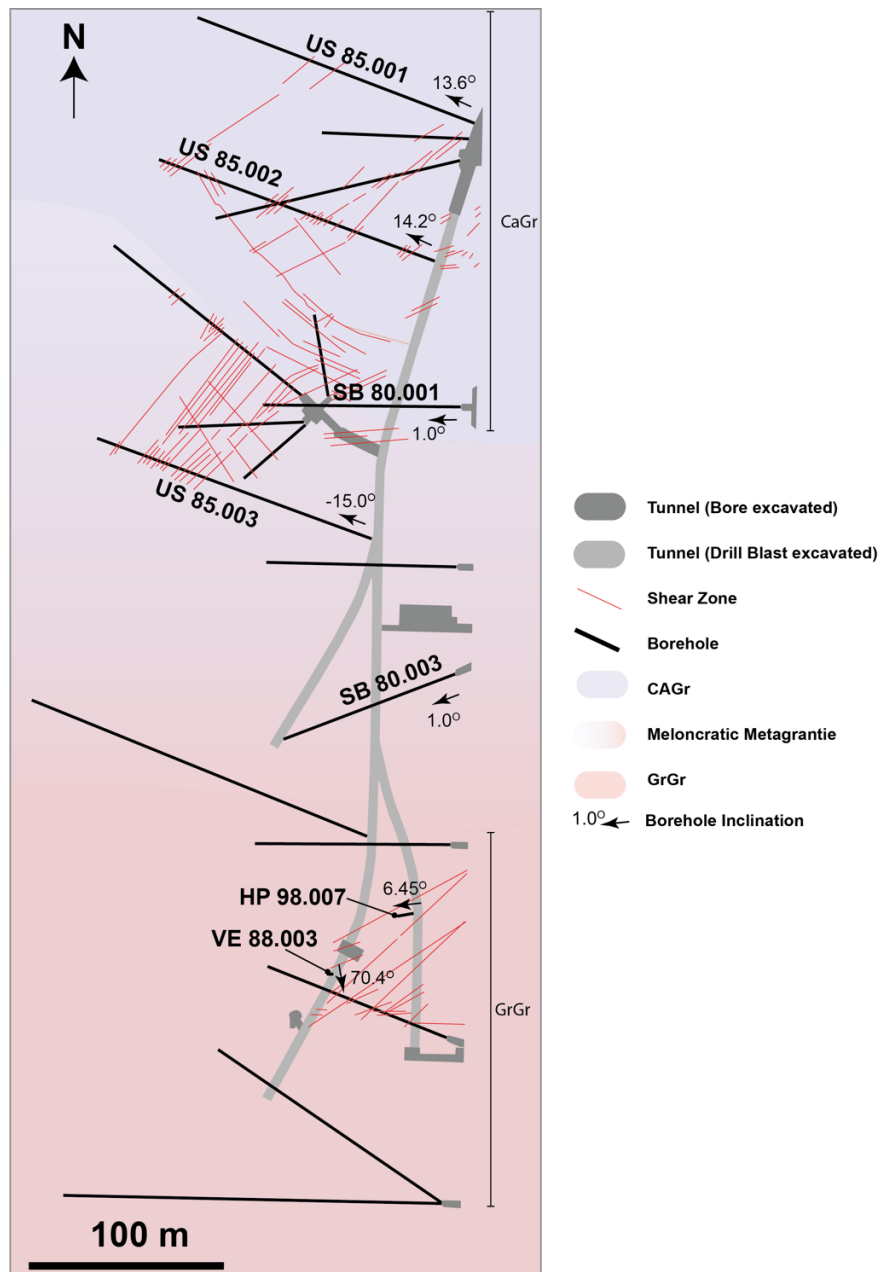


Figure 1.3 Borehole schematic of the GTS. Lithology as mapped at depth (CAGr - lilac, GrGr - Pale Red). Boreholes used through the thesis are labelled; US 85.001, US 85.002, SB 80.001, US 85.003, SB 80.003, HP 98.007 and VE88.003. Shear zones mapped at depth indicated by solid red lines. CAGr – Central Aar Granite, GrGr – Grimsel Granodiorite

2. Controls on groundwater chemistry

2.1 Introduction

This chapter provides an overview of the controls on shallow (200-500m) groundwater chemistry and its chemical evolution. It focuses on the relevant factors that could have a potential impact on, or related to, chemical evolution of groundwater at the Grimsel Test Site (GTS) and other crystalline groundwater systems. Section 2.2 looks at how fluid-rock weathering reactions affect crystalline-hosted groundwater chemistry (section 2.2.7), and the control static and dynamic equilibrium reaction methods have on groundwater evolution. Section 2.3 introduces the impact infiltrating water chemistry can have on groundwater chemistry in the saturated zone. Section 2.3 discusses temporal groundwater fluctuations and the factors which can cause fluctuations in groundwater chemistry and flow (e.g. seasonal climate, earthquakes, glacial cycles, anthropogenic structures).

2.2 Water rock reactions

Groundwater chemistry evolves by different chemical weathering processes and the duration of the associated water rock interaction. These reactions include reduction/oxidation (Redox), carbonation, hydrolysis, and hydration. Aqueous chemical weathering processes act to break down and/or transform minerals, changing the mineral composition, releasing or taking up ions from groundwater. Chemical weathering processes occur at the surface and in the subsurface. Chemical equilibria can be defined to describe the reactions between fluid and rock. Understanding the different equilibrium processes will show if specific minerals are saturated or undersaturated in solution and therefore if precipitation or dissolution should occur. While chemical equilibrium describes the solution with respect to specific minerals or mineral assemblages the dynamic state of equilibrium is defined by chemical kinetics and reaction rate. Chemical reaction rates over geologically long time periods tend to zero as fluid rock equilibrium is reached. If in equilibrium, then kinetics have a minimal control on the composition of groundwater unless the fluid-rock equilibrium state is perturbed. Over short time scales kinetic rate factors play an important role in the evolution of groundwater chemistry. Different minerals react at different rates under different environmental and thermodynamic conditions (i.e. temperature, oxygen availability, microbial activity). Furthermore, physical weathering processes lead to increased reaction rates by increasing surface area for chemical weathering processes to act on.

2.2.1 Hydrochemical equilibrium and saturation index

Chemical equilibrium describes the mass transfer between, solid, liquid and gaseous phases within a chemical system. The key reaction process affecting groundwater chemical evolution are the precipitation or dissolution of mineral phases. Other important chemical reactions described by mass transfer are transformation reactions where ions are removed or replaced from a mineral, these can include oxidation/reduction and complexation reactions. Oxidation/reduction or redox reactions occur by the transfer of electrons and hence the redox conditions will control the valence state of ions. While most elements exist in solution as a lone ion, other elements form complex ions. Complex ions consist of one or more metal ions which become associated with ligands. Ligands surround metal ions when a complex species is formed in solution (e.g. $[\text{Cu}(\text{NH}_3)_4(\text{H}_2\text{O})_2]^{2+}$).

All equilibrium reactions can be defined by a balanced chemical equilibrium reaction (eq. 2.1). Each reaction has an equilibrium constant (K), describing the ratio of the activity of all the products and reactants in an equilibrium reaction. The reaction rate (k) is different for the forward and backward reactions. The Equilibrium constant (K) for the generalised reaction given in equation 2.1 is described by equation 2.2 (Freeze and Cherry, 1979).



Where: a, b, c, d are the moles of the products and reactants. A, B, C, D are the products and reactants.

$$K = \frac{[C]^c[D]^d}{[A]^a[B]^b} \quad (2.2)$$

Where: K is the thermodynamic equilibrium constant.

And $K = k_f/k_r$ (k_f = forward reaction rate constant, k_r = reverse reaction rate constant)

Knowing the state of chemical equilibrium in groundwater shows how saturated species are in solution. This allows a thermodynamic calculator such as PHREEQC (Parkhurst and Appelo, 2013) to determine if further precipitation or dissolution may occur in the groundwater. The activity of ions in a solution (i.e. effective concentration) are used to calculate the saturation of any potential minerals in solution. Saturation index is a numerical representation of the saturation of a solution with respect to one mineral in solution. Saturation index (eq. 2.3) is given by the ratio of the ion activity product (IAP) and the thermodynamic solubility constant at equilibrium (K_{sp}).

$$SI = \log_{10} \frac{IAP}{k_{sp}} \quad (2.3)$$

Where: IAP is the ion activity product calculated from the activity or effective concentration of ions in a measured solution. K_{sp} is the solubility product at equilibrium.

Equation 2.3 essentially shows how far the measured solution (IAP) is away from equilibrium state (k) where there is no net dissolution or precipitation. Thus, for a $SI = 0$ the solution is in equilibrium and no net dissolution or precipitation occurs ($IAP = k$). When; SI is negative the solution is under saturated with respect to a specific mineral and dissolution will continue if there is sufficient mineral available to dissolve. If SI is positive the solution is supersaturated with respect to the mineral phase therefore precipitation is more likely to occur. However just because the saturation index shows something is supersaturated/undersaturated and that precipitation/dissolution should occur this does not mean that precipitation/dissolution will occur. Instead the saturation state only shows in which direction the reaction is expected to happen. Silicate minerals often take a long time to reach equilibrium with groundwater and cannot be properly describe by equilibrium reactions. In this case chemical kinetics can be used to better describe and predict changes to a solution over time.

2.2.2 *Hydrochemical Kinetics and Rate factors*

Before a mineral or compound reaches equilibrium with a solution (i.e. the forward reaction rate is equal to the backward), the reaction can be defined by its chemical kinetics. Kinetic expressions show how a solution evolves with increasing time (Figure 2.1). Often silicate minerals in groundwater systems have not reached equilibrium with the groundwater. If this is the case then equilibrium approximations of the chemical system, may approximately fit, however a kinetic approach is more suitable and can more fully define a chemical system in these cases. In the kinetic realm reaction rates change as the equilibrium of water and solid is approached. The kinetic reaction is controlled by the concentration of products, reactants and the total energy in the system. While kinetic and rate equations should describe a chemical system better than equilibrium chemistry, our understanding of kinetics is based on empirical equations (Appelo and Postma, 2005).

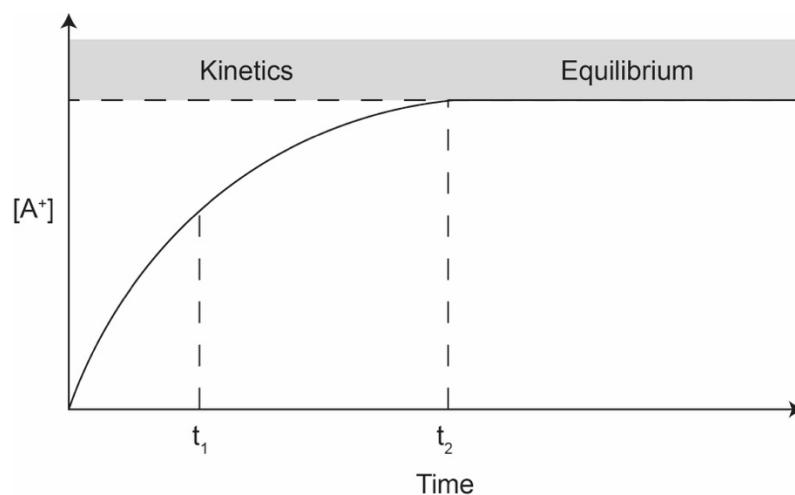


Figure 2.1 Kinetic and equilibrium stages for the evolution of concentration of compound [A+] with time (adapted from Appelo and Postma, 2005).

For a simple reaction where compound X is converted into compounds Y by the reaction:



To describe this reaction, we can measure the concentration of reactants as a function of time. On a plot of concentration versus time (Figure 2.2) the rate of reaction is the change of concentration with time. Rate can be determined from the slope of the tangent to the concentration time curve for the reactants. For concentration curve rate (eq. 2.5) is the differential of concentration and time.

$$Rate = -\frac{dc_x}{dt} \quad (2.5)$$

The rate is given a negative sign as it describes the reactants which decrease in concentration with time. The rate of increase of the product Y is equal and opposite as rate is positive.

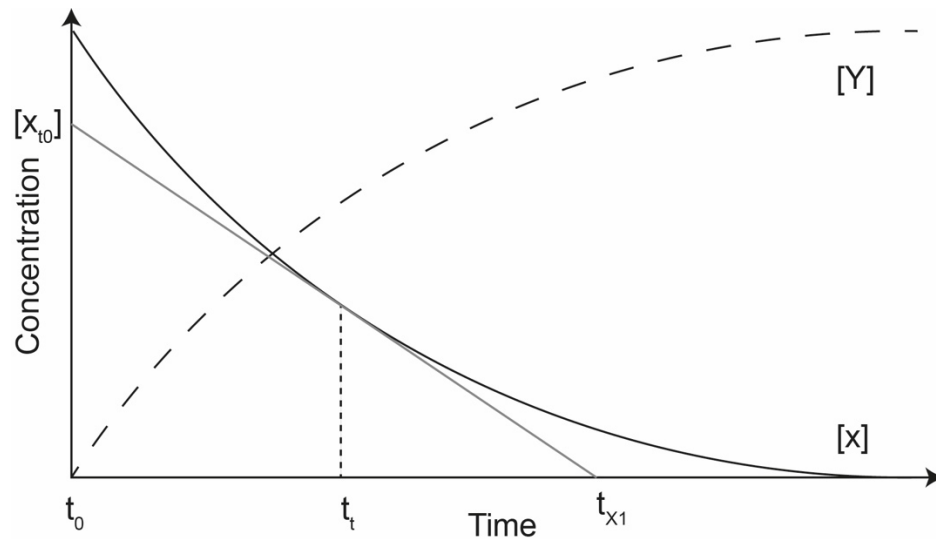


Figure 2.2 concentration of reactants and products for the reaction of $X \rightarrow Y$. Rate of reaction derived from changing concentration over change in time.

Reaction rate is greatly affected by temperature. Increased temperatures increases the kinetic energy in the system and thus increases reaction rate. Temperature effects on rate are governed by the Arrhenius equation (eq. 2.6) where reaction rate changes with temperature.

$$k = A \cdot e^{\left(\frac{-E_a}{RT}\right)} \quad (2.6)$$

E_a is the activation energy (kJ/mol) required to overcome for the reaction to occur, R is the universal gas constant, T is the absolute temperature, and A is the pre-exponent factor, a factor which describes the frequency of collisions. When $E_a \gg RT$ rate of reaction k increases rapidly with increasing temperature. Arrhenius describe activation energy as the energy that reactants are required to gain to transform into products at a given temperature. The total number of reactants with energy greater than the activation energy at a given temperature can be described statistically. The Maxwell-Boltzmann distribution shows the probability that a particle has a specific energy, any particles with an energy greater than the activation energy should then react.

2.2.3 Oxidation and Reduction

Oxidation and reduction, or redox reactions involve a change in valence state of a species. Redox reactions refer to the loss and gain of electrons, thus changing the valence state of a species. Changes in valence state can cause stable species to become more soluble or insoluble affecting their transport mobility in solution. Oxidation is the loss of electrons (e.g. ferrous iron (II) is oxidized to ferric iron (III) by losing an electron), reduction reactions are the gain of electrons decreasing the valence state. Oxygen is the most important redox species in shallow subsurface. Infiltrating water is in equilibrium with atmospheric oxygen. Solid species

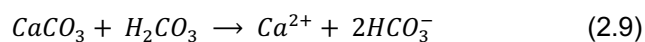
react with dissolved oxygen in groundwater. The mineral is oxidized, this changes the mineral, lowering the energy required for further weathering processes to occur. Once dissolved oxygen is depleted from the water and there are no other sources of oxygen then oxidation reactions by reaction with oxygen cease to occur. However, if there are sources of other electron donors then oxidation reactions will still continue. Other major redox species include nitrogen, iron and sulfur compounds.

2.2.4 Hydration

Hydration or dehydration reactions are the addition or removal of water in a mineral structure. This reaction causes changes to the mineral chemistry and its physical properties (Azam, 2007). Anhydrite (CaSO_4) to Gypsum ($\text{CaSO}_4 \cdot 2\text{H}_2\text{O}$) is a common example of a hydration reaction where water is added into the solid mineral. Hydration reactions often have lower activation energies than dehydration reactions which require an input of energy to remove the water from the mineral. Hydration reactions alone do not generally affect groundwater chemistry but do weather minerals, making them more susceptible to other forms of chemical and physical weathering. This in turn can cause changes to the groundwater chemistry. As well as anhydrite hydration reactions other common hydration reactions occur during metamorphism such as retrograde metamorphism of olivine causing the formation of serpentine and brucite (Kelemen and Hirth, 2012).

2.2.5 Carbonation

Atmospheric CO_2 dissolves into water vapour forming carbonic acid (eq. 2.7). Carbonic acid lowers the pH of the water and acts to dissolve minerals that the water interacts with. This chemical process releases anions and cations into solution as carbonic acid loses a proton, bicarbonate and hydrogen ions (eq. 2.8) are released and react with solids (eq. 2.9).



Carbonic acid is a weak acid. In meteoric-driven groundwater systems with no other CO_2 input, a $p\text{CO}_2$ of 3.5×10^{-4} atm. is expected to dissolve into water vapour in the atmosphere. Atmospheric carbon dioxide concentration in solution behaves by Henry's gas law. Henry's law (White, 2009) states that:

“At a constant temperature, the amount of a given gas that dissolves in a given type and volume of liquid is directly proportional to the partial pressure of that gas in equilibrium with that liquid”

For atmospheric pCO₂ it is expected that the concentration of atmospheric carbon dioxide which goes into solution is given by equation 2.10

$$[CO_2]_{(aq)} = \frac{pCO_2}{k_H} = 3.5 \times 10^{-4} \div 29.76 \quad (2.10)$$



However, not all CO₂ which dissolves into solution remains as [CO₂]_(aq). Hydration equilibrium with water leads to carbonic acid formation (eq. 2.7) which then dissociates (eq. 2.8) and can undergo a further dissociation (eq. 2.11). The second dissociation of HCO₃³⁻ releases a further H⁺ into solution as well as the carbonate ion CO₂⁻². At low pH the products of the second dissociation (eq. 2.11) are negligible. The pH of water is given by the -log[H⁺], the hydrogen ion concentration can be calculated and the predicted pH of a water in equilibrium with atmospheric CO₂ is 5.65.

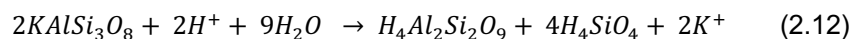
In meteoric groundwaters carbonation via atmospheric CO₂ forms a weak acid. This weak acid increases the dissolution of minerals into solution and will increase the dissolution rates of carbonate minerals as well as other rock minerals. Dissolution will continue until there is no net H⁺ ions for further reactions to take place. Dissolved inorganic carbon will eventually reach an equilibrium and will be in the form of carbonate and bicarbonate. In meteoric systems the main source of CO₂ comes from infiltrating rain and surface waters. CO₂ can also come from microbial processes (Wood et al., 1993) in the soil zone and in subsurface environments (Phelps et al., 1989). Microbially mediated CO₂ production in groundwater generally occurs as a by-product of methanogenesis (Chapelle, 2000). Methanogenesis is the anaerobic respiration of organic matter in the subsurface, and is limited by the availability of electron acceptors in the aquifer (Chapelle and McMahon, 1991). CO₂ can also be introduced into a groundwater system from below from natural CO₂ reservoirs (Shipton et al., 2005) CO₂ rich fluids are carried by buoyancy forces through permeable aquifers as well as faults which can act as a conduit for CO₂ movement (Shipton et al., 2004; Dockrill and Shipton, 2010) through an aquifer.

2.2.6 Hydrolysis

Water reacts with rock forming minerals in aquifers changing the composition and form of different minerals. The result of a hydrolysis reaction is to transform a mineral into a new,

normally weaker mineral, which is not as resistant to further weathering processes (chemical or physical). Hydrolysis reactions also have an impact on the groundwater, as the mineral is changed by adding hydrogen ions into the mineral, cations and anions are then released from the crystal lattice into solution. Release of ions into solution changes the chemistry of the groundwater and over time hydrolysis reactions can evolve groundwater to more concentrated dissolved ion concentrations.

Feldspars undergo weathering by hydrolysis, resulting in cation releases into solution. This reaction evolves groundwater chemistry as ions are released into solution. While groundwater chemistry evolves feldspars are transformed into clay minerals (eq. 2.12), such as kaolinite, and quartz (Nesbitt and Young, 1989). Alkali feldspar hydrolysis is an important process for groundwater evolution, removing protons from solution and releasing cations (Ca^{2+} , Na^+ , K^+ , Mg^{2+}). Removal of protons and addition of alkali ions into solution leads to increasing groundwater pH. The feldspar water interface is the rate determining factor for the weathering rate of feldspars in a groundwater systems (Helgeson et al., 1984). Hydrolysis reactions are limited by the solution mineral interface (Lagache, 1976), and are pH dependent reactions (Aagaard and Helgeson, 1982) that occur at different rates in high and low pH solutions. Reaction rate decreases with time as feldspar surfaces become placated with products stopping the reaction.



2.2.7 Hydrochemical evolution in crystalline rocks

Groundwater evolution in crystalline rocks occurs over much longer time scales than in carbonate rocks. Solution processes are slow in silicate/quartz dominated lithologies. Crystalline igneous or metamorphic hosted groundwater systems are generally in lithologies composed of quartz and aluminosilicates such as feldspars and micas. The slow dissolution rates at low temperatures (20°C) form dilute groundwater solutions which tend to approach high pH. Continental crust is mostly made up of plagioclase feldspar, potassium feldspar and quartz and has the average composition of granodiorite (Hiscock and Bense, 2014). Dependent on local rock type, different secondary minerals are also present.

The evolution of groundwater in crystalline rocks starts with infiltrating meteoric water. Infiltrating meteoric water recharge is not in chemical equilibrium with the rock mass. Rainwater is nominally acidic from atmospheric CO_2 bringing it down to pH 5.65. Carbonic acid from dissolved CO_2 provides the proton source which reacts with the crystalline rock. This carbonation and coeval hydrolysis reactions release cations into solution (Ca^{2+} , Na^+ , K^+). The carbonic acid dissociates and is the source of bicarbonate alkalinity (HCO_3^-). Feldspathic minerals weather by this process and leave behind quartz and kaolinite. Weathering of

feldspathic minerals occurs in accordance with the Goldich weathering sequence, Figure 2.3 (Goldich, 1938). Calcium feldspars are more susceptible to weathering than magnesium sodium and potassium feldspars. Initially waters evolve into a Ca-HCO₃ type groundwater, but as Na-feldspar, K-feldspar weather they react with the groundwater and result in groundwater evolving into a Ca-Na-K-HCO₃ type groundwater. Finally, phyllosilicate minerals dissolve and quartz dissolution occurs last.

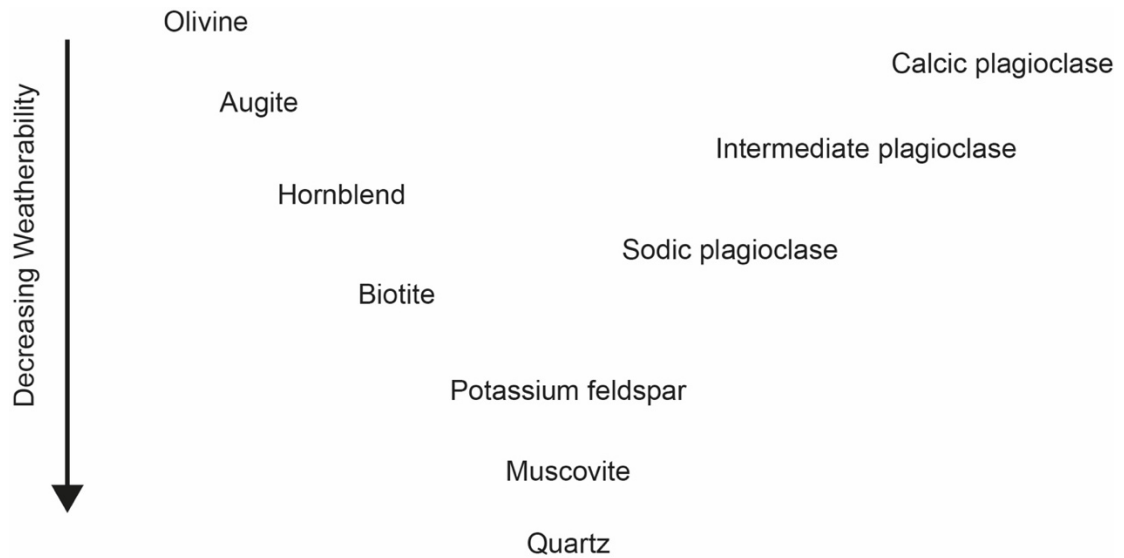


Figure 2.3 Goldich weathering observational based mineral appearance of primary silicate minerals in soils (adapted from Goldich, 1938).

Chemical weathering of secondary minerals occurs along the whole flow path where the mineral is available for dissolution and is not already in equilibrium with groundwater. Non silicic minerals can include; calcite, fluorite, iron sulphides/sulphates, halite and other salts. Most of these salts undergo simple dissolution reactions to release both anions and cations into solution. Dissolution reactions provide the main source of anions into the groundwater system, other sources of chloride and sulphate into crystalline groundwater are from sea water intrusion or atmospheric sources. As a result, Cl⁻ and SO₄²⁻ are normally minor or trace elements in crystalline groundwater. If Cl⁻ and SO₄²⁻ are present in major quantities, it is normally from impurities in rocks and minerals or there is a source chloride or sulphide minerals available to dissolve such as halite or pyrite.

There have been several detailed hydrochemical site investigations in crystalline rock aquifers, which include underground rock laboratories, such as Äspö Hard rock laboratory, Sweden (Laaksoharju et al., 2008; Laaksoharju et al., 2008), Grimsel Test Site (GTS), Switzerland (Keppler, 1995; Schneeberger et al., 2017) both hosted in granitic rock, the Olkiluoto site, Finland (Pitkanen et al., 2004), and plutonic intrusive granitic hosted groundwaters (Frape et al., 1984; Douglas et al., 2000). Hydrochemistry of granitic-gneiss crystalline basement rocks

has been studied in the Black Forest Variscan basement, Germany (Bucher and Stober, 2002) and shallow groundwater systems in Ilesha, Nigeria (Tijani et al., 2014). All of these areas fit the standard groundwater chemical evolution of crystalline aquifers. Groundwater pH is neutral to high (6-9 pH), dilute with low electrical conductivity, and main groundwater type Ca-Na-HCO₃. With time they evolve to the higher pH. Sodium becomes more dominant than calcium and as plagioclase feldspars start to dissolve. Finally, calcite precipitation and ion-exchange with clay minerals occurs along flow paths evolving shallow groundwaters to the composition that has been observed globally.

2.3 How is groundwater evolution affected by infiltrating water conditions?

Meteoric water infiltrates into the ground through the soil zone (1), through the unsaturated zone (2), then into the saturated zone (3) where it remains as groundwater and becomes confined to an aquifer. Figure 2.4a shows the common infiltration route of meteoric water and the potential chemical reactions which may take place as it progresses into the saturated zone. Infiltrating meteoric water reacts with in the unsaturated zone before it reaches the crystalline rock, where chemical evolution occurs through fluid-rock reaction (Section 2.2.7). Infiltrating water undergoes reactions in the unsaturated zone and soil zone/critical zone (Brantley et al., 2007). If there is no soil zone present (Figure 2.4b) then groundwater evolution occurs in accordance with section 2.2.7. However, the critical zone can play an important role in altering the chemistry of infiltrating water, increasing the availability of electron donors and acceptors, changing the redox state, increasing dissolved CO₂, O₂ and other gas partial pressures. All of these factors can change the extent and rate of subsequent chemical reactions in the saturated zone.

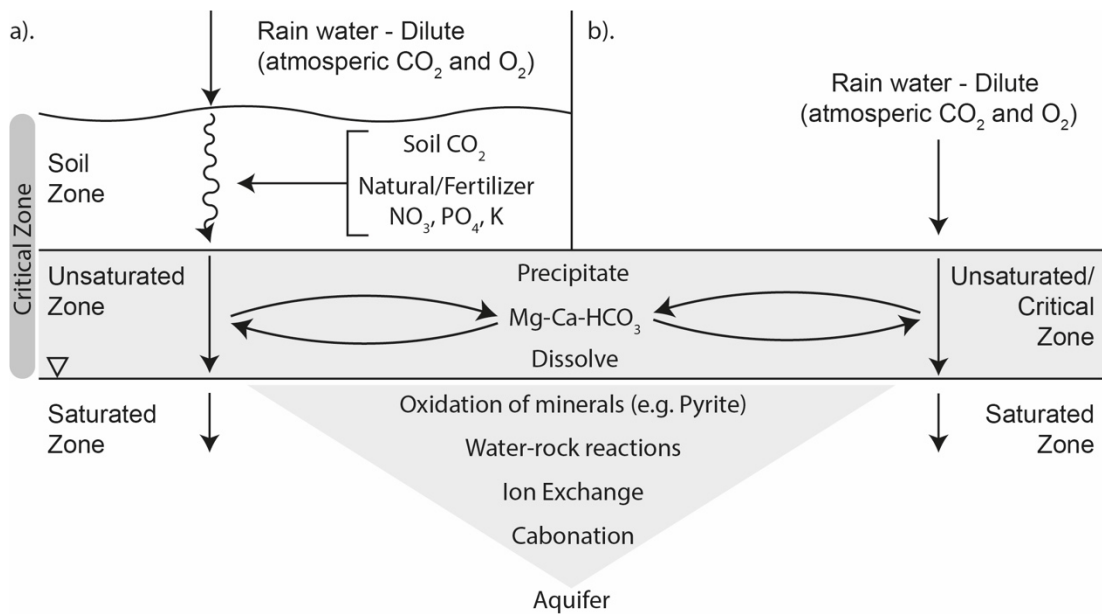


Figure 2.4 Schematic diagram of the evolution of groundwater from infiltrating meteoric water through a). soil and unsaturated zone and b). the unsaturated zone into the saturated zone. Showing important hydrochemical processes in each zone (adapted from Hiscock and Bense, 2014).

Meteoric water is in equilibrium with atmospheric gases (CO₂, O₂, N₂), volatile organic compounds (VOC's) from pollutants and can contain NaCl of marine origin. Gasses are in equilibrium with the atmosphere and will result in carbonation and oxidation reactions to occur. The concentration of NaCl in meteoric water will depend on the proximity of the rainfall site to a marine source. It is expected that there will be a greater influx of NaCl to the groundwater system in costal aquifer systems than in continental land locked areas. VOC's dissolve into water vapour and are in equilibrium with the atmosphere until they reach the saturated zone. VOC's are in low concentrations and will have a negligible impact on groundwater evolution compared to the large impact organic input from the soil zone has on groundwater.

The soil zone plays an important role in the evolution of meteoric water. As well as the availability of H⁺ from dissolution of atmospheric CO₂, increasing the dissolution of clay and other minerals in the soil zone, CO₂ and organic acids also decrease the pH and increase the availability of protons in soil water. As organic compounds in the soil are used up in respiration through biological weathering additional CO₂ and other acids are added into the soil water. Biological reactions such as respiration can increase the acidity of the soil water which can then migrate into the groundwater affecting the rate of chemical weathering in the aquifer more than if there was no soil zone present. While the soil zone has the potential to increase the acidity of infiltrating meteoric water into the unsaturated zone, H⁺ gets neutralized by CaCO₃ and precipitated by hydroxide minerals in the soil. As a result of these reactions the water infiltrating into the unsaturated zone can either be of low pH from carbonic acid and other

organic acids, or becomes enriched in Al, Fe, Mg, and Ca from precipitated minerals in the soil. Soil acidity is greatly influenced by the humidity of the soil. Humid regions with high rainfall tend to lower pH (5-7) whereas arid conditions range to higher pH (7-9) (Tan, 2011).

Nutrients and other contaminants can be introduced in the soil zone and passed into the unsaturated zone. In natural systems phosphorous, sulfur and nitrogen are added into the water system. Nutrients are made available by the breakdown of organic matter (OM) in the soil by bacteria, fungi and plants. In soils with high OM concentration there is a greater input of phosphate, sulfate, nitrite and nitrate into the saturated zone. Conversely soils with low OM content will have a lower nutrient input into the groundwater system. Groundwater systems overlain by cultivated arable land where chemical and natural fertilizers are readily used will have a much higher input of nutrients migrating into the saturated zone.

Other anthropogenic contaminants which input into the soil and saturated zone often include atmospheric pollutants. These include; other acids in rain (H_2SO_4 , HNO_3), oxide gasses (SO_3 , NO_2), radioactive compounds (^{134}Cs , ^{14}C , etc.), compounds released during combustion (Poly Aromatic Hydrocarbons). These additional contaminants have the potential to move from the atmosphere through the soil zone and into the unsaturated zone. This can result in different groundwater composition in the unsaturated zone based on the type of soil meteoric water infiltrated through. Possible results include more acidic initial groundwater composition leading to greater rates of dissolution and a more concentrated groundwater from mineral dissolution in the saturated zone

2.4 What causes dynamic fluctuations in groundwater

Groundwater conditions often do not remain stable over time. This section identifies the key factors which have the potential to influence groundwater chemistry within the course of this thesis. Temporal variation in groundwater flow and chemistry can occur from changes in recharge, caused by seasonal variation. Earthquakes and load changes can alter fluid flow and groundwater level. Groundwater chemical changes have large implications for subsurface infrastructure such as geological disposal facilities and freshwater aquifers. Changes in chemistry can mobilize previously stable contaminants such as toxic metals, which could move them toward the surface environment by fluid flow processes.

2.4.1 Seasonal variability (metrological recharge and mixing)

Seasonal climatic variation causes predictable changes to surface hydrology and chemistry but can also result in changes to groundwater flow and chemistry. Climate seasonality consists of variability in temperature and rainfall. Increases in rainfall have been well documented to change groundwater level (Shamsudduha et al., 2009). Monsoon driven groundwater level

changes cause large effects on groundwater level and they also affect groundwater chemistry. Groundwater chemistry changes vastly from pre to post-monsoon causing groundwater to become unsuitable as a drinking water source (Subba, 2006). Post-monsoon changes often increase the dissolved solids and anthropogenic contaminants (Giridharan et al., 2008) into the groundwater system as a result of meteoric groundwater recharge of different chemistry. Increases in recharge as a result of seasonal climate variation also has impacts on the flow network and can cause shifts in flow direction (Winter, 1999). In some cases the flow direction at the surface-groundwater interface (i.e. lake systems) can change (Anderson and Munter, 1981) due to changes in groundwater recharge. Groundwater level changes can induce earthquakes (Saar and Manga, 2003) in critically stressed fault zones. Fluctuations in recharge driven by seasonal climate have large impacts on the freshwater saline water mixing boundary in coastal environments. Higher meteoric recharge rates control the shift in the salinity boundary in inland coastal groundwater systems (Michael et al., 2005; Heiss and Michael, 2014). Most effects on groundwater level, flow and chemistry are a result of seasonal changes in recharge, however, temperature changes also greatly affect groundwater systems. Post winter periods exhibit warming leading to the melting of snow and ice this changes the chemistry of the soil zone changing the cation concentration (Vitt et al., 1995). Grasby and Lepitzki, (2002) showed that melting snow and ice changes the temperature and dissolved ion concentration of thermal groundwater systems, lowering thermal spring temperature and dissolved ion concentration. Seasonal variation can have a large impact on groundwater level, flow and chemistry through changing recharge and temperatures on yearly time scales.

2.4.2 *Earthquakes groundwater flow and chemistry*

It has been well documented that earthquakes have impact on hydrogeological systems. Inducing transient (Barton et al., 1995) and permanent (Manga and Wang, 2015) permeability changes around fault zones, sustained (Brodsky, 2003) and complex (Shi et al., 2015) groundwater level change, isotopic (Onda et al., 2018) and chemical groundwater anomalies (Skelton et al., 2014), and the expulsions of gasses at the surface such as CO₂ (Sulem and Famin, 2009), H₂ (Sato et al., 1986), ²²²Rn and ³He/⁴He (King et al., 2006).

Changes to hydrogeology occur at different stages in the seismic cycle, often chemical and permeability changes occur prior to slip along critically stressed faults (Ingebritsen and Manga, 2014). It has also been documented that groundwater anomalies can occur around fault zones where no earthquakes occur (Shi et al., 2018). Most documented effects of earthquakes and their precursors have been with respect to hydrogeology and hydrochemical changes, some studies also note the influence of earthquake precursors and tectonic stresses on animal behaviour (Grant et al., 2011; Shi et al., 2018).

Permeability and Flow: Earthquakes have been shown to cause changes in the permeability of fault zones. Experiments show permeability changes are variable over the seismic cycle

(Uehara and Shimamoto, 2004), and field evidence supports this. Field studies have demonstrated how critically stressed faults and fractures also have higher permeability (Barton et al., 1995) than sub optimally oriented fractures and faults. Fluids can exploit changes in permeability, Fischer et al., (2017) found permeability increase and CO₂ release following a M_w 3.5 earthquake. Sustained changes in fault zone permeability can be caused by stress fluctuations prior to earthquake rupture (Min et al., 2004; Baghbanan and Jing, 2008). Earthquakes can cause changes in permeability and flow along fault zones, however they are also documented to affect regional (Manga and Wang, 2015) permeability by seismic wave propagation (Elkhoury et al., 2006).

A much wider impact of earthquakes on hydrogeology is their ability to sustain groundwater level change. Elevation of the water table and associated head change not only changes the phreatic surface but also the sub surface flow regimes resulting in changes to flow direction and redistributing flow within a fracture network. Groundwater level raise has mostly been documented after large magnitude earthquakes (M_w >6 (Wang et al., 2004; Gulley et al., 2013)), a M_w 7.1 earthquake in the Dead Sea Rift Valley resulted in a 6 – 50 cm head change (Yecheili and Bein, 2002). Groundwater level change has been documented proximally and distally from earthquake hypocentres (Parvin et al., 2014) and seen to affect continental scale groundwater head height (Shi et al., 2015), with no clear precursor signals (Itaba et al., 2008). One of the key mechanisms thought to drive sustained groundwater level change is the passing seismic waves (Yan et al., 2016).

Chemical changes: Earthquakes can have a large influence on groundwater chemistry, changing water chemistry or inducing gas migration. Most changes in groundwater chemistry are a result of “tapping” or mixing of different groundwater sources, occurring after (Claesson et al., 2004), and before (M_w > 5) seismic events (Skelton et al., 2014). Mixing of shallow waters with deeper, typically more saline groundwater sources typically increases the concentration of dissolved ions in the shallow groundwater relative to the original shallow groundwater composition. The M_w 7.2 Hyogo-Ken Nanbu earthquake (Japan) caused groundwater mixing between two aquifers and resulted in Cl⁻ increasing from a stable background level, accompanied by similar responses in Mg²⁺, Ca²⁺, Sr²⁺, and Ba²⁺ (Tsunogai and Wakita, 1996). Similar mixing responses of increased ion concentration have been observed in response to 1995 Kobe earthquake (Tokunaga, 1999) and M_w 5.1, Koyna, India where pH drops were also observed (Reddy et al., 2011). While dissolved ion chemical responses have often been observed post-seismic event, changes to oxygen isotope signatures have been observed as pre-cursor anomalies to large magnitude earthquakes. Skelton et al., (2014), Claesson et al., (2004) and Onda et al., (2018) all identify δ¹⁸O isotope anomalies related to large earthquakes (M_w > 5). In most cases the mechanism of temporal chemistry change is mixing, Yecheili and Bein, (2002) did not attribute the chemical change in

response to mixing while Claesson et al., (2004) attribute two mechanisms to the chemical change, pulsing from fault sealing, and from the “tapping” of other groundwater sources.

Chemical changes caused by source mixing only affect chemistry at depth unless fluid pressures drive new water chemistries to the surface. Gas production in response to earthquakes often releases gasses such as CO₂ which migrate to the surface (buoyancy driven) and can cause soil acidification affecting the surface environment. Thermal decomposition of carbonate rich rock requires high temperatures caused by frictional heating along fault zone (Sulem and Famin, 2009) releasing CO₂. CO₂ release along the San Andreas Fault zone has been well documented (King et al., 2006). The San Andreas Fault zone provided a conduit for biogenic gas migration to the surface (Lewicki and Brantley, 2000). Degassing of CO₂ has been attributed to M_w 3.5 earthquake where slip also changes fluid flow rate (Fischer et al., 2017). Other gas anomalies occur including (²²²Rn) radon gas production at the surface. King et al., (1996) associated radon changes with active faulting along different fault sections in California. Increases in hydrogen gas production over active fault systems has been linked to seismic activity and seasonal changes (Sato et al., 1986), the wet grinding in the fault reacts with water and has been shown to produce H₂ gases (Kameda et al., 2003) which migrate to the surface. Earthquakes have also been linked with an increase in ³He/⁴He, the increase in helium ratio suggests a release and flow of mantle (Du *et al.*, 2006) originating fluids.

Influences of earthquakes on groundwater flow can be separated in terms of the changes to the hydrogeology and flow regime or by groundwater geochemical changes. However, all recorded cases of earthquakes causing changes to groundwater flow and chemistry are a result of large magnitude earthquakes. Few cases of small magnitude seismic or microseismic events have been documented to cause even local changes to groundwater level or chemistry.

2.4.3 *Glaciers, permafrost and climate change*

Glacial cycling in response to changes in climate can exert large ($\Delta\sigma > 2000$ MPa) stress changes on the crust. Ice sheets have wide coverage and accompanied permafrost currently covers ~23.9% (Zhang et al., 2008) of exposed Northern Hemisphere land surface. Glacial cycling can result in vertical and flexural lithospheric stress changes (Lemieux *et al.*, 2008). Deglaciation and glacial advance result in hydromechanical changes including; isostasy, permafrost, ice sheet loading, groundwater flow/chemistry, and pore fluid pressure. Deglaciation removes vertical and flexural loads from the lithosphere. Lithospheric rebound occurs, pore fluid pressures change (Neuzil, 2012) in response to the changes in stress. Glacial ice and surrounding permafrost melt and infiltrates into the periglacial groundwater system, changing groundwater flow, causing groundwater to exfiltrate from the subglacial region. Exfiltration occurs during deglaciation when the high-pressure head of ice sheet is

removed (Lemieux *et al.*, 2008) lowering the pressure head and groundwater is expelled from the subglacial zone. Infiltrating meteoric glacial melt water is dilute in composition. Glacial melt water mixes and dilutes groundwater chemistry.

Thermo-hydrological-mechanical (THM) coupling of glacial cycles has been widely studied by numerical modelling. Extensive THM modelling has been carried out in the DECOVALEX (Chan *et al.*, 2005) project to determine the impact of glacial cycling on geological disposal facilities. There is little direct evidence as to the effects of past glaciation on groundwater flow. The impacts of past glaciation on groundwater are largely found as preserved pressure anomalies in aquifers. Neuzil and Provost, (2014) detect pressure anomalies related to changes in flexural loading in response to the Eastern Michigan Basin glaciation (Ontario, Canada). Pressure anomalies are evidence that groundwater pressure changed during the Pleistocene glaciation (Khader and Novakowski, 2014), forming the conceptual basis of hydro-mechanical numerical models. Stable isotopes and solute chemistry do confirm that glacial water had infiltrated up to 1km (McIntosh *et al.*, 2012) during the Pleistocene glaciation in the Michigan basin. Hydraulic jacking of fractures under glaciers provides more infiltration pathways. Water pressure in the upper 1km is driven by the water pressure at the water ice interface driving flow into the ground at the base of the glacier (Lönqvist and Hökmark, 2013). High pressures water pressures during periods of ice coverage increasing permeability by hydraulically open fractures. Numerical modelling of past glacial cycles is widely used to study the impact of glaciation on groundwater flow. Models show that changes in groundwater flow and recharge vary sub-glacially and periglacially (Person *et al.*, 2012) over the glacial cycle. Numerical models highlight the importance of understanding how permafrost, glacial load and pore pressure change (Vidstrand *et al.*, 2008) during deglaciation and the affect this has on the groundwater flow regime. Sedimentary units undergo permeability changes during glaciation altering fluid pathways sub-glacially (Boulton *et al.*, 1996), in response to the stress of deglaciation flow pathways can shift further.

Groundwater chemistry as well as flow fluctuates during the glacial cycle. Studies of the Laurentide ice sheet, Wisconsin glaciation and Pleistocene glaciation across North America show that brine formation, movement and infiltrating meltwater mixing have huge impacts during deglaciation. Brines concentrate during cold glacial periods under permafrost. Cryogenic brine formation occurs when water freezes (Starinsky and Katz, 2003), solutes are not stored in ice and concentrated in the remaining water. Cryogenic brines are produced during permafrost formation (McIntosh, Garven and Hanor, 2011) in the near surface and concentrate saline sea water under the coastal regions of ice sheets (McIntosh and Walter, 2005). Saline brines formed from permafrost are stored as halite minerals in the shallow subsurface. During static glacial periods brines are stable, however, during glacial advance they are forced deeper and glacial retreat leads to the upwelling of saline brines (Starinsky

and Katz, 2003). Deglaciation has the largest chemical impact on groundwater where saline brines are driven to shallower depths. Melt water infiltrates and dissolves halite minerals (deposited during permafrost formation in glacial periods). Infiltrating melt water triggers microbially mediated methanogenesis (McIntosh and Walter, 2005). Melt water and halite rich melt water infiltrates and mix with upwelling saline waters changing the chemical composition of shallow and deep groundwater. Other studies where glaciation events have been modelled and predict similar chemical evolutions (Auqué et al., 2007) to groundwaters.

2.4.4 *Reservoirs/Dam Draining and refilling*

Reservoir/dam construction and operation have been documented over the past 75 years to result in earthquakes and changes to groundwater. Several reviews (Simpson, 1986; Gupta, 1992, 2002) have explored Reservoir Triggered Seismicity (RTS) associated with the construction and operation of manmade reservoirs and dams. Over 90 sites have been investigated (Gupta, 2002) developing RTS. RTS has been investigated in several sites worldwide, the Koyna dam in Koyna-Warna region of central India has been the focus of many investigations since construction was completed. Koyna dam operation has directly triggered 200+ $M_w > 4$ and 22 $M_w > 5$ earthquakes (Yadav et al., 2016) since its construction was completed in 1964. An increase in surface pressure of 0.1 MPa (~100m water head) has been shown to be sufficient (Gupta, 2002) to trigger a seismic response at the Koyna dam (Pandey and Chadha, 2003). Reservoir refilling and draining in India have been shown to trigger earthquakes up to 35km away (Yadav et al., 2016). The seismic response to reservoirs worldwide is often accompanied by changes to groundwater level and pore pressure change. Simpson et al., (1988) highlighted two types of RTS: (1) Rapid response to reservoir level changes. (2) Delayed response, water level change is accompanied by a lagged response in seismicity and groundwater. Seismicity has been shown to be induced by the increase in poroelastic stress associated with filling of the reservoir (Simpson et al., 1988). An investigation at the Rihan dam, central India showed earthquakes are triggered during water high stand period (Gahalaut et al., 2007). Gahalaut et al., (2007) find that increase in water level at high stand raised the Coulomb stress, on nearby optimally oriented faults, sufficiently to trigger seismic events. Fault orientation with relation to the changing surface stresses, caused by reservoir draining and refilling, and the local and regional stress field determine which faults are likely to be seismically activated (Roeloffs, 1988) at reservoir low and high stand. Water level changes investigated around the Koyna reservoir (Gupta, 2002) and changes in hydraulic head, stream and groundwater flow (Francis et al., 2010) downstream of dams is also experienced in response to reservoir water level fluctuations.

3. Spatial Groundwater Chemistry

Geological controls on the spatial variability in groundwater chemistry at the Grimsel Test Site (GTS), Switzerland.

3.1 Introduction

Developing an understanding of how groundwater chemistry evolves and flows in fractured crystalline rock networks is of key interest to geothermal projects, nuclear waste disposal and even basement hydrocarbon plays. This research measures and analyses the groundwater chemical evolution around the Grimsel Test Site (GTS), Switzerland. Groundwater is hosted in two lithologies the Central Aar Granite (CAGr) and the Grimsel Granodiorite (GrGr). Flow through the rock mass is dominated in brittle reactivated ductile shear zones. Groundwater chemistry is analysed using multivariate statistical analysis using principal component analysis and hierarchical clustering. Statistical analysis identifies four distinct groundwater types. The main control on groundwater type is the major host rock lithology, minor differences in other groundwater groups are the result of pyrite oxidation and fluorite dissolution. Differences in surface infiltration result in slight differences in groundwater chemistry and isotopic composition. A comparison of isotopic values of ground and surface water show that infiltration does not necessarily occur directly above the GTS. Instead infiltration sources are more complex and isotopic values are likely the result of mixing of infiltrating sources. While the spatial chemical variability is small between the two key lithologies at the GTS, the data show that structural controls (fracture connectivity and lithology) on groundwater chemistry are important at this small scale. Over a larger scale, such as a reservoir or repository scale, understanding structural controls on groundwater chemistry could be important for safety case development, since they have a significant effect on migration pathways and dilution.

3.2 Introduction

The study area is located in the upper Hasli valley, Canton of Bern, Switzerland. The Grimsel Test Site (GTS) is an underground rock laboratory (URL) on the eastern flank of Juchlistock. The GTS sits ~ 37m below the top of Räterichsbodensee, a hydro-dammed reservoir, and is located within the mountainside 200 to 600m away from the reservoir's western edge (Figure 3.1). The Grimselsee hydro-dammed reservoir is situated nearby, south of the study area. The GTS, operated by NAGRA, is accessed via tunnel networks owned and managed by KWO (Kraftwerke Oberhasli hydroelectric power company).

The GTS is hosted in late post-Variscan calc-alkaline (Schaltegger, 1990) intrusions of the Central Aar Granite (CAGr U/Pb ages 298 ± 2 Ma) and Grimsel Granodiorite (GrGr 299 ± 2 Ma) (Schaltegger, 1993). CAGr is the dominant lithology in the north of the GTS and GrGr in the south. A gradual magmatic transition zone defined by; 'schlieren' structures between the two lithologies implies a coeval emplacement (Schneeberger *et al.*, 2016). Metabasic dykes cross-cut the granitic rocks (Oberhänsli, 1985; Keusen *et al.*, 1989), and are later cut by aplitic dykes (Wehrens, 2015). Esperanza and Holloway (1987) attribute an extensional tectonic regime to the emplacement of metabasic dykes.

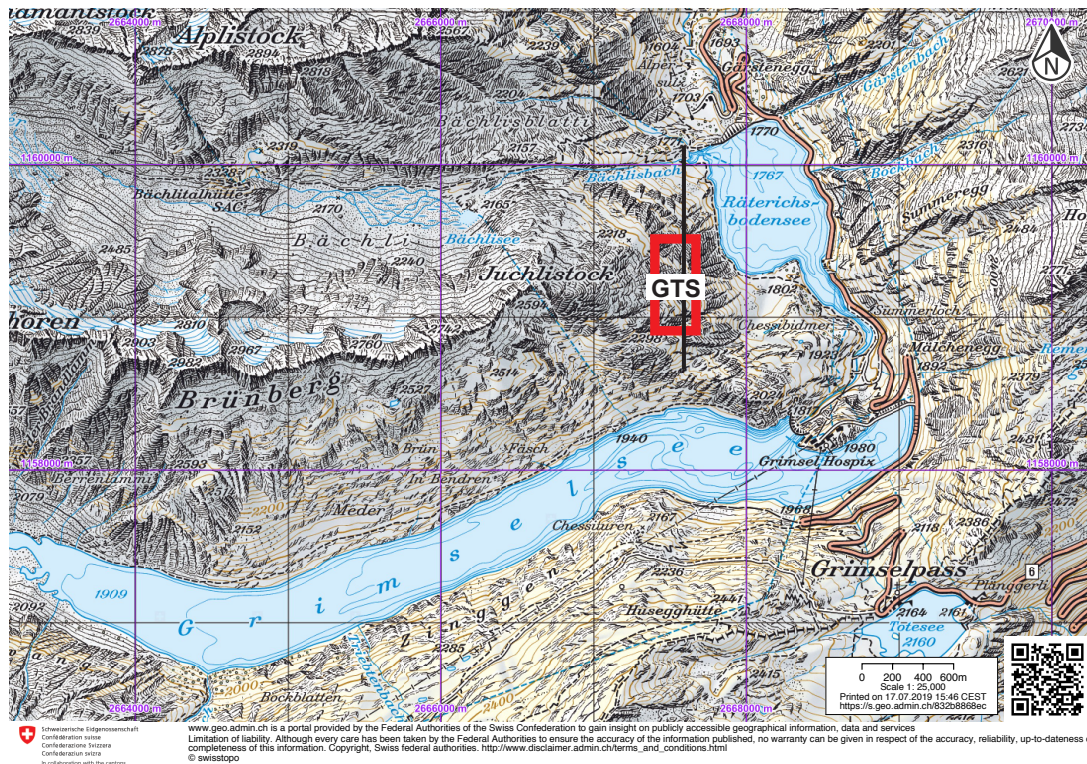


Figure 3.1 Map of the Grimsel Valley and the location of the GTS (red box). Top of Juchlistock to the west of the GTS.

The GTS area underwent Alpine deformation, peak metamorphism of greenschist facies (Challandes *et al.*, 2008; Goncalves *et al.*, 2012) at 20 Ma (Rolland, Cox and Corsini, 2009). Alpine deformation is accommodated by ductile and brittle features, with higher strain (Choukroune and Gapais, 1983; Wehrens, 2015) in the south shown by pervasive steep southerly dipping mineral foliation. Localized deformation is focused on south-dipping ductile shear zones (Schneeberger *et al.*, 2016), later overprinted by cataclastic brittle deformation. Brittle deformation is concentrated on lithological boundaries, where the damage zone is more pervasive in the footwall (Schneeberger *et al.*, 2019). Wehrens (2015) separated Alpine deformation into two phases of ductile deformation (1) Handeggphase and (2) Oberaarphases

based on kinematics of: (1) SE dipping shear zones with vertical movement, and (2) Strike-slip and oblique E-W, NW-SE and NNE-SSW structures.

Hydrologically, the Grimsel area has considerable seasonal variability. Average surface temperature are lowest in February (-5.4°C) and warmest in July (10.0°C) (MeteoSwiss, 2016a, 2016b). Precipitation in the region is lowest in summer, between June and October (~129 mm/month), and highest in November to February (~180 mm/month) (MeteoSwiss, 2016a, 2016b). Seasonal meteoric changes are likely to have the greatest impact on recharge. However, at Grimsel, temperature variation will have a larger impact on the groundwater system because in the colder months (November to April) maximum average daytime temperatures do not go above freezing. Continuous freeze thaw cycle develops discontinuous permafrost (Delaloye and Lambiel, 2005). This results in a drop in the recharge to the groundwater system below. Permafrost development acts to decrease the surface area available for water soil/rock interactions and at the same time lower temperatures slow the dissolution rates. The permeability in the critical zone (Brantley *et al.*, 2007) is reduced significantly and water recharge into the subsurface is retarded (Lemieux *et al.*, 2008). Chemical reactions at the surface are therefore delayed as is the recharge of surface water into the critical zone during winter periods. Conversely, in summer and during permafrost thawing, permeability in the critical zone increases, as does the dissolution rate of water rock interactions. It is therefore expected that the winter surface water should have a lower concentration of dissolved ions compared to summer water and that any recharge effects in the critical zone and groundwater system will be low, compared to other seasons. Seasonality in, temperature and precipitation will affect the surface water system (Sutcliffe *et al.*, 1982; Whitehead *et al.*, 2009) both at the present day and in future glaciations. Surface water plays a key role in the recharge of the groundwater system above the GTS. Recharge has the potential to affect the groundwater flow paths and the groundwater chemistry as more surface water mixes with the granitic groundwater, acting to dilute the equilibrated groundwater.

Hydrogeologically, the crystalline granitoid host rock has a very low matrix permeability, which means that brittle structures form the main conduits for fluid flow in the rock mass. The most recent increase in permeability occurred due to northern hemisphere deglaciation. Associated topographic exfoliation joints and brittle fracturing created a fracture system at the surface, potentially increasing the permeability through horizontal and vertically dipping fractures. Topographic stress fractures are generated when the lithosphere is in tectonic compression while a surface load such as a glacier is removed. Topographic stress fractures have been documented to penetrate up to 300m (Martel, 2006, 2011; Slim *et al.*, 2015) and are well studied in the Aar valley (Ziegler *et al.*, 2014; Ziegler *et al.*, 2016). Topographic stress fractures are visible in surface exposure and could provide hydraulic connectivity from the surface to the level of the GTS. Keusen *et al.* (1989) documented two types of inflow to the

GTS: (1) minimal climatic influence (low variations in flow rate), and (2) high flux variation at shallower depths with strong climatic influence in the near surface (high variations in flow rate). Conceptual groundwater models indicate meteoric recharge (Schneeberger, Mäder and Waber, 2017) from surface infiltration. There is little geochemical evidence to-date to suggest that the lake is hydraulically connected to the GTS groundwater system (Keppler, 1995; Schneeberger et al., 2017). Water infiltrates through exfoliation joints, topographic stress fractures and steep southerly dipping brittle reactivated ductile shear zones. The fracture network forms the main infiltration paths from the surface into the test site. Inflow and fluid flow in the GTS is predominantly hosted in fractures (Le Borgne *et al.*, 2006) of high porosity 10-30 vol% (Bossart *et al.*, 1991) rather than the low matrix porosity 0.8-1.53 vol% (Bossart *et al.*, 1991) host rock. The GTS and KWO tunnel systems form a fixed low pressure head and exert an anthropogenic influence on the surrounding flow regime. An unperturbed flow regime would have the Aare river and valley flow creating the lowest pressure head regionally (Voborny *et al.*, 1991; Voborny et al., 1995) rather than the underground tunnel network. Hoehn *et al.*, 1998 show an average hydraulic conductivity of 10-100 ms⁻¹ for test intervals. Hence, the key flow pathways (Bense *et al.*, 2013; Stober and Bucher, 2015) where water rock reactions occur, are along fracture systems or faults (Berkowitz, 2002). The structural geology in the Grimsel region therefore controls flow path formation and is likely to be the largest dominant factor governing the spatial variation of groundwater chemistry at the GTS.

3.3 Methods

3.3.1 Ground and surface water sampling locations

Groundwater sampling for this research covers the extent of the GTS using a pre-existing borehole system. Boreholes cut different lithologies, fracture sets and fault rock types. Boreholes were drilled between 1980 and 1998 and packers were installed to allow sampling of isolated individually packed borehole intervals. Twelve sampling intervals were chosen for this study (Figure 3.2), which cover a large area of the GTS as well as sampling different geological features.

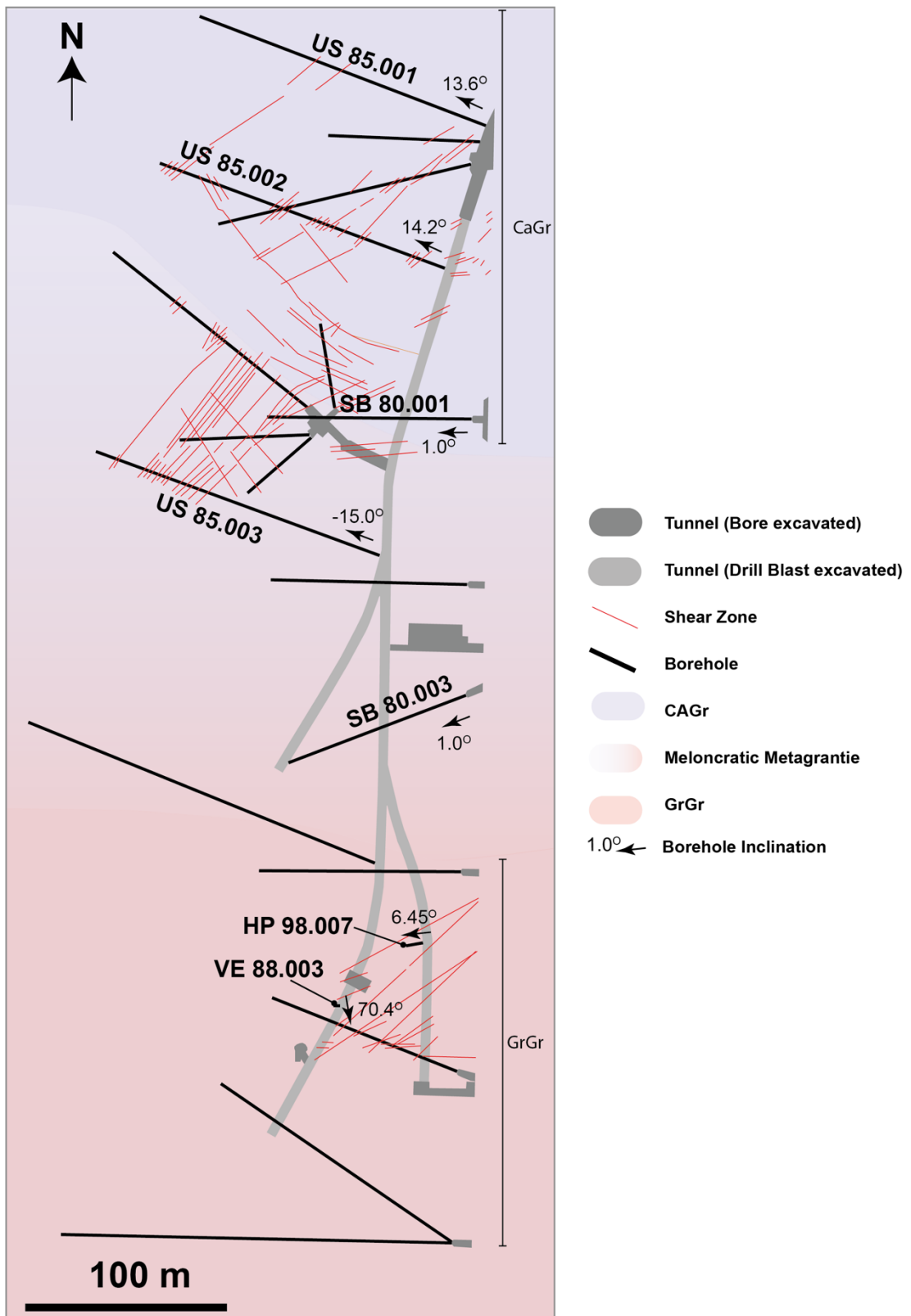


Figure 3.2 Borehole plan view schematic showing access tunnels in grey, boreholes (black), Shear Zones (red line) and host rock lithology.

Surface sample locations were chosen to take into account potential infiltration sources. The accessible samples were taken from Grimsensee (S2), Räterichsbodensee (S3), glacial melt water (S1), from higher up in the catchment, sampled from a stream above Grimsensee and surface runoff (S4) collected on the bank of Räterichsbodensee (Figure 3.3).

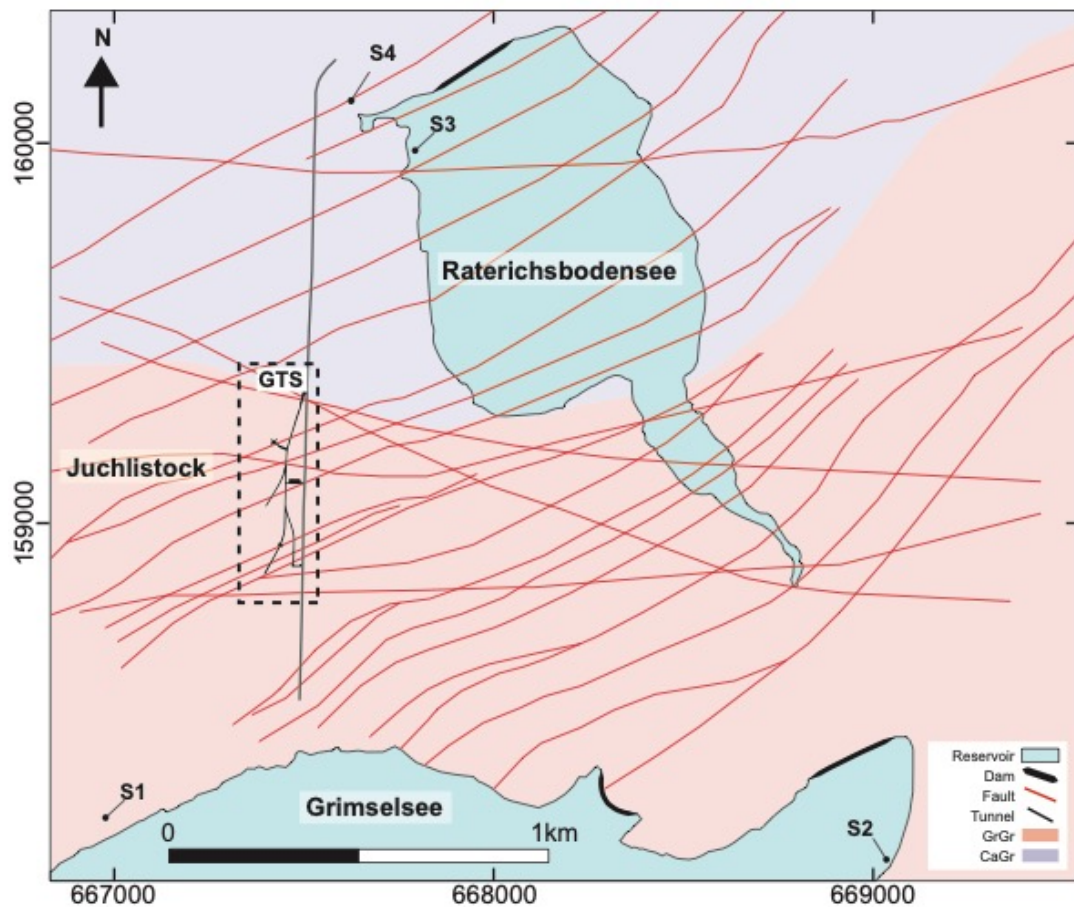


Figure 3.3 Map of the Grimsel valley. Surface water sample sites (S1) river flowing into Grimsensee, (S2) Grimsensee, (S3) Räterichsbodensee, (S4) surface runoff into Räterichsbodensee. Host rock lithology faults from liniment tracing at the surface (Schneeberger *et al.*, 2016).

3.3.2 Sample Collection and Preservation

Groundwater samples were collected over a three-month period (Feb-Mar) in 2016. Surface and groundwater samples were collected in Aug-2015 and again in Aug-2017. Groundwater sample locations consist of 6 boreholes and 12 intervals (Figure 3.2).

Eh, pH, EC, Temperature and Dissolved Oxygen were measured during sampling, using a daily calibrated YSI Pro Plus MultiMeter. Eh measured using ORP probe was calibrated with a one point calibration using Reagecon 250mV (± 5 mV) Redox Oxidation/Reduction (ORP) standard (measurement accuracy ± 20 mV). 3-point pH calibration was carried out using Reagecon buffer solutions pH 4.00 (± 0.01), pH 7 (± 0.01), pH 10 (± 0.01) (measurement

accuracy ± 0.2). Electrical conductivity one-point calibration using Reagecon 84 $\mu\text{S}/\text{cm}$ ($\pm 1\%$) (measurement accuracy $\pm 1\%$). Dissolved Oxygen probe calibration was carried out using a one-point calibration of 100% humidity air (measurement accuracy $\pm 1\%$). Surface waters were measured directly in the water body while groundwater was measured using a flow through cell. Water samples, Flow rate and physiochemistry data were collected every 30 seconds during and after the borehole interval was flushed. Flushing involved flowing through three times the interval volume prior to collecting a water sample to ensure formation water was being sampled and not residual water in the flow lines or borehole. Flow rate was measured using a measuring cylinder and stopwatch. Water samples were taken for analysis of dissolved ions, and alkalinity. Samples were collected in duplicate for Cation and Anion analysis, filtered through a 0.45 μm cellulose acetate filter, sealed in HDPE centrifuge tubes, and stored at 4°C. Cations were acidified to pH 2 using analytical grade HNO_3 prior to storage. Unfiltered samples were collected for alkalinity titration using a Hach digital field titrator the same day, titrations were completed within six hours of sample collection. Alkalinity titrations are time sensitive as CO_2 in-gassing and degassing causes a change in the carbonate/bicarbonate/carbon dioxide equilibrium, which could potentially lead to anomalous alkalinity results.

3.3.3 Lab Analysis

Major and minor ions (University of Strathclyde, Glasgow), stable isotope analysis (SUERC, East Kilbride) analysis were performed under laboratory conditions, on collected and preserved samples. Anion analysis (Br^- , Cl^- , F^- , NO_2^- , NO_3^- , PO_3^{3-} , SO_4^{2-}) was carried out using Ion Chromatography (Metrohm 850 Professional IC). Calibration was performed using a 7-point calibration, standards were prepared from stock 10000 mg/l solutions of certified reference material (CRM) TraceCERT[®] diluted by 18.2 M Ω -cm ultrapure water. Quantification limits for each analyte are as follows: $\text{Cl}^-/\text{F}^-/\text{SO}_4^{2-}$ – 0.01 mg/l, $\text{Br}^-/\text{NO}_2^-/\text{NO}_3^-/\text{PO}_3^{3-}$ – 0.1 mg/l. Cation (Al^{3+} , Ba^{2+} , Ca^{2+} , Fe_{tot} , K^+ , Li^+ , Mg^{2+} , Mn^{2+} , Na^+ , Sr^+ , $\text{Si}_{\text{dissolved}}$) analysis, and Inductively Coupled Plasma Optical Emission Spectra (ICP-OES) iCAP 6000 Series (ThermoFisher). Calibration was performed using 3-point calibration. Calibration standards were prepared from a stock solution 10000 mg/l solution in HNO_3 2-3% (CRM) Centipur[®] diluted by 18.2 M Ω -cm ultrapure water. The matrix matched to the acidified sample. Quantification limits for each analyte are as follows: $\text{Al}^{3+}/\text{Ba}^{2+}/\text{Fe}_{\text{tot}}/\text{Mg}^{2+}/\text{Mn}^{2+}/\text{Li}^+/\text{Sr}^+$ -- 0.001 mg/l, K^+ -- 0.097 mg/l, Na^+ -- 0.052 mg/l, $\text{Si}_{\text{dissolved}}$ – 0.003 mg/l, Ca^{2+} -- 0.52 mg/l. $\delta^{18}\text{O}$ and $\delta^2\text{H}$ were analysed on ThermoFischer Delta V, Isotope Ratio Mass Spectrometer (IRMS) with gas-bench and Optima Duel inlet IRMS with Cr furnace respectively. Oxygen and Hydrogen measurements were calibrated relative to three (low/medium/high) water standards.

3.3.4 *Geochemical modelling PHREEQC*

Speciation, inverse mass balance and kinetic modelling have been carried out using PHREEQC thermodynamic software (Parkhurst and Appelo, 2013). Speciation modelling was carried out on all groundwater samples to determine if minerals present in the lithologies at the GTS; over saturated and may precipitate from solution, under saturated and can still dissolve or at saturation and in equilibrium with the groundwater. To determine the mass of minerals dissolved or precipitated along flow pathways inverse mass balance models were carried out. Inverse modelling calculates the moles of minerals and gasses transferred into and out of solution along different flow paths, by mass balance calculation. The mass balance calculation takes the known starting composition and final groundwater composition, it then carries out a series of simultaneous equations to calculate the moles of each mineral precipitated or dissolved to reach the final water composition from a starting composition. Modelling takes into account the user-specified minerals present within the host lithology and is used to determine potential chemical reactions occurring along flow paths. Positive values of mole transfer reflect mineral dissolution; negative values indicate precipitation. Kinetic modelling in PHREEQC is used to determine if chemical evolution is feasible through water rock interaction along fracture dominated flow paths. Kinetic modelling is carried out, checking the feasibility of dissolution and precipitation reactions, indicated by inverse and speciation modelling. Kinetic modelling demonstrates that the water chemistry evolution by fluid rock interaction is feasible the time scale of indicated by tritium ages (>65 years) of groundwater previously recorded (Schneeberger et al., 2017).

3.4 Results and Discussion

3.4.1 Physiochemical Properties

Surface water collected from the reservoirs (S2, S4), glacial meltwater (S1) and surface run off (S3) were used to assess the chemistry of infiltrating meteoric water into the groundwater system. Conductivity values for surface water range from 14 – 35 μScm^{-1} with a neutral pH. Groundwater of Na–Ca–HCO₃–SO₄ type, and dilute (EC 10 – 250 μScm^{-1}), reflecting the low reactivity of weathered granitic rock at the surface and the low reactivity of any particulates in reservoir waters over short time periods.

Table 3-1 Average groundwater values (n= 27) and measured surface water values for temperature, conductivity and pH are presented in the table along with the host rock lithology.

Location/ Borehole	Interval	Host Rock Lithology	Geological Feature*	Temp	Ec (μScm^{-1})	pH	Eh (SHE)
US85.001	i2	CaGr		11.5	84.51	7.51	215.87
US 85.002	i6	CaGr	DS	11.9	84.09	8.98	195.69
US 85.002	i5	CaGr	DS	11.9	77.06	8.96	180.18
US 85.002	i4	CaGr	MBD	12.2	83.76	9.04	172.27
US 85.002	i3	CaGr	MBD	12.1	79.39	8.83	177.86
US 85.002	i2	CaGr	DS	12.7	76.96	9.12	182.50
SB80.001		CaGr	DS	11.7	68.54	8.97	241.04
US85.003		CaGr	MBD/DS	13.4	84.35	9.32	227.98
SB80.003	i4	Ca/GrGr	MBD/DS	12.6	80.40	9.23	199.27
HP98.007	i3	GrGr		12.6	85.36	9.49	308.24
HP98.007	i2	GrGr		12.6	76.69	9.40	188.46
VE88.003	i3	GrGr		13.1	81.64	9.18	175.15
VE88.003	i2	GrGr	DS	12.7	75.97	9.39	182.40
S1	River			11.2	16.70	6.67	117.40
S2	Lake			7.0	35.00	7.00	93.70
S3	River			8.1	14.70	6.85	55.60
S4	Lake			10.4	30.30	7.13	58.70

*CaGr = Aar Granite, GrGr= Grimsel Granodiorite, DS = Ductile Shear zone, MBD = Meta Basic Dyke.

Surface water chemical data (Table 3-2) gives the dissolved ion chemistry sampled from each location (S1-S4). Lake water samples are marginally higher in Ca²⁺, K⁺, Mg²⁺, Sr⁺, SO₄²⁻, and Alkalinity compared to the river water samples.

Table 3-2 Major and Minor dissolved ion chemistry for surface water sample, locations given in Figure 3.3. Concentrations are given in mg/l.

Location	Al ³⁺	Ca ²⁺	Fe ²⁺	K ⁺	Mg ²⁺	Mn ⁺	Na ⁺	Si	Sr ⁺	F ⁻	Cl ⁻	Br ⁻	NO ₂ ⁻	NO ₃ ⁻	PO ₄ ³⁻	SO ₄ ²⁻	Alkalinity
S1	0.064	0.812	0.103	0.537	0.116	0.008	0.946	0.802	0.002	0.19	0.98	BDL	BDL	0.70	BDL	1.79	2.2
S2	0.033	2.785	0.052	0.829	0.329	0.008	1.430	0.622	0.008	0.05	0.59	BDL	BDL	0.77	BDL	5.24	6.2
S3	0.030	2.485	0.060	0.857	0.261	0.006	0.905	0.621	0.007	0.05	0.43	BDL	BDL	0.78	BDL	4.14	5.2
S4	0.042	0.711	0.050	0.273	0.084	0.002	0.056	0.771	0.003	0.04	0.04	BDL	BDL	0.57	BDL	0.65	1.6

*BDL = Below Detection Limit.

Groundwater temperature is between 11.4°C and 17.3°C. Figure 3.4 shows the spatial distribution of average temperatures in each borehole interval. Borehole intervals are at an elevation of ~1730m above sea level and the surface elevation above the boreholes varies from 2000 to 2200m from north to south. Depth below surface therefore increases from 270 to in the north 470m in the south. Average geothermal gradients in the area correspond to ~25°C/km of depth (Toth and Bobok, 2017; Waber *et al.*, 2017). With this geothermal gradient, we would expect borehole temperatures to rise from the annual average surface temperature (5°C) by 6.75°C in the north and 11.75°C in the south. Temperatures are not out of the range for a standard lithospheric geothermal gradient implying that the temperature variation could be a function of the increased overburden in the south compared to the north.

Conductivity varies between 64.23 – 81.18µS/cm⁻¹ and is higher than surface water conductivity (14 – 35 µScm⁻¹). When compared to general freshwater aquifer systems (0-1000 ppm TDS (Hiscock and Bense 2015) both the surface (14-35 ppm) and ground (41-52 ppm) waters in the GTS are extremely dilute. Spatial variation of conductivity is likely controlled by dissolution reactions of minerals along flow paths; however, there is no correlation between factors such as flow rate and host rock type which could account for the variation in conductivity. In fact, in the same borehole (US 85.002) in the north of the GTS we see adjacent intervals with large variation in EC, this may imply that fracture type, orientation, or other structures like meta-basic dykes could be controlling the spatial variation in EC.

Values of pH range from 5.86 to 9.82 and relate to the change in host rock lithology. The spatial distribution of pH, (Figure 3.4) shows that lower pH values are typically < 9.0 associated with CAGr in the north of the GTS, while values >9.0 usually occur in GrGr. This relationship indicates a lithological control on pH in the GTS. Temperature does not seem to affect the pH as slightly higher temperatures in the south of the GTS correspond to a higher pH. If temperature did affect the spatial distribution of pH the converse would be expected.

Borehole flow rate is generally below 3.5m³day⁻¹ with three exceptions (Figure 3.4); 'US 85.001', 'US. 85.003' and 'SB80.001' have significantly higher flow rates of up to 13m³day⁻¹ compared with the other boreholes.

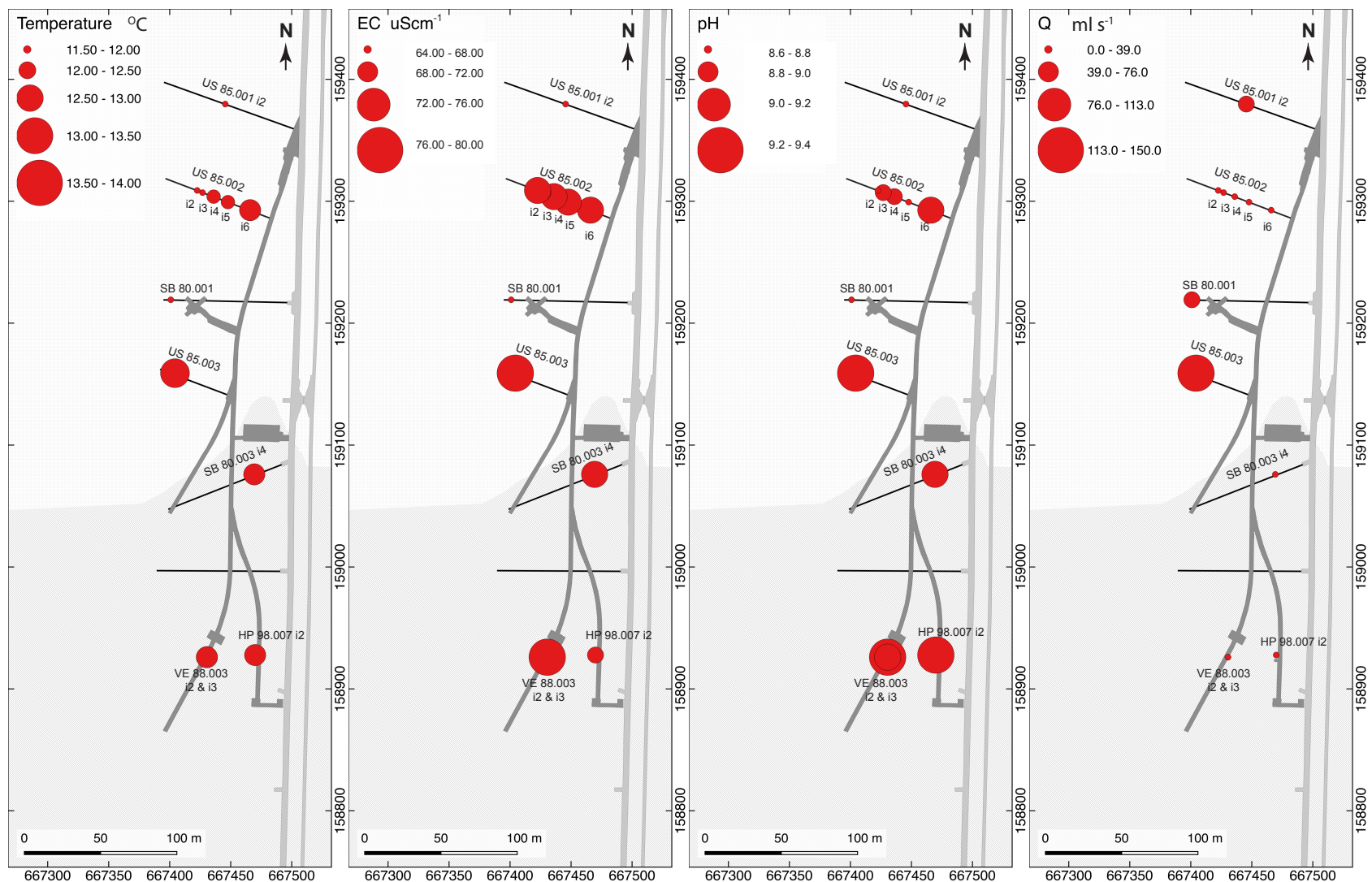


Figure 3.4 Tunnel schematic showing the spatial distribution in size categorised red bubbles (left to right) of temperature, electrical conductivity (EC), pH and borehole flow rate (Q). CAGr (white) GrGr (light grey), boreholes (black lines), tunnels (Dark grey).

3.1.1. Major Element + Spatial Changes

Physiochemical data shows a difference in pH and EC between ground and surface water: groundwater, being generally more alkaline and more concentrated than surface water. We observe a difference in major dissolved ions making groundwater distinctly different from surface waters as well as showing separate groundwater groups (Figure 3.5). Groundwater is clustered based on major dissolved ions and seems to correlate with boreholes hosted in each of the two major rock types (GrGr and CAGr). The piper diagram (Figure 3.5) shows that the relative concentration of Ca^{2+} , Mg^{2+} , SO_4^{2-} and Cl^- to Na^+ , K^+ , alkalinity is relatively lower in surface waters than in the groundwaters. We also see progressively higher concentrations of Na^+ , K^+ and alkalinity to other major ions in the granodiorite (GrGr) comparatively to the granite (CAGr). This change in composition could be a result of different water-rock reactions occurring in the granodiorite compared with the granite (the mineralogy of lithological features in the GTS is given in table 3.2) or a feature of the increased overburden in the south of the GTS leading to potentially longer flow paths and residence time where GrGr is the dominant lithology. Alternatively, the difference we see in major ion groundwater composition could be a combination of these factors, host rock lithology and longer residence times in the south.

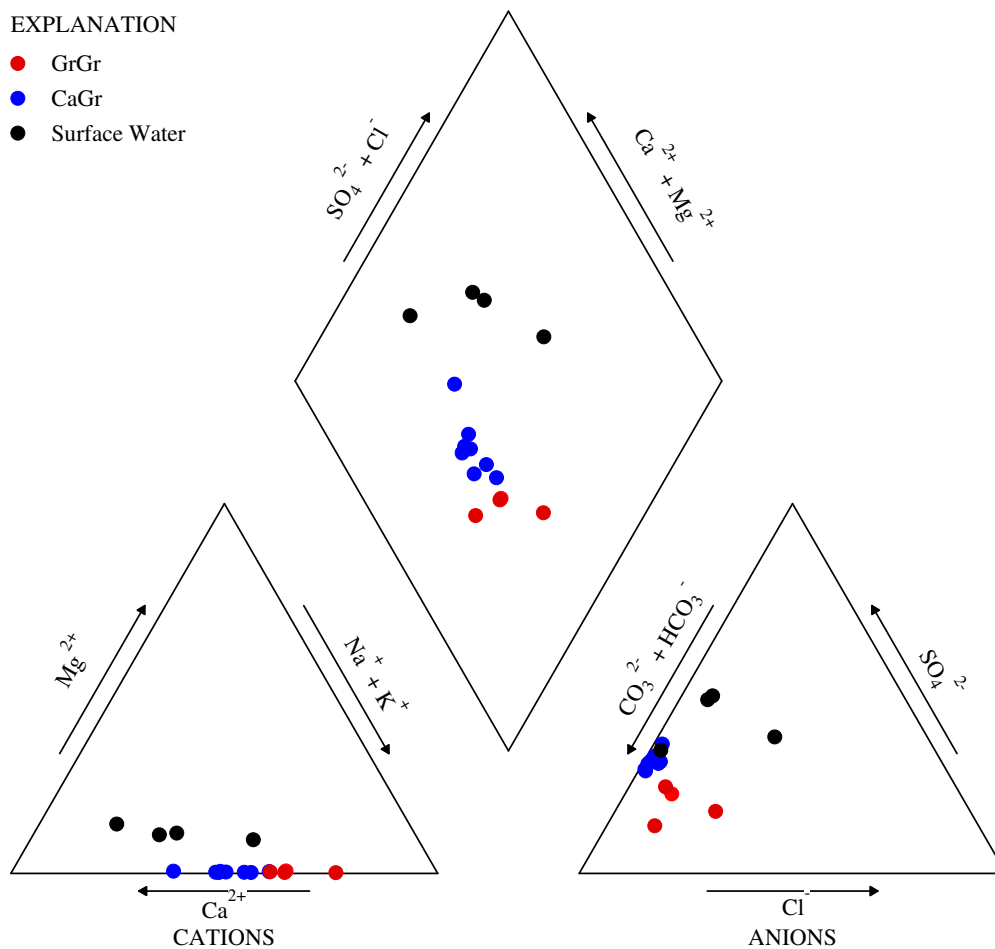


Figure 3.5 Piper diagram of groundwaters hosted in GrGr (red), CAGr (blue) and surface water (black).

The spatial distribution of major ions seems to reflect a difference between the north and south of the GTS. Figure 3.6 and 3.7 show the average major and minor dissolved ions across the sampled intervals. There is a higher concentration of Ca²⁺, SO₄²⁻, Mg²⁺ in the North whereas Na⁺, K⁺, Li⁺, F⁻, and Cl⁻ are in higher concentration in the south. Total alkalinity remains constant across the GTS. However, carbonate alkalinity is higher in the south and bicarbonate alkalinity is lower, with the reverse being true in the north of the GTS. Analysis of the spatial distribution of dissolved ions shows indicates presence of two main groups, which is also reflected in the pH data. Both show the same clear trends that separate the northern and southern groundwater endmembers.

Table 3-3 Composition of rock types in the GTS outlining the key mineralogy CAGr: Central Aar Granite, GrGr: Grimsel Granodiorite, MBD: Metabasic dyke. Taken from Schneeberger *et al.*, 2019 compiled from: Keusen *et al.*, 1989; Mäder *et al.*, 2006; Wehrens, 2015

Property/ Mineral	CAGr	GrGr			MBD*
	Unfractured rock matrix	Unfractured rock matrix	Mylonite	Fault gouge	Unfractured rock matrix
Quartz	32.6 [wt-%]	31 [wt-%]	27 [wt-%]	22 [wt-%]	
K-feldspar	33.6 [wt-%]	28 [wt-%]	17 [wt-%]	18 [wt-%]	0-6.8 [wt-%]
Plagioclase	21.5 [wt-%]	25 [wt-%]	18 [wt-%]	17 [wt-%]	12.4-17.7 [wt-%]
Biotite	6.5 [wt-%]	8 [wt-%]	10 [wt-%]	12 [wt-%]	57.2-71.6 [wt-%]
Chlorite**	1 [wt-%]	0.1 [wt-%]	0 [wt-%]	0 [wt-%]	
Muscovite	1 [wt-%]	6 [wt-%]	24 [wt-%]	27 [wt-%]	
Epidote	3.0 [wt-%]	0.4 [wt-%]	0.3 [wt-%]	0.3 [wt-%]	16-18.3 [wt-%]
Titanite	0.2 [wt-%]	1 [wt-%]	0.3 [wt-%]	0.3 [wt-%]	
accessories	< 1 [wt-%]	0.2 [wt-%]	3 [wt-%]	3 [wt-%]	
Clay Minerals		0 [wt-%]	0.4 [wt-%]	0.4 [wt-%]	

*MBS = Meta basic Dike, ** Chlorite formed in conjunction with white mica during Alpine metamorphism.

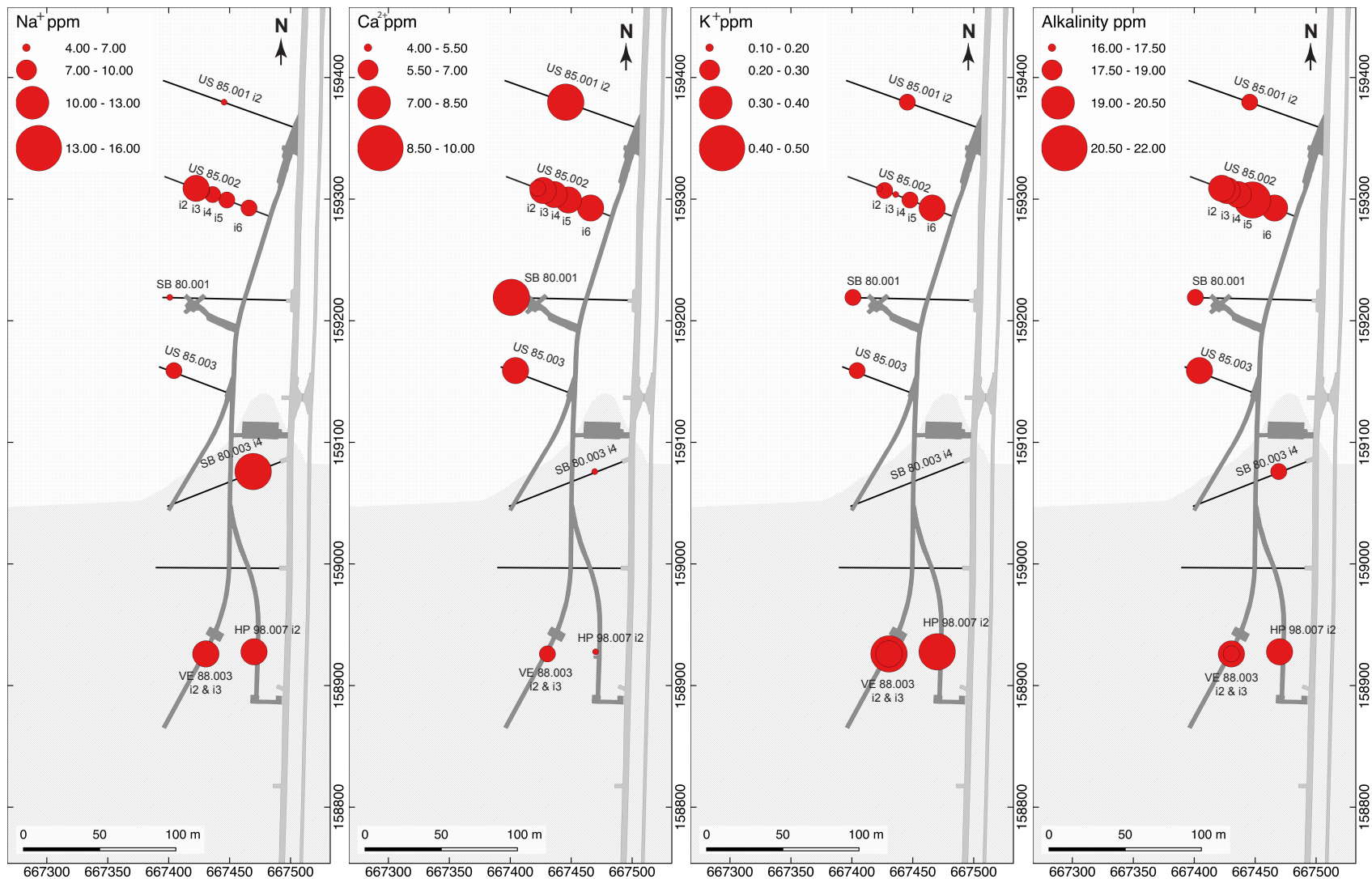


Figure 3.6 Tunnel schematic showing the spatial distribution in size categorised red bubbles (left to right) of Na⁺, Ca²⁺, K⁺, Alkalinity (ppm). CAGr (white background) GrGr (light grey), boreholes (black lines), tunnels (Dark grey).

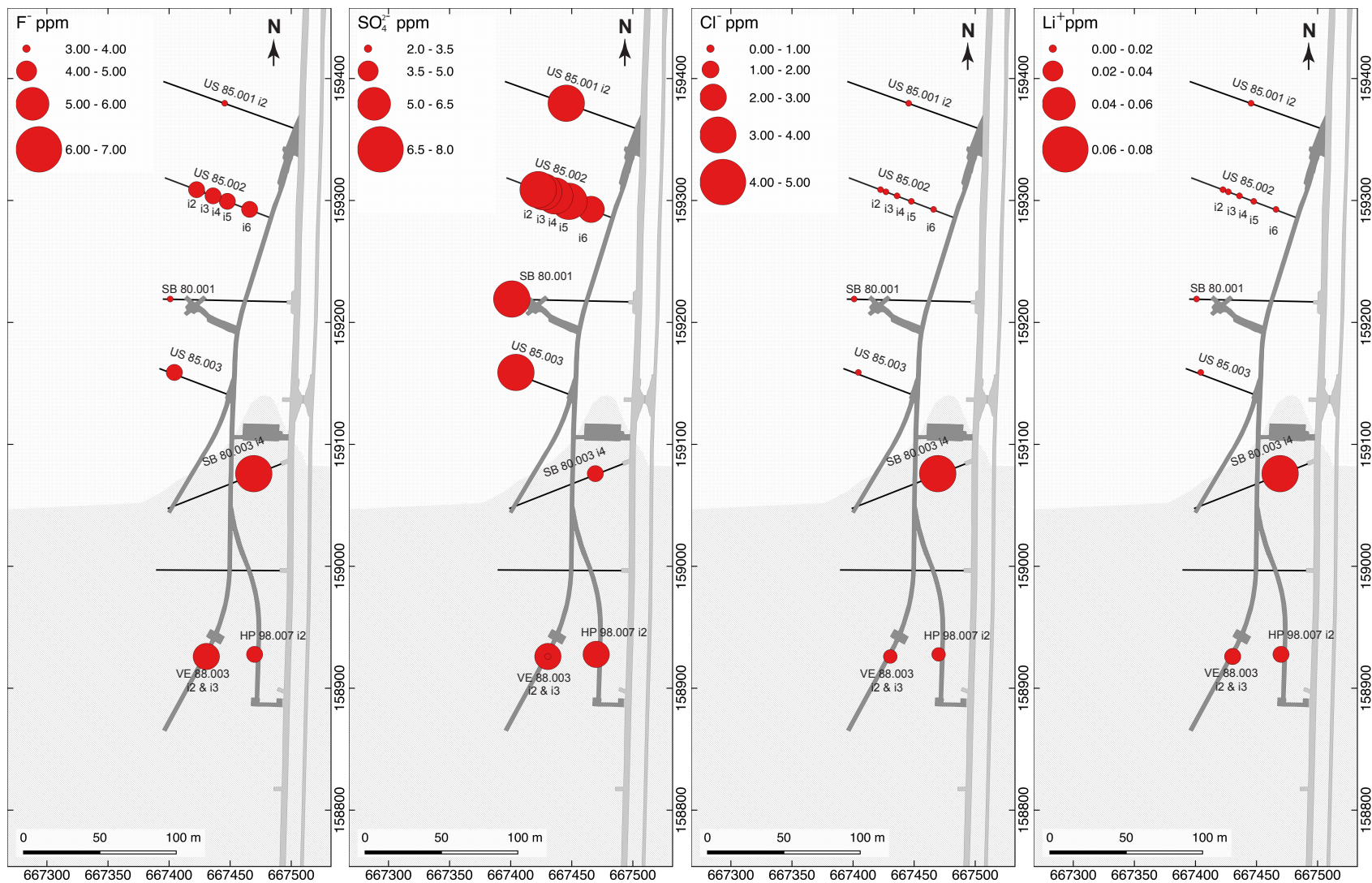


Figure 3.7 Tunnel schematic showing the spatial distribution in size categorised red bubbles (left to right) of F⁻, SO₄²⁻, Cl⁻, Li⁺ (ppm). CAGr (white background) GrGr (light grey), boreholes (black lines), tunnels (Dark grey).

Stable isotope analysis carried out on ground and surface water samples is compared with the Swiss metrological database, Figure 3.8. Our analysis is consistent with previous groundwater studies (Schneeberger et al., 2017). Groundwater lies along the Local decadal Meteoric Water Line (LMWL) of surface precipitation (IAEA/WMO, 2020) as do the surface water samples collected. LMWL sits parallel to the Global Meteoric Water Line (GMWL). Small differences between the two meteoric water lines exist but can be accounted for by orographic effects, namely the change in altitude and wind direction. Figure 3.8 shows how groundwater collected during lake draining in 2014 lie in the same cluster as the summer groundwater samples Aug 2015, showing groundwater isotope are seasonally stable.

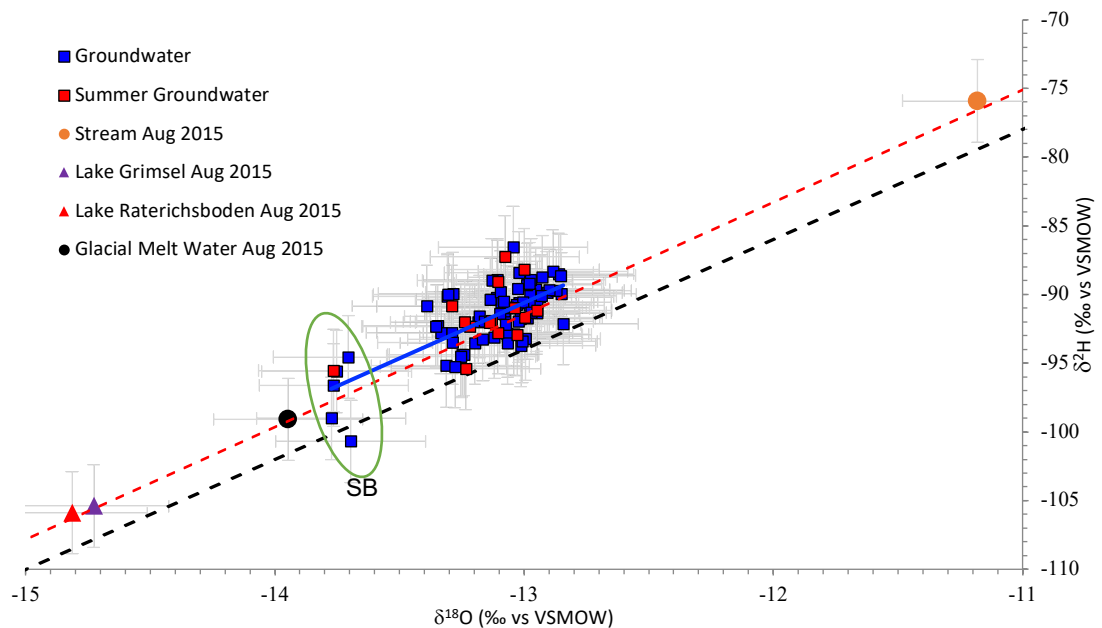


Figure 3.8 Groundwater stable isotope data (2014-15) $\delta^{18}\text{O}$ vs $\delta^2\text{H}$ in comparison with local decadal meteoric water (LMWL blue line) and the global meteoric water line (GMWL yellow line). Winter lake draining 2014/15 blue, clusters with summer groundwater Aug 2015. Surface river water and lake water plot outside the groundwater cluster.

Groundwater plots in two clusters. Isotopically, with lighter groundwater samples all correspond to samples taken from one borehole 'SB 80.003' (Figure 3.8). All other groundwater samples plot as isotopically heavier, distributed along the LMWL. Surface water samples sit along the LMWL. Samples taken from lakes Räterichbodensee and Grimselsee are the lightest isotopically. Whereas the runoff from summer rainfall (Aug 2015) is the isotopically heaviest sample collected. River water fed by lake Bächliensee through the tunnel system into Grimselsee has an isotopic signature closest to the groundwater from the Grimsel test site. The groundwater sits along the mixing line between lake, meltwater and summer rainfall.

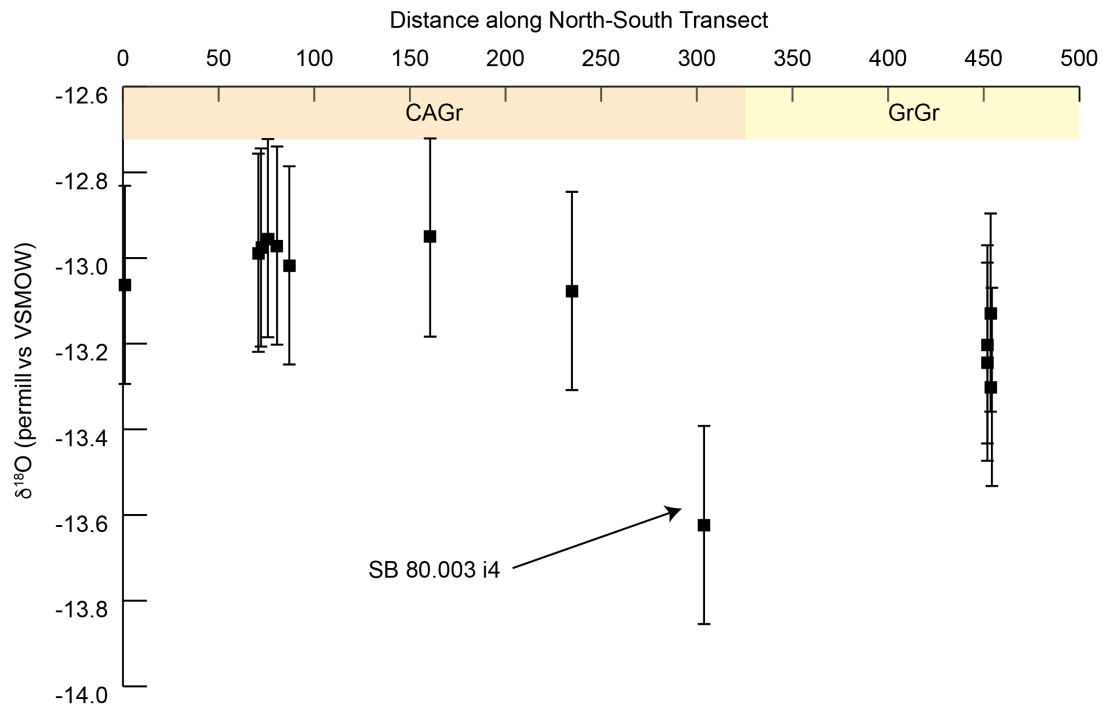


Figure 3.9 Average (n=7) borehole interval $\delta^{18}\text{O}$ isotope values (black squares) versus distance along a north to south transect through the GTS. Standard error isotope measurement $\delta^{18}\text{O} \pm 0.2$ ‰.

Figure 3.9 shows how the isotopic composition along a North-South transect through the GTS. Isotopic compositions generally go from heavier to lighter from North to South. There is notable isotopically lighter water at SB 80.003 (300m). Stable isotope data is comparable with previous studies (Schneeberger et al., 2017) and shows that the groundwater likely originates from meteoric water.

Schneeberger et al., (2017) suggest that the isotopic signature of the ground water reflects the infiltration altitude directly above the sample site. All of our sample sites except 'SB80.003' agree with their findings. SB 80.003 could be fed by a source at higher altitude, glacial melt, lake water or a mixture of each.

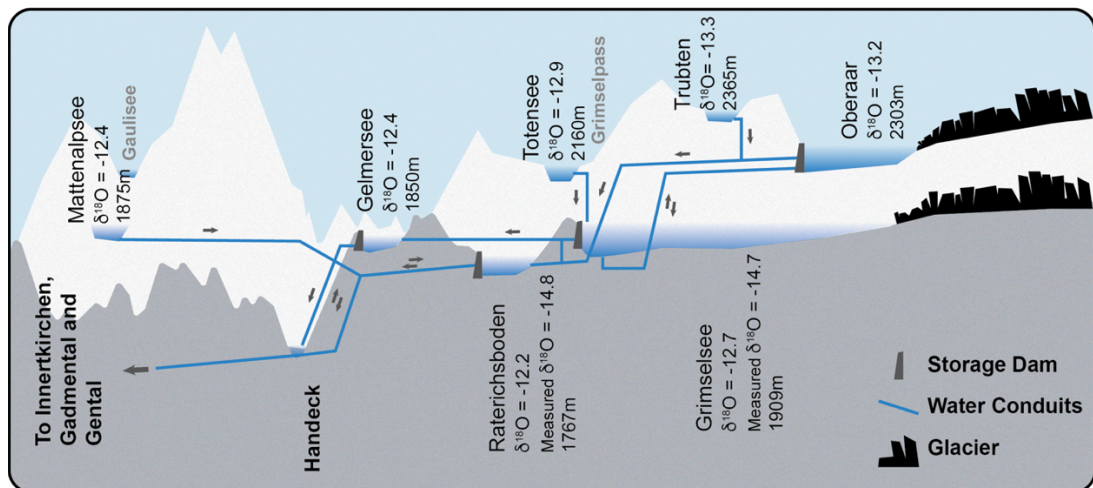


Figure 3.10 Schematic diagram of part of the hydropower network. Showing lake altitude, calculated oxygen isotope values based on altitude (Schotterer, 2010) and measured oxygen isotope values for Grimselsee and Räterichsbodensee. Glaciers directly feed into Oberaar and Grimselsee.

There is a wide isotopic distribution of meteoric water in the Grimsel valley. Reservoir water is a function of all the meteoric water precipitated in the catchment above the reservoir, and due to the pumping for hydropower there is a large degree of mixing between the lakes. As a result of this the isotopic value of Grimselsee and Räterichsbodensee can vary with time. Could these lakes be the source of infiltrating meteoric water into the GTS? Figure 3.10 shows the layout of a small part of the hydropower network, the isotopic values estimated by altitude (Schotterer, 2010) are given. It can be seen from the calculated versus measured values from Grimselsee and Räterichsbodensee that oxygen isotope values are lighter than predicted. The changes in groundwater isotope ratio with overburden thickness might suggest that the water infiltrates from directly above the GTS (excluding SB 80.003 which does not follow this trend) suggesting a higher altitude of infiltration to the south. Or, as groundwater has been shown to be greater than 50 years old (Schneeberger et al., 2017), the groundwater measured could reflect mixing water from different surface water sources that infiltrated over a 50-year period. Additionally, melting of glaciers and mixing of hydro-reservoirs could cause the shift to a lighter isotopic value on average.

3.1.2. Multivariate analysis of dissolved ion species

Principal component analysis (PCA) and k-means factor analysis were carried out on the concentrations of dissolved ions to investigate if there are any other distinctive groundwater groups (Figure 3.11). PCA works by reducing the number of variables (dissolved ion concentrations) in a data set into fewer components, where the first and second components (Principal components) can be used to describe most of the variance in the data. The data set is standardized (i.e. individual concentrations are normalised) making the variables comparable over the same scale. The covariance matrix is calculated, and the eigenvectors

and eigenvalues of the covariance matrix computed to give the principle components. Principal components one (PC1) and two (PC2) for each sample are plotted. A Plot of PC1 versus PC2 for all samples shows how interrelated individual samples are (Figure 3.11). Samples with similar dissolved ion properties plot in the, (HP i2) same areas, and the differences in water type become more apparent.

PCA carried out using groundwater major and minor ions shows how chemically different the groundwater from different sample sites are (Figure 3.11). All boreholes except 'HP 98.007 i2' plot in a relatively tight cluster. In this case, PC1 separates groundwater based on the variation in host rock lithology, GrGr is more positive in PC1 compared with CAGr. PC2 highlights the variance in SO_4^{2-} , K^+ , and Cl^- , the largest variance with PC2 is in GrGr hosted groundwaters. Alongside PCA analysis, hierarchical cluster analysis was carried out using a K-mean method to determine how samples from different boreholes cluster based on their dissolved ion chemistry. Cluster analysis shows that four clusters can best describe the variance in the dissolved ion data. Clusters analysis (Table 3.3) identify similar groups to those observed in the PCA analysis (Figure 3.11).

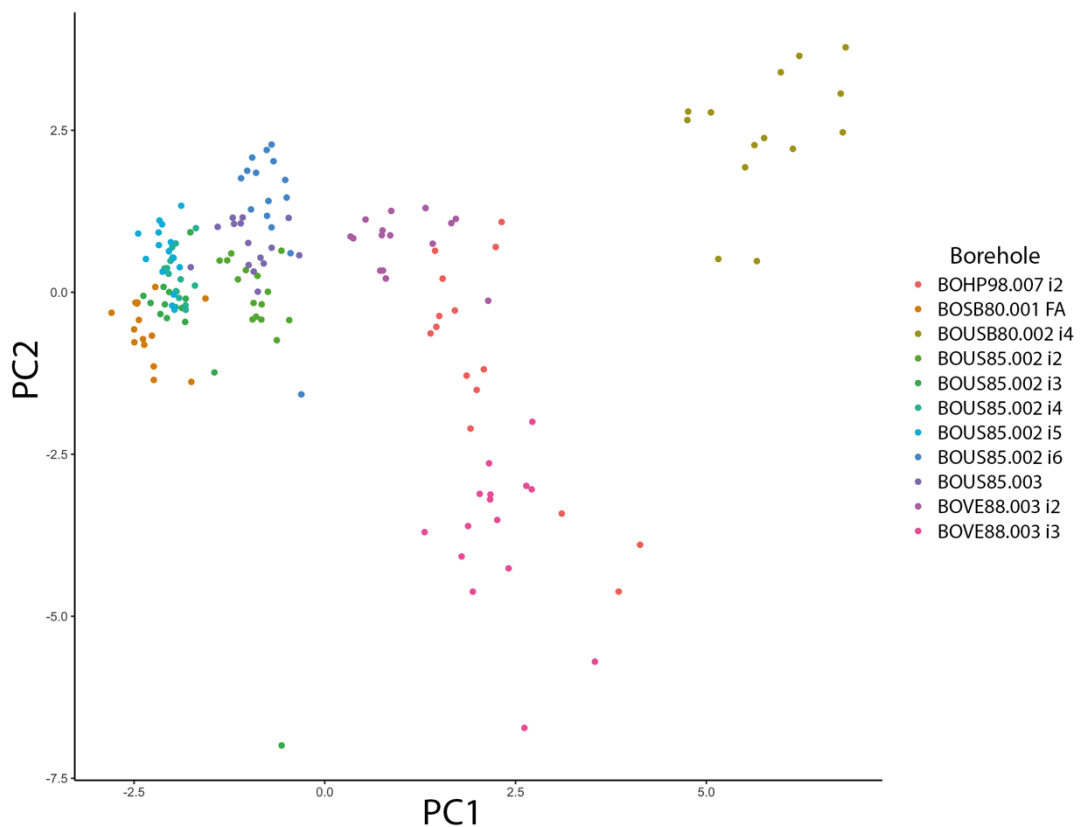


Figure 3.11 PCA analysis of all borehole geochemical data from the GTS.

Hierarchical cluster analysis (Figure 3.12) separates the groundwater into 4 groups (table 3.3). Group 1 represents the groundwaters hosted in CAGr and groups 2 and 3 are hosted in the GrGr. Group 4 is made of samples from one borehole (SB 80.004) and plots furthest from the other clusters. SB 80.004 also has more negative oxygen and hydrogen isotope values compared with all other samples. Group 2 and 3 separates two intervals in the same borehole VE 88.003 i2 from VE 88.002 i3 respectively. HP 98.007 i2 is split between cluster 2 and 3. Host rock lithology of groundwaters in clusters 2 and 3 are the same, therefore there must be another chemical factor separating them.

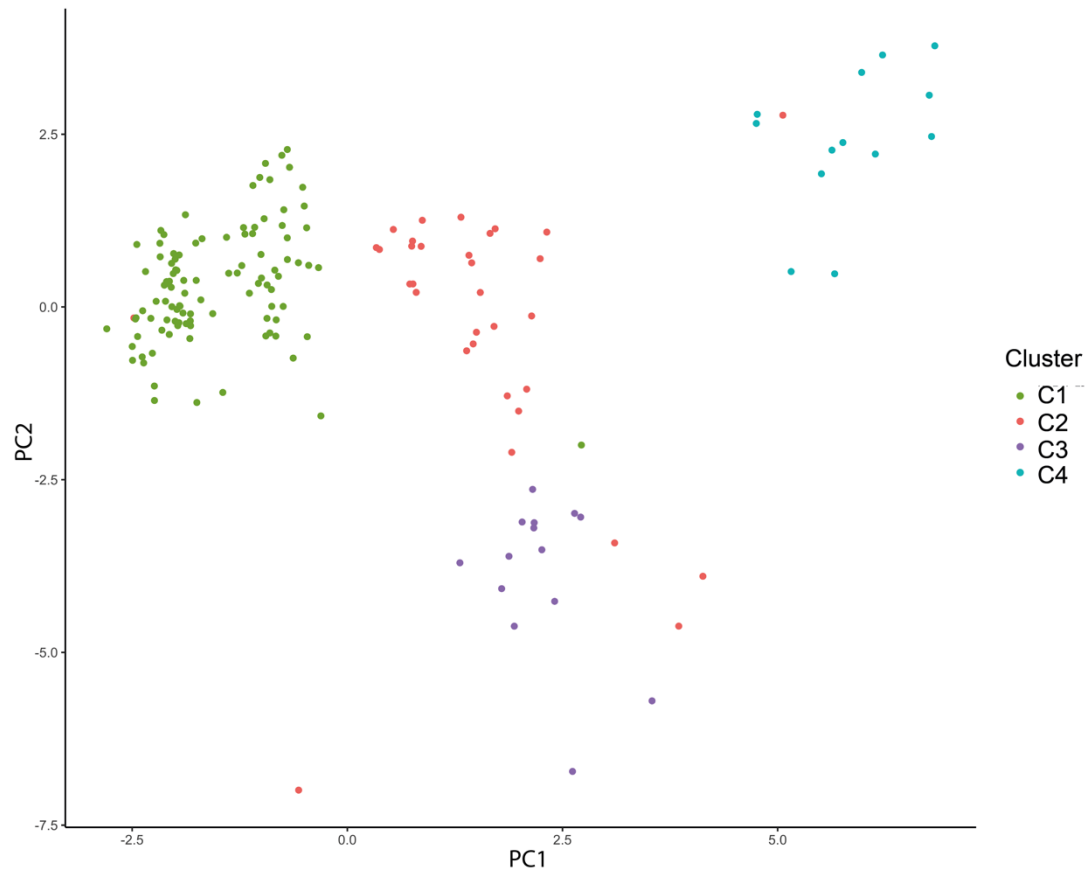


Figure 3.12 PCA plot of scaled ion groundwater chemistry data. Colours correspond to cluster analysis by k-mean, fit of 4 clusters.

Chemical factors controlling PC1 seem to be a change in groundwater dominated by Ca^{2+} to groundwater dominated by Na^+ , Cl^- , F^- . Changes in Ca^{2+} and Na^+ could reflect the change in host rock lithology. PC2 separates cluster 2 from cluster 3. Group 3 seems to be a result of an increase in K^+ , Mg^{2+} . Table 3.3 shows how the properties of each cluster and the borehole(s) making up each cluster.

Table 3-4 Table of the Principal component analysis groups displayed in Figure 3.9.

Cluster	Borehole interval	Relationship
1	US 80.002 i2, US 80.002 i3, US 80.002 i4, US 80.002 i5, US 80.002 i6, US 80.003, SB80.001	<ul style="list-style-type: none"> • Negative PC1 • High in Ca²⁺, SO₄²⁻, • Low in Na⁺, F⁻, CO₃⁻, Cl⁻
2	VE 88.003 i2, HP 98.007 i2	<ul style="list-style-type: none"> • Close to Zero in PC1 & PC2
3	VE 88.003 i3, HP 98.007 i2	<ul style="list-style-type: none"> • Negative PC2 • High in Mg²⁺, K⁺ • Low in Si_{tot}
4	SB 80.003 i4	<ul style="list-style-type: none"> • Positive PC1 & PC2 • High in Na⁺, F⁻, CO₃⁻, Cl⁻ • Low in Si_{tot}, Ca²⁺, SO₄²⁻, Mg²⁺, K⁺

To discover how flow path mineralogical properties control groundwater chemistry, further analysis of water rock interaction will delimit the reactions separating each cluster. As fracture flow is the dominant water transport facilitator in the GTS fracture mineralogy, is likely to have a much larger effect on spatial groundwater differences than host rock mineralogy. Any mineral dissolution and water rock reactions will involve the minerals lining the fracture surfaces. Potential mineral linings of fractures can differ from the host rock. Fractures either have no fill or contain biotite, gouge or breccia. Minerals in fault rocks are often more weathered and contain hydrated host rock or clay minerals arising feldspar weathering along the flow path.

What causes the variation shown in PCA and cluster analysis? The variation of dissolved calcium and sodium across the GTS seems to be the controlling factor on spatial groundwater chemistry. Figure 3.13 emphasises the correlation between Ca and Na concentrations ($r^2 = 0.7779$), where individual boreholes still plot in their respective groups and cluster in agreement with the K-means cluster analysis. Groundwater changes from Ca²⁺ dominated in the north of the GTS to Na⁺ dominant groundwater in the south of the GTS. Groundwater

change from north to south in the GTS could be due to a change in feldspar dissolution from albite to anorthite along flow paths.

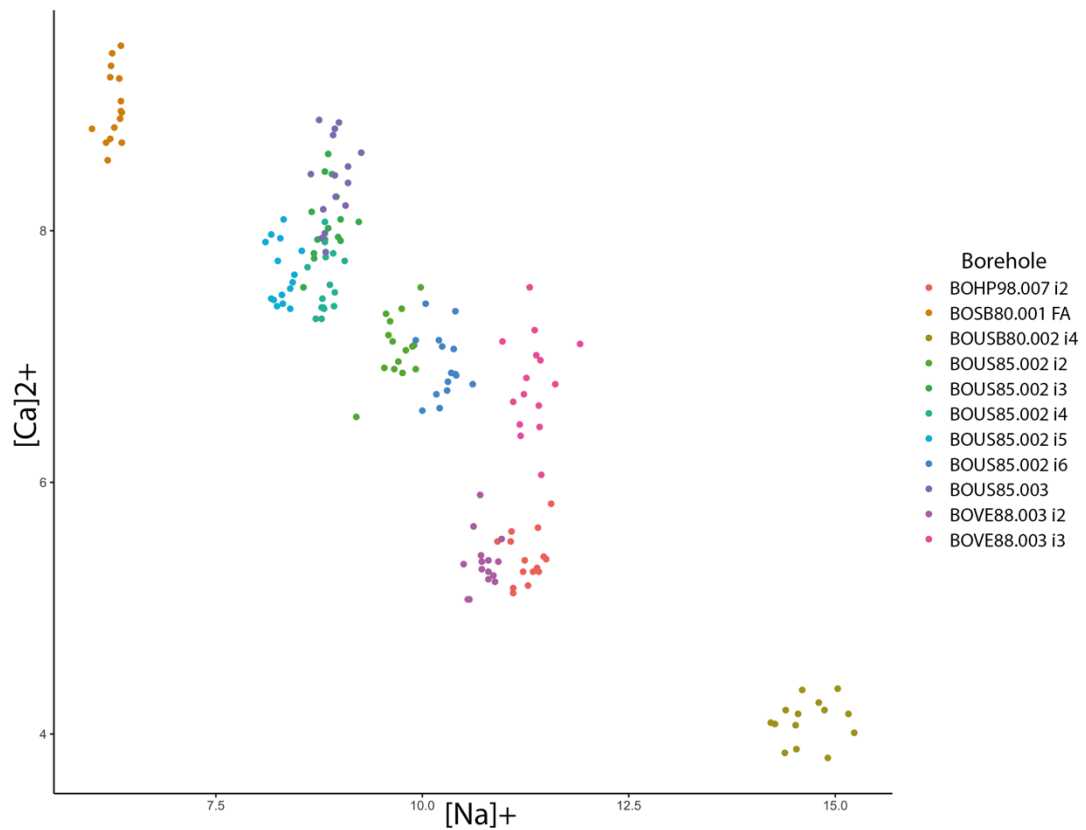


Figure 3.13 Graph of Sodium vs Calcium ion borehole groundwater concentrations.

Consequently, a change in Ca^{2+} to Na^{+} dominated groundwater could mean a change in the feldspathic minerals on fracture surfaces. A shift in feldspar mineralogy along fractures is likely to reflect a change in the host rock lithology between the granite in the north and granodiorite in the south. Continued albite and anorthite dissolution along the flow path would not only evolve the groundwater composition but also hydrate and weather feldspar minerals along fractures. Over time, this Weathering process within fractures would act to make fracture surfaces less reactive and lead to progressively slower reaction rates.

Table 3-5 Whole rock major oxide geochemistry for the different lithologies in the GTS.

Wt%	CAGr	GrGr	Mylonite	Fault Gouge	MBD	Aplite	Altered Gr
SiO ₂	71.75	67.524	72.7	62.6	52.1	75.84	66.9
TiO ₂	0.32	0.522	0.4	0.5	1.17	0.11	0.5775
Al ₂ O ₃	14	15.6	13.5	17.6	15.6	12.29	16.45
Fe ₂ O ₃ total	n.d	n.d	1	1.6	8.6	0.81	2.4375
FeO	2.2	3.3	1.1	1.7			
MnO	0.068	0.074	0.04	0.07	0.17	0.02	0.055
MgO	0.472	0.72	1.4	2.1	6.99	0.04	0.605
CaO	1.566	2.1	0.8	1.5	7	0.89	2.328
Na ₂ O	4.11	4.5	3.3	3.8	2.69	3.32	5.218
K ₂ O	4.188	3.9	4.1	6.1	2.7	5.33	3.953
P ₂ O ₃	0.1	0.166	0.1	0.1	0.39	0.03	0.17

As well as the change in Ca²⁺ and Na⁺ groundwater type from North to south based on rock lithology, there is also a change in Ca²⁺ and K⁺. Ca²⁺ increases from north to south, in all boreholes except 'SB 80.003' both Na⁺ and K⁺ show a general increase in concentration in the groundwater. Similar to the relationship between Ca²⁺ and Na⁺, the association of Ca²⁺ and K⁺ is also most likely governed by an increase in potassium feldspar dissolution along groundwater flow paths. Changes in fracture mineralogy seem to control groundwater chemistry in the GTS. However, SB 80.003 has a different geochemistry. SB 80.003 has a high concentration of Na⁺ and a low Ca²⁺ and K⁺ and does not follow the chemical groundwater trend associated with changes in host rock composition. However, meta basic dykes (MBD) in the GTS have low K⁺ and Ca²⁺. It can be inferred that groundwater sampled from SB 80.003 is in contact with MBD giving high Na⁺ and low Ca²⁺ and K⁺. As flow in the GTS is predominantly fracture fed, it is hypothesised that the fractures in the south of the GTS expose the groundwater to a different mineralogy, or different degrees of weathered fracture mineralogy.

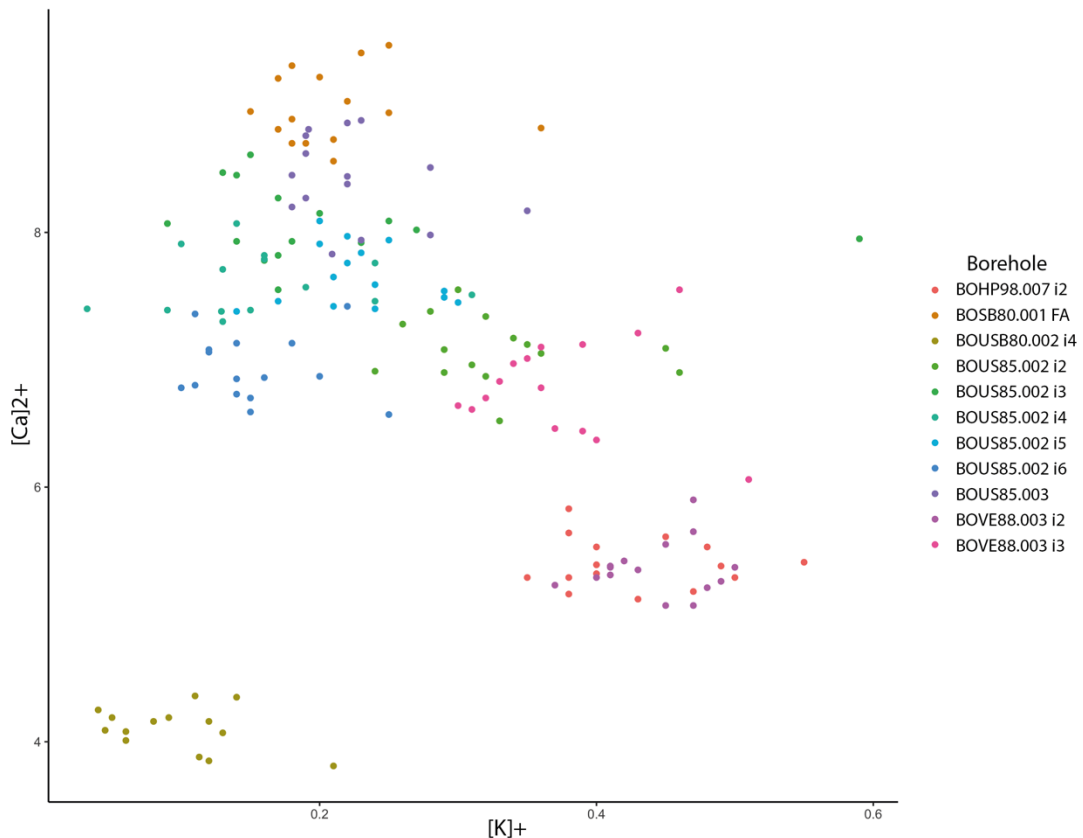
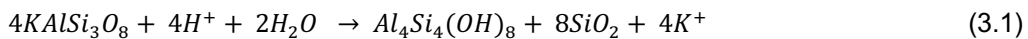
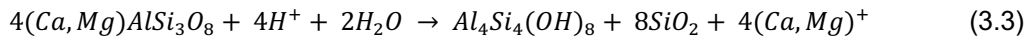
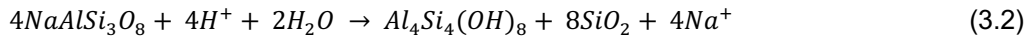


Figure 3.14 Graph of Potassium vs Sodium ion borehole groundwater concentrations.

Feldspar minerals react with groundwater along the flow paths, releasing metal ions into solution. This hydrolysis reaction forms clay minerals such as kaolinite along the flow path. Formation of clay minerals occurs by hydrolysis of feldspars. This is a result of a replacement reaction where H^+ is substituted for the metal ion in the mineral lattice, which in turn forms an OH^- in the clay mineral lattice. As the metal ion is leached from the fracture surface following reactions eq. 3.1-3 the mineral, is transformed into kaolinite. Metal (Na^+ , K^+ or Ca^{2+}) ions are no longer available to react on the mineral surface. Over time this will reduce the total exposed reactive surface area of feldspar along flow paths. The uptake of H^+ ions during hydrolysis causes a net drop in H^+ compared with OH^- in the groundwater and, consequently, increases the pH of the groundwater. Water-feldspar reactions are the main control on groundwater pH, leading it to turn moderately alkaline pH 8.67 - 9.34. The availability of H^+ in this case is likely a function of dissolved CO_2 forming carboxylic acid. Once infiltrated into the fracture network, the groundwater system no longer undergoes atmospheric gas exchange. Hydrolysis of feldspar acts as a buffer over time, with hydrogen ions being taken into solution. With no CO_2 added along the flow path, this leads to the increased pH in Grimsel groundwaters compared to surface waters.

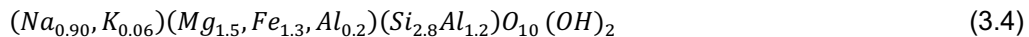




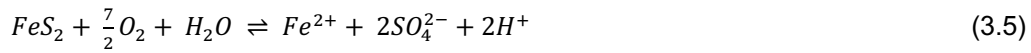
Lithium varies spatially in the GTS. Li⁺ is higher in the south than the north. The distribution of lithium in groundwater follows the same trend as sodium and is related to the changes in lithology. As Li is enriched in the later stage magmatic phase resulting in Li enriched Granodiorite emplacement. We expect to see higher lithium concentrations in the K-feldspar and albite (Na-feldspar) dominated groundwaters. Low concentrations of lithium in the north of the GTS reflect the lower levels of Na and higher levels of anorthite (Ca-feldspar). The presence of lithium in the host rock is most likely a result of lithium enrichment during the earlier stages of the pluton emplacement.

Fluoride concentration differs spatially across the GTS. However, it not likely to be controlled by the same water-rock reactions governed by the feldspathic minerals present along flow paths. It is more likely the increase in fluoride concentration is related to fluorite dissolution along the flow path. 'Alpine clefts' aligned with ductile deformation structures, formed when the pluton was still ductile and have been known to host fluorite minerals (McKinley *et al.*, 1987) in the Grimsel region. Flow paths that intersect alpine clefts can explain the presence of fluoride in groundwater. Fluorite deposited in alpine clefts may provide the source of fluoride and calcium ions into the GTS groundwater system. The spatial distribution of fluoride in the GTS therefore depends on the fracture network and flow paths. As only flow paths intersecting alpine clefts have a source of fluoride which is taken into the groundwater by dissolution.

Changes in Mg²⁺, Al³⁺, and Fe²⁺ in southern borehole intervals can be attributed to biotite (eq. 3.4) dissolution along the flow path. Biotite is the dominants mineral in-contact and dissolves into groundwater flowing through biotite lined fractures. Biotite weathering releases Fe, Mg and Al increasing the concentration of these metal ions in the groundwater.



Sulfate and chloride concentrations vary across the GTS, chloride is more concentrated in the south and sulfate concentrations are higher in the north of the GTS. The source of sulfate is likely to be pyrite oxidation along flow paths as this is the only sulphide mineral found in the host rock. Sulphide in pyrite is oxidized to sulfate (eq. 3.5) and dissolved into the groundwater. The Eh measurements in the north being higher than those in the south supports increased pyrite oxidation as the higher source of sulphates in solution.



Pyrite oxidation requires oxygen in the system to release sulfates into solution. Therefore, pyrite dissolution likely occurs in the near-surface where rock is oxidised by dissolved oxygen in infiltrating meteoric water. Dissolved oxygen in infiltrating rainwater is normally consumed by organic C in soil, however, the soil cover directly above the GTS is sparse with patchy peat development in topographic depressions. Consequently, dissolved oxygen from meteoric water would remain in solution and become available for the oxidative dissolution of sulphide minerals and Fe(II) minerals. Sulphide minerals are more reactive and thus react faster to oxidative dissolution than Fe(II) minerals (eq.3.6). A by-product of oxidative dissolution is the release of Fe(II), which is immediately oxidised and precipitates on fracture surfaces as amorphous Fe(OH)₂ (eq. 3.6).



Infiltrating groundwater loses oxygen to these reactions. The sources of sulfate in other groundwaters has found to be the result of pyrite oxidation in the near surface (Massmann *et al.*, 2003) while also relating sulfate in groundwater to residual paleo-Baltic seawater from inundation at the Litorina stage (ca. 8000 y ago - these are coastal sites) in Sweden (Laaksoharju *et al.*, 2008). In the case of Grimsel there is no possibility of sulfate originating from relict sea water, so the most likely origin is solely the oxidation of pyrite at the near surface. Low dissolved iron concentrations found at the GTS are then explained by the precipitation of amorphous Fe(OH)₂ in the near surface. We see no evidence for this precipitation along fractures at depth. Over time the pyrite along fractures is accessible for oxidation by dissolved oxygen in groundwater and will be gradually depleted by the oxidation process. The 'redox front' will gradually move to greater depth and will eventually lead to the precipitation of iron-oxide-hydroxide at greater depths over time. Variables which will affect the SO₄²⁻ concentration in the GTS are: the abundance of accessible pyrite along the flow path, the residual dissolved oxygen after depletion by the organic carbon at the in the critical zone (Brantley *et al.*, 2007) as well as reducing compounds which are transported from the surface such as (i.e. DOC) or diffuse from microbially mediated release (i.e. CH₄ or H₂), or the abundance of reactivity of accessible Fe(II)-containing minerals along the flow path other than pyrite (i.e. biotite, chlorite). Finally, sulfate concentration can also be affected by microbial reactions where depending on the different redox conditions where H₂S oxidizes to SO₄²⁻ or alternatively microbes can facilitate the reduction of SO₄²⁻ to H₂S. The sulfur system has probably undergone several oxidation and reduction reactions along the flow path. Redox reactions with sulfur can account for the release of H₂S into solution and for the sulphide smell that was recorded during sampling in certain borehole intervals.

3.1.3. Geochemical Modelling

Initial calculations of speciation and saturations: Appendix 1. Saturation index (SI) is calculated for the main rock-forming minerals known to be present in the GTS, as well as $p\text{CO}_2$. During this calculation step, the quality of data is assessed via an ion balance; the percentage error in the ion balance is calculated. Percentage errors of less than 10% are considered acceptable and < 5% is excellent. $\text{SI}_{\text{quartz}}$ is greater than or near zero; therefore, it is in equilibrium with the groundwater in both the north and south of the GTS. Quartz is more saturated in the CaGr groundwaters than the GrGr but only slightly. Most boreholes are saturated by K-feldspar and are generally more saturated in GrGr waters. The exception is borehole "1", which is undersaturated in K-feldspar. Anorthite and albite are undersaturated. Albite is closer to saturation in the GrGr hosted groundwaters than the CaGr waters, however, the opposite is true for anorthite. Amorphous iron oxyhydroxide is approaching equilibrium but is more saturated in the GrGr than the CaGr.

Speciation and saturation calculations support the findings that dissolution of different feldspathic minerals (i.e. albite and anorthite) dissolving along flow paths control the major chemical difference between the CaGr and GrGr hosted groundwaters. The supersaturation of clay minerals (kaolinite, illite) is indicative of alteration of feldspathic minerals along flow paths by a hydrolysis reaction.

Table 3-6 maximum and minimum mole transfer of phases from inverse modelling of surface water to the average cluster water composition. Where 'n' is the number of potential models. Positive mole transfer record dissolution and negative mole transfer indicate precipitation.

Phase	Formulae	mmol/l transfer for Cluster:							
		1 (n=4)		2 (n=11)		3 (n=6)		4 (n=11)	
		Max	Min	Max	Min	Max	Min	Max	Min
Albite	NaAlSi ₃ O ₈	0.336	0.331	0.398	0.398	0.392	0.236	0.544	0.543
Anorthite	CaAl ₂ Si ₂ O ₈	-	-	3.003	0.438	-	-	4.691	0.696
Calcite	CaCO ₃	-0.009	-0.012	0.516	-2.971	0.031	0.046	0.120	-4.811
Fluorite	CaF ₂	0.117	0.117	0.117	0.117	0.152	0.152	0.159	0.158
Clinocllore	Mg ₅ Al ₂ Si ₃ O ₁₀ (OH) ₈	0.226	0.221	0.277	-0.653	0.294	0.161	0.424	-0.996
Muscovite	KAl ₃ Si ₃ O ₁₀ (OH) ₂	0.364	0.357	0.454	-0.110	0.482	0.260	0.691	-0.019
Pyrite	FeS ₂	-0.001	-0.001	0.000	0.000	0.115	0.001	0.000	-0.001
Kaolinite	Al ₂ (Si ₂ O ₅)(OH) ₄	-0.001	-0.750	0.471	-2.532	-0.533	0.966	0.754	-3.937
CO ₂ (g)		0.231	0.219	0.252	-3.003	0.243	0.197	0.278	-4.691
Halite	NaCl	-0.005	-0.005	0.033	0.031	0.039	0.039	0.109	0.001
PhlogopiteK	KMg ₃ Si ₃ AlO ₁₀ (OH) ₂	-0.373	-0.380	0.969	-0.465	-0.027	0.494	0.019	-0.710
H ₂ S(g)		0.143	0.001	0.001	0.001	0.000	0.002	1.422	0.001
MgCO ₃		-	-	3.255	0.252	-	-	4.969	0.278

Inverse modelling carried out in PHREEQC using the SIT thermodynamic database calculates the potential different mass balance solutions from which mineral precipitation and dissolution can create groundwater from surface meteoric waters. Table 3.5 shows the inverse modelling results where O₂(g) and CO₂(g) atmospheric equilibrated pure water underwent a dissolution reaction with primary mineral phases (Albite, Anorthite, Fluorite, Quartz), other mineral phases are allowed to precipitate or dissolve (Calcite, Clinocllore, Muscovite, Pyrite, Kaolinite, Halite, Phlogopite, MgCO₃). Gas phases CO₂ and H₂S are allowed to exsolve and dissolve into solution. Cluster 1 represents all samples contained within the CAGr. Clusters 2 and 3 are hosted in GrGr, and Cluster 4 is in the magmatic transition zone between CAGr/GrGr, also cut by a meta-basic-dyke. Kinetic modelling by Schneeberger et al., (2017) shows that pH evolution is reasonable for reaction times of 50-100 years. Modelling results agree with groundwater chemical data indicating hydrolysis of feldspars is the key reaction in the evolution of groundwater chemistry in the GTS.

3.2. Discussion and Conclusions

Geochemically, the groundwater in the GTS has evolved from the chemistry of the meteoric water source(s) at the surface, via water rock interactions with the different rock chemistries during fracture transport to depth. Two distinct groundwater compositions are found that match the main lithologies in the GTS, distinguished largely by higher pH (8-9.5) in the GrGr to the north than the CAGr in the south (pH 7.5-8.5). Groundwater can be characterized as $\text{Na-HCO}_3\text{-F} \pm \text{SO}_4$ type in the South of the GTS hosted in GrGr and $\text{Ca-HCO}_3\text{-F} \pm \text{SO}_4$ type groundwater in the north of the GTS hosted in CAGr. Surface waters taken from Räterichsbodensee, Grimsensee and two rivers are near neutral pH 6.67-7.13. Several studies (Keusen *et al.*, 1989; Schneeberger *et al.*, 2016) assess groundwater chemistry at the GTS, all studies agree with this investigation that at the GTS elevation, groundwater is fed by infiltrating meteoric water.

Attention needs to be paid to the host rock lithology and fracture properties as those properties likely control subtle spatial variation in groundwater chemistry within the same main lithology. CAGr) and GrGr have undergone several orogenic deformation phases. From a hydrological viewpoint brittle deformation is most important as this affects the fluid pathways. Ductile deformation does not significantly alter permeability or porosity to have a significant effect on flow. Understanding the controls on brittle fracturing during the alpine orogeny will help to determine which fractures are critically stressed and may have relatively higher flow rates (Barton *et al.*, 1995; Schneeberger, 2017) compared to less critically stressed fractures. Fracture properties also play a key role in the evolution of groundwater chemistry.

Groundwater chemistry is related to changes in fracture mineralogy. Four major changes in mineralogy along flow paths are found to affect the groundwater chemistry. These findings are summarised in the conceptual model in Figure 3.15 and supported by geochemical modelling of mass transfer of these key minerals in the groundwater:

- 1) Changes in feldspathic mineralogy along flow paths, most likely reflect the host rock lithology.
- 2) Flow along biotite and chlorite lined fractures increases Fe, Cl, Mg and Mn in groundwater as biotite dissolves.
- 3) Intersection of flow paths with Alpine clefts allows groundwater to interact with fluorite in the Alpine clefts. This increases the levels of fluorine in groundwater
- 4) Oxidation of pyrite along flow paths in the shallow subsurface contributes to higher levels of sulfate in the groundwater.

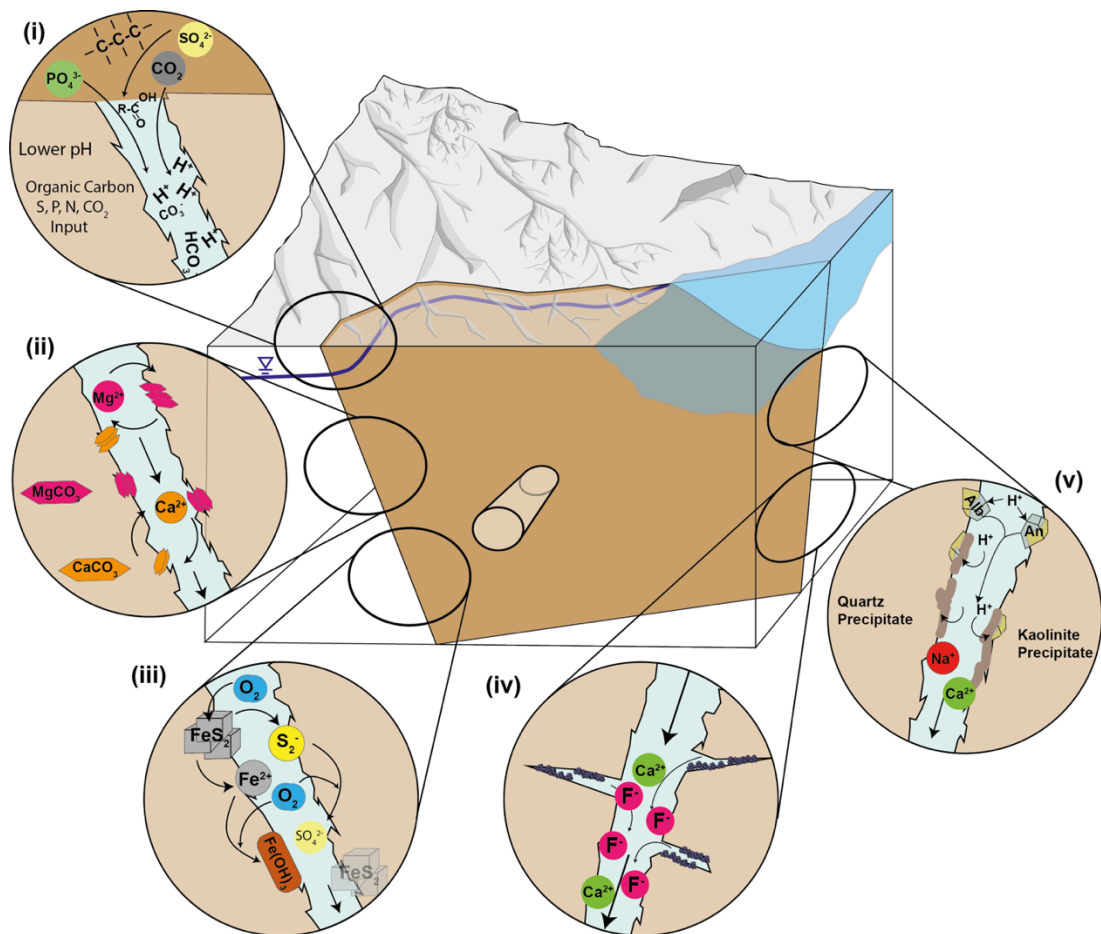


Figure 3.15 Conceptual diagram showing the key reaction processes leading to the evolution of groundwater from infiltrating meteoric water along a fracture path (Brown plane). (i) Influx of organic compounds, organic acids, Sulfur/Phosphorus compounds, and CO_2 added from the soil zone dissolving and forming bicarbonate and carbonate in groundwater. (ii) Precipitation and dissolution reactions of Mg^{2+} and Ca^{2+} at the start of the flow path forming $(\text{Mg}/\text{Ca})\text{CO}_3$ precipitates depending on water conditions. (iii) Pyrite oxidation and potential precipitation of iron oxyhydroxides. (iv) Fluorite dissolution from intersecting 'alpine clefts' adding F^- and Ca^{2+} into groundwater. (v) Feldspar weathering (Alb = Albite, An = Anorthite) by hydrolysis releasing cations forming Quartz and Kaolinite on fracture surface.

In summary, mineralogical changes in the fractures which host flow through the subsurface, are the main control on the spatial evolution of groundwater chemistry at the GTS. The differences between the different groundwater geochemistries is small but detectible. Given that flow in the GTS is fracture dominated, flow paths and geological structures play an important role in controlling flow in the rock mass and the evolution of groundwater chemistry. Where several fractures cross-cut a borehole sampling interval, only the fractures making up a flow path will affect the groundwater chemistry. This is an important distinction as fracture flow models often use all fractures to describe the flow in a fractured rock network. However, the groundwater geochemical evidence implies that, where multiple fractures intersect one sampling interval, only a subset of these fractures are contributing to flow.

4. Tracing the source of surface infiltration

Tracing the source of surface infiltration into a groundwater system using organic fingerprinting

4.1. Abstract

Tracing the sources of water into groundwater systems is inherently difficult and the problem is exacerbated in fracture-dominated rocks. Current methods for understanding groundwater origins rely on either additive tracing or isotope geochemistry. Recovery rates of additive tracers in fractured rocks are notoriously low and they can only be used to trace flow over very short time periods, and hence over very short distances. By contrast, isotopes can trace groundwater origins over long time periods, but only where potential source waters can be distinguished by variations in atmospheric composition at the time of precipitation. In this paper we present a new method of groundwater tracing based on organic fingerprinting. In the past, researchers have used specific organic molecules found in sediments to distinguish between terrestrial and marine sediment origins. Here, we take an entirely new approach. We create unique organic fingerprints of individual water samples and soil samples, based on sequencing the full range of organic molecules present using 2D-Gas Chromatography. We then use this technique to determine groundwater origins. We validate our approach by sampling groundwater, surface soils and lake water at the Grimsel Test Site in Switzerland, which is located within a fractured granite. We derive organic fingerprints for all samples. Using principal component analyses, we show that individual groundwater samples can be clearly identified as having derived from identifiable surface water sources. Our findings are consistent with previous isotope investigations, yet complimentary. The organic fingerprinting provides additional detail; we can determine the different soil types through which meteoric water infiltrated, as opposed to only knowing the approximate source water altitude.

4.2. Introduction

Methods for tracing the sources of meteoric infiltration into a groundwater system should ideally be able to distinguish between the contribution of many sources, either tracing groundwater to a unique source or determining the combination of different mixed sources. However current tracing techniques have severe limitations. Additive tracers e.g. fluorescein, DNA, salt (Field *et al.*, 1995; Sabir *et al.*, 1999) cannot be used in systems with long travel

times (greater than weeks or months) as this results in tracer diffusion and 'lost' tracers. Even over short periods, additive tracers used in fracture networks are often not recovered because flow along fractures is highly complex and occurs along sparse, linked subsets of the total fracture network, thus by-passing monitoring wells. Further, the addition of tracers at the surface can only be achieved at a small number of discrete sites and, hence, does not necessarily take account of the full surface water catchment. Some tracers (e.g. salt, fluorescein) can also have negative impacts on surface and downstream environments (Field *et al.*, 1995).

Other methods of determining infiltration location rely on large differences in major and minor ion chemistries; these methods are only applicable where infiltrating waters contain key differences in dissolved ion content. Further, mixing often gives a non-unique answer where infiltration sources cannot be delineated with certainty from each other or from chemical changes driven by water-rock reaction. Combining major and trace elements with stable isotopes to 'isolate' a given supply (Kalbus *et al.*, 2006) is a more powerful approach. Orographic climate change effects alter stable isotope composition, making them a powerful tool for determining palaeoclimatic versus meteoric water origins. For meteoric waters, stable isotopes can be used to estimate infiltration altitude (Boronina *et al.*, 2005), narrowing down infiltration sources. However, they cannot distinguish meteoric water sources in areas with little-to-no surface elevation variation. In locations where groundwaters of different ages are mixed, the use of stable isotopes is limited.

Organic matter that was once living at the surface leaves signature organic compounds dissolved in groundwater. For instance, decayed vascular plant matter in peat soils will produce characteristic compounds such as n-alkanes (Pancost *et al.*, 2002) and sterols (Lehtonen and Ketola, 1993) some of which become part of the preserved DOC in the groundwater. Current studies of dissolved organics in groundwater and surface water systems focus on contamination from landfill (Christensen *et al.*, 1998), pharmaceuticals (Barnes *et al.*, 2008), hydrocarbons (Allan *et al.*, 2012; Payne and Driskell, 2018), and other organic pollutants (Lapworth *et al.*, 2012). The majority of studies investigate bulk dissolved organic carbon (DOC) content rather than studying the individual compounds. DOC is used to successfully determine characteristics and organic contamination levels in ground and surface waters. Artinger *et al.*, (2000) showed that by separating humic and fluvic fractions, the influences of sedimentary systems on groundwater can be determined, and that the mixing and turnover of organic carbon can be estimated (Huang *et al.*, 2015; Stegen *et al.*, 2016). While grouping the DOC from groundwater into these organic groups can give a lot of information about a system, much of the information is lost as these groups are comprised of several hundreds of different organic compounds.

In this paper we explore whether the sheer diversity of organic compounds in groundwater can be used to discriminate between sites of surface water infiltration. We hypothesize that regions with similar organisms and organic matter decay paths will result in characteristic, identifiable suites of organic compounds that give a unique signature to individual surface water sources. This unique signature may then be preserved, or a fraction of it preserved, in the groundwater. We test this hypothesis at the Grimsel Test Site (GTS), an underground rock characterization laboratory in Switzerland.

4.3. Field Site

The GTS is situated within granitoid host rocks and has the potential to be fed by several surface water sources. To test our hypothesis, we collected groundwater samples from boreholes within the GTS, sampled surface soils and collected water samples from rivers, lakes and exposures on the mountainside above the GTS. We create unique organic signatures of individual samples, based on sequencing the full range of organic molecules present using 2D-Gas Chromatography. We then use this technique to determine groundwater origins.

The GTS is a system of tunnels and boreholes that sits 200m to 400m beneath the eastern flank of a mountain (Juchlistock). Lake Räterichsbodensee lies 200m to 600m laterally to the West of the GTS, with the lake surface being ~37m above the level of the GTS tunnels. (Figure 4.1). Lake Räterichsbodensee is fed by the far larger Lake Grimselsee, which is at the toe of the Unteraar glacier. Both lakes are part of the KWO hydropower network and are connected by a system of tunnels and rivers. The hydropower network is mixed on a daily basis by pumping water around the reservoir system across the Grimsel Valley. The GTS is hosted within a post-Variscan calc-alkaline granitoid (Schaltegger, 1990; Schaltegger and von Quadt, 1990). The host rock underwent Alpine deformation (Wehrens, 2015) which led to the development of a complex, poorly connected fracture network dominated by steeply dipping fractures (Schneeberger *et al.*, 2016) (Figure 4.1). Hydraulically, the GTS imposes an artificially low (atmospheric) pressure at depth within the subsurface, which consequently drains groundwater from the surrounding rocks. Due to the low matrix porosity, groundwater flow into the GTS is concentrated along the fracture network. This groundwater potentially derives from several sources: 1) Meteoric water that can infiltrate where the sub-vertical fractures intersect the mountainside and the surrounding valleys, this surface infiltration may be enhanced by topography-parallel unloading fractures (Ziegler *et al.*, 2016); 2) lake water that connects reservoirs (to the East and the South of the GTS) and river/stream beds through the fracture network ; 3) upwelling groundwater from depth.

Surface sampling of soil organic materials was severely limited by the topographic access at the site (1-6, Figure 1). Sample sites were located, as far as possible, to cover a North-South transect above the GTS, which resulted in three soil sampling locations and one sediment river bed sample (Figure 4.1). At each site (numbered numerically) two samples were collected (labelled a and b) to examine how variable the organic signature is at each location. Clear differences are apparent from a visual inspection between sites. Site 3 is dark, waterlogged and has very little sand/gravel content, site 4 is brown, not as waterlogged as site 3 and contains fragments of roots/plant matter, site 5 consists mostly of crushed up granite and is light brown in colour. Site 6 is the riverbed of a tributary to Räterichsbodensee, mostly containing crushed rock and fine rock flour.

Lake water was sampled (Figure 4.1) at a location where the water was readily accessible, and where the predominant SW/NE fracture set within the GTS (Figure 4.2) might plausibly intersect the lake. It is important to bear in mind with the lake water that, due to the highly connected nature of the pump-storage hydropower system, any sample is likely to represent an integrated mixture of the surface water both upstream and downstream in the hydropower network.

Groundwater was sampled from within the GTS (a-g, Figure 4.1). Horizontal boreholes are fitted with isolated packer systems integrated with water sampling flow lines. Each interval is instrumented with a pressure transducer. It is possible to sample volumes of groundwater produced from individually packed intervals. A total of 7 groundwater sampling intervals were selected for this study (Figure 4.2). Groundwater sampling intervals (labelled alpha numerically) were chosen based on the host rock lithology and structural geology, as well as providing spatial coverage across the GTS. Groundwater sample sites are shown in Figure 4.2, locations a to d relate to the Central Aar granite, sample g lies in the Grimsel granodiorite whereas e and f sit within the transition zone between the two lithologies.

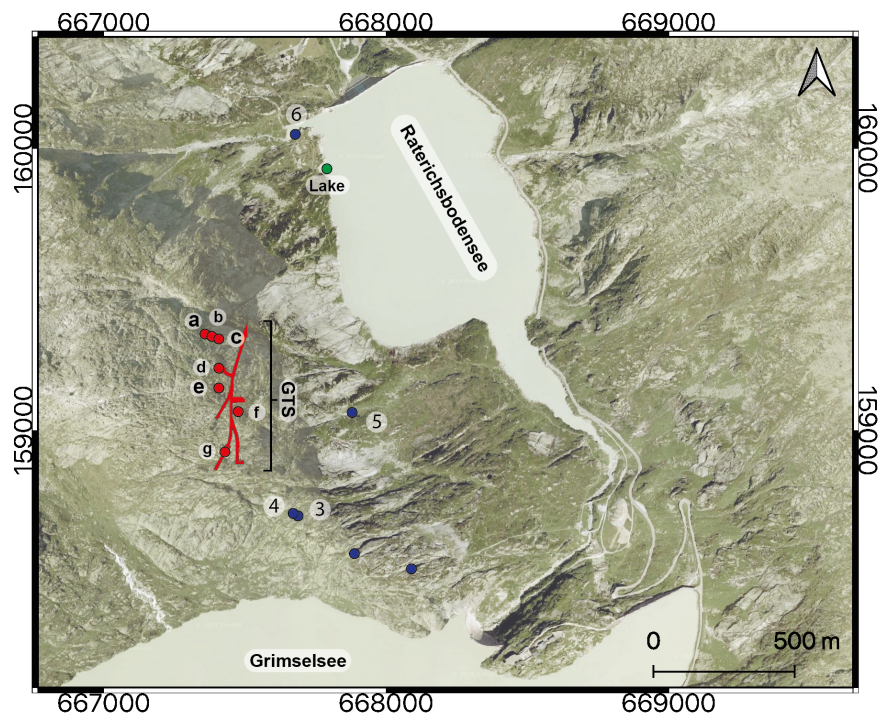


Figure 4.1 Satellite map (Google Maps) of sample locations; groundwater a-g (red circles), Soil and sediment samples 3-6 (blue circles), and lake water sample (green circle). The footprint of the Grimsel Test Site tunnel is shown in red.

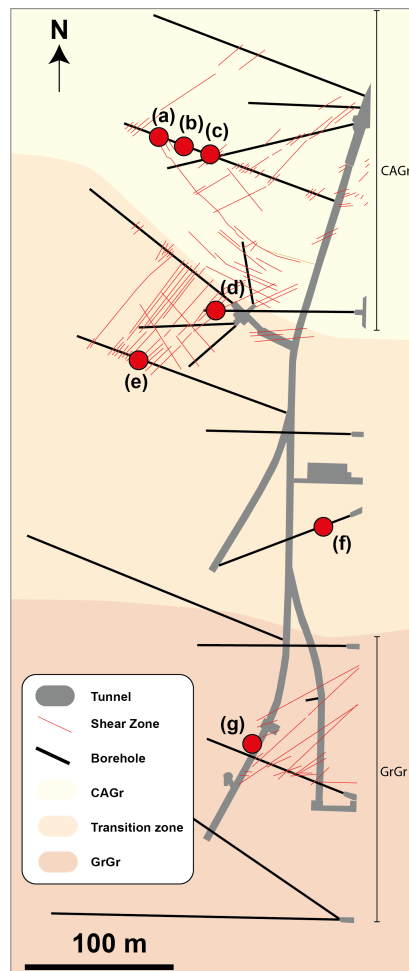


Figure 4.2 Borehole map, groundwater sample locations (red circles), shear zones (red lines, tunnels (grey), boreholes (black lines), CAGr (pale yellow), GrGr (orange) and magmatic transition zone (pale orange)

4.4. Materials and Methods

4.4.1. Surface site, and groundwater sampling

Surface soils were collected using organic free metal trowels, and placed into foil parcels, prepared by heating at 550°C for 8 hours prior to sampling. This heating process ensures that there is no residual organics present on the aluminium foil. The samples were double wrapped and stored at 4°C for transport (i.e. below ambient soil temperature) until sample preparation could take place. Water samples are collected in 125ml boston rounds (borosilicate glass). Prior to groundwater sampling the borehole interval was drained three times the volume of the borehole sampling interval and sample lines. Draining of borehole intervals is to remove any water that has been in contact with plastic in the packer system ensuring that only formation water is sampled. Groundwater is used to flush the 125ml sample bottle 3 times. Samples are collected and sealed underwater with PTFE foil lined caps to ensure no atmospheric gases

enter the sample (Geological Survey, 2006). Physiochemistry was measured during sampling, water samples of dissolved inorganic ions were taken.

4.4.2. Sample preparation for organic analysis

Soil samples were freeze dried and homogenized, then extracted with dichloromethane (DCM): methanol (MeOH) (9:1, v:v) (Toney *et al.*, 2010) using Accelerated Solvent Extractor ASE 350 (Dionex). ASE extraction cells are packed with deactivated silica (10% deactivated w:w) as an in-cell clean up step during extraction (McGregor *et al.*, 2011). Ground and lake water samples were extracted by separatory funnel liquid-liquid extraction, using the EPA method 3510C as a guideline (EPA Publication, 1996), it was not feasible to transport large volumes of groundwater, so extraction was carried out on 125ml of sample. Extraction was carried out three times with a solvent mixture DCM:MeOH (9:1, v:v). Due to the dilute nature of dissolved organics in groundwater; extracted samples were concentrated using a combination of heat and vacuum concentration (Buchi Syncore Analyst, DCM method) to 1.0 ml volume. Where further sample concentration was required solvent evaporation with a constant stream of pure N₂ to lower volumes. Samples were made up with DCM to the desired sample volume. During sample preparation surface samples 1 and 2 did not stay airtight, as a result were spoiled, therefore site 1 and 2 were not included in GCxGC analysis.

4.4.3. Analysis by GCxGC-ToF

Regular chromatography methods do not give sufficient separation or detection limits to build a detailed organic signature of the different organic compounds within an individual sample. In standard GC an individual chromatogram peak may represent several compounds; the advantage of GC x GC mass spectrometers is that individual compounds can be uniquely identified by both a two-dimensional retention time, as well as a mass spectrum for each sample peak.

The following GC x GC method was used to analyse soil and water extracts, which was adapted from LECO application note (LECO Corporation USA, 2019). Comprehensive signatures of the samples were collected using a LECO (St. Joseph, Michigan) time of flight mass spectrometer (Pegasus 4D), with an Agilent 7890A gas chromatography equipped with a LECO thermal modulator (Figure 4.3). The column set up was reverse phase, 1st dimension column DB-17MS (60m x 0.25mm i.d. x 0.25 µm; Agilent) polar phase, 2nd dimension column less polar phase Rxi-5Sil MS (1.4m x 0.25mm i.d. x 0.25 µm; Restek) less polar phase. Sample injection was splitless using a split/splitless injector set at 260°C, with a helium flow rate of 1.4 ml/min for the entirety of the run. The primary oven temperature program is as follows; initial temperature 50°C, hold for 0.2 min, ramp 3.5 °C/min to 320°C, hold for 20 min. The secondary oven and thermal modulator had an offset of +10°C and +20°C respectively from the primary

oven. Thermal modulator period of 5 seconds and the Mass Spectrometer transfer line temperature is 300°C with the spectra acquisition rate of 200 spectra/second. This method gave repeatable analyte separation and produces enough detectable peaks to build a picture of all the organic compounds contained within each sample.

Processing of 2-Dimensional gas chromatography data to detect peaks and identify compounds was carried out using LECO ChromaTOF software. Processing was carried out twice using a low and high signal-to-noise ratio of 50 and 100 respectively, removing any compounds related to column bleed, or the DCM solvent. The end result for each sample is a 2D chromatograph and peak table which contains the retention time, intensity, the mass spectra and the NIST library database match for each peak.

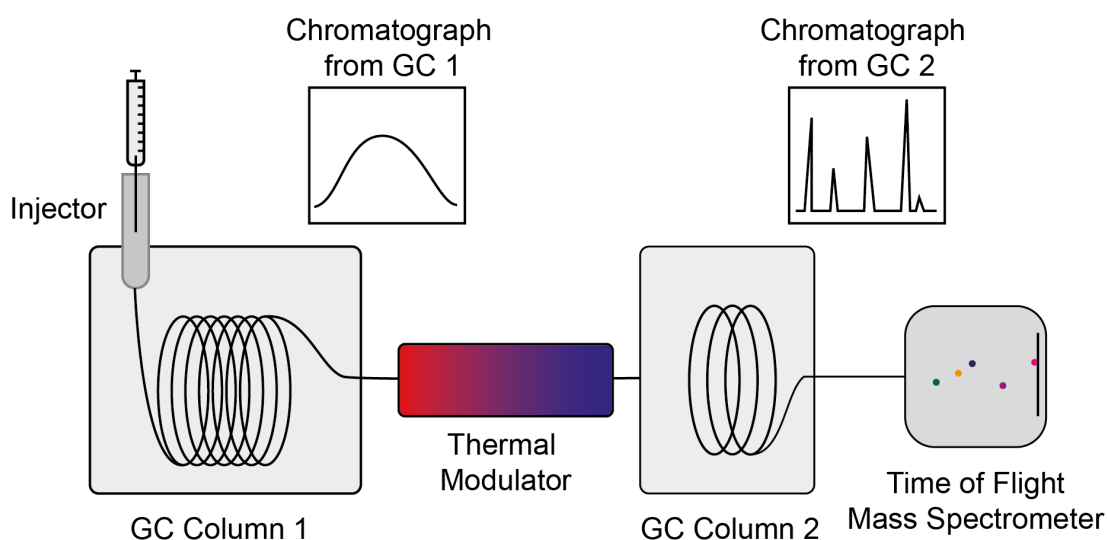


Figure 4.3 Schematic diagram of the GCxGC ToF system with thermal modulator. While displayed as separate sections; GC column 1, thermal modulator and GC column 2 are all enclosed in the Agilent 7890A. Column 2 is in a secondary oven enclosed in the primary oven. The time of flight (ToF) mass spectrometer is connected to GC column 2 via a heated transfer line.

The GCxGC-ToFms system works similarly to a regular GC-MS system. However, the two columns and thermal modulation leads to better analyte separation and greater peak intensity. The sample is injected into a heated GC inlet. The sample vaporises and a carrier gas of pure helium (purity 99.9999%) carries the sample vapour through through GC column 1 (Figure 4.3). As the sample flows through the column the analytes are separated based on their molecular size and affinity to the columns stationary phase, giving a peak. The sample then flows into the thermal modulator which cools and heats the column in two places. This alternate heating and cooling process, slows (cold) and releases (hot) the analytes flowing through the column. Each burst of cold takes a time slice of the chromatograph (a product of this cooling is an increase in peak amplitude as the analytes are concentrated on to a small section of the column). The cool zone is then heated and the analytes released onto the second column where analytes separated based on size and affinity of the compounds to the stationary phase

in GC Column 2. On leaving column 2 the compounds travel into the time of flight mass spectrometer, where they are ionised and accelerated towards a detector.

4.4.4. Peak Alignment

The peak tables output from GC x GC analysis section 4.4.3 can have in excess of 2000 analytes of interest (peaks). A peak alignment process is required to determine whether peaks with close retention times are genuinely different compounds, or whether they are merely misaligned due to minor changes between sample runs. A manual comparison of all peaks based on their retention times and mass spectra would be impractical with this number of analytes. Instead peak tables are compared using the R package, R2DGC (Ramaker et al., 2018). R2DGC aligns compound peaks from peak tables output by ChromaTOF. Alignment is based on their 2D retention time index and the mass spectra for each peak and a peak alignment table of matching compounds between samples is generated. Optimization of the processing method and R2DGC was carried out to ensure there was minimal bias. R2DGC uses one or more baseline samples (seed files) to compare the other samples to for alignment. In order to remove bias in this process toward aligning with either the water samples or the soil samples, one of each were selected as the seed files. For a compound to be included in the alignment table generated by R2DGC, it must appear in at least 80% of the peak tables output by ChromaTOF. A number of pairs of samples were trialled as the seed samples, and soil sample 4b paired with groundwater a, resulted in the highest number of aligned peaks between all samples.

4.5. Results

4.5.1. Groundwater pressure and physiochemistry

None of the selected groundwater sampling intervals showed any hydraulic response to nearby lake level changes, either before, during or after the sampling period (Appendix 3). This is typical of almost all boreholes within the GTS. However, some limited connectivity between the surrounding fracture network and Lake Grimsensee exists as one GTS borehole, not sampled in this study, is known to respond to water level changes in Lake Grimsensee, which is located to the South of the GTS.

Groundwater in the GTS is dilute and alkaline, (pH 9.0 – 9.5 in the CAGr and GrGr respectively). Dissolved ion chemistry shows a very slight variation governed by water-rock interactions with the host rock. Groundwater hosted in CAGr has higher Ca^{2+} and lower Na^+ than groundwater in the GrGr which has higher Na^+ and lower Ca^{2+} . Stable isotope measurements show that groundwater is meteoric (Schneeberger et al., 2017). The oxygen isotopic values vary with the depth of individual boreholes below the ground surface (Schneeberger et al., 2017), suggesting a vertical flow path from the surface to the groundwater sample location and little influence of the nearby lake on the groundwater system.

Table 4-1 Groundwater sample locations and their respective physiochemical, major ion stable isotope and tritium and age. *Tritium and stable isotope values from Schneeberger, Mäder and Waber, 2017

	<i>Groundwater Sample Locations</i>						
	a	b	c	d	e	f	g
<i>Temperature °C</i>	12.7	12.1	12.2	11.7	13.4	12.6	12.7
<i>EC uS/cm</i>	77	79	83	69	84	80	76
<i>pH</i>	9.12	8.83	9.04	8.97	9.32	9.23	9.39
<i>Na⁺ mg/l</i>	9.7	8.85	8.83	6.26	8.93	14.66	10.74
<i>Ca²⁺ mg/l</i>	7.07	8.07	7.58	8.98	8.41	4.09	5.36
<i>K⁺ mg/l</i>	0.33	0.27	0.16	0.21	0.22	0.05	0.44
<i>* δ¹⁸O</i>	-12.68	-12.66	-12.68	-12.61	-	-	-12.99
<i>* δH</i>	-89.43	-89.34	-89.44	-88.97	-	-	-92.06
<i>*Tritium (TU)</i>	<0.6	<0.6	<0.6	<0.6	-	-	<0.6
<i>*Inferred</i>	>65	>65	>65	>65	-	-	>65
<i>Age (years)</i>							

4.5.2. Analysis of GCxGC data

Two of the GC x GC chromatographs, for soil sample (5a) and groundwater sample (A), are shown in Figure 4.4. These plot the raw 2D mass spectrometry data (prior to alignment) where high intensity areas are denoted by the colour temperature scale and each high point represents an individual compound peak. Since the same extraction method has been applied to each sample, the same compound in each sample should occupy approximately the same retention time in the both the first (x-axis) and second dimensions (y-axis) and hence will plot at approximately the same location on each chromatograph. Similar compounds or groups of compounds elute along predictable trends in the chromatograph. Changes in carbon number is often expressed by a small change in retention time along the x-axis as larger molecules are retained longer in the first GC column. Different groups of compounds have different affinities to the stationary phase in the second-dimension column causing a separation by compound group in the secondary column. A visual inspection of the two chromatographs in Figure 4.4 shows that each is highly complex with hundreds of peaks in each sample, there are areas of similarity and also clear differences between the two samples. As might be anticipated, the soil sample contains a greater number of organic compounds than the groundwater samples, with higher intensity peaks.

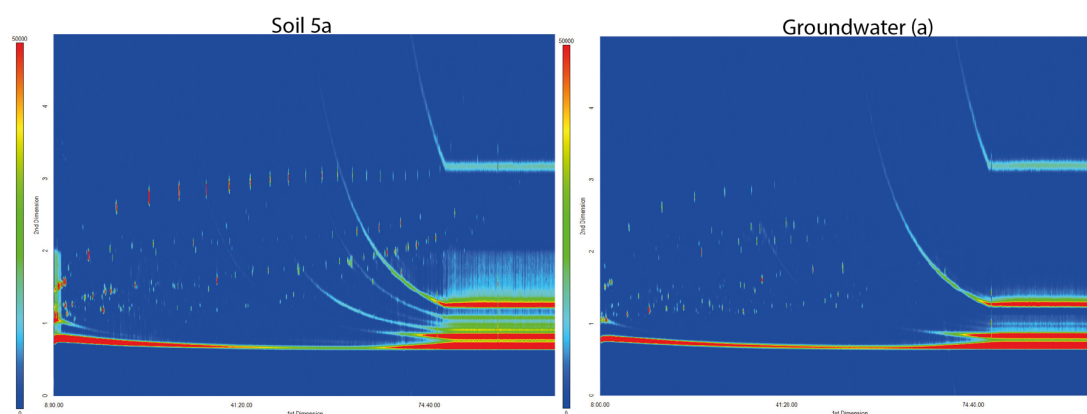


Figure 4.4 GCxGC 2D chromatographs; soil '5a' (left) and groundwater 'g' (right). The x-axis represents the first dimension of separation in column one, y-axis represents the separation of compounds in the shorter second column. Colour temperature reflects the Total Ion Count (TIC) of the Mass Spectrometer. Red is a high TIC and blue is low TIC, Red to light blue dots represent individual compounds. Long coloured streaks parallel to the x-axis are artefacts from the sample matrix and the GC column stationary phases.

228 organic compounds were successfully aligned for all samples (Appendix 2). To allow comparison of the relative concentrations of individual compounds between samples, all samples were then normalised by their total mass i.e. by the total mass of the 228 compounds. Figure 4.5 is a coloured bar plot of the normalized concentration data for all 228 aligned compounds for each sample; the width of each coloured rectangle represents the relative concentration. Comparing samples (Figure 4.4) there are clear similarities and differences. For example, all surface soil samples contain the blue and orange compounds (on the left of

Figure 4.5), as does the lake water (LW), although the LW and site 6 have lower relative concentration of these two compounds, when compared with the rest of the soils. The only groundwater samples which contain both of these compounds are a, d, e and g. Indicating that these samples have a soil-derived surface infiltration source. If we now focus on the grey and brown compounds, making up the majority of surface sample site 6, the only other sample that contains a similar prevalence of these is groundwater sample g. Implying that groundwater g could be derived from infiltration through a riverbed system (site 6). Displaying the data from the alignment tables as colour bars (Figure 4.4) is useful to visually inspect clear similarities and differences between samples and to provide a preliminary verification of results. However, in order to robustly analyse for similarities within the entire dataset, a multivariate analysis is required.

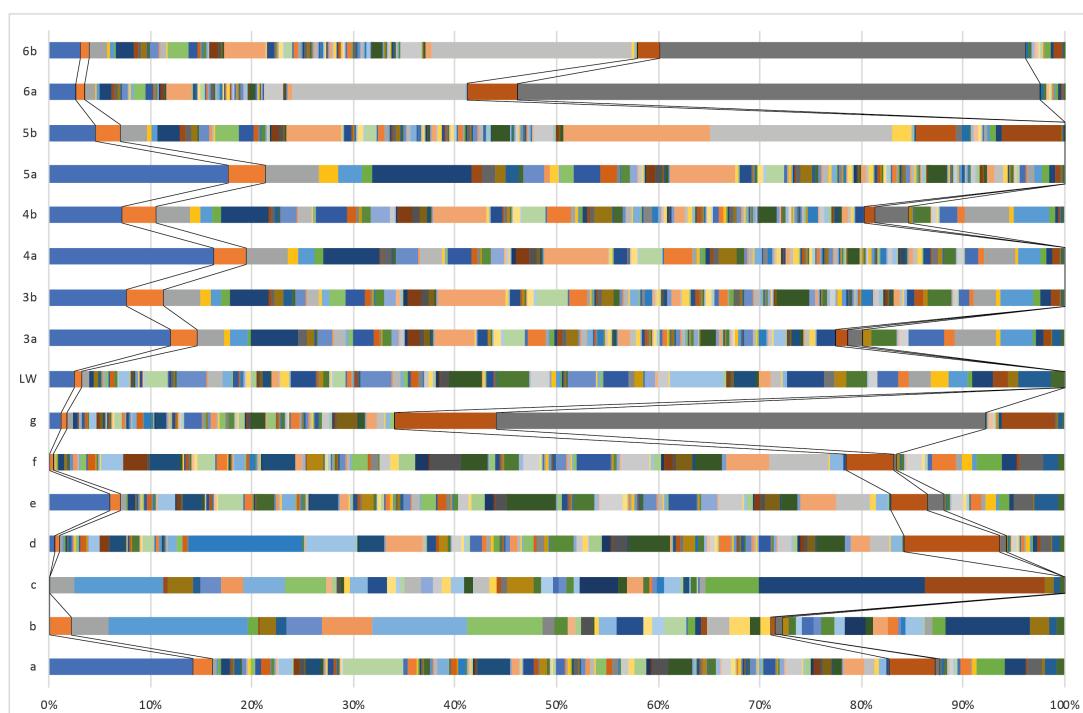


Figure 4.5 Coloured bar plot of the normalized concentration data for all 228 aligned compounds for each sample; each multi-coloured bar represents one sample (labelled right) soil samples '3'-'6', groundwater samples 'a'-'g' and lake water 'LW', the width of each coloured rectangle represents the relative concentration of the organic compound with respect to the total concentration of all 228 compounds presented in the plot. Black lines connect selected matching compounds between samples to display similarities and differences between compound presence.

4.5.3. Principal Component Analysis (PCA)

The relative ratios of each organic compound are taken from the peak alignment table and statistically compared with every other sample using Principal Component Analysis (PCA). PCA of the GC x GC alignment table was carried out using R open source code and is a standard technique employed in the analysis of GC x GC data (McGregor et al., 2012;

Gauchotte-Lindsay et al., 2019). PCA determines a set of orthogonal axes, or components (linear combinations of the relative concentrations of the organic compounds), that explain the greatest variance within the data using the fewest components. The underlying similarity between samples can then be elucidated by displaying the samples as coordinates of the first two, most explanatory, principle components. Samples that plot at similar locations will contain similar combinations (or patterns) of the organic compounds.

PCA was carried out using all 228 explanatory variables (aligned organic compounds) from the peak alignment table (Appendix 2). Analyses used all samples (surface soil, lake and sediment and groundwater) in order to determine whether the different groundwater samples had clearly distinct organic signatures that could be matched to any of the surface organic signatures.

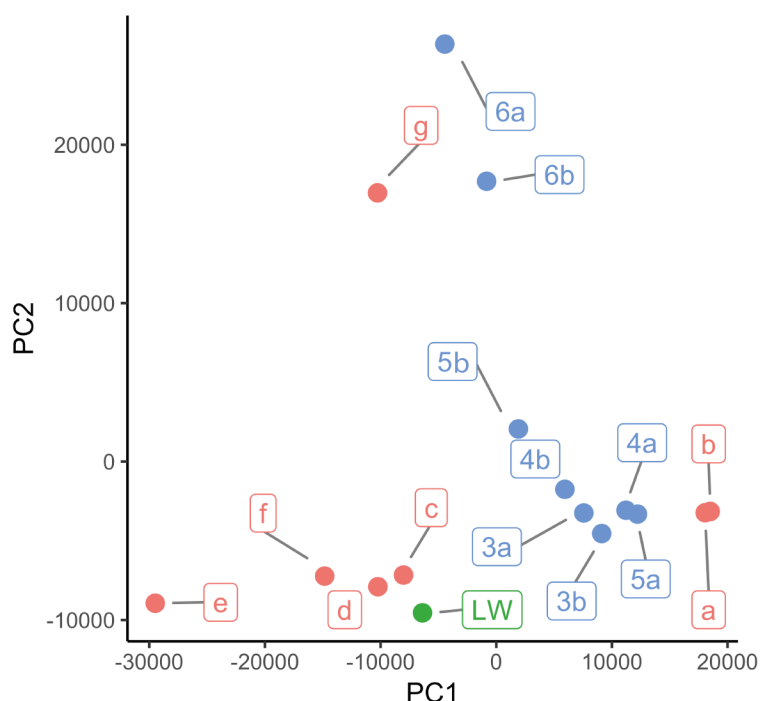


Figure 4.6 Ratio transformed PCA scores plot of all organic sample analysis. All points are labelled with the sample id corresponding to Figure 4.1 and 4.2; soil/sediment (blue), lake (green), groundwater (red). Principal Component 1 (PC1), and Principal Component 2 (PC2).

Results from the PCA are shown in Figure 4.6. Principal component 1 (PC1) explains 64% of the variance and comprises 16 individual compounds and Principal component 2 (PC2) explains 12% of the variance and comprises 145 individual compounds. The lake water (green) plots in a distinctly different location to any of the soil samples (Figure 4.5), indicating it contains different organic signatures. Most soils cluster in the bottom right quadrant of the graph alongside two groundwater samples, **a** and **b**. However, the sediment samples from site 6 (**6a** and **6b**), the river, plot a long way from the other soils, alongside one of the groundwater samples **g**. Site 6 is located in the riverbed, where the river enters lake Räterichsbodensee. The sediment at site 6 was comprised of angular rock particles with no visible organic matter

content, and as such likely reflects the different organic compounds present in the stream water, as well as those in soils that may have been washed down from surface runoff. We could infer from this, that water infiltrating into borehole interval **g** is derived from a riverine source at the surface, as it does not contain a soil or lake signature but plots most closely to the river sediment (Site 6).

Groundwater samples **c**, **d**, and **f** all plot close to the lake water signature and likely derive predominantly from the lake. Whereas groundwater **a** and **b** plot near the main soil cluster (Figure 4.6), indicating they have similar organic signatures to the soils and have originated from surface soil infiltration. Groundwater sample **e** plots at a separate location and appears to have an organic signature that is unique from the rest of the samples.

Interestingly, groundwater samples **a**, **b**, and **c** are all from the same borehole, taken from adjacent isolated intervals. Despite this, they have very different organic signatures, suggesting that the local fracture network is poorly connected.

4.6. Discussion

4.6.1. Why do different groundwaters contain different characteristic signatures - what are we detecting?

Different surface environments are host to different species of flora and fauna. These site-specific organisms die, and decay; meteoric rainfall/runoff dissolves the organic decay products creating a dissolved organic signature, reflecting a specific surface environment. Meteoric water containing this dissolved signature then infiltrates into the groundwater system. At the GTS, groundwater signatures are separated by some specific changes in the major compound functional groups of the individual samples. The first principal component (PC1), which explains 64% of the variance in these samples, is comprised of fatty acid methyl esters (FAMES) and other natural fats. This finding is consistent with research in related fields; FAMES have been used to profile microbial communities (Haack *et al.*, 1994), and a FAMES signature has previously been used by researchers to identify the presence of microbial activity in soils (Ritchie *et al.*, 2000). It is most likely that the differences in FAME composition between samples at the GTS reflect the differing microbial communities within the soils, the river sediment and the lake water.

Amines, esters, alkanolic acids, methyl esters, aromatics and n-alkanes separate along the second principal component at the GTS (PC2). Different amines present in samples likely originate from the breakdown of amino acids in protein chains or from neurotransmitters by released microbes (Skelley *et al.*, 2007) in the soil zone. Alkanes are common in algal marine and terrigenous, bacterial, and vascular plants (Eglinton and Hamilton, 1967; Volkman *et al.*,

1994). Soils are characterised by a higher proportion of n-alkanes, that derive from the decay of vascular plants and bacteria. Alkanoic acids would indicate bacterial organic decay (Cranwell, 1982). At the GTS, PC2 acts to discriminate the organic-poor river-bed sediments and groundwater sample (g), from the other samples.

4.6.2. *How are compounds preserved over time i.e. when and where will this technique work?*

For organic fingerprinting to be an effective groundwater tracing technique at any given site, the surface signatures must be sufficiently well-preserved over time, so as to be identifiable at depth. We know from Konno *et al.*, (2013) that microbial communities exist along fractures in the GTS and in other groundwater systems. Microbial metabolism of the organic components in groundwater will lead to progressive degradation of organic parent molecules over time and, hence, along the groundwater flow paths. The peak alignment process only matches those molecules present in both surface soils/waters and in groundwaters. Degradation of parent molecules will create daughter products, and eventually will result in no parent products remaining in the groundwater; thus, ruling parent molecules out of the PCA analysis. If daughter products are formed along the flow path, but not at the surface, these also will not be usable. Hence, for the technique to be applicable, the timescales for degradation must be such that either the parent or the daughter products (or both) are present both at the surface and at depth. Despite this restriction, specific organic compounds have been found by researchers in related fields, and used as indicators of surface deposition environment (Peters *et al.*, 2004) for petroleum source rocks, for Jurassic age sediments (Korkmaz and Gülbay, 2007).

Microbial degradation may cause a change in the ratio of abundance of different compounds, if different organic compounds are broken down at different rates. Uneven degradation rates of critical compounds may skew the PCA analysis and result in the groundwater plotting as a separate cluster. However, groundwater samples **a**, **b**, **c**, **d**, **f** and **g** all plot near surface samples (Figure 4.6), which must imply one of two things: 1) that degradation processes tend to maintain the concentration ratios of parent-to-daughter compounds or 2) after 50-years (the approximate age of groundwater at the GTS) any compounds that were broken down too rapidly are simply not present in the peak alignment table, hence, do not affect the PCA analysis.

One sample, groundwater sample e has very low concentrations of dissolved organics and does not plot near any of the surface samples collected in this study. Borehole interval e also has an anomalously high flow rate (when compared with the other sampled intervals). If interval e has a more rapid connection to the ground surface, dissolution of some organic compounds into groundwater may not have had time to occur. Alternatively, the differing

organic signature in sample e may be a result of uneven degradation of parent molecules or may simply reflect a differing surface water source that is not captured by our limited number of surface sampling sites.

4.6.3. Are there any sub-surface sources of organic molecules?

The contribution of organics from the granitic host rock at the GTS is considered as negligible, however, if this technique were applied to a sedimentary environment consideration should be taken of the organic input from the host rock. Decay of microbes hosted in fractures will add new organic compounds to the system. However, if the products of this decay are not present at the surface, they will not affect the PCA analysis, since they will be eliminated during peak alignment.

4.6.4. Are the findings consistent with those of other tracers at the GTS?

Stable isotopes indicate that water is meteoric in source (Schneeberger et al., 2017) which is consistent with our findings from the dissolved organics, that groundwater is derived from meteoric infiltration. Infiltration altitude is known to affect water isotopes. Higher altitudes lead to a lighter water isotope signature. The infiltration altitude is approximately 2,000 m for an oxygen isotopic ratio of -13.0 (Schotterer, 2010). The only measured oxygen isotope value for the lake is -14.8, which theoretically corresponds to an altitude of 3,134m, while the Räterichsbodensee only sits at 1767m. However, the lake is part of a regional pump storage hydropower system, so it is likely that this value varies significantly over time and that water within the reservoir is a mixture of meteoric water from the upstream catchment and water pumped up from the reservoir below. The elevation of the ground surface above the GTS is approximately 2100-2300 m from North to South. The elevation rises to 2594m. This corresponds to a range in the rainfall isotope ratio of -12.8 – 13.8. At first sight, these data might lead one to assume that isotopes can be used to discriminate surface infiltration origins. However, at Grimsel Hospice (1,900m), meteoric oxygen isotope signatures in rainwater range from -7 to -20, in an approximately sinusoidal manner over the course of a year (IAEA/WMO, 2020). The average value at the Hospice is ~ -13 and at the time of groundwater sampling (August) the meteoric isotopic ratio was ~ -10. Comparing the range of surface (lake and meteoric) isotope data with the oxygen isotope values in the borehole sampling intervals, all values lie within this range (-14 to -10); in fact, they only vary between -12.61 and -12.99: a-d have oxygen isotopes of $\sim 12.66 \pm 0.05$; g is ~ -12.99 . The age of the groundwater in the GTS, as estimated from tritium data, is > 65 years (Schneeberger, Mäder and Waber, 2017). Hence, considering a ~65-year travel time (from surface to the GTS) diffusion will result in a homogenized isotopic signature representative of the average water isotope ratio that infiltrated into an individual flow pathway.

In summary, the findings from the organic signature data are consistent with the isotope data. It is clear from both the isotopes and the organic signatures that groundwater is meteoric in source. However, the organic signatures are sensitive to the local organic soil infiltration environment, which unlike the surface isotopic signature does not vary significantly over short timescales. Hence, the organic signatures are a useful tool for identifying groundwater derived from differing surface infiltration sources, such as characteristic soils, riverbeds and lakes.

4.7. Summary and Conclusions

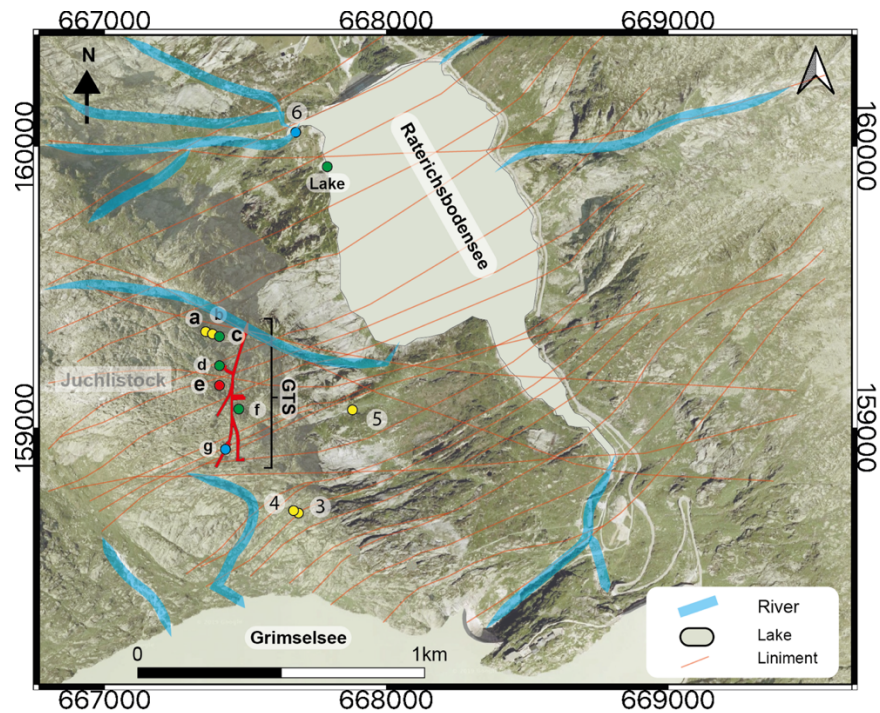


Figure 4.7 Conceptual diagram updated sample location colours reflect the surface water origins as determined by organic signature comparison; green dots (c, d, f and Lake) reflect water samples with lake surface signature, yellow dots (a, b, 3, 4 and 5) are water/soil samples with a soil surface origin, light blue dots (g and 6) are samples localities containing an stream signature (ephemeral and long-lived streams at the surface are highlighted in transparent blue. Liniments are given by red lines (Schneeberger *et al.*, 2016, 2017; Schneeberger, 2017). GTS tunnel exposure is given as a red polygon outlined in black.

The results of this investigation show that the signatures of naturally dissolved organic compounds in groundwater can be a useful, and complementary, tool in hydrogeology to identify different meteoric infiltration sources (Lake, soil and river). The technique can distinguish between different infiltration environments (soils, riverbeds, lake water) and has the potential to distinguish different soil types, although more surface sample sites are required to confirm this. The research demonstrates that individual surface environments have unique, and predictable, organic signatures. The findings for the GTS are summarised in Figure 4.6, with groundwater sampling locations coloured by infiltration origin. Intervals **a** and **b** are

indicative of soil infiltration, **c**, **d** and **f** contain a component of lake water, **e** does not match the signature of any surface sample and likely originates from an unknown 'unsampled' soil type. Finally, sample interval **g** contains an infiltration signature typical of the ephemeral riverbed sediment found at location **6**. Similar riverbed channels, from which the groundwater may have originated, are marked and common above the GTS (Figure 4.7).

5. Temporal Groundwater Change

5.1. Microseismic events cause significant pH drops in Groundwater

Earthquakes can impact hydrogeological systems, inducing changes in rock permeability (Fischer *et al.*, 2017) and groundwater levels (Brodsky *et al.*, 2003), altering isotopic ratios and groundwater chemistry (Claesson *et al.*, 2007), and expelling gases at the surface (Sato *et al.*, 1986). These impacts occur because existing fractures are propagated, and new ones created, that act to “tap” or mix distinctly different groundwater bodies (Skelton *et al.*, 2014). Observations of earthquake-induced hydrogeochemical changes are all from earthquakes of magnitude (ML) greater than 3.5 (Fischer *et al.*, 2017). Effects of microseismicity (ML<2) on groundwater chemistry have not previously been demonstrated. Here we show that microseismic events can cause significant changes in in-situ groundwater pH, of 1 to 3 units. We present observations, taken at the Grimsel Test Site (GTS) in Switzerland, of groundwater pH fluctuations that are concurrent with nearby shallow (< 1 km below ground surface) microearthquakes ML < 1 (and as low as -1.2ML). These pH changes were not accompanied by changes in the water chemistry, and hence cannot be explained by tapping or mixing of other groundwater sources. We conducted experiments to crush granite from the GTS, in the presence of equilibrated groundwater, that produced pH drops with no change to the water chemistry. These drops occur due to the creation of fresh rock surfaces containing silanols and silica radicals (Saruwatari *et al.*, 2004) that, in the absence of oxygen, interact with in situ groundwaters, increasing the relative concentration of H⁺ thus lowering pH. Evidence is emerging that microseismic events are frequent and spatially pervasive (Ross *et al.*, 2017), potentially making microseismically-induced pH drops ubiquitous in the shallow crust. pH exerts a fundamental control on the rate and outcome of most aqueous geochemical reactions. Hence, our findings have significant implications for interpreting evidence of fluid-rock interactions in the geological record.

Fracturing during earthquakes can alter groundwater hydrogeochemistry; post-seismic observations reveal significant changes to the permeability and connectivity of regional flow networks (Brodsky *et al.*, 2003), expressed as increases in gas release rates (CO₂ (Sulem and Famin, 2009; Cappa and Rutqvist, 2012), H₂ (Sato *et al.*, 1986), ²²²Rn and ³He/⁴He (King, Zhang and Zhang, 2006)) and isotope anomalies from the tapping of new groundwater sources (Skelton *et al.*, 2014b; Onda *et al.*, 2018). During larger magnitude events, the creation and propagation of fractures can provide a conduit for the transport and mixing of previously isolated fluids. Observations of earthquake-induced groundwater chemistry changes are all

from events of magnitude (ML) > 3.5 (Fischer et al., 2017). Gas expulsion has been observed for an event of magnitude ML = 3.5 (Fischer et al., 2017). Smaller magnitude (ML < 2) microseismic events have not previously been reported to affect groundwater hydrogeochemistry.

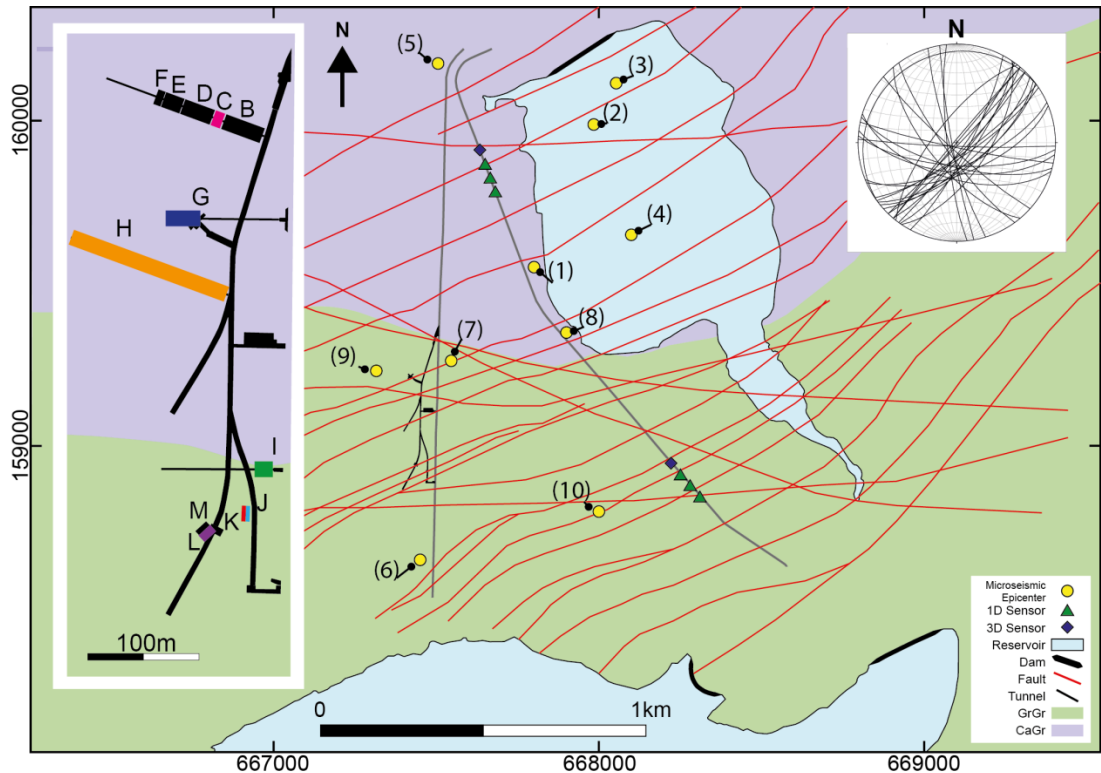


Figure 5.1 Map of the Grimsel Test Site (GTS). Solid red lines are fault traces mapped from surface lineaments (Schneeberger et al., 2017) grey lines represent tunnels including the GTS. Microseismic epicentres are chronologically numbered (yellow circles). The main map shows the lithological contact between Aar Granite (purple) and Grimsel Granodiorite (green) at the surface. The enlarged GTS map (inset left) shows the contact at 1728 m AMSL and the sampled borehole intervals B to K. Intervals with a pH change are coloured to match Fig2. The stereonet shows orientations of open fractures in the GTS (Schneeberger et al., 2017) and other tunnels.

We monitored groundwater chemistry and microseismic activity at the GTS during two periods within which the neighbouring Lake Räterichsboden was drained and refilled (Nov-2014; Feb-2016). The GTS is hosted in fractured Central Aar Granite (CAGr) to the North and Grimsel Granodiorite (GrGr) to the South (Figure 5.1). Stable isotope measurements ($\delta^{18}\text{O}$, δH) confirm a meteoric groundwater source (Schneeberger et al., 2017). Chemical modelling shows groundwater chemistry is in equilibrium with the host rock reflecting localised water-rock interaction (Schneeberger et al., 2017): groundwater from boreholes cutting the CAGr have slightly higher Ca^{2+} and lower Na^+ , Li^+ and Cl^- concentrations than those in the GrGr (Schneeberger, Mäder and Waber, 2017). Groundwater has low electrical conductivity (< 90 μScm^{-1}), temperature range 11.4-17.3°C and pH that reflects the differing host rocks; mean pH is 9.03 and 9.40 in the CAGr and GrGr, respectively.

During lake drainage we took regular water samples from fractures cutting 12 packed borehole intervals (marked B-M, Figure 5.1) in the GTS: Nov-2014 weekly sampling; Feb-2016 daily sampling during drainage, weekly thereafter. Short-term drops in pH were observed (instrument accuracy ± 0.2) in several, but not all, of the borehole intervals (Figure 5.2); drops were on different days for different intervals (each cutting different fractures). In Nov-2014, two of seven borehole intervals (C and H) in the North of the GTS (Figure 5.2) experienced pH drops of 0.56 and 2.09 units respectively, and 4 of 5 Southern intervals were affected; two (J and L) on two occasions. In Feb-2016, similar behaviour was observed, this time in two monitoring intervals, I and K in the South and in one original and three new intervals (C, B, E and G) in the North. Interval 'I' experienced particularly large pH drops: 1.48 units (11/02/16) and 3.31 units (09/03/16). All observed pH drops were short-lived, recovering to background levels by the following sample implying that pH recovers in 24 hours or less.

Microseismicity was recorded by two surface microseismic arrays we had installed 500 m east of the GTS, at an average depth of 120 m below surface. We scanned the 48-hour period preceding each pH drop in Figure 5.2 for nearby microseismic events; the timing of detected events within a 2km radius of the GTS (as determined by the difference between the P-wave and S-wave arrival times) are shown on Figure 5.2. All pH drops are preceded by at least one event. Figure 5.1 shows the epicentres of all those events that were locatable. Events that were not locatable were either not detected by a sufficient number of sensors, or occurred so close to the sensors that the sampling rate was insufficiently high to distinguish the p-wave arrival times between individual sensors. The local magnitudes for the events in Figure 5.1 were between -1.2 ML and 1 ML following the formula suggested in Föh *et al.*, (2011) for local magnitudes in Switzerland. Using Brune's model (Brune, 1970), the estimated slip patch fracture surface areas for these events are 1,300 - 6,350 m². NE-SW and NW-SE striking fracture sets (Schneeberger *et al.*, 2017) have been previously mapped at the ground surface (Figure 5.1), these fractures are of sufficient length to host seismic events of this range in magnitudes and slip-patch surface areas. The same fracture sets are observed cutting the tunnels and boreholes within the GTS (stereonet Figure 5.1). The presence of fracture sets with a wide range of strike orientations suggests that fracture connectivity would be sufficient for groundwater to propagate from the microseismic event locations to the GTS.

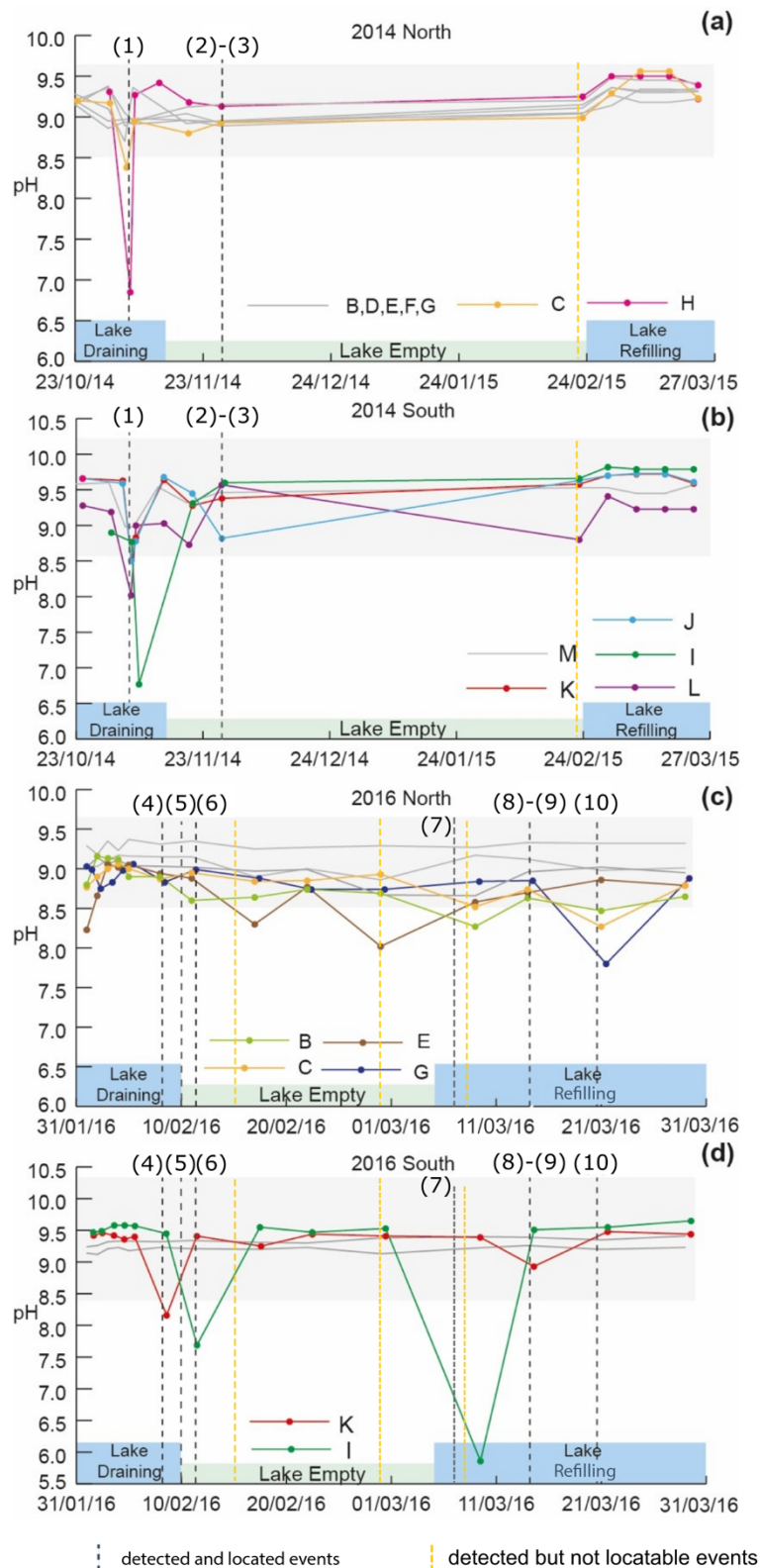


Figure 5.2 Groundwater pH measurements during periods of increased microseismicity due to lake drainage. Lines with markers show pH in borehole intervals coloured to match locations in Figure 5.1. Dark grey lines denote boreholes with no detectable change. Graphs are separated by year and host rock lithology a. and c. come from the Aar Granite whereas b. and d. are sampled in the Grimsel granodiorite. The grey shaded area shows 95 percentiles for background pH. Located microseismic events corresponding to the numbered epicentres in Figure 5.1 are denoted by vertical black lines. Unlocated events are vertical yellow lines.

For larger magnitude seismic events investigated elsewhere (Yeichieli and Bein, 2002), observed hydrogeochemical changes are attributed to 'tapping' and mixing of distinct groundwater bodies by co-seismic fracture network propagation. Documented water body types in the GTS region are groundwater of meteoric origin, surface water (lake and rainwater) and deep thermal waters, each with a distinct geochemistry (Waber *et al.*, 2017). Dissolved ion analyses were performed on all water samples taken during the two drainage and refilling periods. No changes in dissolved ion chemistry associated with the pH drops were observed (Appendix 3), nor were there any detectable changes in groundwater pressure (Appendix 4). Hence, there is no evidence for mixing or 'tapping' of other water sources.

Laboratory studies have shown that fracturing of silica-based rocks leads to the splitting of siloxane bonds: where the electrons are split evenly between the Si and the O, this results in the formation of surface radicals; where the split is such that both electrons are taken by the oxygen, charged Si^+ and SiO^- surface species are formed. In both cases, on reaction with water the surface species form silanol groups, which then dissociate releasing H^+ into solution, lowering the pH and forming hydrogen gas (Section 5.2). Three studies have associated this mechano-chemical reaction with large magnitude earthquakes (Kita *et al.*, 1982; Sato *et al.*, 1986) or subglacial rock comminution (Telling *et al.*, 2015). In these studies, laboratory experiments have been conducted exploring mechano-chemical hydrogen production by crushing rock grains with deionised water (Kameda *et al.*, 2003; Telling *et al.*, 2015). Conditions in these studies are not reflective of the GTS, only one showed that a change in pH also occurs (Kameda *et al.*, 2003).

We conducted three sets of laboratory experiments. First, to explore the effect on pH of the cracked rock surface area, we used a ball mill to crush quartz adding between 1g and 15g of quartz to 40g of synthetic GTS groundwater that had been equilibrated with the rock. We observed in situ pH drops (instrument accuracy ± 0.06), which increased from 0.3 to 0.9 units as the rock-to-groundwater mass ratio increased from 1:40 to 3:8 (Figure 5.3a) i.e. the more grain crushing, the higher the magnitude of the pH drop. Second, to more closely replicate conditions in the GTS at 430m below surface, a single experiment was conducted in the absence of oxygen (i.e. under argon) on 1.25g of crushed granodiorite using 10g of the same synthetic water equilibrated with crushed granodiorite for 2 weeks. This resulted in a pH drop of 1.3 units over a period of 66 hours (Figure 5.3b). Finally, ball mills achieve grain size reduction through ball-grain-mortar impacts that crack grains, and by grain-grain surface abrasion. To investigate the magnitude of mechanochemical reactions without surface abrasion (i.e. from the formation of new fractures) hydraulic press experiments were conducted. In situ fluid pressures between 0.1 to 0.8 GPa were applied in a rigid uniaxial cell

to crack 2g of quartz grains in 2g of synthetic groundwater (ratio of 1:1), producing drops in pH of 0.3 to 0.8 (Figure 5.4). Increasing pressure correlated with a decrease in the final pH.

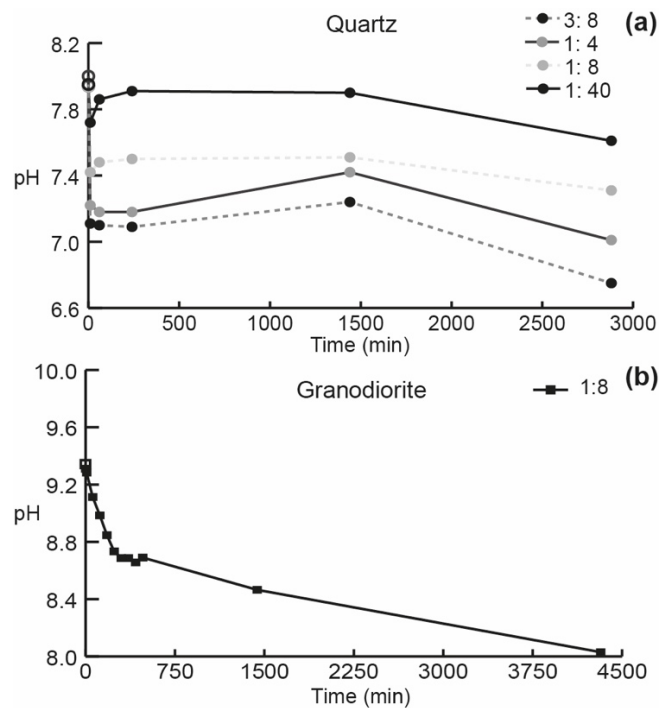


Figure 5.3 Quartz and Granodiorite grain crushing and abrading experiments. Experimental results showing evolution of pH as a result of grain crushing with different mass ratios of rock to water. a. quartz and b. pH evolution with time for granodiorite grains crushed in granodiorite-equilibrated water under an argon atmosphere.

Our experiments demonstrate that mechanical activation of mineral surfaces is a viable mechanism to explain the short-lived pH drops observed in GTS groundwaters. Experiments that vary the ratio of cracked mineral grains to water, imply that for the microseismically-driven pH drops at the GTS to be as large as 1 to 3 units, the abraded surface area during each microseismic event (1,300 - 6,350 m² from the Brune model (Brune, 1970)) must be in contact with a relatively small volume of groundwater. We postulate that at the GTS, a pH drop occurs in the groundwater within the slip patch during each microseismic event, and is then propagated by an in situ pressure rise from the slip event (Pytharouli *et al.*, 2011), through the local fracture network, to the monitoring boreholes. The variability in pH measurements between individual boreholes, and indeed between adjacent monitoring intervals in the same borehole, implies that whilst regionally connected, individual fractures are locally hydraulically isolated from each other, as is common in fracture-dominated flow systems (Birgersson *et al.*, 1993). This focussing of groundwater flow within a few individual channels will tend to preserve the pH peaks, rather than rapidly disperse them.

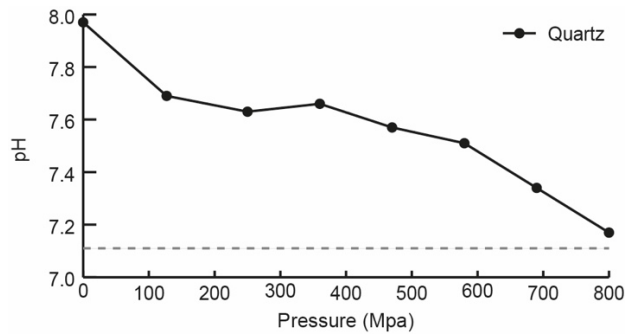


Figure 5.4 Effect on pH of hydrostatic grain fracturing at increasing pressures. Hydrostatic fracturing of quartz sand grains in the same synthetic groundwater solution used in Figure 3a shows increasing pH change with pressure. Measurements of pH taken 10 minutes after uniaxial cell reaches the desired pressure. Dashed grey line shows the pH evolution for ball-mill-crushed Quartz (Figure 3a) after 10 minutes for a rock to water mass ratio of 3:8.

To determine how common microseismically-driven pH events might be, we consider the frequency of microseismic events. The standard Gutenberg-Richter frequency-magnitude distribution (GRF, Gutenberg and Richter, 1994) predicts that event frequency should logarithmically increase with decreasing event magnitude. Microseismic event frequency is rarely quantified, since magnitude 2 is less than the complete magnitude (M_c) threshold (detection threshold) of most permanent seismic networks. However, one study shows that the GRF remains applicable for small events (Abercrombie and Brune, 1994) and, by implication that microseismic events are very common on geological timescales. For example, the GRF would predict over 17 million earthquakes of magnitude -1 or above per thousand years in the UK, which is tectonically quiet, and over 2 billion in Switzerland, all with slip patches $> 1200\text{m}^2$ in area. Hence, localised temporal pH drops within groundwater may be common, particularly with respect to geological timescales.

Frequent significant changes to pH, even if short-lived, could radically alter our interpretation of common geological observations. For example, alteration halos around fractures are commonplace and are interpreted as being due to fluid influx with differing chemical composition (e.g. hydrothermal (Ogata *et al.*, 2014), hydrocarbon (Eichhubl *et al.*, 2009) or CO_2 -rich (Dockrill and Shipton, 2010) groundwaters). This may not always be the case. A temporal drop in pH implies a relative increase in the number of hydrogen ions in solution. Hydrogen ions react with minerals by hydrolysis (Helgeson *et al.*, 1984) which can remove metal ions from minerals in the surrounding rock, releasing them into solution. Hydrolysis would alter the rock composition (Helgeson *et al.*, 1984) surrounding the fracture and potentially mobilise the metals to be transported and precipitated elsewhere. Hence, microseismically-driven mechanochemical reactions have the potential to form alteration halos and mobilise metals without requiring a fluid influx with differing chemical composition to the system. This is just one example. pH exerts a fundamental control on the rate and outcome of most aqueous geochemical reactions. Hence, microseismically-driven pH drops could have

significant implications for interpreting evidence of fluid-rock interactions in the geological record.

5.2. Methods

5.2.1. Microseismic monitoring system

We installed two short-period microseismic arrays in the Gerstenegg tunnel which is located 500 m east of the GTS and has an average elevation of 1730 m ASL. Each microseismic array consisted of one 3-component and three vertical-component 1 Hz seismometers. The flat response of all seismometers is between 1 Hz and 100 Hz. The sampling rate was 250 Hz and recordings were taken continuously between November 2014 – August 2017.

The arrays were synchronised using GPS, with the GPS antenna installed outside the Gerstenegg tunnel. The GPS signal was transmitted distances of up to 2km via fibre optic cables. Data were streamed, at near real-time, to the University of Strathclyde in Glasgow.

5.2.2. Microseismic event selection

Microseismic event selection was targeted to 48 hours prior to the time of each recorded significant pH drop. In total, ten events were located (three in 2014 and seven in 2016).

Prior to undertaking visual inspection of the recordings they were filtered to remove anthropogenic noise. This was undertaken using a high-pass, 2nd order, bidirectional Butterworth filter with a cut-off frequency of 10 Hz. Specific noise at 50Hz, associated with an AC electric power supply, was removed using a band-stop, 2nd order, bidirectional Butterworth filter at between 48 Hz and 52 Hz.

Only those microseismic events that satisfied all of the criteria listed below are presented in this work:

- The event should have had an impulsive P arrival
- The event should be 'locatable', i.e. have been detected by either all channels of the 3D seismometer of the array, or by four different seismometers, with arrival times that differ by at least one sample point (4 msec),
- The time difference between P and S wave arrival times is a maximum of 0.3 sec. This time has been defined based on the area of interest, defined as a 2km radius, around the GTS. The P-wave and S-wave velocities were estimated using a nearby event (approximately 2 km away) from the Swiss catalogue. This resulted in a velocity for $V_p = 4.5$ km/sec and a S-wave velocity of $V_s = 2.64$ km/s for the GTS area. These

values are within the reported range of wave velocities for typical granites (Bourbie *et al.*, 1992). A typical value for the difference between the S and P wave arrival times for a 2 km radial distance is equal to 0.3 sec. Microseismic events with longer S-P times were assumed to have occurred beyond this 2 km boundary, and hence are unlikely to have caused the observed changes in the pH.

Ten events were detected that satisfied the above selection criteria, these fall into the one of the three main categories:

- (1) Events detected by all four seismometers of the North array only and located using P and S arrivals from all four seismometers of the array (event no (1), (4)-(8) in Figure 1). These events had very short durations, less than 0.5 sec. They were typically part of a 'sequence' of short duration events (rather than an isolated event) which occurred within less than 1 sec of each other with the total sequence lasting up to 13 seconds. On 5/11/2014, these 'sequences' of microearthquakes appear over whole hours, e.g. 13:00 – 14:00, and 15:00 – 17:00 UTC (Coordinated Universal Time).
- (2) Events detected by, and located using, the P and S arrivals from all seismometers of the North and South array (event no (9) – (10), Figure 1).
- (3) Events detected by the North array for which picking of arrival times was not possible at the different seismometers. For these events (no (2) and (3) in Figure 1), the location was based on the recordings of the 3D seismometer only (single station location, see section on event hypocentral determination below).

5.2.3. Selected microseismic event hypocentral determination

Microseismic events were located based on a modified version of the grid search algorithm proposed by Stiros and Saltogianni, 2014. This algorithm only solves for the hypocentral location, not the origin time.

The origin time was estimated by the Wadati plots using the P arrival and S-P times. For those events recorded on the 3D seismometers only, the single station location method (Havskov and Schweitzer, 2002) was applied for the estimation of their location.

Location errors vary depending on the location method used. For the grid search method, the algorithm resulted in a root mean square (RMS) of less than 50 m.

The errors for the distance depend on the errors of the picking of the P phase arrival times, which were within 2 sampling points i.e. ± 0.008 sec. For a P wave velocity equal to $V_p = 4.5$ km/sec and a maximum distance between seismometer and epicentre of 1 km, these errors translate to a maximum epicentral distance error of approximately 270 m.

A varying V_p/V_s ratio was found using the arrival times of P and S phases for the events that were detected by at least 4 seismometers. These variations were within 2% of the range of values of $V_p/V_s = [1.65 - 1.7]$.

5.2.4. *Selected microseismic event local magnitude and source dimensions estimation*

Local magnitudes for these events were calculated based on the local magnitude relationship for Switzerland as suggested by (Fäh *et al.*, 2011). The local magnitudes ranged between -1.2 and 1.04.

The source dimensions were based on the methodology suggested by (Brune, 1970). Corner frequencies for events 1-8 were within the range 13 and 20 Hz, while events 9-10 had corner frequencies 96 and 100Hz, respectively. These corner frequencies correspond to rupture patches of radii between 21 and 38 m for events 1-8 and 8 and 9m for events 9-10.

5.2.5. *Groundwater Sampling*

Groundwater was sampled from thirteen intervals from within seven boreholes. The boreholes were selected to isolate different structural features, flow rates, lithologies and to give good spatial coverage across the test site.

Packers were installed in the boreholes in ~1980, with the packers positioned near to the borehole opening. The packer system allows water volumes to be sampled from each interval via independent flow lines. Each borehole generally has three lines exiting for each interval, (i) hydraulic packer line, (ii) interval line with piezometer and pressure transducer attached and (iii) flow line for sample extraction, each being labelled accordingly.

Digital pressure monitoring was measured across the borehole intervals of interest.

Real time pressure monitoring occurred in each borehole, with monitoring and logging undertaken every 15 minutes. For geochemical sampling, the interval was emptied, then allowed to refill, after which time samples were taken (so as to ensure that geochemical signals were not diluted by the relatively large volume of the borehole interval). This process significantly disturbs the local groundwater pressure, which then takes several hours to recover prior to the next sample being taken. Consequently, pressure monitoring could not be used to record ambient groundwater pressure.

Flow rate, pH (± 0.2 units), Eh (± 20 mV), conductivity ($\pm 1\%$ of reading), temperature (± 0.1 °C) and Dissolved oxygen (DO) ($\pm 1\%$ of reading) were measured within a flow-through cell located at the borehole headworks. These physicochemical parameters were logged every 30 seconds using a YSI Pro Plus Multi meter which was calibrated daily. Calibration for

physiochemical parameters was carried out using reference standards. Three-point calibration for pH (pH 4.00 (± 0.01), 7.00 (± 0.01), 10.00 (± 0.01)) using Reagecon buffer solution. Eh and conductivity used a one-point calibration using 250mV (± 5 mV) and 84 μ S/cm ($\pm 1\%$) Reagecon calibration solutions respectively, DO used a one-point calibration of 100% saturated air and water. Readings were only recorded once values had stabilized for each of the parameters recorded.

The physicochemical properties of the surface water (river / lake) were measured using the YSI meter with the probe submerged below the surface. Measurements were recorded after the readings had stabilized, which was typically in around 15 minutes.

Water samples were collected into labelled HDPE 50 ml plastic centrifuge tubes. Depending on the analysis required, samples were either filtered using a 4 μ m cellulose acetate filter (anions), filtered and acidified (cations) with HNO₃ (concentrated nitric acid), or unfiltered (alkalinity). All centrifuge tubes were sealed with tape and stored at +4 °C until appropriate testing could be carried out.

5.2.6. Alkalinity determination

The concentration of alkalinity in water samples deteriorates following collection due to the in-gassing / outgassing of CO₂. Alkalinity was recorded on site at the GTS laboratory using an alkalinity test kit (AL-DT, Hach). An unfiltered sample was titrated against 0.0016 N sulfuric acid using a hand held digital titrator. A combination of two indicators were used (phenolphthalein and bromocresol green/methyl red) in order to determine the specific type of alkalinity present in the sample (i.e. carbonate and/or bicarbonate).

5.2.7. Laboratory Determinants

Anion analysis (Br⁻, Cl⁻, F⁻, NO₂⁻, NO₃⁻, PO₃³⁻, SO₄²⁻) was undertaken using a Metrohm 850 Professional Ion Chromatograph fitted with a Metrosep A Supp 5 – 150/4.0 column with a sodium carbonate/sodium hydrogen carbonate eluent. Calibration was performed using a 7-point calibration, standards were prepared from stock 10000 mg/l solutions of certified reference material (CRM) TraceCERT® diluted by 18.2 M Ω -cm ultrapure water. Quantification limits for each analyte are as follows: Cl⁻/F⁻/SO₄²⁻ – 0.01 mg/l, Br⁻/NO₂⁻/NO₃⁻/PO₃³⁻ – 0.1 mg/l. The eluents, acid solutions, chemical standards, water and acid rinses were prepared using analytical grade reagents. For all analytical analysis degassed Ultra pure water (18.2 m Ω /cm) was used.

The concentration of dissolved metals and silica in solutions (Al³⁺, Ba²⁺, Ca²⁺, Fe_{tot}, K⁺, Li⁺, Mg²⁺, Mn²⁺, Na⁺, Sr⁺, Si_{dissolved}) was determined by ICP-OES (inductively coupled plasma optical emission spectroscopy) using iCAP 6000 Series ICP-OES (ThermoFisher). Calibration was performed using 3-point calibration. Calibration standards were prepared from a stock

solution 10000 mg/l solution in HNO₃ 2-3% (CRM) Centipur® diluted by 18.2 MΩ-cm ultrapure water. The matrix matched to the acidified sample. Quantification limits for each analyte are as follows: Al³⁺/Ba²⁺/Fe_{tot} /Mg²⁺/Mn²⁺/Li⁺/Sr⁺ -- 0.001 mg/l, K⁺ -- 0.097 mg/l, Na⁺ -- 0.052 mg/l, Si_{dissolved} – 0.003 mg/l, Ca²⁺ -- 0.52 mg/l.

5.2.8. Experiments

The following experiments were undertaken to determine the effects of grain crushing, in the presence of water, on pH:

- Experiment (1) - Investigated the effect of the sand: water ratio on the evolution of pH over time
- Experiment (2) - Examined the effect of Grimsel Granodiorite on equilibrated synthetic groundwater
- Experiment (3) - Investigated the effect of the mechanism of grain fracturing on the evolution of pH

The experimental methodologies used are outlined below:

- Experiment 1 – A series of experiments were conducted using quartz sand, of 125 – 500 μm diameter grain size, which was washed with deionised water and dried at 100°C for 24h's. 30g of Sand was crushed using a Retsch PM100 planetary agate ball mill for 30 minutes at 100 rpm. Crushed sand fractions of 15, 10, 5, and 1g were added to 50ml HDPE centrifuge tubes to which 40g of synthetic water was also added (composition of Ca²⁺= 6.93, K⁺= 7.09, Mg²⁺= 0.24, Na⁺= 32.7, Si = 6.14, Cl⁻=41.7, F⁻=0.34 mg/l). The pH of the initial solution was recorded using a Jenway 3510 pH meter, subsequent pH readings were taken at 10, 60, 240, 1440, 2880 minutes after the initial reading. Once a pH meter reading (error ± 0.06 unit) was taken the centrifuge tube was sacrificed to ensure no atmospheric CO₂ in-gassing effected the pH of the rock water solution. A control of uncrushed quartz sand was measured and treated in the same way as the crushed samples.
- Experiment 2 - a limited volume of GTS granodiorite was available, and a single rock water mass ratio test was performed within an argon atmosphere. The granodiorite was prepared by crushing, washing in deionised water, drying at 100°C for 24h and sieving to extract the 125-500μm granodiorite sand fraction. 1.25g of the resulting granodiorite sand was placed in a pestle and mortar inside a glove-bag that was filled and continually flushed for the entirety of the experiment with argon gas. The experiment used a synthetic water that had equilibrated with Grimsel granodiorite fines (< 63μm) in an end-over-end shaker. The fines were equilibrated over a 3-week period using a fines-to-water mass ratio of 1:10. The granodiorite equilibrated solution was filtered through 0.2 μm cellulose acetate filter, and 10g of the filtered solution was added to the pestle containing the granodiorite sand.

The initial pH of the sand water solution was measured. The granodiorite sand was then crushed in the pestle and mortar under the argon atmosphere for 2 minutes. Subsequent pH measurements (error ± 0.06 unit) were then taken at 1 minute, 10 minutes, and 1, 2, 3, 4, 5, 6, 7, 8, 24 and 48 hours after crushing.

- Experiment 3 - Experiments were conducted using a hydraulic press which fractures mineral grains by increasing hydrostatic pressure (Hutchison *et al.*, 2015). A series of experiments were conducted from atmospheric pressures to 0.8 GPa using 2g of quartz sand to 2g of synthetic water (using the quartz sand from Experiment 1). Samples were placed into a PTFE capsule, with the full volume taken up by the 2g of sand and 2g of liquid. The capsule was sealed with a PTFE cap and PTFE tape. The capsule was then placed in a BERYLCO-25 alloy uniaxial pressure cell. Pressures were generated inside the cell by a hydraulic press and load frame. Samples were then loaded to the desired pressure (0.1, 0.2, 0.3, 0.4, 0.5, 0.6, 0.7 and 0.8 GPa) held at the desired pressure for 10 minutes, then unloaded from the cell and pH measurements are taken 10 minutes after the maximum pressure was attained, and the sample recovered.

5.2.9. Geochemical Modelling

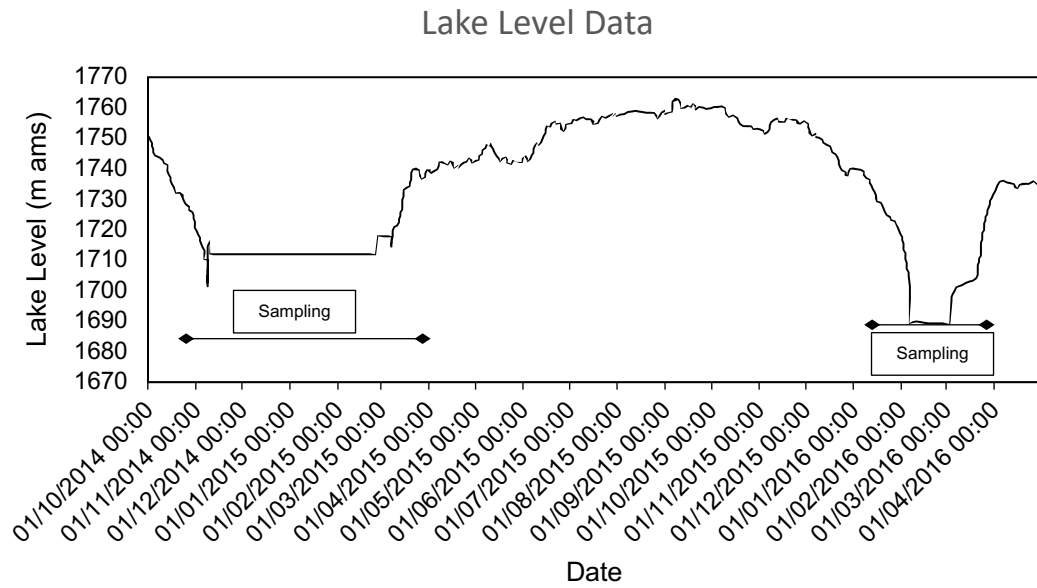
Geochemical speciation modelling was carried out using PHREEQC thermodynamic modelling software (Parkhurst and Appelo, 2013). Geochemical modelling was conducted using the samples collected from each borehole interval. Speciation and saturation indices were calculated for each sample.

Findings of the modelling showed that major minerals, making up the host rock lithology within the Grimsel Test Site, are over saturated, at saturation, or very close to saturation, which indicates that groundwater does reach equilibrium with the host rock.

5.3. Supplementary Information

5.3.1. Supplementary Figures

Lake level data has been recorded in Lake Räterichsboden and is displayed below. The timing of the two geochemical sampling periods is indicated. *ams (above mean sea level)



5.3.2. Supplementary Table(s)

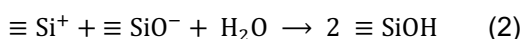
Table 5-1 Table of saturation index from groundwater modelling in PHREEQC(Parkhurst and Appelo, 2013).

Saturation Index Range For Each Borehole Interval											
Borehole	Lithology	Calcite	Kaolinite	K-feldspar	Illite	CO2(g)	Quartz	Albite	Anorthite	Clinochlore-14A	Fe(OH)3
B	CaGr	-0.273 to -1.095	4.019 to 2.042	0.977 to 0.027	2.941 to 0.822	-4.070 to -5.000	0.169 to 0.130	-0.187 to -1.120	-3.509 to -5.549	-3.014 to -12.341	0.173 to -2.195
C	CaGr	-0.300 to -1.070	2.843 to 1.539	0.776 to 0.142	1.908 to 0.717	-4.059 to -4.877	0.170 to 0.123	-0.656 to -1.285	-4.182 to -5.546	-4.840 to -13.059	-0.781 to -2.218
D	CaGr	-0.237 to -0.653	2.748 to 1.790	0.800 to -0.316	1.962 to 0.816	-4.426 to -4.983	0.137 to 0.110	-0.495 to -1.007	-3.949 to -4.984	-4.382 to -9.403	-0.782 to -2.120
E	CaGr	-0.239 to -1.331	5.454 to 2.016	1.713 to 0.047	4.825 to 1.066	-3.667 to -4.843	0.181 to 0.124	0.216 to -1.003	-2.739 to -5.011	-4.442 to -14.829	0.463 to -2.254
F	CaGr	-0.243 to -0.587	2.888 to 2.028	1.286 to 0.779	2.485 to 1.736	-4.650 to -5.011	0.165 to 0.118	-0.325 to -0.635	-3.894 to -4.408	-3.275 to -6.407	-0.654 to -2.150
G	CaGr	-0.252 to -1.446	4.939 to 2.707	1.118 to 0.672	3.483 to 2.088	-3.561 to -4.878	0.122 to 0.085	-0.575 to -0.831	-3.655 to -4.128	-3.358 to -14.047	-0.641 to -2.095
H	CaGr	-0.023 to -0.311	2.237 to 1.326	0.867 to 0.400	1.894 to 0.901	-5.022 to -5.323	0.106 to 0.073	-0.577 to -0.941	-3.924 to -4.667	-2.367 to -4.398	-0.753 to -2.216
I	GrGr	-0.162 to -3.742	2.023 to -5.163	0.931 to -6.227	1.893 to -10.453	-1.668 to -5.778	0.188 to 0.063	-0.208 to -7.223	-3.891 to -18.340	-0.113 to -47.422	-0.566 to -3.308
K	GrGr	-0.157 to -1.384	5.586 to 1.729	2.009 to 0.999	5.065 to 1.685	-4.000 to -5.547	0.192 to 0.075	0.351 to -0.509	-2.904 to -4.205	2.128 to -7.884	-0.046 to -2.260
L	GrGr	-0.156 to -1.571	2.219 to 0.739	0.848 to 0.102	1.907 to 0.250	-4.916 to -6.450	-0.029 to -0.072	-0.776 to -1.403	-4.072 to -5.440	-2.460 to -4.357	0.513 to -1.054
M	GrGr	-0.176 to -0.438	2.139 to 1.151	1.212 to 0.723	2.064 to 0.952	-5.099 to -5.331	0.128 to 0.073	-0.416 to -0.873	-4.140 to -4.890	-2.831 to -4.440	-0.974 to -2.232

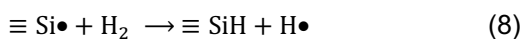
Average Saturation Index For Each Borehole Interval											
Borehole	Lithology	Calcite	Kaolinite	K-feldspar	Illite	CO2(g)	Quartz	Albite	Anorthite	Clinochlore-14A	Fe(OH)3
B	CaGr	-0.660	2.800	0.600	1.950	-4.564	0.153	-0.575	-4.400	-8.762	-1.481
C	CaGr	-0.546	2.241	0.532	1.492	-4.615	0.140	-0.912	-4.793	-8.167	-134.615
D	CaGr	-0.410	2.173	0.420	1.467	-4.785	0.124	-0.793	-4.554	-6.263	-1.567
E	CaGr	-0.638	2.871	0.628	2.062	-4.439	0.145	-0.703	-4.430	-7.987	-1.451
F	CaGr	-0.358	2.426	1.046	2.118	-4.884	0.147	-0.489	-4.152	-4.741	-1.580
G	CaGr	-0.504	3.102	0.837	2.488	-4.622	0.097	-0.698	-3.883	-5.714	-1.554
H	CaGr	-0.095	1.700	0.633	1.365	-5.165	0.086	-0.773	-4.332	-3.315	-1.674
I	GrGr	-0.551	0.962	-0.149	0.167	-5.272	0.088	-0.940	-5.419	-6.088	-1.608
K	GrGr	-0.337	2.595	1.405	2.643	-5.202	0.109	-0.108	-3.643	-1.308	-0.952
L	GrGr	-0.344	1.837	0.569	1.442	-5.125	-0.045	-0.959	-4.476	-3.323	-0.369
M	GrGr	-0.265	1.620	0.961	1.489	-5.229	0.098	-0.665	-4.519	-3.477	-1.702

5.3.3. Supplementary Equations

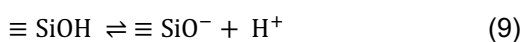
Silica radical reaction with water



Subsequent radical reactions



Silanol dissociation



Equation 1a and 1b (Saruwatari et al., 2004) show how silicon and siloxane radicals from homolytic cleavage of silica-oxygen covalent bonds produce surface silanols, as well as hydrogen and hydroxide radicals. The combination of hydroxide radicals (5) (Tranter, 2015) results in the production of hydrogen peroxide and the combination of hydrogen radicals produces hydrogen gas (4) in solution (Kita et al., 1982; Telling *et al.*, 2015). Hydrogen radicals (6) and hydroxide radicals (7) (Tranter, 2015) can also neutralise surface siloxane and silica radicals respectively. Equations 1, 2, 3, 6 and 7 all form a surface silanol species which dissociates to add H⁺ into solution following reaction 9 and, under rare occasions with very low pH, hydrogen ions form from the dissociation of $\equiv\text{SiOH}_2^+$ (Saruwatari et al., 2004). Hydrogen gas produced from equation 4 can subsequently further react with surface silica radicals to produce hydrogen radicals (8).

Equation 2 shows how heterolytic cleavage produces positively charged silica and negatively charged oxygen surface species, which both react with in situ water to form surface silanol species, which undergo the reactions outlined in 9 to dissociate and release hydrogen ions (Saruwatari et al., 2004).

6. Discussion and Conclusions

Conceptual models of hydrogeology and hydrogeochemistry enhance our understanding of how water interacts with the surface and subsurface. These models provide the base concept and appropriate boundary conditions for detailed numerical models of groundwater flow and water rock interactions. This chapter takes the findings of Chapters 3, 4, and 5 as well as previous site investigations at the GTS to produce a conceptual understanding of groundwater chemical evolution and flow. The chapter explores how lake level change affects the conceptual model. Finally, the chapter assesses the use of lake draining experiments as an analogue for glacial perturbation of the subsurface with respect to hydrogeology and geochemistry.

6.1. Spatial Hydrogeochemical Model of the GTS

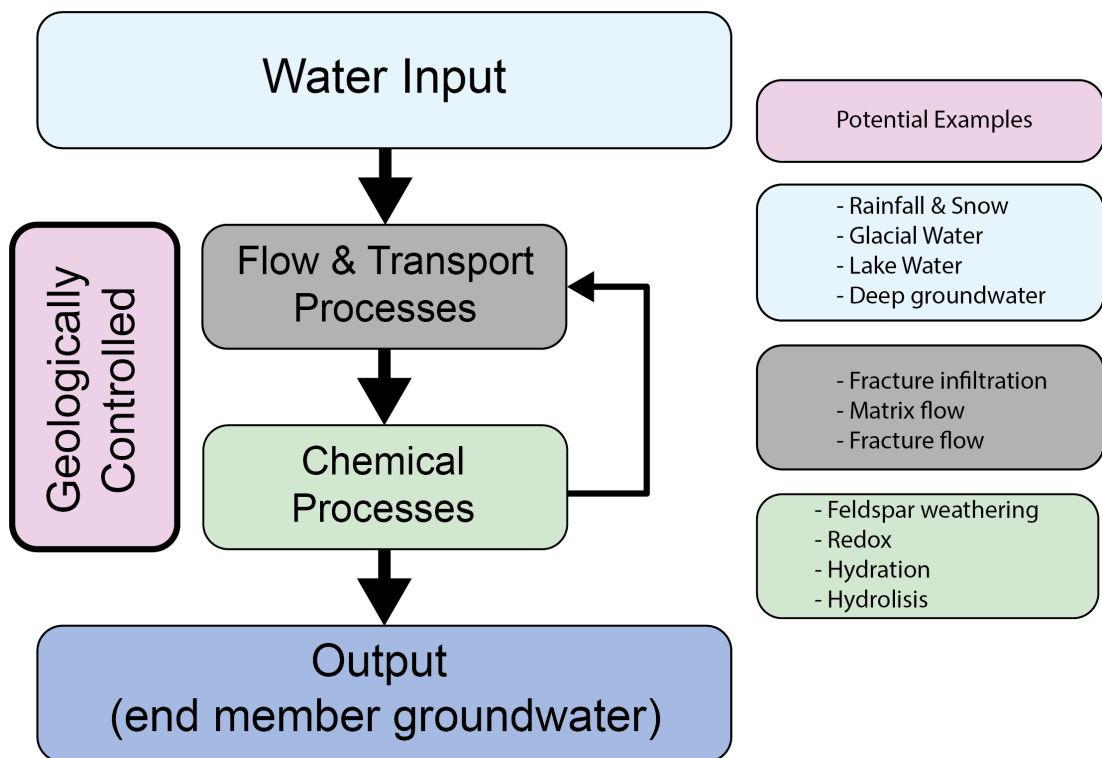


Figure 6.1 Flow diagram for the different factors involved in the hydrogeochemical model of the GTS.

The conceptual model for the hydrogeological conditions at the GTS can be separated into four different components (Figure 6.1). Each component has strong geological controls. These components are inputs to the hydrogeological system; processes of water transport; water-rock interaction processes and the final range of hydrogeological observations within the GTS. By examining the hydrogeological system in these component parts, the system as a whole becomes easier to understand and model numerically.

Development of the initial conceptual model for the GTS requires constraints on the end member groundwaters and surface water inputs into the system. Chapter 3 outlines the end member groundwater composition as type Ca-Na-HCO₃ and Na-Ca-HCO₃ in the North and south of the GTS respectively.

6.1.1. Input

Historic studies at the GTS have shown water input into the GTS is from infiltrating meteoric water (Keusen et al., 1989; Schneeberger et al., 2017). Chapter 3 shows there is very little evidence from major and minor dissolved ion chemistry to distinguish the location of meteoric water recharge, entering the groundwater system. Schneeberger et al., 2017 use groundwater isotopic evidence as a justification for removing lake water and glacial melt infiltration as meteoric water sources. Groundwater isotopic ratios correspond with the predicted isotopic ratio from meteoric water infiltrating directly above the GTS. This hypothesis makes the assumption that the $\delta^{18}\text{O}$ and δD of precipitation has remained at the same constant average ratio for the past ~50 years the estimated groundwater residence time from Schneeberger et al., (2017). Monthly isotopic data from the Grimsel GNIP station (IAEA/WMO, 2020) shows isotope precipitation values in the Grimsel valley at the same altitude vary annually over a 46-year sampling period. Precipitation is more negative $\delta^{18}\text{O}$ in winter months and more positive in summer months. Changes to meteoric isotopic ratio is a result of changes in the average monthly temperature, the mean value over the full year, however, remains at a $\delta^{18}\text{O}$ of -13.61 ‰. The altitude infiltration hypothesis (Schneeberger et al., 2017) assumes that only direct infiltration at altitudes above the GTS can result in the isotopic ratio observed in the groundwater samples. However, isotopic data from lake water and surface runoff (Chapter 3) indicate that mixing of water sources within lake water, glacial meltwater and surface runoff can result in $\delta^{18}\text{O}$ comparable to the groundwater isotopic measurements. Stable isotopes may not be able to identify precise water infiltration locations; however, they do give an indication of mean infiltration altitude and, hence, suggest there is no contribution from deep old or hydrothermal groundwaters.

Evidence from the organic fingerprinting of groundwater in Chapter 4 indicates multiple meteoric water sources at the surface. While not all boreholes are measured for organic analysis in Chapter 4, it is clear that groundwater in the GTS derives from both lake water and

direct infiltration through the soil zone. Stillings et al (Chapter 4) shows that free-draining granite sand-rich soils have a different organic fingerprint to other more organic-rich non-free draining soils. Further, by comparing the organic fingerprints found within groundwater samples from the GTS, it can be shown that groundwaters mostly derive from lake water and from surface sites with organic-rich soils, however, one borehole is fed by infiltrating water from a low-organic content, free-draining soil.

Figure 6.2 indicates the different potential meteoric water inputs into the GTS groundwater system. Precipitation is the key source of water input into the GTS; however, the surface sites for infiltration are different. The historic GTS literature indicates infiltration derives from ground surface directly above the GTS site, which is characterised by high altitudes and soils with a low organic content. Instead, the evidence from organic fingerprinting supports infiltration occurring from two or three soil types. These are:

- Dark water logged soils (most common)
- Light coloured free draining, high granitic sand content soils (only found in one sample site)
- Free draining fast infiltration areas with little-to-no surface soil (only found in one sample)

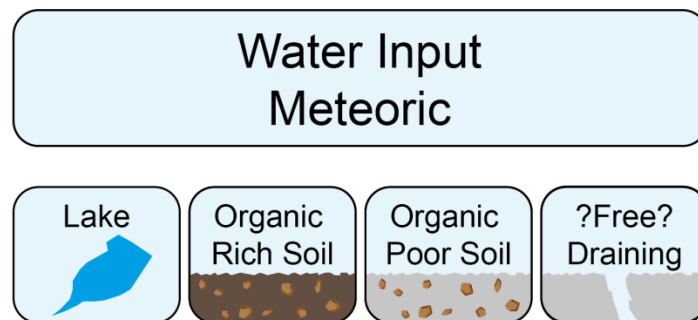


Figure 6.2 Schematic diagram building on Figure 6.1 adding the potential water inputs into the GTS groundwater system. Including Lake water, organic poor and rich soils and infiltration with no soil zone. Water origin is meteoric in source i.e. precipitation as rain or snow.

It is clear that water input to the GTS is complex and, that flow regimes will be influenced by the construction of the underground tunnels due to the presence of atmospheric pressure within the tunnel system. To demonstrate the underpinning for the conceptual hydrogeological model, the following text and diagrams sequentially build up the individual component parts of the systems. The conceptual model is finalised as a diagram in Figure 6.4 and displayed as a 3D representation of the GTS and its surroundings in Figure 6.5 and 6.6.

6.1.2. Infiltration and Water transport processes

Meteoric water infiltrates at the surface and then flows through the subsurface. Runoff is the main transport process at the surface, whereas fracture flow is dominant in the subsurface,

particularly in granitic rocks. Water may also flow along surface parallel fractures after infiltration into the soil zone. Meteoric water also infiltrates from the lake, either through the soil zone at the lakebed or directly via fractures exposed at the surface with no soil zone. At the GTS, topography is the driving force for water movement, even in the subsurface. Water infiltrating at high altitude generates a high-pressure head forcing water to areas of lower pressure such as in the tunnels or further downstream where the altitude is lower. Matrix porosity and permeability in the granite are very low compared to the fracture network permeability (Bossart et al., 1991). Hence, the dominant transport mechanism considered in the conceptual model is fracture flow.

Meteoric water hits the land surface and then either infiltrates into the soils zone or is transported by gravity down the mountain side. Surface water can still infiltrate as it runs off the mountain. Infiltration occurs at the base of slopes and along the banks of the reservoir. Infiltration pathways for surface runoff will differ depending on the range of geological features interacting with surface runoff. Most infiltration sources will include the soil zone, passing through different soil types. Water in the soil zone increases in CO₂ concentration and takes on water soluble organics. Gravity then transports the soil water via drainage within connecting open fractures. Where fractures are exposed at surface, water infiltrates directly without any interaction with the soil zone.

Infiltrating meteoric water exploits exfoliation and topographic stress fractures in the near surface. Topographic stress fractures are common in the top 300m (Martel, 2006; Slim *et al.*, 2015) of the lithosphere in glacial tectonic regions. Topographic stress fractures increase the bulk permeability in the top 300m and provide key infiltration and flow pathways connecting to tectonic brittle fractures. Tectonic brittle fractures extend deeper into the lithosphere than topographic stress fractures. The GTS lies between 300 and 460m below ground surface, hence, tectonic fractures form the main conduits of fluid transport into the GTS (Schneeberger et al., 2017) as topographic stress fractures will not extend to the depth of the GTS. Lake water infiltrates using a combination of different fractures in a complex poorly connected network. The hydraulic head gradient drives water flow from the lake into the GTS, where the pressure head is lower. If the GTS were not present, the Valley and the lake would likely form the lowest head, with groundwater contributing to the lake and being transported down the valley via the river network (Voborny et al., 1991).

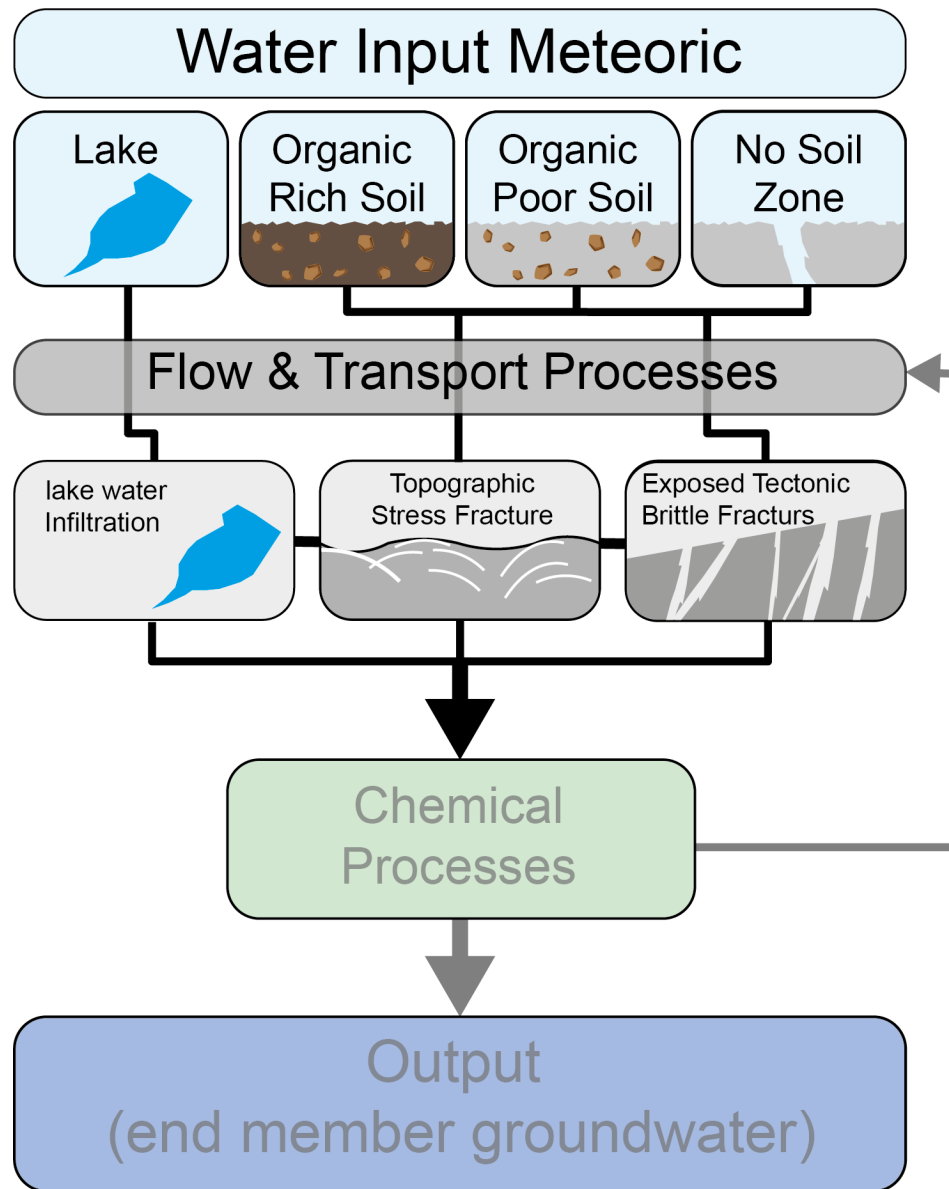


Figure 6.3 Schematic flow diagram building on Figure 6.2 adding flow and transport pathways from the surface to the GTS groundwater system. Including Lake water, topographic stress fractures extending to ~300m and brittle overprinting to ductile shear zones.

Fractures host flow by advective transport (Bossart *et al.*, 1991; Barton *et al.*, 1995; Caine *et al.*, 1996). Matrix porosity is low in crystalline rocks, such as those in the GTS (0.8 – 1.53 vol%) as compared to the fracture porosity (10-30 vol%; Bossart *et al.*, 1991). Local and regional stresses control the permeability of the fractures within the fracture network. Fracture permeability decreases with increasing depth below ground surface due to increases in the vertical stress, which decreases the fracture aperture and reduces the permeability. Critically stressed fractures, where the ratio of shear to normal stress is in excess of 0.6 of the failure envelope, are thought to have higher permeability (Rogers, 2003) and thus, depending on their connectivity to infiltration sources, are more likely to have high flow rates. Fractures in

the GTS formed as brittle overprinting to alpine ductile deformation. Brittle overprinting of ductile strain localizing zones is more pervasive in the south of the GTS in the GrGr than in the north in CAGr (Choukroune and Gapais, 1983; Rolland et al., 2009; Wehrens, 2015). Brittle deformation in the GTS is shown by Schneeberger et al., 2016 as; fracturing, cataclasites and fault gouges. Fractures filled with fault gouge or lined with biotite, often form at the boundary between metabasic dykes and granite. Open fractures are present in the granitic pluton (Schneeberger et al., 2016). Brittle fracturing seen in the host rock localizes along shear zones in the GTS. Shear zone development is more pervasive in the south of the GTS forming steep planar (dip >80°) South, South East and South West dipping fractures extending km to tens of kilometres (Wehrens, 2015; Schneeberger et al., 2016).

The fracture network encompassing the GTS hosts the majority of fluid flow from the surface to depth. Tectonic brittle fractures are the key transport conduit from the surface to the GTS. Topographic stress fractures, parallel to topography, intersecting with brittle tectonic fractures, NE-SW oriented form conduits for fluid flow. Flow conduits form along the strike of the vertical tectonic fractures and flow parallel to the surface. While the junctions between these fracture sets does not extend down to the depth of the GTS, they do provide connection from the surface to ~300m depth below ground surface. Surface liniment mapping indicates few intersections between tectonic brittle fractures, meaning fracture connectivity perpendicular to the brittle fractures will be poor. Findings from chapter 4 suggest this to be true. Figure 6.4 shows that two adjacent borehole sample intervals can have distinctly different infiltration sources, highlighting the poor fracture connectivity perpendicular to tectonic fracture at the GTS. Groundwater pressure monitoring in isolated borehole intervals (Appendix 4) at the GTS shows that, in the same borehole, pressure can vary depending on the fracture/geological feature each interval intersects. High pressure boreholes/intervals are found adjacent to lower pressure ones, and this supports the findings from chapter 4 that the fracture network in the GTS is poorly connected.

Groundwater at the GTS derives from; (1) infiltrating meteoric water, (2) lake water infiltrating from fractures, or (3) a combination of infiltrating meteoric (terrigenous) and lake water. Waters travelling through different fracture sets may have the same dissolved ion chemistry but could contain waters derived from a combination of sources. The poorly connected fracture network is likely to result in different mixing patterns along each individual flow path, thus explaining the observed differences in organic content (Chapter 4). Boreholes with pressures greater than the lake are more likely to originate purely from infiltrating topographically driven meteoric water.

6.1.3. Chemical processes: Water-rock interactions along flow paths

Schneeberger et al (2019) highlighted the change in groundwater chemistry between the north and the south of the GTS. Groundwater hosted in Grimsel granodiorite (GrGr) has a slightly different dissolved ion chemistry than in the Central Aar granite (CaGr). Here the original conceptual groundwater model of the GTS is updated from the new insights into dissolved ion chemistry (Chapter 3) and from the sites of surface infiltration input to the groundwater system (Chapter 4).

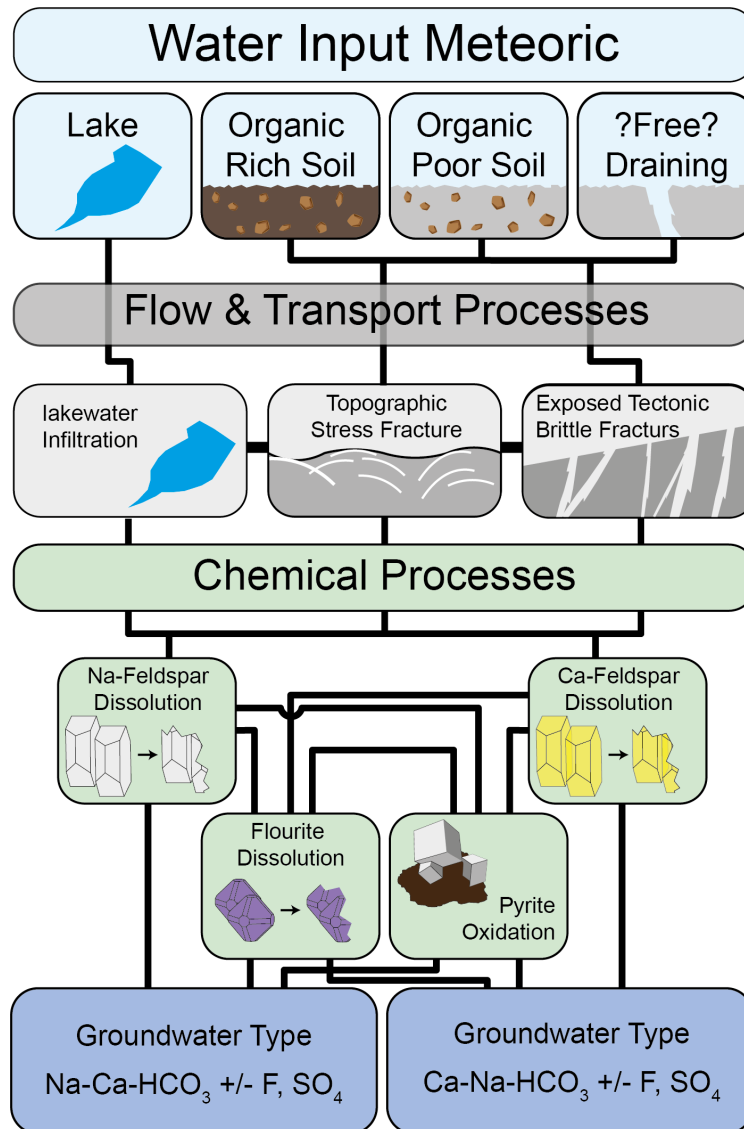


Figure 6.4 Schematic diagram building on Figure 6.3 adding flow and transport pathways from the surface to the GTS groundwater system. Including key chemical reactions occurring in the top ~300m of the crust surrounding the GTS.

Chapter 3 discusses four key chemical reactions leading to the evolution of meteoric water to groundwater at the GTS. Host rock lithology is the major control on groundwater chemistry; the Aar granite in the north (CAGr) and Grimsel granodiorite (GrGr) in the south have differing Ca/Na ratio. Feldspar type is the dominant control on this; Ca-feldspars in CAGr dissolve

leading to Ca-HCO₃±F,SO₄ type groundwaters to the north, Na-feldspars in GrGr dissolve forming Na-HCO₃±F,SO₄ type groundwaters in the south of the GTS.

While host rock mineralogy plays an important role in groundwater chemical evolution, the presence of other accessory minerals present along a flow path also has an influence. Alpine clefts aligned with, or intersect, flow pathways hosting fluorite, calcite and amorphous quartz minerals. Dissolution of these minerals by groundwater results in increased F⁻, Ca²⁺ and Si_(tot) dissolved in groundwater. Dissolution reactions in alpine clefts along flow paths change the water composition only in cleft-intersecting flow paths. The poor connectivity in the fracture network results in adjacent borehole intervals with highly variable Fluoride concentrations. Oxidation of pyrite releases sulfur into groundwater. Pyrite oxidation requires an electron donor, dissolved oxygen concentration is dependent on the oxygen in infiltrating groundwater. Infiltration pathways with high oxygen are likely to release more SO₄²⁻ and precipitate iron oxides near to the ground surface on fracture surfaces. This process will continue until the redox front passes the GTS then sulfate concentration will no longer evolve and could potentially reduce as meteoric water continues to infiltrate.

Infiltration processes exert a control on groundwater chemistry. Infiltration water from the lake and the open free-draining fractures will be in equilibrium with atmospheric gasses and have low dissolved ion concentrations. The high dissolved oxygen concentration will promote oxidation processes in these fracture pathways. Comparatively, water infiltrating through the soil zone should have higher dissolved CO₂ and lower dissolved oxygen, but higher concentrations of dissolved ions from the soil. Increased organic acid concentration from soil infiltration will lead to increased water-rock reaction rates. Higher H⁺ concentrations from the organic acid will also result in increased hydrolysis of feldspar minerals. Infiltration through the soil zone can also add or remove Calcium and magnesium from the infiltrating meteoric water depending on soil reaction processes.

In summary, whilst the host rock exerts the greatest control on groundwater chemistry, variations in infiltration sources will influence the rates of individual water-rock reactions during fracture transport.

6.1.4. Groundwater Hydrogeological Conceptual model for the GTS

Collating the findings from relevant literature (chapter 2), spatial chemistry (Chapter 3), infiltration sources (chapter 4) and hydrogeology (Section 6.1) at the GTS into one model builds an in-depth picture of groundwater flow and geochemical evolution at the GTS. The main source of water into the hydrological system is meteoric, precipitation in the form of rain and snow. This water infiltrates through the soil, or directly into open fractures, above the GTS.

Infiltration also occurs from lakes fed by surface runoff from precipitation and glacial melt further up the catchment.

Once in the subsurface, the main flow paths are near-surface (<300m depth) topographically near-parallel stress-relief fractures (Martel, 2006; Ziegler et al., 2016) and steeper near-vertical tectonic fractures. High flow rates are associated with critically stressed fractures that are optimally oriented to the stress field.

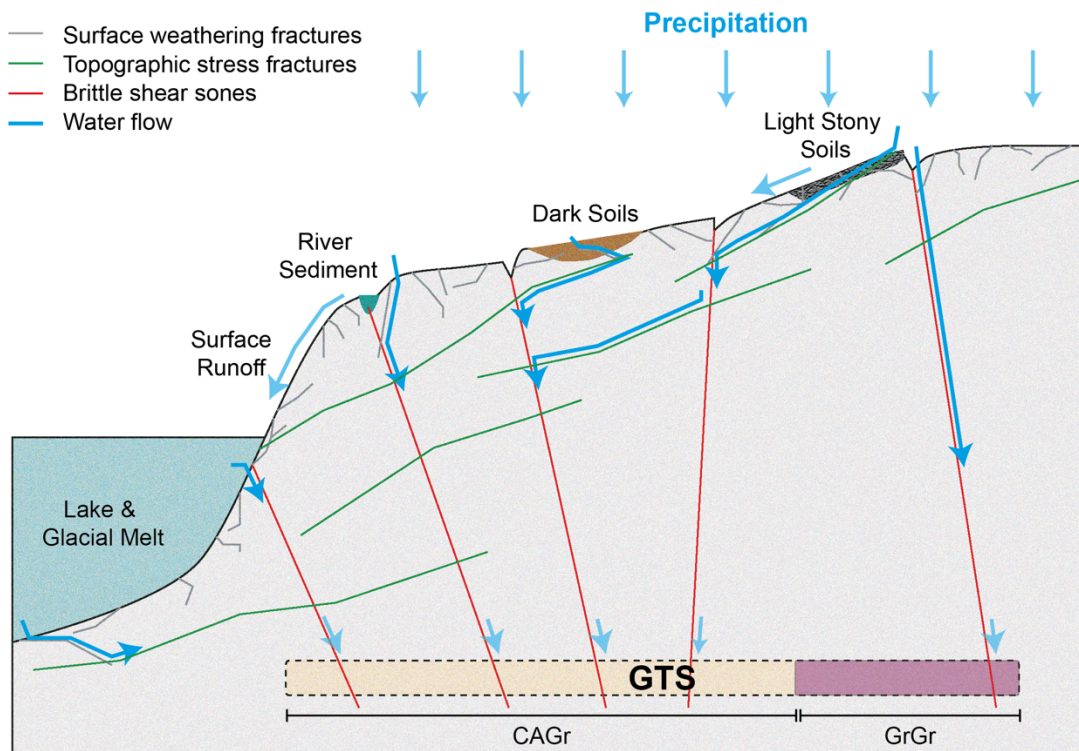


Figure 6.5 Conceptual diagram of water flow pathways. Meteoric water source from precipitation, infiltrates from different surface environments; lake/glacial melt, river sediment, dark soil, light stony soil, direct infiltration to shear zones. Water follows several fracture pathways; surface weathering fractures, topographic stress fractures and brittle shear zones. Fractures hosted in two main lithologies Central Aar Granite (CAGr) and Grimsel Granodiorite (GrGr). Brittle shear zones and other fractures can contain different mineralogies for water rock reaction (i.e. biotite, fault gauge, epidote, quartz, fluorite, meta-basic dyke).

Lithology is the main control on chemical groundwater evolution. It is difficult to determine from the water chemistry the exact mineralogy lining the fractures. Each interval hosts a number of fractures all with differing mineralogies (i.e. granite, mylonite, biotite). As a number of fractures are likely to contribute to flow in a single interval, the chemical differences in each interval reflect a mix of the chemical evolution and groundwater age along each fracture path. As only subtle differences in chemistry are visible, it is not possible to determine the exact fracture mineralogy from groundwater chemical evolution. Flow is topographically driven towards the GTS, which is at atmospheric pressure. Fracture flow is more connected in a NE-SW and

ENE-WSW direction following the strike of the main tectonic fracture sets. Poor connectivity perpendicular to these fractures will be a major constraint on groundwater mixing at a regional and local scale.

Using the developed conceptual model (Figure 6.5) what can be delineated about the flow path and chemical reactions feeding each fracture system from infiltration to sample site? Figure 6.6 shows there are four identified different surface infiltration sources feeding the groundwater sampled at the GTS. Soil infiltration feeds groundwater samples site 'a' and 'b', Lake water feeds 'c', 'd', and 'f', while groundwater site 'e' seems to be fed by a low organic content or high infiltration site and 'g' closely reflects a river source.

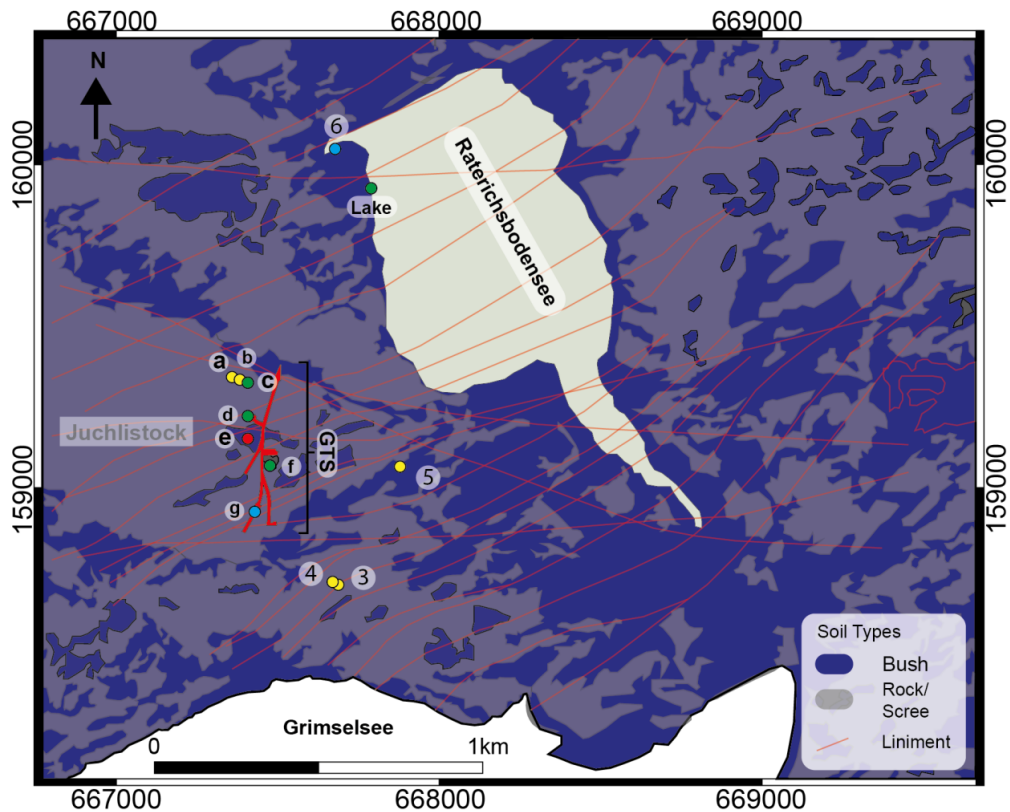


Figure 6.6 Soil map of the Grimsel region, showing the groundwater (alpha numeric) and surface organic sampling sites (numeric). Sample sites are colour coded by origin; lake in green circle, soil yellow circle, river blue circle, low organic red circle. The GTS access tunnels are in red.

Following infiltration at surface, water undergoes water rock interactions with the mineralogy along the fracture flow path. Findings from Chapter 3 determine the probable mineralogy water interacted with along flow path, the full reaction path is summarised in table 6.1. The composition of groundwater from most of sample sites (a,b,c,d, and g) is consistent with water rock interactions with the host rock. This thesis shows that water from sample sites 'a' and 'b' infiltrates through the soil zone and undergoes water rock interaction with the Central Aar granite (CAGr), transport is most likely along the brittle tectonic fractures intersecting the borehole sample interval. Groundwater sample site 'c' and 'd' infiltrate from a lake/reservoir

source, undergoing water rock interaction with CAGr along fracture flow paths. Sample location 'g' shows a riverine infiltration source, reacting with Grimsel Granodiorite (GrGr) along the flow path.

Most sampled groundwaters undergo water rock interactions giving a predictable chemistry indicative of the host rock. Groundwater sample sites 'f' and 'e' indicate different fluid rock interactions than the reactions while their infiltration sources are from Lake and low organic sources respectively. Dissolved ion chemistry in 'f' has abnormally low K^+ , SO_4^{2-} and higher Li^+ , Cl^- and F^- compared with the other sample sites in GrGr. It is likely the lower sulfate results from lower incidence of pyrite along the flow path, while higher chloride can indicate an increase in biotite. High fluoride concentration may be a result of more fluorite being presence. Fluorite exists in Alpine clefts host, and presence of fluoride in groundwater at the GTS could mean the fracture flow pathway intersects with alpine clefts. Groundwater sample location 'e' has a higher concentration of sodium than expected for water rock interaction with just CAGr and is more indicative of water rock interactions with GrGr and CAGr. Location 'e' is proximal to the magmatic transition zone, it is most feasible that water travelled along a fracture network with both CAGr and GrGr lithologies present.

Table 6-1 Summary of the key findings for each sample site; water input, water rock interactions and dissolved chemical ion differences. Showing if water rock interactions are consistent with the expected groundwater chemistry in that lithology

Groundwater Site	Surface Source	Host Rock	Ion Chemistry	Water Rock Interactions consistent with host rock
a	Soil	CAGr	High: Ca^{2+} , K^+ Low: Na^+	Consistent CAGr
b	Soil	CAGr	High: Ca^{2+} , K^+ Low: Na^+	Consistent CAGr
c	Lake	CAGr	High: Ca^{2+} , K^+ Low: Na^+	Consistent CAGr
d	Lake	CAGr	High: Ca^{2+} , K^+ Low: Na^+	Consistent CAGr
e	Low organic	GrGr	Medium: Na^+ , Ca^{2+} , K^+	Transition between CAGr and GrGr
f	Lake	GrGr	High: Na^+ , Li^+ , Cl^- , F^- Low: Ca^{2+} , K^+ , SO_4^{2-}	Not consistent with either host rock
g	River	GrGr	High: K^+ , Na^+ Low: Ca^{2+}	Consistent with GrGr

6.1.5. *How does the GTS hydrogeology and groundwater geochemistry respond to transient stress changes from Lake Draining?*

The conceptual hydrogeological model presented thus far is based on there being no significant changes to annual infiltration patterns at the GTS site. Data show that seasonal surface climate has little-to-no effect on groundwater chemistry at the GTS. However, over the lifespan of a geological disposal facility (<1Ma) it is important to account for temporal change, such as changing climate, anthropogenic surface land use change, earthquakes, glaciation and tectonic stress changes.

This study investigated the changes to groundwater chemistry and flow in response to lake draining and refilling. Lake draining removes a potential source of groundwater recharge to the GTS during drainage and subsequently increases recharge during refilling. These changes to groundwater recharge could potentially have changed flow pathways and groundwater pressures. However, no change in groundwater pressure was detected in response to the draining and refilling of Räterichbodensee (Appendix 4).

We might expect to see a change in groundwater chemistry reflecting either an increase or decrease of lake water mixing with the groundwater. With less lake water infiltration, we would expect changes in pH, TDS and major ion concentration as surface water no longer dilutes groundwater. The converse to this would be true if there is an increase in recharge from the lake water. No chemical evidence of changes in groundwater composition at the GTS was observed.

During the two drainage and refilling periods, short-lived drops in pH were the only detected temporal groundwater changes observed at the GTS (Chapter 5). These pH drops were clearly associated with microseismic events, that largely occurred concurrent to lake drainage (as opposed to refilling). Chapter 5 showed that mechanical activation of fracture surfaces during slip generates H^+ ions in groundwater, decreasing the pH. These microseismic events are most likely to have been triggered by changes to the local stress field as a result of surface unloading (during lake drainage). In addition to the observed drops in pH, these microseismic events may have caused localised changes to fracture permeability and connectivity.

Localised short-lived changes in pH, in response to microseismic events, have implications for interpretation of the geological record, in particular for interpreting the flow history at a site. Whilst over a 1Ma-year lifespan of a repository, local events may be relatively infrequent, over geological timescales they may leave a notable imprint on the surrounding rocks. While this is an important finding for interpreting the geological record, a GDF in the UK will not be placed in an area with a fault and earthquake hazards. Therefore the UK site for a GDF is not directly comparable to that at the GTS.

During site investigation, there is a particular interest in analysing evidence of past flow regimes, particularly where evidence may exist for upwelling geothermal waters. This is often in the form of mineral and metal precipitates in fractures and the presence of alteration halos surrounding fractures due to dissolution or oxidation; all of which are interpreted as evidence of a change to the groundwater chemistry within the fracture network and hence of incoming waters. Localised drops in pH, due to mechanochemical reactions during fracture formation and fracture slip will increase the dissolution rates of minerals along fracture zones, mobilize metals and alter redox processes. These perturbations over time could result in the transport of metal ions from minerals to other locations without significant changes to groundwater flow. Hence, observations of fracture precipitates and fracture alteration halos may be incorrectly interpreted as being due to changes in the chemistry of incoming groundwaters as opposed to small microseismic events. Such an error could lead to an overly conservative characterisation of a potential GDF site.

6.2. How does the lake draining compare as an analogue for Glacial loading and unloading?

To assess whether lake draining is an applicable modern analogue to deglaciation it is necessary to consider the induced stress changes and the hydrological effects in the two systems. Stress change from the draining and refilling of Räterichsbodensee (Chapter 5) was $\Delta\sigma \sim 0.1$ MPa, this is an order of magnitude smaller than the expected stress change from a large glacier or ice sheet $\Delta\sigma \sim 1-2$ MPa. While lake draining is a smaller stress change, the stress change is imposed over a shorter time period ~ 2 months compared to glacial time scales on the order of 1,000-10,000 years. Rapid, small stress change from the lake drainage resulted in multiple small microseismic events $M_w < 2$. Larger stress changes from ice sheet unloading should result in more frequent small magnitude events and some potentially larger seismic events.

Small magnitude events $M_w < 2$ proximal to the GTS caused localised pH drops of 1-3 units. Larger more frequent seismic events will likely result in similar or larger magnitude pH drops, acidifying the groundwater locally to the slip plane. Dilation and compression of fractures during slip events will lead to the propagation of this chemical change. So, whilst the magnitude of unloading due to lake drainage is smaller than that due to glacial unloading, it might be expected that the effect on pH is similar but more frequent for small magnitude events, with more extreme pH drops being associated with larger less frequent events. For each specific groundwater chemistry there is likely to be an extent of water buffering reducing the magnitude of the pH decrease.

During deglaciation, ice melting increases the volume of basal glacial water for recharge. This effect is not reproduced during lake drainage, in fact, groundwater heads will drop local to the lake. Seismic events are triggered by the effective shear stress exceeding the stress required for shear failure on the fracture/fault. The effective stress can be increased either by changes in the tectonic stresses or by increases in pore pressure. Since glacial melting will also result in a rise in groundwater pressure, the frequency of seismic events during glacial melting is likely to be further increased by the increased fluid pressure along fault zones generated by addition head of meltwater from the melting glacier. This reduced the principal stresses acting on the fracture there by bringing the fracture closer to failure.

Monitoring groundwater chemistry during lake drainage and recharge at the GTS has given a unique insight into the potential temporal effects of mechanochemical reactions on groundwater geochemistry. To determine the likely magnitude and frequency of these effects during deglaciation, further laboratory work would be required, alongside microseismic monitoring of glacial melt sites.

6.3. Implication for Siting a GDF in the UK

This research funded in part by RWM and EPSRC doctoral training program. A key output is to develop new methods for site investigation and to show how these new methods are used in conjunction with standard existing site investigation techniques. The thesis also aimed to assess the potential long-term variations in groundwater chemistry at a GDF. Chapter 6.1 demonstrated how new site investigation methods in conjunction with temporal data collection, better informs and develops a more in-depth site model. Section 6.3 firstly discusses the implications for organic tracing and the application and integration of organic tracing into UK GDF siting programs. Secondly the section considers the implications of temporal groundwater acidification associated with microseismicity at a GDF.

6.3.1. Siting method and implications

Site characterisation is a vital stage of the UK Radioactive Waste disposal program. Site Characterisation is needed to understand the potential geological and hydrogeological setting of a potential GDF and to inform design and safety case for considerations.

Initial site investigations are likely to be surface based using 2/3D and passive seismic and other geophysical techniques. Borehole drilling would follow the surface characterisation. Detailed site investigations carried out by international organizations tasks with developing a GDF highlight the need for multiple geochemical and hydrogeological techniques to be used in parallel to develop a detailed model of the subsurface. Minimally invasive hydrogeological techniques could be used at an early stage in a site characterisation programme. They would not, however, replace the need for groundwater samples collected from boreholes, since

information on deep groundwater chemistry would still be needed. The early information would be valuable to help inform and guide drilling locations and inform on recharge / catchment areas for the site. Non-invasive techniques such as using organic molecules as tracers, could, following validated testing, be used to support evaluations of surface water recharge catchments, and conversely provide an indication of potential flow paths from the GDF depth to the surface which could then be further evaluated as part of intrusive / numerical investigations.

Characterising the hydrogeology and geochemistry of the subsurface requires drilling of boreholes. The process of collecting groundwater samples from boreholes perturbs the groundwater system. New techniques such as CHEMLAB developed by SKB (Karnbranslehantering, 2000) and used at Äspö hard rock laboratory allow samples to be collected that preserve the pressure at depth and have minimal disruption to the groundwater (i.e. without pumping and draining of a borehole are advantageous and could be deployed first which preserves conditions for other subsequent forms of testing. Many of the initial techniques of characterizing groundwater chemistry are outlined in Chapter 3. This include physiochemical measurements during sample collection and analysis for major, minor and trace ions, and stable isotopes. Such techniques are well described in the literature and their benefit is that they are easily accessible and low cost. Attention should be taken when characterizing groundwater chemistry as to the sampling conditions. In-situ conditions will be different from the chemistry measured at surface pressures and temperatures. When samples taken from depth equilibrate with atmospheric gasses precipitates will form and gasses will exsolve and dissolve from the groundwater changing the recorded chemistry. Additional geochemical analysis techniques can be used in combination build up the lines of evidence to infer; groundwater age, travel times, and mixing of water sources. More complex analytical techniques are often expensive, and facilities in the UK limited. Other techniques often require large volumes of groundwater causing significant perturbations to the groundwater system, and in some settings large volumes of what may not exist due to the properties of the rock. Apparent groundwater age determination can use Nobel gases (Kr, Ar, Ne, He), tritium and tritium with helium, Radiocarbon, or CFC and SF₆ analysis. Determining surface infiltration origin is difficult and current techniques struggle to isolate surface regions contributing to the make-up of groundwater. Chapter 4 presents the forensic analysis of the organic component of groundwater to determine the surface origin of the meteoric component in a groundwater system.

RWM need to characterise the groundwater setting, chronology and evolution at potential sites in the UK. The dissolved organic approach outlined in chapter 5 has potential, in combination with other analytical tools, to further our understanding of groundwater origin and age that cannot be determined by other methods alone. It is vital to understand how organics can be

used and their limitations / uncertainties for determining groundwater infiltration. The technique has currently been used to determine infiltration from lake, soil and different soil types. However, for this method to be used in support of site characterisation activities it must be further validated after the promising results of an initial small pilot study at the GTS. The technique could be a promising screening tool, as such the presence or absence of certain compounds on a first pass can help determine, which samples are more similar to each other. If compounds are present in groundwater and also present in lake water but absent in soils, the groundwater is likely derived from lake origin.

Further testing and validation of the organic analytical technique (Section 4) for the tracing of groundwater movement is required before it can be applied to GDF siting. The objectives for future work should be to understand the opportunities, and the limitations of the technique. Topics to investigate in the future to validate and explore where this new technique is suitable include:

- Understand the fate and transport of the biomarkers.
- Evaluate fracture surface mineralogy as sorption sites.
- Influence of changes in physio/chemistry in the groundwater with depth.
- The mode of transport of the biomarkers (diffusive / advective).
- Potential for 'filtering' within the rock mass.
- Applicability of the technique to different rocks / geological settings.
- Travel time / residence time estimation, ability to calculate flow velocity depth of penetration from the from the surface.

To determine how ubiquitously this technique can be used we need to apply it to different host rock aquifer types. In clastic and carbonate aquifers there will be an organic component contributed to the groundwater. Perhaps this technique can identify the matrix water contribution into a fractured sedimentary aquifer system. While the fate and transport of bulk Dissolved Organic Matter (DOM) is well documented, there are very few investigations into the transport mechanisms of different organic groups through different rock types, pores and fractures. Understanding degradation rates of different organic groups and analysing the parent and daughter degradation products could be used in determination groundwater ages, as could the application of compound specific isotope analysis (CSIA) of these parent compounds. Sorption rate onto mineral and fracture surfaces should be different depending of the organic group and compound polarity. By comparison of the ratio of key compounds with different sorption rates could show flow path length and perhaps constrain groundwater age.

While the different investigations described above validate how different site characteristics and processes could be examined with this technique, further validation of the analytical

technique is required. At present sample extraction method is different for soil and water samples, a comparison of the recovery rate and methods to compare the absolute concentration of compounds between these sample types is needed. Validation of the sample concentration step, although following published methodologies, should be done to determine how this affects compound presence in the final sample volume. Detailed organic analysis can tell the site investigator a lot at the site characterisation stage. However, when combined with other geochemical techniques more in-depth understanding of the geochemistry and transport is attained.

6.3.2. *Implication of temporal groundwater acidification*

Chapter 5 shows how microseismic events, induced by lake draining and refilling, cause ground water pH changes. Mechano-chemical reactions occurring during rock comminution, generate siloxanes and silica radicals, producing H^+ and peroxide respectively in groundwater. This is a process not previously considered in the interpretation of the features in the geological record. Chapter 5 shows a significant pH drop from the release of hydrogen ions into solution, Telling *et al.*, 2015 show peroxide production by combination of hydroxide radicals. Peroxide formation as well as drops in pH will result in changes to the redox potential. However, no significant change in redox is measured during the experiment at the GTS. From a radioactive waste point of view, temporal changes in groundwater chemistry need to be assessed for their impact on the mobility, and transport of radionuclides. Acidification and change to redox of groundwater over time is important. Sorption of radionuclides onto mineral surfaces are pH and ionic strength dependent (Wallace *et al.*, 2012). Over long time periods repeated small changes in groundwater chemistry will have a cumulative effect on sorption, mobility and transport distance of radionuclides from a source. It is therefore vital to fully understand the extent of seismically induced changes to pH and redox in groundwater and the compounded effect of repeated mechanochemical reaction of radionuclides. A safety case for a GDF could consider the impact of increased mobility of radionuclides due to fracture slip.

Alteration halos around rock fractures are pervasive and understood to be due to the influx of fluids with differing chemical composition (e.g. hydrothermal fluids, hydrocarbons, CO_2 -rich groundwaters). Perhaps this is not always the case? Changes to groundwater chemistry in fractures can cause alterations to fracture mineralogy. Decreasing pH and changing redox in-situ from faulting leads to the mobility of metals from the minerals lining fractures leading to the formation of alteration halos. Silica radical production during fracturing not only acts to drop pH and produce H_2 gas in solution, but also results in the production of hydrogen peroxide through the combination of OH radicals (Telling *et al.*, 2015; Tranter, 2015). Hydrogen peroxide is a strong oxidizer and will act to change the redox potential of the in-situ porewater in and adjacent to the slipped fracture surface. This process could lead to the formation of alteration halos by reduction, without requiring a fluid flux into the system.

Carbonate-silicate weathering is known to lock-up atmospheric CO₂. Models of silicate weathering at the ground surface are included in global climate models (Lasaga et al., 1985) but are recognised as being highly conservative and account for some of the greatest model uncertainties (St Clair *et al.*, 2015). A drop-in surface or groundwater pH as a result of landslides/rockfalls and shallow subsurface microseismic events will cause increased dissolution of Mg and Ca from the surrounding rocks. In regions of high topography, such as the Alps, surface waters travel to depths of several hundred meters before emerging in lakes and rivers, so groundwater may play an important role in the silicate weathering cycle as well as surface water.

Drops in in situ pH observed during the breaking of silicon-bearing rocks is a key, currently unaccounted for, crustal process that can have a significant impact on our current understanding of chemical weathering, carbon cycling and mineral precipitation, dissolution and alteration processes. Given the highly localised nature of flow within sparse fracture networks it is extremely unlikely that a similar result could be replicated in a standard borehole experiment.

Presently little is known as to the groundwater conditions leading to a drop-in groundwater pH from mechano-chemical reaction or constraints on the frequency of cracking events at depths where the mechano-chemical process is likely to occur. Cracking of silica can occur as a result of shallow seismic events or landslides/rockfalls. Whilst prediction of large event frequency is well understood, small magnitude ($< 2 M_w$) seismicity has rarely been the object of studies in the international literature, mainly because it falls below the detection threshold of permanent seismic networks. Natural microseismic event records are thus incomplete at low magnitudes below $2 M_w$. Further, such shallow, small-magnitude microseismic events are well-documented as being triggered by climatic processes such as rainfall, snow melt and glacial retreat (Fischer et al., 2017). Further investigation could be carried out:

- To determine the mineralogical and environmental controls on the production of silica radicals, and the rate and magnitude of the subsequent pH drop, for a range of common rock types and groundwater compositions; experiments will include investigation of the temperature range over which this process occurs.
- To determine the frequency of occurrence, depth and fractured surface area of such pH drop events, as a function of geographic location; controlled in the subsurface by the frequency, magnitude and location of shallow microseismic events within silica-bearing rocks, and at the ground surface by the frequency of landslides and rockfalls.
- To determine the global significance of mechano-chemically-driven pH drops for crustal processes; initial experiments would focus on three such crustal processes,

the formation of fracture alteration halos, the global carbonate-silicate cycle and the mineral trapping of dissolved CO₂ in basalt.

- Acidification of groundwater has implications in a wide range of fields. Further research is required to fully understand the extent and magnitude of mechano chemical reactions. Potential implications of in-situ acidification of fracture systems and the effect on interpretation of the geological record can have important implication for our understanding of alteration halos, and contaminant transport through fault systems.

6.4. Conclusions

Investigation into the spatial hydrogeochemistry at the GTS confirmed the results of previous studies by Keppler, (1995) and more recently Schneeberger et al., (2017). **Groundwater at the GTS is meteoric in source, infiltrating from the surface. Groundwater chemistry evolves by water rock reaction, and the final chemical composition is largely controlled by the lithology it interacts with along flow pathways.** Two key controls on groundwater chemical endmember evolution are the slight changes in lithology between the north and south of the GTS and minor differences in groundwater chemistry explained by the reaction of secondary minerals such as pyrite and fluorite along the flow path. Alpine clefts host fluorite implying they may form part of flow path into specific intervals.

This thesis concludes that there is very poor fracture connectivity in the rocks surrounding the GTS. First, there is a consistent difference in groundwater chemistry between boreholes in the north and the south of the GTS, which are separated by ~500m. This is consistent with the previous observations of (Schneeberger, 2017). More compelling evidence though, is provided by the observed differences in the organic signatures between adjacent boreholes, and between adjacent sampling intervals in the same borehole, showing that fracture flow pathways are locally isolated. The technique developed in this thesis for characterising organic water/soil signatures should be transferable to other sites and could form a powerful tool for determining groundwater origins as part of site investigation. The range of host rocks and groundwater ages this technique is appropriate to will require further investigation.

The dissolved organic content of groundwater is highly complex. Non targeted organic analysis at the GTS showed that groundwater contains in excess of 2,000 different organic compounds in what is considered a 'relatively clean 'modern low dissolved solids groundwater. The complexity of the dissolved organic component in groundwater is traditionally simplified into one or two bulk components. While studies on bulk organic fractions are useful, this thesis shows that oversimplifying the organic content of groundwater results in a loss of information

about groundwater origins. Based on the testing to date, the organic groundwater tracing technique indicates that additional information about the groundwater system can identify subtle differences in groundwater origins that cannot be determined from inorganic chemical evidence alone.

The contributing sources of infiltrating meteoric water can be determined from the dissolved organic signature preserved in the groundwater. In this thesis I demonstrate how the relative concentrations of organic compounds present in multiple groundwater, surface water and soil samples can be used to identify and trace the signature of different infiltration environments. As meteoric water infiltrates it picks up the water-soluble organic signature within surface soils/sediments and transports them along fracture flow pathways to the GTS. Comparing the signature of groundwater with different surface environments for similarities in organic components allowed different infiltration sources to be determined. Since the groundwater in the GTS is known for be > 50 years old, this implies that **the organic signatures of these surface environments are preserved in groundwater for at least 50 years.**

Dissolved organic signatures can differentiate between visibly different soil/sediment types. Findings of the organic study show that visibly different soils/sediments have clearly different organic signatures. Chapter 4 shows how darker soils are distinctly different from lighter river sediments and that these different organic signatures can be used to determine water origins.

This thesis shows that soil, lake, and riverbed surface infiltration environments all contribute to the groundwater system at the GTS. Organics analysis identified that two different types of soil environment contribute to the groundwater system, as does the lake water. Lake water was not previously considered as a groundwater source based on past hydrogeological reports at the GTS (Keppler, 1995; Schneeberger et al., 2017) largely because little-to-no hydraulic connectivity has been observed between the lake levels and the pressure in borehole test intervals at the GTS. Previous isotope studies also concluded that water infiltrates from altitudes directly above the GTS. This thesis shows that organic signatures are complimentary to existing techniques, and that their use can result in a more nuanced understanding of groundwater origins.

In addition to the spatial variations in groundwater chemistry, this thesis also investigated the potential for temporal variations in groundwater chemistry that could result from hydro mechanical changes in the rock mass. **Lake drainage causes changes to the effective stress around and beneath a water reservoir due to both direct removal of the water**

load and to the associated drop in groundwater head. This results in induced microseismicity in the rock mass surrounding, and beneath, the reservoir.

During both episodes of lake drainage and refilling, groundwater pH drops were recorded. Drops in pH are short lived (< 24hours) and associated with a prior microseismic event. These pH drops are a result of a microseismically induced mechano-chemical reaction. Mechano-chemical reactions are shown to occur as a result of fractured siloxane bonds interacting with water, in the absence of oxygen, and producing silanol on cracked mineral surfaces. Silanol dissociates and releases excess H^+ into solution lowering pH. These mechano-chemical processes have been shown experimentally to cause the release of H_2 (g) and H_2O_2 into solution, which will potentially result in a change to the redox conditions in groundwater.

Combining the findings from the spatial observations of organic and inorganic groundwater chemistry, with the observations of temporal variations in pH, a picture can be constructed of the groundwater system. **Groundwater at the GTS flows through highly isolated fracture systems that are connected to surface soils, river beds and in one instance, the lake. The water chemistry in individual fractures is largely stable and is dependent on the infiltration source and the rock mineralogy along the flow path. Rock fracturing events (i.e. microseismicity) cause perturbations to the groundwater pH in the fracture that can be preserved over several days. These perturbations likely result in short-term changes to redox chemistry which could produce short-duration localised 'bursts' of mineral/metal precipitation or dissolution on fracture surfaces.**

7. Future work and Recommendations

7.1. Recommendations for future site investigation practice

The results of the analyses in the study have implications for future site investigation. In addition, the opportunity to work on a multi-national, multi-institution project highlighted some key learnings that will be of relevance to RWM as the site characterisation for a UK GDF proceeds.

When considering groundwater investigations, a number of factors should be considered when devising, implementing and analysing the results of groundwater studies. My recommendations for future approaches to support the characterisation of a site are separated into 4 categories; (1) devising the sampling program, (2) sampling methodologies and analysis practices, (3) separating raw data from data interpretation and (4) and conveying different data types to non-discipline specific stakeholders.

7.1.1. Devising a site investigation program

Planning a site investigation program is complex. Great care must be taken to ensure the timing of each investigative technique is scheduled as that it does not impact the results of the next technique. At the GTS there have been ~30 years of investigations, but in some cases earlier investigations have effectively removed some areas of rock from being useful for future studies – e.g. because of previous experiments one borehole had to be removed from the data analysis due to corrosion of the borehole isolation packer system, it was not possible to determine if the groundwater chemistry had been altered due to packer corrosion. If site investigation techniques cause significant perturbation to the system, they should be used minimally.

When devising a borehole groundwater monitoring system, attention should be paid to appropriate logging and recording of geological core. My studies identified specific challenges to the ability to characterise the fracture network arise where photos of borehole cores are not orientated, or where image logs are absent rendering future scrutiny of previous interpretations impossible. This presented limitations in my project, which could have been overcome had image logs or oriented core been available since it would have been possible to check if different orientations of fractures, or fractures with different fracture fills, were delivering water with different chemistry, pH evolution or organic content to the boreholes.

For the purposes of my project, boreholes would ideally have been packed off to isolate as many individual structural features so as to not artificially connect previously isolated fracture systems. However, the packers at the GTS had been placed since the 1980's, it was out of the scope of the project to remove and realign packers to isolate specific fractures of interest.

7.1.2. Flexibility in site model evolution

It is important that the siting program is designed to be flexible. Initial geophysical techniques provide a guide but have limitations, when the next step of site investigation takes place new information may challenge the previous conceptual site model. As new evidence is gathered the site model should be updated, then new next steps in the site investigation can be planned and devised. During the construction of this thesis, several new insights into how the GTS groundwater system behaves were discovered i.e. temporal changes in pH, new meteoric infiltration sources. As a result, further research questions arose. If the site model is fixed and not flexible these results would have been considered as anomalous (because they did not fit the model) rather than determining the cause of the anomalies i.e. the pH changes were discounted as temporal data did not always fit the current GTS groundwater model.

7.1.3. Sampling and analysis methodologies

When site investigation moves from non-invasive to invasive techniques, perturbation to the groundwater system will occur and can start to effect the results of future site characterisation efforts. Attention to recording all activities at the site is essential to understand if other activity is affecting data collection. During sampling, replicate samples should be taken of sufficient size to ensue optimal analysis, and the date, time, sample technique, storage, chain of custody and person(s) involved should be recorded. This information should be stored as metadata with any analysis. A similar approach should be taken during sample analysis. A number of samples from each batch should be analysed multiple times to evaluate precision of results, and data correction undertaken according. Certified reference standards samples should be analysed to determine machine / instrument accuracy allowing data correction as required. Blank samples should be analysed to monitor for sampling and analytical contamination. Reserve sample should remain stored as a backup if analysis fails. Samples are to be stored in accordance to guidance and analysed within their holding times. Again, metadata should be recorded regarding every aspect of the analysis, and combined with the sampling metadata. In specific cases and depending on the type of analysis, samples should be analysed by two separate laboratories for comparison. Emphasis on metadata means that even if analysis is not considered excellent, understanding what has happened to the sample before during and after sampling can show the scientist interpreting the data how significant the data might be or if it should be discounted. This recommendation is based on experience gained during field works undertaken for this thesis. Samples were collected from a site

designed for underground characterisation. Having the knowledge of previous experiments was vital to understand how the past experiments may have affected my current investigation. Most of the difficulties encountered were a result of a lack of recording of sample treatment i.e. reports did not clearly say what the experimental approaches involved or the reports on past experiments were not available to be examined as they contained preparatory information. Often the knowledge of past experiments or findings are not recorded but are known as rumour or hearsay.

7.1.4. Data storage and interpretation

Raw data and associated metadata should be stored in non-editable files. The stored raw data should be the actual output from the instrument, i.e. chromatograph, spectra. The calibrated concentration should be stored alongside the calibration used to gain that value. If data are stored in this way the raw data generated by the instrument can then be reprocessed and reinterpreted if required. Data reporting should include final measurement reference to the raw data, experimental or analytical error, method detection limits or metadata i.e. methodology. Data interpretation needs to be kept separate from the raw data. Errors made during interpretation can be identified when the analyst reprocesses the raw data. When devising a site investigation, planning should include how data and what data should be stored. Sampling frequency is important as increasing frequency rapidly increases the volume of data storage required. Carrying out temporal analysis showed the pH changes in the groundwater never seen before by using a seasonal (quarterly) sampling frequency.

7.1.5. Conveying different data types

Displaying different formats of data at a specific site is complex due to the nature of multiple different measurement variables, for example how to represent seismic, stress and chemical data. This thesis uses a combination of GIS to display groundwater data, and rudimentary 3D models and image manipulation to present conceptual 3D models of the GTS and surroundings. However, as more and more different data types accumulate from a site, displaying this data visually becomes more difficult. Building Information Modelling (BIM) is a technique used in civil engineering. In principle, Geological-BIM (GEO-BIM) could allow all the information about a site to be presented in a usable interactive 3D model. GEO-BIM would allow users from different scientific and engineering fields to visualise all of the geological data gathered about the site and design a repository from these data, and also to reactively evolve the site conceptual model. While not used in this project, if it were adopted by NAGRA or RWM it would go a long way to addressing the other issues and lessons learned while conducting this thesis.

7.2. Recommendations for Future research

Recommendations for future research are largely based on new discoveries made in this thesis. Here I focus on developments in organic groundwater tracing, and mechanochemical reactions as a result of fracture and fault slip.

7.2.1. Geochemical evolution in fracture networks

The results of this thesis showed that the fracture networks of very poorly connected – this is very common in fracture-dominated systems. Tracer tests are notoriously difficult due to dilution and lack of return of the tracer. The chemistry of the groundwater itself contains information on the flow pathways. Further research should determine what the chemistry of the groundwater can show about the pathway the water travelled and reacted with on route to the groundwater sample location. This is not only useful in URL's but also in other fracture dominated systems where little is known about the fracture system or the dominant geological features that provide pathways for fluid flow. By analysis the chemical reaction which occur in a flow path to get a specific groundwater there is the potential elucidate the mineralogy of the flow pathway as well as the travel times along the flow path from reaction kinetics.

7.2.2. Organic Tracing

Future research in the application of organic fingerprinting groundwaters can be split in to 3 research channels; verification and validation; age tracing; processing development. Verification and validation of the method outlined in section 4. Verification should be carried out by comparison of findings from organic tracing with conventional additive tracer testing. Validation of the methods used however is a lot more costly and complex. Sample extraction methods and potential derivatizations should be completed to ensure the repeatability and compound recovery of the organic extraction step. Further validation of the sample concentration step should be done, because potentially sample volume could cause discrepancies. Finally, improvement and efficiency of the GCxGC method will better separate compounds and improve sample to sample reproducibility. Analytical standards should be utilised to quantify compound concentration, internal standards should be used to help with sample to sample alignment.

Further to the analytical method more research into how organics are transported and change along flow path is needed. Perhaps some compound groups are better suited (i.e. more long lived and less prone to sorption and degradation) than others? Identifying the parent-daughter degradation relationships could be used to identify the groundwater age or travel time from surface. This would be a vital technique for modern groundwater dating as common techniques such as tritium and CFC's become obsolete.

While the R code used is the best at aligning compounds at the time of study, further development of a compound alignment code and comparison tool is vital. Presently raw data processing is done through “black box” software with minimal user interface. This poses a severe issue in how detailed peak identification and how well compound alignment codes can work. A recommendation would be to firstly improve raw data processing, then increase the reliability of compound alignment, finally developing a scientific reasoning to identify parent and daughter degradation products in the chromatograph.

Organic tracing of groundwater through detailed compound analysis opens up a new field of organic research. Having the potential to gain more information about ground and surface water systems. Applied to soil science organic tracing such as this can be combined with metabolomic analysis to deconvolute different processes occurring in the soil zone and their result on the soil system. Applied in the ocean and to ocean sediment cores, organic tracing could have the potential to show how ocean circulation has changed in the past and is presently changing. While some of these are speculative future research themes, they are all based around the complexity of different organic compounds in different environments.

7.2.3. Seismic induced mechano-chemical reactions

Future work should investigate where in the crust this process can occur, and how environmental conditions affect the production rates of silica radicals and surface silanol. All previous experiments in the literature have investigated H₂ gas production using deionised, de-gassed waters with various rock types and minerals (Kameda et al., 2003; Saruwatari et al., 2004; Telling *et al.*, 2015). Experiments under geologically realistic groundwater compositions would determine the extent of silica radical and surface siloxane production and its effect on in situ groundwater pH.

Experiments should examine the effects of rock mineralogy, temperature, and groundwater chemistry on the mechanochemical reaction rate and magnitude of the pH drop. Continuous measurements of pH and Eh, alongside monitoring of hydrogen gas evolution, could be used to determine reaction rates.

Further to this, the effect of mechano-chemical reactions should be explored with respect to the formation of fracture alteration halos. Alteration halos around rock fractures are pervasive and understood to be due to the influx of fluids with differing chemical composition (e.g. hydrothermal fluids, hydrocarbons, CO₂-rich groundwaters). Perhaps this is not always the case? Silica radical production during fracturing not only acts to drop pH and produce H₂ gas in solution, but also results in the production of hydrogen peroxide through the combination of OH radicals (Tranter, 2015). Hydrogen peroxide is a strong oxidizer and will act to change the redox potential of the in-situ porewater in and adjacent to the slipped fracture surface. This

process could lead to the formation of alteration halos by oxidation/reduction, without requiring a fluid flux into the system | The global carbonate-silicate cycle: Carbonate-silicate weathering is known to lock-up atmospheric CO₂. Models of silicate weathering at the ground surface are included in global climate models but are recognised as being highly conservative and account for some of the greatest model uncertainties (St Clair *et al.*, 2015). A drop-in surface or groundwater pH as a result of landslides/rockfalls and shallow subsurface microseismic events will cause increased dissolution of Mg and Ca from the surrounding rocks. In regions of high topography, such as the Alps, surface waters travel to depths of several hundred meters before emerging in lakes and rivers, so groundwater may play an important role in the silicate weathering cycle as well as surface water.

Mineral trapping of dissolved CO₂ in basalt: Mineral trapping considered a secure for CO₂ trapping. Mineral trapping can be significant in basaltic rocks due to the availability of reactive minerals with up to 95% of injected CO₂ mineralised within 2 years (Elango and Kannan, 2007). The rate and magnitude of mineral trapping is partly controlled by the pH of the fluids; an order of magnitude increase in reaction rate occurs with a decrease of one pH unit (Loiko *et al.*, 2017).

REFERENCES

- Aagaard, P. and Helgeson, H. C. (1982) 'Thermodynamic and kinetic constraints on reaction rates among minerals and aqueous solutions; I, Theoretical considerations', *American Journal of Science*. American Journal of Science, 282(3), pp. 237–285. doi: 10.2475/ajs.282.3.237.
- Abercrombie, R. E. and Brune, J. N. (1994) 'Evidence for a constant b -value above magnitude 0 in the southern San Andreas, San Jacinto and San Miguel Fault Zones, and at the Long Valley Caldera, California', *Geophysical Research Letters*. John Wiley & Sons, Ltd, 21(15), pp. 1647–1650. doi: 10.1029/94GL01138.
- Allan, S. E., Smith, B. W. and Anderson, K. A. (2012) 'Impact of the Deepwater Horizon Oil Spill on Bioavailable Polycyclic Aromatic Hydrocarbons in Gulf of Mexico Coastal Waters', *Environmental Science & Technology*. American Chemical Society, 46(4), pp. 2033–2039. doi: 10.1021/es202942q.
- Anderson, M. P. and Munter, J. A. (1981) 'Seasonal reversals of groundwater flow around lakes and the relevance to stagnation points and lake budgets', *Water Resources Research*. John Wiley & Sons, Ltd, 17(4), pp. 1139–1150. doi: 10.1029/WR017i004p01139.
- Appelo, C. A. J. and Postma, D. (2005) *Geochemistry, groundwater and pollution*. Balkema.
- Artinger, R. Buckau, G. Geyer, P. Fritz, P. Wolf, M. Kim, J. I. (2000) 'Characterization of groundwater humic substances: influence of sedimentary organic carbon', *Applied Geochemistry*. Pergamon, 15(1), pp. 97–116. doi: 10.1016/S0883-2927(99)00021-9.
- Auqué, L. F. Gimeno, M. J. Gómez, J. B. (2007) 'Groundwater chemistry around a repository for spent nuclear fuel over a glacial cycle Evaluation for SR-Can'. SKB, Technical Report, TR-06-31. Available at: www.skb.se (Accessed: 9 July 2019).
- Azam, S. (2007) 'Study on the geological and engineering aspects of anhydrite/gypsum transition in the Arabian Gulf coastal deposits', *Bulletin of Engineering Geology and the Environment*. Springer-Verlag, 66(2), pp. 177–185. doi: 10.1007/s10064-006-0053-2.
- Baghbanan, A. and Jing, L. (2008) 'Stress effects on permeability in a fractured rock mass with correlated fracture length and aperture', *International Journal of Rock Mechanics and Mining Sciences*, 45(8), pp. 1320–1334. doi: 10.1016/j.ijrmms.2008.01.015.
- Barnes, K. K. Kolpin, D. W. Furlong, E. T. Zaugg, S. D. Meyer, M. T. Barber, L. B. (2008) 'A national reconnaissance of pharmaceuticals and other organic wastewater contaminants in the United States-I) Groundwater'. *Science of the total environment*. 402, pp. 192-200 doi: 10.1016/j.scitotenv.2008.04.028.
- Barton, C. A., Zoback, M. D. and Moos, D. (1995) 'Fluid flow along potentially active faults in crystalline rock', *Geology*, 23(8), pp. 683–686. doi: 10.1130/0091-7613(1995)023.
- Bense, V. F. Gleeson, T. Loveless, S. E. Bour, O. Scibek, J. (2013) 'Fault zone hydrogeology', *Earth-Science Reviews*, 127, pp. 171–192. doi: 10.1016/j.earscirev.2013.09.008.
- Berkowitz, B. (2002) 'Characterizing flow and transport in fractured geological media: A review', *Advances in Water Resources*, 25(8–12), pp. 861–884. doi: 10.1016/S0309-1708(02)00042-8.
- Birgersson, L. Moreno, L. Neretnieks, I. Widén, H. Ågren, T. (1993) 'A tracer migration experiment in a small fracture zone in granite', *Water Resources Research*. 29(12), pp. 3867–3878. doi: 10.1029/93WR02340.
- Le Borgne, T. Bour, O. Paillet, F. L. Caudal, J. -P. (2006) 'Assessment of preferential flow path connectivity and hydraulic properties at single-borehole and cross-borehole scales in a

- fractured aquifer'. *Journal of Hydrology*, 328, pp. 347-359 doi: 10.1016/j.jhydrol.2005.12.029.
- Boronina, A. Balderer, W. Renard, P. Stichler, W. (2005) 'Study of stable isotopes in the Kouris catchment (Cyprus) for the description of the regional groundwater flow', *Journal of Hydrology*. Elsevier, 308(1-4), pp. 214-226. doi: 10.1016/J.JHYDROL.2004.11.001.
- Bossart, P. Mazurek, M. Hellmuth, K. H. Siitari-Kauppi, M. Schneebeli, M. (1991) 'Grimsel test site: structural geology and water flow-paths in the migration shear-zone'. NAGRA-NTB-91-12. Available at: https://inis.iaea.org/search/search.aspx?orig_q=RN:23047598 (Accessed: 16 July 2019).
- Boulton, G. S. Caban, P. E. Van Gigssel, K. Leijnse, A. Punkari, M. Van Weert, F. H. A. (1996) 'The impact of glaciation on the groundwater regime of Northwest Europe', *Global and Planetary Change*, 12(1-4), pp. 397-413. doi: 10.1016/0921-8181(95)00030-5.
- Bourbie, T. Coussy, O. and Zinszner, B. (1992) 'Acoustics of Porous Media', *The Journal of the Acoustical Society of America*. Acoustical Society of America, 91(5), pp. 3080-3080. doi: 10.1121/1.402899.
- Brantley, S. L. Goldhaber, M. B. and Ragnarsdottir, K. V. (2007) 'Crossing Disciplines and Scales to Understand the Critical Zone', *Elements*, 3(5). Available at: <http://elements.geoscienceworld.org/content/3/5/307> (Accessed: 8 May 2017).
- Brantley, S. L., Goldhaber, M. B. and Ragnarsdottir, K. V. (2007) 'Crossing Disciplines and Scales to Understand the Critical Zone', *Elements*. GeoScienceWorld, 3(5), pp. 307-314. doi: 10.2113/gselements.3.5.307.
- Brodsky, E. E. Roeloffs, E. Woodcock, D. Gall, I. Manga, M. (2003) 'A mechanism for sustained groundwater pressure changes induced by distant earthquakes', *Journal of Geophysical Research*. 108(B8), p. 2390. doi: 10.1029/2002JB002321.
- Brune, J. N. (1970) 'Tectonic stress and the spectra of seismic shear waves from earthquakes', *Journal of Geophysical Research*. 75(26), pp. 4997-5009. doi: 10.1029/JB075i026p04997.
- Bucher, K. and Stober, I. (2002) 'Water-rock reaction experiments with Black Forest gneiss and granite', in: Springer, Dordrecht, pp. 61-95. doi: 10.1007/978-94-010-0438-1_3.
- Caine, J. S., Evans, J. P. and Forster, C. B. (1996) 'Fault zone architecture and permeability structure', *Geology*. 24(11), p. 1025. doi: 10.1130/0091-7613(1996)024<1025:FZAAPS>2.3.CO;2.
- Cappa, F. and Rutqvist, J. (2012) 'Seismic rupture and ground accelerations induced by CO₂ injection in the shallow crust', *Geophysical Journal International Geophys. J. Int*, 190, pp. 1784-1789. doi: 10.1111/j.1365-246X.2012.05606.x.
- Challandes, N. Marquer, D. and Villa, I. M. (2008) 'P-T-t modelling, fluid circulation, and 39Ar- 40Ar and Rb-Sr mica ages in the Aar Massif shear zones (Swiss Alps)', *Swiss Journal of Geosciences*, 101(2), pp. 269-288.
- Chan, T. Christiansson, R. Boulton, G. S. Ericsson, L. O. Hartikainen, J. Jensen, M. R. Mas Ivars, D. Stanchell, F. W. Vistrand, P. Wallroth, T. (2005) 'DECOVALEX III BMT3/BENCHPAR WP4: The thermo-hydro-mechanical responses to a glacial cycle and their potential implications for deep geological disposal of nuclear fuel waste in a fractured crystalline rock mass', *International Journal of Rock Mechanics and Mining Sciences*. Pergamon, 42(5-6), pp. 805-827. doi: 10.1016/J.IJRMMS.2005.03.017.
- Chapelle, F. H. (2000) *The significance of microbial processes in hydrogeology and geochemistry*, *Hydrogeology Journal*. Springer-Verlag. Available at: <https://link.springer.com/content/pdf/10.1007%2FPL00010973.pdf> (Accessed: 24 June 2019).
- Chapelle, F. H. and McMahon, P. B. (1991) 'Geochemistry of dissolved inorganic carbon in a Coastal Plain aquifer. 1. Sulfate from confining beds as an oxidant in microbial CO₂ production', *Journal of Hydrology*. Elsevier, 127(1-4), pp. 85-108. doi: 10.1016/0022-1694(91)90110-4.
- Choukroune, P. and Gapais, D. (1983) 'Strain pattern in the Aar Granite (Central Alps): orthogneiss developed by bulk inhomogeneous flattening.', *Journal of Structural Geology*, 5, pp. 411-418.

- Christensen, J. B. Jensen, D. L. Grøn, C. Flip, Z. Christensen, T. H. (1998) 'Characterization of the dissolved organic carbon in landfill leachate-polluted groundwater', *Water Research*. Pergamon, 32(1), pp. 125–135. doi: 10.1016/S0043-1354(97)00202-9.
- Claesson, L. Skelton, A. Graham, C. Dietl, C. Mörth, M. Torssander, P. Kockum, I. (2004) 'Hydrogeochemical changes before and after a major earthquake', *Geology*, p. 641. doi: 10.1130/G20542.1.
- Claesson, L. Skelton, A. Graham, C. Mörth, C. (2007) 'The timescale and mechanisms of fault sealing and water-rock interaction after an earthquake', *Geofluids*. (10.1111), 7(4), pp. 427–440. doi: 10.1111/j.1468-8123.2007.00197.x.
- Cranwell, P. A. (1982) 'Lipids of aquatic sediments and sedimenting particulates', *Progress in Lipid Research*. Pergamon, 21(4), pp. 271–308. doi: 10.1016/0163-7827(82)90012-1.
- Delaloye, R. and Lambiel, C. (2005) 'Evidence of winter ascending air circulation throughout talus slopes and rock glaciers situated in the lower belt of alpine discontinuous permafrost (Swiss Alps)', *Norsk Geografisk Tidsskrift - Norwegian Journal of Geography*. Routledge, 59(2), pp. 194–203. doi: 10.1080/00291950510020673.
- Department for Business, E. & I. S. and T. R. H. C. S. (2019) *UK becomes first major economy to pass net zero emissions law*, Gov.uk. Available at: <https://www.gov.uk/government/news/uk-becomes-first-major-economy-to-pass-net-zero-emissions-law>.
- Dockrill, B. and Shipton, Z. K. (2010) 'Structural controls on leakage from a natural CO₂ geologic storage site: Central Utah, U.S.A.', *Journal of Structural Geology*, 32(11), pp. 1768–1782. doi: 10.1016/j.jsg.2010.01.007.
- Douglas, M. Clark, I. D. Raven, K. Bottomley, D. (2000) 'Groundwater mixing dynamics at a Canadian Shield mine', *Journal of Hydrology*, 235(1–2), pp. 88–103. doi: 10.1016/S0022-1694(00)00265-1.
- Du, J. Cheng, W. Xiang, Y. Jie, C. Guan, Z. Liu, W. Bai, L. (2006) 'Helium and carbon isotopic compositions of thermal springs in the earthquake zone of Sichuan, Southwestern China', *Journal of Asian Earth Sciences*, 26(5). doi: 10.1016/j.jseaes.2004.11.006.
- Eglinton, G. and Hamilton, R. J. (1967) 'Leaf Epicuticular Waxes', *Science*, 156, pp. 1322–1335. doi: 10.1126/science.156.3780.1322.
- Eichhubl, P., Davatzes, N. C. and Becker, S. P. (2009) 'Structural and diagenetic control of fluid migration and cementation along the Moab fault, Utah', *AAPG Bulletin*. GeoScienceWorld, 93(5), pp. 653–681. doi: 10.1306/02180908080.
- Elango, L. and Kannan, R. (2007) 'Chapter 11 Rock–water interaction and its control on chemical composition of groundwater', *Developments in Environmental Science*. Elsevier, 5, pp. 229–243. doi: 10.1016/S1474-8177(07)05011-5.
- Elkhoury, J. E., Brodsky, E. E. and Agnew, D. C. (2006) 'Seismic waves increase permeability', *Nature*. Nature Publishing Group, 441(7097), pp. 1135–1138. doi: 10.1038/nature04798.
- EPA Publication (1996) *Method 3510c, Revision 3 December 1993, Final Update III to the Test Methods for Evaluating Solid Waste, Physical/Chemical Methods, EPA Publication SW-841*.
- Esperança, S. and Holloway, J. R. (1987) 'On the origin of some mica-lamprophyres: experimental evidence from a mafic minette', *Contributions to Mineralogy and Petrology*. Springer-Verlag, 95(2), pp. 207–216. doi: 10.1007/BF00381270.
- Fäh, D. Giardini, D. Kästli, P. Deichmann, N. Gislser, M. Schwarz-Zanetti, G. Alvarez-Rubio, S. Sellami, S. Edwards, B. Allmann, B. Bethmann, F. Wössner, J. Gassner-Stamm, G. Fritsche, S. Eberhard, D. (2011) *ECOS-09 earthquake catalogue of Switzerland release 2011 report and database. Public catalogue, 17. 4. 2011. Swiss Seismological Service ETH Zurich, Risk*. Available at: <http://citeseerx.ist.psu.edu/viewdoc/download?doi=10.1.1.464.8258&rep=rep1&type=pdf> (Accessed: 12 June 2019).
- Field, M. S. Wilhelm, R. G. Quinlan, J. F. Aley, T. (1995) 'An assessment of the potential adverse

- properties of fluorescent tracer dyes used for groundwater tracing', *Environmental Monitoring and Assessment*. 38(1), pp. 75–96. doi: 10.1007/BF00547128.
- Fischer, T., Matyska, C. and Heinicke, J. (2017) *Earthquake-enhanced permeability – evidence from carbon dioxide release following the ML 3.5 earthquake in West Bohemia*, *Earth and Planetary Science Letters*. doi: 10.1016/j.epsl.2016.12.001.
- Francis, B. A., Francis, L. K. and Cardenas, M. B. (2010) 'Water table dynamics and groundwater-surface water interaction during filling and draining of a large fluvial island due to dam-induced river stage fluctuations', *Water Resources Research*. 46(7). doi: 10.1029/2009WR008694.
- Frape, S. K., Fritz, P. and McNutt, R. H. (1984) 'Water-rock interaction and chemistry of groundwaters from the Canadian Shield', *Geochimica et Cosmochimica Acta*, 48(8), pp. 1617–1627. doi: 10.1016/0016-7037(84)90331-4.
- Freeze, R. A. and Cherry, J. A. (1979) *Groundwater*. Prentice-Hall.
- Gahalaut, K., Gahalaut, V. K. and Pandey, M. R. (2007) 'A new case of reservoir triggered seismicity: Govind Ballav Pant reservoir (Rihand dam), central India', *Tectonophysics*, 439(1), pp. 171–178. doi: 10.1016/j.tecto.2007.04.003.
- Gauchotte-Lindsay, C. Aspray, T. J. Knapp, M. Ijaz, U. Z. (2019) 'Open Access Article'. doi: 10.1039/c9fd00020h.
- Geological Survey, U. S. *U.S. Geological Survey, (2006). Reston, VA, Chlorofluorocarbon Laboratory Website. Available at: https://water.usgs.gov/lab/chlorofluorocarbons/sampling/bottles/ (Accessed: 29 August 2019).*
- Giridharan, L., Venugopal, T. and Jayaprakash, M. (2008) 'Evaluation of the seasonal variation on the geochemical parameters and quality assessment of the groundwater in the proximity of River Cooum, Chennai, India', *Environmental Monitoring and Assessment*. Springer Netherlands, 143(1–3), pp. 161–178. doi: 10.1007/s10661-007-9965-y.
- Goldich, S. S. (1938) 'A Study in Rock-Weathering', *The Journal of Geology*. University of Chicago Press, 46(1), pp. 17–58. doi: 10.1086/624619.
- Goncalves, P. Oliot, E. Marquer, D. Connolly, J. A. D. (2012) 'Role of chemical processes on shear zone formation: an example from the Grimsel metagranodiorite (Aar massif, Central Alps)', *Journal of Metamorphic Geology*, 30(7), pp. 703–722.
- GOV.UK (2014) *Implementing Geological Disposal A Framework for the long-term management of higher activity radioactive waste*. Available at: www.nationalarchives.gov.uk/doc/open-government-licence/ (Accessed: 14 January 2020).
- Grant, R. A. Halliday, T. Balderer, W. P. Leuenberger, F. Newcomer, M. Cyr, G. Freund, T. (2011) 'Ground Water Chemistry Changes before Major Earthquakes and Possible Effects on Animals', *International Journal of Environmental Research and Public Health*. Molecular Diversity Preservation International, 8(6), pp. 1936–1956. doi: 10.3390/ijerph8061936.
- Grasby, S. E. and Lepitzki, D. A. . (2002) 'Physical and chemical properties of the Sulphur Mountain thermal springs, Banff National Park, and implications for endangered snails', *Canadian Journal of Earth Sciences*. NRC Research Press Ottawa, Canada, 39(9), pp. 1349–1361. doi: 10.1139/e02-056.
- Gulley, A. K. Dudley Ward, N. F. Cox, S. C. Kaipio, J. P. (2013) 'Groundwater responses to the recent Canterbury earthquakes: A comparison', *Journal of Hydrology*, 504. doi: 10.1016/j.jhydrol.2013.09.018.
- Gupta, H. K. (1992) *Reservoir-induced earthquakes*. Developments in Geotechnical Engineering, 64. Elsevier.
- Gupta, H. K. (2002) 'A review of recent studies of triggered earthquakes by artificial water reservoirs with special emphasis on earthquakes in Koyna, India', *Earth-Science Reviews*, 58(3), pp. 279–310. doi: 10.1016/S0012-8252(02)00063-6.
- Gutenberg, B. and Richter, C. F. (1994) *FREQUENCY OF EARTHQUAKES IN CALIFORNIA**.

Available at: <https://core.ac.uk/download/pdf/33111762.pdf> (Accessed: 12 June 2019).

- Haack, S. K. Garchow, H. Odelson, D. A. Forney, L. J. Klug, M. J. (1994) 'Accuracy, reproducibility, and interpretation of Fatty Acid methyl ester profiles of model bacterial communities.', *Applied and environmental microbiology*. American Society for Microbiology, 60(7), pp. 2483–93. Available at: <http://www.ncbi.nlm.nih.gov/pubmed/16349327> (Accessed: 28 August 2019).
- Havskov, J. and Schweitzer, J. (2002) *Topic Earthquake location compiled*, Available at: http://gfzpublic.gfz-potsdam.de/pubman/item/escidoc:4109:4/component/escidoc:4110/IS_11.1rev1.pdf (Accessed: 20 June 2019).
- Heiss, J. W. and Michael, H. A. (2014) 'Saltwater-freshwater mixing dynamics in a sandy beach aquifer over tidal, spring-neap, and seasonal cycles'. doi: 10.1002/2014WR015574.
- Helgeson, H. C., Murphy, W. M. and Aagaard, P. (1984) 'Thermodynamic and kinetic constraints on reaction rates among minerals and aqueous solutions. II. Rate constants, effective surface area, and the hydrolysis of feldspar', *Geochimica et Cosmochimica Acta*. Pergamon, 48(12), pp. 2405–2432. doi: 10.1016/0016-7037(84)90294-1.
- Hiscock, K. M. (2005) *Hydrogeology: principles and practice*. Blackwell Publishing.
- Hoehn, E. Eikenberg, J. Fierz, T. Drost, W. Reichlmayr, E. (1998) 'The Grimsel Migration Experiment: field injection–withdrawal experiments in fractured rock with sorbing tracers', *Journal of Contaminant Hydrology*. Elsevier, 34(1–2), pp. 85–106. doi: 10.1016/S0169-7722(98)00083-7.
- Huang, S. Wang, Y. Ma, T. Tong, L. Wang, Y-y. Liu, C-r, Zhao, L. (2015) 'Linking groundwater dissolved organic matter to sedimentary organic matter from a fluvio-lacustrine aquifer at Jiangnan Plain, China by EEM-PARAFAC and hydrochemical analyses', *Science of The Total Environment*. 529, pp. 131–139. doi: 10.1016/J.SCITOTENV.2015.05.051.
- Hutchison, I. B. Delori, A. Wang, X. Kamenev, K. V. Urquhart, A. J. Oswals, I. D. H. (2015) 'Polymorphism of a polymer precursor: metastable glycolide polymorph recovered via large scale high-pressure experiments', *CrystEngComm*. 17(8), pp. 1778–1782. doi: 10.1039/C5CE00119F.
- Wakita, H. Nakamura, Y. (1980). *Hydrogen Release: New Indicator of Fault Activity*. Science. 210(4466). pp. 188-190.
- IAEA/WMO (2020) *Global Network of Isotopes in Precipitation. The GNIP Database*.
- Ingebritsen, S. E. and Manga, M. (2014) 'Hydrogeochemical precursors', *Nature Geoscience*. Nature Publishing Group, 7(10), pp. 697–698. doi: 10.1038/ngeo2261.
- Itaba, S. Koizumi, N. Toyoshi, T. Kaneko, M. Sekiya, K. Ozawa, K. (2008) 'Groundwater changes associated with the 2004 Niigata-Chuetsu and 2007 Chuetsu-oki earthquakes', *Earth, Planets and Space*. 60(12), pp. 1161–1168. doi: 10.1186/BF03352873.
- Kalbus, E., Reinstorf, F. and Schirmer, M. (2006) *Measuring methods for groundwater? surface water interactions: a review* *Measuring methods for groundwater? surface water interactions: a review. Hydrology and Earth System Sciences Measuring methods for groundwater-surface water interactions: a review*. Hydrogeology and Earth System Sciences Discussions, *European Geosciences Union*. 10(6). pp. 873-887
- Kameda, J., Saruwatari, K. and Tanaka, H. (2003) 'Hydrogen Generation by Wet Grinding of Quartz Powders and Its Dependence on the pH and Ionic Strength of Liquid Media', *Bulletin of the Chemical Society of Japan*. 76(11), pp. 2153–2154. doi: 10.1246/bcsj.76.2153.
- Karnbranslehantering, S. (2000). *Aspo Hard Rock Laboratory Annual Report 1999, SKB*.
- Kelemen, P. B. and Hirth, G. (2012) 'Reaction-driven cracking during retrograde metamorphism: Olivine hydration and carbonation', *Earth and Planetary Science Letters*. Elsevier, 345–348, pp. 81–89. doi: 10.1016/J.EPSL.2012.06.018.
- Keppler, A. (1995) *Hydrogeologische, hydrochemische und isotopenhydrologische Untersuchungen*

an den Oberflächen- und Kluftwässern im Grimselgebiet, Schweiz.

- Keusen, H. R. Ganguin, J. Schuler, P. Buletti, M. (1989) Grimsel Test Site Geology. NAGRA Technical Report 87-14 E.
- Khader, O. and Novakowski, K. (2014) 'Impacts of Pleistocene glacial loading on abnormal pore-water pressure in the eastern Michigan Basin', *Geofluids*, 14(2), pp. 200–220. doi: 10.1111/gfl.12074.
- King, C.-Y. King, B-S. Evans, W. C. (1996) 'Spatial radon anomalies on active faults in California', *Applied Geochemistry*. 11(4), pp. 497–510. doi: 10.1016/0883-2927(96)00003-0.
- King, C.-Y. Zhang, W. and Zhang, Z. (2006) 'Earthquake-induced Groundwater and Gas Changes', *Pure and Applied Geophysics*. Birkhäuser-Verlag, 163(4), pp. 633–645. doi: 10.1007/s00024-006-0049-7.
- Kita, I. Matsuo, S. and Wakita, H. (1982) 'H₂ generation by reaction between H₂O and crushed rock: An experimental study on H₂ degassing from the active fault zone', *Journal of Geophysical Research: Solid Earth*. John Wiley & Sons, Ltd, 87(B13), pp. 10789–10795. doi: 10.1029/JB087iB13p10789.
- Konno, U. Kouduka, M. Komatsu, D. D. Ishii, K. Fukuda, A. Tsunogai, U. Ito, K. Suzuki, Y. (2013) 'Novel Microbial Populations in Deep Granitic Groundwater from Grimsel Test Site, Switzerland', *Microbial Ecology*. Springer-Verlag, 65(3), pp. 626–637. doi: 10.1007/s00248-013-0184-5.
- Korkmaz, S. and Gülbay, R. K. (2007) 'Organic geochemical characteristics and depositional environments of the Jurassic coals in the eastern Taurus of Southern Turkey', *International Journal of Coal Geology*. doi: 10.1016/j.coal.2006.07.001.
- Laaksoharju, M. Smellie, J. Tullborg, E-L. Gimeno, M. Molinero, J. Gurban, I. Hallbeck, L. (2008) 'Hydrogeochemical evaluation and modelling performed within the Swedish site investigation programme', *Applied Geochemistry*, 23(7), pp. 1761–1795. doi: 10.1016/j.apgeochem.2008.02.015.
- Laaksoharju, M., Gascoyne, M. and Gurban, I. (2008) 'Understanding groundwater chemistry using mixing models', *Applied Geochemistry*, 23(7), pp. 1921–1940. doi: 10.1016/j.apgeochem.2008.02.018.
- Lagache, M. (1976) 'New data on the kinetics of the dissolution of alkali feldspars at 200°C in CO₂ charged water', *Geochimica et Cosmochimica Acta*. Pergamon, 40(2), pp. 157–161. doi: 10.1016/0016-7037(76)90173-3.
- Lapworth, D. J. Baran, N. Stuart, M. E. Ward, R. S. (2012) 'Emerging organic contaminants in groundwater: A review of sources, fate and occurrence', *Environmental Pollution*. 163, pp. 287–303. doi: 10.1016/J.ENVPOL.2011.12.034.
- Lasaga, A. C., Berner, R. A. and Garrels, R. M. (1985) 'An improved geochemical model of atmospheric CO₂ fluctuations over the past 100 million years.', *The carbon cycle and atmospheric CO*. doi: 10.1029/gm032p0397.
- LECO Corporation USA (2019) *Instrument: Pegasus BT 4D ® Determining Terpene Profiles of Cannabis Strains Using GC and GCxGC with High Performance TOFMS Application Note*. Available at: https://www.leco.com/images/Products/massspec/PegasusBT4D/PEGBT4D_CANNABIS_TERPENE_PROFILES_203-821-558.pdf.
- Lehtonen, K. and Ketola, M. (1993) 'Solvent-extractable lipids of Sphagnum, Carex, Bryales and Carex-Bryales peats: content and compositional features vs peat humification', *Organic Geochemistry*, 20(3), pp. 363–380. doi: 10.1016/0146-6380(93)90126-V.
- Lemieux, J.-M. Sudicky, E. A. Peltier, W. R. Tarasov, L. (2008) 'Dynamics of groundwater recharge and seepage over the Canadian landscape during the Wisconsinian glaciation', *Journal of Geophysical Research*, 113(F1), p. F01011. doi: 10.1029/2007JF000838.
- Lewicki, J. L. and Brantley, S. L. (2000) 'CO₂ degassing along the San Andreas Fault, Parkfield,

- California', *Geophysical Research Letters*. John Wiley & Sons, Ltd, 27(1), pp. 5–8. doi: 10.1029/1999GL008380.
- Loiko, S. V. Pokrovsky, O. S. Raudina, T. V. Lim, A. Kolesnichenko, L. G. Shirokova, L. S. Vorobyev, S. N. Kirpotin, S. N. (2017) 'Abrupt permafrost collapse enhances organic carbon, CO₂, nutrient and metal release into surface waters', *Chemical Geology*. 471, pp. 153–165. doi: 10.1016/J.CHEMGEO.2017.10.002.
- Lönnqvist, M. and Hökmark, H. (2013) 'Approach to estimating the maximum depth for glacially induced hydraulic jacking in fractured crystalline rock at Forsmark, Sweden', *Journal of Geophysical Research: Earth Surface*, 118(3), pp. 1777–1791. doi: 10.1002/jgrf.20106.
- Mäder, U. K. Fierz, T. Frieg, B. Eikenberg, J. Rütli, M. Albinsson, Y. Möri, A. Ekberg, S. Stille, P. (2006) 'Interaction of hyperalkaline fluid with fractured rock: Field and laboratory experiments of the HPF project (Grimsel Test Site, Switzerland)', *Journal of Geochemical Exploration*. 90(1–2), pp. 68–94. doi: 10.1016/J.GEXPLO.2005.09.006.
- Manga, M. and Wang, C. Y. (2015) 'Earthquake Hydrology', in *Treatise on Geophysics: Second Edition*. doi: 10.1016/B978-0-444-53802-4.00082-8.
- Martel, S. J. (2006) 'Effect of topographic curvature on near-surface stresses and application to sheeting joints', *Geophysical Research Letters*, 33(1), doi: 10.1029/2005GL024710.
- Martel, S. J. (2011) 'Mechanics of curved surfaces, with application to surface-parallel cracks', *Geophysical Research Letters*, 38(20), p. n/a-n/a. doi: 10.1029/2011GL049354.
- Massmann, G. Tichomirowa, M. Merz, C. Pekdeger, A. (2003) 'Sulfide oxidation and sulfate reduction in a shallow groundwater system (Oderbruch Aquifer, Germany)', *Journal of Hydrology*. 278(1–4), pp. 231–243. doi: 10.1016/S0022-1694(03)00153-7.
- McGregor, L. A. Gauchotte-Lindsay, C. Daéid, N. N. Thomas, R. Daly, P. Kalin, R. M. (2011) 'Ultra resolution chemical fingerprinting of dense non-aqueous phase liquids from manufactured gas plants by reversed phase comprehensive two-dimensional gas chromatography', *Journal of Chromatography A*. Elsevier, 1218(29), pp. 4755–4763. doi: 10.1016/J.CHROMA.2011.05.045.
- McGregor, L. A. Gauchotte-Lindsay, C. Daéid, N. N. Thomas, R. Kalin, R. M. (2012) 'Multivariate Statistical Methods for the Environmental Forensic Classification of Coal Tars from Former Manufactured Gas Plants', *Environmental Science & Technology*. American Chemical Society, 46(7), pp. 3744–3752. doi: 10.1021/es203708w.
- McIntosh, J. C., Garven, G. and Hanor, J. S. (2011) 'Impacts of Pleistocene glaciation on large-scale groundwater flow and salinity in the Michigan Basin', *Geofluids*. J, 11(1), pp. 18–33. doi: 10.1111/j.1468-8123.2010.00303.x.
- McIntosh, J. C., Schlegel, M. E. and Person, M. (2012) 'Glacial impacts on hydrologic processes in sedimentary basins: evidence from natural tracer studies', *Geofluids*, 12(1), pp. 7–21. doi: 10.1111/j.1468-8123.2011.00344.x.
- McIntosh, J. C. and Walter, L. M. (2005) 'Volumetrically significant recharge of Pleistocene glacial meltwaters into epicratonic basins: Constraints imposed by solute mass balances', *Chemical Geology*. Elsevier, 222(3–4), pp. 292–309. doi: 10.1016/J.CHEMGEO.2005.07.010.
- McKinley, I. G. Alexander, W. R. Bajo, C. Frick, U. Hadermann, J. Herzog, F. A. Höhn, E. (1987) 'The Radionuclide Migration Experiment at the Grimsel Rock Laboratory, Switzerland', *MRS Proceedings*. Cambridge University Press, 112, p. 179. doi: 10.1557/PROC-112-179.
- MeteoSwiss (2016a) 'Climate normals Grimsel Hospiz 1961-1990', *Federal Office of Meteorology and Climatology MeteoSwiss*, climsheet.
- MeteoSwiss (2016b) 'Climate normals Grimsel Hospiz 1981-2010', *Federal Office of Meteorology and Climatology MeteoSwiss*, climsheet. Available at: <https://www.meteoswiss.admin.ch/home/climate/swiss-climate-in-detail/climate-normals/climate-diagrams-and-normals--per-station.html?region=Table>.
- Michael, H. A., Mulligan, A. E. and Harvey, C. F. (2005) 'Seasonal oscillations in water exchange

- between aquifers and the coastal ocean', *Nature*. Nature Publishing Group, 436(7054), pp. 1145–1148. doi: 10.1038/nature03935.
- Min, K.-B. Rutqvist, J. Tsang, C-F. Jing, L. (2004) 'Stress-dependent permeability of fractured rock masses: a numerical study', *International Journal of Rock Mechanics and Mining Sciences*, 41(7), pp. 1191–1210. doi: 10.1016/j.ijrmms.2004.05.005.
- Nesbitt, H. W. and Young, G. M. (1989) 'Formation and Diagenesis of Weathering Profiles', *The Journal of Geology*, 97(2), pp. 129–147. doi: 10.1086/629290.
- Neuzil, C. E. (2012) 'Hydromechanical effects of continental glaciation on groundwater systems', *Geofluids*. John Wiley & Sons, Ltd (10.1111), 12(1), pp. 22–37. doi: 10.1111/j.1468-8123.2011.00347.x.
- Neuzil, C. E. and Provost, A. M. (2014) 'Ice sheet load cycling and fluid underpressures in the Eastern Michigan Basin, Ontario, Canada', *Journal of Geophysical Research: Solid Earth*, 119(12), pp. 8748–8769. doi: 10.1002/2014JB011643.
- Oberhänsli, R. (1985) 'Mineralogy and geochemistry of meta-lamprophyres from the Central Swiss Alps.', *Unpubl. Habilitationsschrift, Univ. Bern*.
- Ogata, K. Senger, K. Braathen, A. Tveranger, J. (2014) 'Fracture corridors as seal-bypass systems in siliciclastic reservoir-cap rock successions: Field-based insights from the Jurassic Entrada Formation (SE Utah, USA)', *Journal of Structural Geology*. doi: 10.1016/j.jsg.2014.05.005.
- Onda, S. Sano, Y. Takahata, N. Kagoshima, T. Miyajima, T. Shibata, T. Pinti, D. L. Lan, T. Kim, N. K. Kusakabe, M. Nishio, Y. (2018) 'Groundwater oxygen isotope anomaly before the M6.6 Tottori earthquake in Southwest Japan', *Scientific Reports*. Nature Publishing Group, 8(1), p. 4800. doi: 10.1038/s41598-018-23303-8.
- Pancost, R. D. Baas, M. Van Geel, B. Damsté, J. S. S. (2002) 'Biomarkers as proxies for plant inputs to peats: An example from a sub-boreal ombrotrophic bog', *Organic Geochemistry*. doi: 10.1016/S0146-6380(02)00048-7.
- Pandey, A. P. and Chadha, R. K. (2003) 'Surface loading and triggered earthquakes in the Koyna–Warna region, western India', *Physics of the Earth and Planetary Interiors*, 139, pp. 207–223. doi: 10.1016/j.pepi.2003.08.003.
- Parkhurst, D. and Appelo, C. (2013) 'Description of input and examples for PHREEQC version 3—A computer program for speciation, batch-reaction, one-dimensional transport, and inverse geochemical calculations: U.S. Geological Survey Techniques and Methods'. USGS, p. 497p. Available at: <http://pubs.usgs.gov/tm/06/a43>.
- Parvin, M. Tadakuma, N. Asaue, H. Koike, K. (2014) 'Delineation and interpretation of spatial coseismic response of groundwater levels in shallow and deep parts of an alluvial plain to different earthquakes: A case study of the Kumamoto City area, southwest Japan', *Journal of Asian Earth Sciences*. doi: 10.1016/j.jseaes.2014.01.011.
- Payne, J. R. and Driskell, W. B. (2018) 'Macondo oil in northern Gulf of Mexico waters – Part 1: Assessments and forensic methods for Deepwater Horizon offshore water samples', *Marine Pollution Bulletin*. 129(1), pp. 399–411. doi: 10.1016/J.MARPOLBUL.2018.02.055.
- Person M. Bense, V. Cohen, D. Banerjee, A. (2012) 'Models of ice-sheet hydrogeologic interactions: a review', *Geofluids*. 12(1), pp. 58–78. doi: 10.1111/j.1468-8123.2011.00360.x.
- Peters, K. E., Walters, C. C. and Moldowan, J. M. (2004) *The Biomarker Guide, The Biomarker Guide*. doi: 10.1017/cbo9780511524868.
- Phelps, T. J. Raione, E. G. White, D. C. Fliermans, C. B. (1989) 'Microbial activities in deep subsurface environments', *Geomicrobiology Journal*. 7(1–2), pp. 79–91. doi: 10.1080/01490458909377851.
- Pitkanen, P., Partamies, S. and Luukkonen, A. (2004) *Hydrogeochemical Interpretation of Baseline Groundwater Conditions at the Olkiluoto Site. Posiva Report 2003-07*.
- Pytharouli, S. I. Lunn, R. J. Shipton, Z. K. Kirkpartick, J. D. Nascimento, A. F. (2011) 'Microseismicity

- illuminates open fractures in the shallow crust', *Geophys. Res. Lett.*, 38, p. 2402. doi: 10.1029/2010GL045875.
- Ramaker, R. C., Gordon, E. R. and Cooper, S. J. (no date) 'R2DGC: threshold-free peak alignment and identification for 2D gas chromatography-mass spectrometry in R'. doi: 10.1093/bioinformatics/btx825.
- Reddy, D. V., Nagabhushanam, P. and Sukhija, B. S. (2011) 'Earthquake (M 5.1) induced hydrogeochemical and $\delta^{18}\text{O}$ changes: validation of aquifer breaching-mixing model in Koyna, India', *Geophys. J. Int.*, 184, pp. 359–370. doi: 10.1111/j.1365-246X.2010.04838.x.
- Ritchie, N. J., Schutter, M. E., Dick, R. P., Myrold, D. D. (2000) 'Use of length heterogeneity PCR and fatty acid methyl ester profiles to characterize microbial communities in soil.', *Applied and environmental microbiology*. American Society for Microbiology, 66(4), pp. 1668–75. doi: 10.1128/aem.66.4.1668-1675.2000.
- Roeloffs, E. A. (1988) 'Fault stability changes induced beneath a reservoir with cyclic variations in water level', *Journal of Geophysical Research*. John Wiley & Sons, Ltd, 93(B3), p. 2107. doi: 10.1029/JB093iB03p02107.
- Rogers, S. F. (2003) 'Critical stress-related permeability in fractured rocks', *Geological Society, London, Special Publications*. Geological Society of London, 209(1), pp. 7–16. doi: 10.1144/GSL.SP.2003.209.01.02.
- Rolland, Y., Cox, S. F. and Corsini, M. (2009) 'Constraining deformation stages in brittle–ductile shear zones from combined field mapping and $^{40}\text{Ar}/^{39}\text{Ar}$ dating: The structural evolution of the Grimsel Pass area (Aar Massif, Swiss Alps)', *Journal of Structural Geology*, 31(11), pp. 1377–1394. doi: 10.1016/j.jsg.2009.08.003.
- Ross, Z. E., Hauksson, E. and Ben-Zion, Y. (2017) *Abundant off-fault seismicity and orthogonal structures in the San Jacinto fault zone*. *Sci. Adv.*, 3:e1601946 .
- Saar, M. O. and Manga, M. (2003) 'Seismicity induced by seasonal groundwater recharge at Mt. Hood, Oregon', *Earth and Planetary Science Letters*, 214(3), pp. 605–618. doi: 10.1016/S0012-821X(03)00418-7.
- Sabir, I. H., Torgersen, J., Haldorsen, S., Aleström, P. (1999) 'DNA tracers with information capacity and high detection sensitivity tested in groundwater studies', *Hydrogeology Journal*. Springer-Verlag, 7(3), pp. 264–272. doi: 10.1007/s100400050200.
- Saruwatari, K., Kameda, J. and Tanaka, H. (2004) 'Generation of hydrogen ions and hydrogen gas in quartz? water crushing experiments: an example of chemical processes in active faults', *Physics and Chemistry of Minerals*. Springer-Verlag, 31(3), pp. 176–182. doi: 10.1007/s00269-004-0382-2.
- Sato, M., Sutton, A. J., McGee, K. A., Russell-Robinson, S. (1986) 'Monitoring of hydrogen along the San Andreas and Calaveras faults in central California in 1980-1984', *Journal of Geophysical Research: Solid Earth*. 91(B12), pp. 12315–12326. doi: 10.1029/JB091iB12p12315.
- Schaltegger, U. (1990) 'Post-magmatic resetting of Rb-Sr whole rock ages — a study in the Central Aar Granite (Central Alps, Switzerland)', *Geologische Rundschau*, 79(3), pp. 709–724. doi: 10.1007/BF01879210.
- Schaltegger, U. (1993) 'The evolution of the polymetamorphic basement in the Central Alps unravelled by precise U-Pb zircon dating', *Contributions to Mineralogy and Petrology*, 113(4), pp. 466–478. doi: 10.1007/BF00698316.
- Schaltegger, U. and von Quadt, A. (1990) 'U-Pb zircon dating of the Central Aar Granite (Aar massif, Switzerland)', *Schweizerische Mineralogische und Petrographische Mitteilungen*, 70(361–370).
- Schneeberger, R., Berger, A., Herwegh, M., Eugster, A., Korber, F., Spillmann, T., Blechschmidt, I. (2016) *Arbeitsbericht NAGRA NAB 16-27 GTS Phase VI - LASMO: Geology and Structures of the GTS and Grimsel region*.
- Schneeberger, R., de La Varga, M., Egli, D., Berger, A., Kober, F., Wellmann, F., Herwegh, M. (2017)

- 'Methods and uncertainty estimations of 3-D structural modelling in crystalline rocks: a case study', *Solid Earth*, 8(5), pp. 987–1002. doi: 10.5194/se-8-987-2017.
- Schneeberger, R. Kober, F. Lanyon, B. Mäder, U. K. Spillmann, T. Blechschmidt. I. (2019) 'NTB-19-01, Grimsel Test Site: Revisiting the site-specific geoscientific knowledge'. Nagra.
- Schneeberger, R. B. (2017) *Interplay in 3D between faults and water flow paths in crystalline bedrock (Grimsel, Switzerland)*.
- Schneeberger, R., Mäder, U. K. and Waber, H. N. (2017) 'ScienceDirect Hydrochemical and isotopic (d^2H , $d^{18}O$, 3H) characterization of fracture water in crystalline rock (Grimsel, Switzerland)', *Procedia Earth and Planetary Science*, 17, pp. 738–741. doi: 10.1016/j.proeps.2016.12.187.
- Schotterer, U. (2010) 'Wasserisotope in der Schweiz - Neue Ergebnisse und Erfahrungen aus dem nationalen Messnetz ISOT', *Wasser | EAUX*.
- Shamsudduha, M. Chandler, R. E. Taylor, R. G. Ahmed, K. M. (2009) 'Recent trends in groundwater levels in a highly seasonal hydrological system: the Ganges-Brahmaputra-Meghna Delta', *Hydrology and Earth System Sciences*, 13(12), pp. 2373–2385. doi: 10.5194/hess-13-2373-2009.
- Shi, Z. Wang, G. Manga, M. Wang, C. Y. (2015) 'Continental-scale water-level response to a large earthquake', *Geofluids*, 15(1–2). doi: 10.1111/gfl.12099.
- Shi, Z. Wang, G. Liu, C. Che, Y. (2018) 'Tectonically Induced Anomalies Without Large Earthquake Occurrences', *Pure and Applied Geophysics*. Springer International Publishing, 175(7), pp. 2513–2526. doi: 10.1007/s00024-017-1596-9.
- Shipton, Z. Evans, J. P. Dockrill, B. Heath, J. Williams, A. (2005) 'Natural leaking CO₂-charged systems as analogs for failed geologic storage reservoirs', *Carbon Dioxide Capture for Storage in Deep Geologic Formations*, pp. 699-712
- Shipton, Z. K. Evans, J. P. Kirschner, D. Kolesar, P. T. Williams, A. P. Heath, J. (2004) 'Analysis of CO₂ leakage through "low-permeability" faults from natural reservoirs in the Colorado Plateau, east-central Utah', *Geological Society, London, Special Publications*, 233(1), pp. 43–58. doi: 10.1144/GSL.SP.2004.233.01.05.
- Simpson, D. W. (1986) *Triggered Earthquakes*. Annu. Rev. Earth Planet. Sci. 14, pp. 22-42.
- Simpson, D. W., Leith, W. S. and Scholz, C. H. (1988) *Two Types of Reservoir-Induced Seismicity*, *Bulletin of the Seismological Society of America*.
- Skelley, A. M. Aubrey, A. D. Willis, P. A. Amashukeli, X. Ehrenfreund, P. Bada, J. L. Grunthaler, F. J. Mathies, R. A. (2007) 'Organic amine biomarker detection in the Yungay region of the Atacama Desert with the Urey instrument', *Journal of Geophysical Research: Biogeosciences*. 112(G4), doi: 10.1029/2006JG000329.
- Skelton, A. Andrén, M. Kristmannsdóttir, H. Stockmann, G. Mörth, C-M. Sveinbjörnsdóttir, Á. Jónsson, S. Sturkell, E. Guðrúnardóttir, H. R. Hjartarson, H. Seigmund, H. Kockum I. (2014) 'Changes in groundwater chemistry before two consecutive earthquakes in Iceland', *Nature Geoscience*. Nature Publishing Group, 7, p. 752.
- Slim, M. Perron, J. T. Martel, S. J. Singha, K. (2015) 'Topographic stress and rock fracture: a two-dimensional numerical model for arbitrary topography and preliminary comparison with borehole observations', *Earth Surface Processes and Landforms*, 40(4), pp. 512–529. doi: 10.1002/esp.3646.
- St Clair, J. Moon, S. Holbrook, W. S. Perron, J. T. Riebe, C. S. Martel, S. J. Carr, B. Harman, C. Singha, K. Richter, Dd (2015) 'Geophysical imaging reveals topographic stress control of bedrock weathering.', *Science (New York, N.Y.)*. American Association for the Advancement of Science, 350(6260), pp. 534–8. doi: 10.1126/science.aab2210.
- Starinsky, A. and Katz, A. (2003) 'The formation of natural cryogenic brines', *Geochimica et Cosmochimica Acta*. Pergamon, 67(8), pp. 1475–1484. doi: 10.1016/S0016-7037(02)01295-4.

- Stegen, J. C. Fredrickson, J. K. Wilking, M. J. Konopka, A. E. Nelson, W. C. Arntzen, E. V. Chrisler, W. B. Chu, R. K. Danczak, R. E. Fansler, S. J. Kennedy, D. W. Resch, C. T. Tfaily, M (2016) 'Groundwater-surface water mixing shifts ecological assembly processes and stimulates organic carbon turnover', *Nature Communications*, 7. doi: 10.1038/ncomms11237.
- Stiros, S. C. and Saltogianni, V. (2014) 'Solution of underdetermined systems of equations with gridded a priori constraints', *SpringerPlus*. SpringerOpen, 3(1), p. 145. doi: 10.1186/2193-1801-3-145.
- Stober, I. and Bucher, K. (2015) 'Hydraulic conductivity of fractured upper crust: insights from hydraulic tests in boreholes and fluid-rock interaction in crystalline basement rocks', *Geofluids*. Blackwell Publishing Ltd, 15(1–2), pp. 161–178. doi: 10.1111/gfl.12104.
- Subba, R. N. (2006) 'Seasonal variation of groundwater quality in a part of Guntur District, Andhra Pradesh, India', *Environmental Geology*. Springer-Verlag, 49(3), pp. 413–429. doi: 10.1007/s00254-005-0089-9.
- Sulem, J. and Famin, V. (2009) 'Thermal decomposition of carbonates in fault zones: Slip-weakening and temperature-limiting effects', *Journal of Geophysical Research*, 114(B3), p. B03309. doi: 10.1029/2008JB006004.
- Sutcliffe, D. W. Carrick, T. R. Heron, J. Rigg, E. Talling, J. F. Woof, C. Lund, J. W. G. (1982) 'Long-term and seasonal changes in the chemical composition of precipitation and surface waters of lakes and tarns in the English Lake District', *Freshwater Biology*. 12(5), pp. 451–506. doi: 10.1111/J.1365-2427.1982.TB00640.X.
- Tan, K. H. (2011) *Principles of soil chemistry*. CRC Press.
- Telling, J. Boyd, E. S. Bone, N. Jones, E. L. Tranter, M. MacFarlane, J. W. Martin, P. G. Wadham, J. L. Lamarche-Gagnon, G. Skidmore, M. L. Hamilton, T. L. Hill, E. Jackson, M. Hodgeson, D. A. (2015) 'Rock comminution as a source of hydrogen for subglacial ecosystems', *Nature Geoscience*. Nature Publishing Group, 8(11), pp. 851–855. doi: 10.1038/ngeo2533.
- Tijani, M. N., Oke, S. A. and Olowookere, A. T. (2014) 'Hydrogeochemical characterization of a shallow groundwater system in the weathered basement aquifer of Ilesha area, southwestern Nigeria', *Proceedings of the International Association of Hydrological Sciences*, 364, pp. 475–480. doi: 10.5194/piahs-364-475-2014.
- Tokunaga, T. (1999) 'Modeling of earthquake-induced hydrological changes and possible permeability enhancement due to the 17 January 1995 Kobe Earthquake, Japan', *Journal of Hydrology*, 223(3–4), pp. 221–229. doi: 10.1016/S0022-1694(99)00124-9.
- Toney, J. L. Huang, Y. Fritz, S. C. Baker, P. A. Grimm, E. Nyren, P. (2010) 'Climatic and environmental controls on the occurrence and distributions of long chain alkenones in lakes of the interior United States', *Geochimica et Cosmochimica Acta*, 74(5), pp. 1563–1578. doi: 10.1016/j.gca.2009.11.021.
- Toth, A. and Bobok, E. (2017) 'What Is Geothermal Energy?', in *Flow and Heat Transfer in Geothermal Systems*. Elsevier, pp. 1–19. doi: 10.1016/b978-0-12-800277-3.00001-3.
- Tranter, M. (2015) 'Grand challenge for low temperature and pressure geochemistry—sparks in the dark, on Earth, Mars, and throughout the Galaxy'. doi: 10.3389/feart.2015.00069.
- Tsunogai, U. and Wakita, H. (1996) 'Anomalous Changes in Groundwater Chemistry. Possible Precursors of the 1995 Hyogo-ken Nanbu Earthquake, Japan.', *Journal of Physics of the Earth*. The Seismological Society of Japan, The Volcanological Society of Japan, The Geodetic Society of Japan, 44(4), pp. 381–390. doi: 10.4294/jpe1952.44.381.
- Uehara, S. and Shimamoto, T. (2004) 'Gas permeability evolution of cataclasite and fault gouge in triaxial compression and implications for changes in fault-zone permeability structure through the earthquake cycle', *Tectonophysics*. Elsevier, 378(3–4), pp. 183–195. doi: 10.1016/J.TECTO.2003.09.007.
- Vidstrand, P. and Wallroth, T. (2008) 'Coupled HM effects in a crystalline rock mass due to glaciation: indicative results from groundwater flow regimes and stresses from an FEM study'. doi:

10.1007/s10064-008-0123-8.

- Vitt, D. H., Bayley, S. E. and Jin, T.-L. (1995) 'Seasonal variation in water chemistry over a bog-rich fen gradient in Continental Western Canada', *Canadian Journal of Fisheries and Aquatic Sciences*. NRC Research Press Ottawa, Canada, 52(3), pp. 587–606. doi: 10.1139/f95-059.
- Voborny, O. Adank, P, Hürlimann, W. Vomvoris, S. Mishra, S. (1991) *Technical Report 91-03 Grimsel Test Site. Modeling of Groundwater Flow in the Rock Body Surrounding the Underground Laboratory*.
- Voborny, O., Vomvoris, S. and Lanyon, G. W. (1995) 'Simulations of Groundwater Flow in Fractured Crystalline Rocks of Northern Switzerland', *Bull. Swiss Assoc. of Petroleum Geol. and Eng.*, 62(140), pp. 17–28.
- Volkman, J. K. Barrett, S. M. Blackburn, S. I. Mansour, M. P. Sikes, E. L. Gelin, F. (1998) 'Microalgal biomarkers: A review of recent research developments'. *Org. Geochem.* 29(5-7), pp. 1163-1179.
- Volkman, J. K., Barrett, S. M. and Dunstan, G. A. (1994) 'C25 and C30 highly branched isoprenoid alkenes in laboratory cultures of two marine diatoms', *Organic Geochemistry*. Pergamon, 21(3–4), pp. 407–414. doi: 10.1016/0146-6380(94)90202-X.
- Waber, H. N. *et al.* (2017) 'ScienceDirect Constraints on evolution and residence time of geothermal water in granitic rocks at Grimsel (Switzerland)', *Procedia Earth and Planetary Science*, 17, pp. 774–777. doi: 10.1016/j.proeps.2017.01.026.
- Wallace, S. H. *et al.* (2012) 'Effect of groundwater pH and ionic strength on strontium sorption in aquifer sediments: Implications for 90Sr mobility at contaminated nuclear sites', *Applied Geochemistry*. doi: 10.1016/j.apgeochem.2012.04.007.
- Wang, C.-Y., Wang, C.-H. and Kuo, C.-H. (2004) 'Temporal change in groundwater level following the 1999 (Mw = 7.5) Chi-Chi earthquake, Taiwan', *Geofluids*. John Wiley & Sons, Ltd (10.1111), 4(3), pp. 210–220. doi: 10.1111/j.1468-8123.2004.00082.x.
- Wehrens, P. (2015) *Structural evolution in the Aar Massif (Haslital transect): Implications for mid-crustal deformation*. University of Bern, Bern, Switzerland.
- White, B. (2009) 'A Dictionary of Chemistry (6th edition) Edited by John Daintith. *A Dictionary of Chemistry (6th edition)*. Oxford: Oxford University Press 2008. ISBN: 978 0 19 920463 2. doi: 10.1108/09504120910935291.
- Whitehead, P. G. Wilby, R. L. Battarbee, R. W. Kernan, M. Wade, A. J. (2009) 'A review of the potential impacts of climate change on surface water quality', *Hydrological Sciences Journal*. Taylor & Francis Group, 54(1), pp. 101–123. doi: 10.1623/hysj.54.1.101.
- Winter, T. C. (1999) 'Relation of streams, lakes, and wetlands to groundwater flow systems', *Hydrogeology Journal*. Springer-Verlag, 7(1), pp. 28–45. doi: 10.1007/s100400050178.
- Wood, B. D., Keller, C. K. and Johnstone, D. L. (1993) 'In situ measurement of microbial activity and controls on microbial CO₂ production in the unsaturated zone', *Water Resources Research*. John Wiley & Sons, Ltd, 29(3), pp. 647–659. doi: 10.1029/92WR02315.
- Yadav, A., Bansal, B. K. and Pandey, A. P. (2016) 'Five decades of triggered earthquakes in Koyna-Warna Region, western India – A review', *Earth-Science Reviews*. Elsevier, 162, pp. 433–450. doi: 10.1016/J.EARSCIREV.2016.09.013.
- Yan, R., Wang, G. and Shi, Z. (2016) 'Sensitivity of hydraulic properties to dynamic strain within a fault damage zone', *Journal of Hydrology*, 543, pp. 721–728. doi: 10.1016/j.jhydrol.2016.10.043.
- Yecheili, Y. and Bein, A. (2002) 'Response of groundwater systems in the Dead Sea Rift Valley to the Nuweiba earthquake: Changes in head, water chemistry, and near-surface effects', *J. Geophys. Res.*, 107(B12), p. 2332. doi: 10.1029/2001JB001100.
- Zhang, T. Barry, R. G. Knowles, K. Heginbottom, J. A. Brown, J. (2008) 'Polar Geography Statistics and characteristics of permafrost and ground-ice distribution in the Northern Hemisphere'. doi:

10.1080/10889379909377670.

- Ziegler, M., Loew, S. and Amann, F. (2016) 'Near-surface rock stress orientations in alpine topography derived from exfoliation fracture surface markings and 3D numerical modelling', *International Journal of Rock Mechanics and Mining Sciences*, 85, pp. 129–151. doi: 10.1016/j.ijrmms.2016.03.009.
- Ziegler, M., Loew, S. and Bahat, D. (2014) 'Growth of exfoliation joints and near-surface stress orientations inferred from fractographic markings observed in the upper Aar valley (Swiss Alps)', *Tectonophysics*, 626, pp. 1–20. doi: 10.1016/j.tecto.2014.03.017.

APPENDICES

Appendix I

Consists of the PHREEQC input file used to generate the speciation table also attached. Enclosed is the input file for generating the Mass Balance equilibrium model, average groundwater composition from each borehole was taken to reduce the number of different combinations of Mass Balance models required.

Speciation Input File

DATABASE C:\Program Files (x86)\USGS\Phreeqc Interactive 3.3.8-11728\database\llnl.dat
TITLE Calculation of Saturation Index for 2016 Data Set

SOLUTION_SPREAD

```
-temp 13
-units mg/l
Number pH pe Alkalinity Al Ca Fe K
Li Mg Mn Na Si Sr F Cl S
charge
1 9.42 2.014174266 15.57377049 0.057 5.18 0.025 0.47 0.04
0.03 0.001 11.28 4.5 0.176 4.663 1.979 5.029
2 9.46 1.64581018 15.73770492 0.071 5.64 0.03 0.38 0.04
0.045 0.001 11.4 4.83 0.19 4.595 1.906 5.052
3,4,5,6, ..... #All data not included but found in Appendix 3 for reference
```

SELECTED_OUTPUT 1

```
-file F:\Modeling SC8\OutPut\selected_output_1.sel
-simulation false
-state false
-distance false
-time false
-step false
-reaction false
-alkalinity false
-ionic_strength true
-water false
-charge_balance true
-percent_error true
-saturation_indices Calcite Kaolinite K-feldspar Illite
CO2(g) Quartz Albite Anorthite
Clinochlore-14A Fe(OH)3
```

END

Output Saturation Index data found in table over leaf ...

Saturation Index Range for Each Borehole Interval

Borehole	Host										
	Lithology	Calcite	Kaolinite	K-feldspar	Illite	CO2(g)	Quartz	Albite	Anorthite	Clinochlore-14A	Fe(OH)3
B	CaGr	-0.273 to -1.095	4.019 to 2.042	0.977 to 0.027	2.941 to 0.822	-4.070 to -5.000	0.169 to 0.130	-0.187 to -1.120	-3.509 to -5.549	-3.014 to -12.341	0.173 to -2.195
C	CaGr	-0.300 to -1.070	2.843 to 1.539	0.776 to 0.142	1.908 to 0.717	-4.059 to -4.877	0.170 to 0.123	-0.656 to -1.285	-4.182 to -5.546	-4.840 to -13.059	-0.781 to -2.218
D	CaGr	-0.237 to -0.653	2.748 to 1.790	0.800 to -0.316	1.962 to 0.816	-4.426 to -4.983	0.137 to 0.110	-0.495 to -1.007	-3.949 to -4.984	-4.382 to -9.403	-0.782 to -2.120
E	CaGr	-0.239 to -1.331	5.454 to 2.016	1.713 to 0.047	4.825 to 1.066	-3.667 to -4.843	0.181 to 0.124	0.216 to -1.003	-2.739 to -5.011	-4.442 to -14.829	0.463 to -2.254
F	CaGr	-0.243 to -0.587	2.888 to 2.028	1.286 to 0.779	2.485 to 1.736	-4.650 to -5.011	0.165 to 0.118	-0.325 to -0.635	-3.894 to -4.408	-3.275 to -6.407	-0.654 to -2.150
G	CaGr	-0.252 to -1.446	4.939 to 2.707	1.118 to 0.672	3.483 to 2.088	-3.561 to -4.878	0.122 to 0.085	-0.575 to -0.831	-3.655 to -4.128	-3.358 to -14.047	-0.641 to -2.095
H	CaGr	-0.023 to -0.311	2.237 to 1.326	0.867 to 0.400	1.894 to 0.901	-5.022 to -5.323	0.106 to 0.073	-0.577 to -0.941	-3.924 to -4.667	-2.367 to -4.398	-0.753 to -2.216
I	GrGr	-0.162 to -3.742	2.023 to -5.163	0.931 to -6.227	1.893 to -10.453	-1.668 to -5.778	0.188 to 0.063	-0.208 to -7.223	-3.891 to -18.340	-0.113 to -47.422	-0.566 to -3.308
K	GrGr	-0.157 to -1.384	5.586 to 1.729	2.009 to 0.999	5.065 to 1.685	-4.000 to -5.547	0.192 to 0.075	0.351 to -0.509	-2.904 to -4.205	2.128 to -7.884	-0.046 to -2.260
L	GrGr	-0.156 to -1.571	2.219 to 0.739	0.848 to 0.102	1.907 to 0.250	-4.916 to -6.450	-0.029 to -0.072	-0.776 to -1.403	-4.072 to -5.440	-2.460 to -4.357	0.513 to -1.054
M	GrGr	-0.176 to -0.438	2.139 to 1.151	1.212 to 0.723	2.064 to 0.952	-5.099 to -5.331	0.128 to 0.073	-0.416 to -0.873	-4.140 to -4.890	-2.831 to -4.440	-0.974 to -2.232

Average Saturation Index For Each Borehole Interval

Borehole	Host										
	Lithology	Calcite	Kaolinite	K-feldspar	Illite	CO2(g)	Quartz	Albite	Anorthite	Clinochlore-14A	Fe(OH)3
B	CaGr	-0.660	2.800	0.600	1.950	-4.564	0.153	-0.575	-4.400	-8.762	-1.481
C	CaGr	-0.546	2.241	0.532	1.492	-4.615	0.140	-0.912	-4.793	-8.167	-134.615
D	CaGr	-0.410	2.173	0.420	1.467	-4.785	0.124	-0.793	-4.554	-6.263	-1.567
E	CaGr	-0.638	2.871	0.628	2.062	-4.439	0.145	-0.703	-4.430	-7.987	-1.451
F	CaGr	-0.358	2.426	1.046	2.118	-4.884	0.147	-0.489	-4.152	-4.741	-1.580
G	CaGr	-0.504	3.102	0.837	2.488	-4.622	0.097	-0.698	-3.883	-5.714	-1.554
H	CaGr	-0.095	1.700	0.633	1.365	-5.165	0.086	-0.773	-4.332	-3.315	-1.674
I	GrGr	-0.551	0.962	-0.149	0.167	-5.272	0.088	-0.940	-5.419	-6.088	-1.608
K	GrGr	-0.337	2.595	1.405	2.643	-5.202	0.109	-0.108	-3.643	-1.308	-0.952
L	GrGr	-0.344	1.837	0.569	1.442	-5.125	-0.045	-0.959	-4.476	-3.323	-0.369
M	GrGr	-0.265	1.620	0.961	1.489	-5.229	0.098	-0.665	-4.519	-3.477	-1.702

Example of Inverse Mass Balance Input File

DATABASE C:\Program Files (x86)\USGS\Phreeqc Interactive 3.3.8-11728\database\llnl.dat
TITLE Inverse Modeling of Surface to groundwater
#RR VS Grimsel groundwater

SOLUTION 20
temp 10
pH 7
pe 4
redox pe
units mmol/kgw
density 1
-water 1 # kg

#RR
SOLUTION 1
temp 8.1
pH 6.85
pe 0.93
redox pe
units mg/l
density 1
Al 0.0418
Alkalinity 1.31
Ca 0.7114
Cl 0.036
F 0.04
Fe 0.0001
K 0.2726
Mg 0.084
Na 0.056
S(6) 0.652
Si 0.7708
-water 1 # kg

#RS
SOLUTION 2
temp 10.4
pH 7.13
pe 0.99
redox pe
units mg/l
density 1
Al 0.0303
Alkalinity 4.26
Ca 2.485
Cl 0.431
F 0.05
Fe 0.0001
K 0.857
Mg 0.2606
Na 0.905
S(6) 4.141
Si 0.6211
-water 1 # kg

#GR
SOLUTION 3
temp 11.2
pH 6.67
pe 1.98
redox pe
units mg/l
density 1
Al 0.0638
Alkalinity 1.8
Ca 0.8122
Cl 0.978
F 0.189
Fe 0.0001
K 0.5373
Mg 0.1163
Na 0.9462
S(6) 1.786
Si 0.8019
-water 1 # kg

#GS
SOLUTION 4
temp 7
pH 7
pe 1.58
redox pe
units mg/l
density 1
Al 0.0327
Alkalinity 5.08
Ca 2.785
Cl 0.586
F 0.048
Fe 0.0001
K 0.8291
Mg 0.3293
Na 1.43
S(6) 5.24
Si 0.6222
-water 1 # kg

#US 85.003 06/04/16
SOLUTION 5
temp 12
pH 9.31
pe 0.96
redox pe
units mg/l
density 1
Al 0.0022
Alkalinity 16.88
Ca 8.44
Cl 0.717
F 4.39
Fe 0.014
K 0.22
Mg 0.025

Na 8.94
S(6) 7.325
Si 4.39
-water 1 # kg

#HP i2 06/04/16

SOLUTION 6

temp 12
pH 9.34
pe 0.14
redox pe
units mg/l
density 1
Al 0.046
Alkalinity 16.07
Ca 5.29
Cl 1.824
F 4.727
Fe 0.01
K 0.38
Mg 0.029
Na 11.41
S(6) 4.971
Si 4.73
-water 1 # kg

#SB i1

SOLUTION 7

temp 12
pH 8.89
pe 0.68
redox pe
units mg/l
density 1
Al 0.004
Alkalinity 16.39
Ca 8.73
Cl 0.195
F 3.731
Fe 0.01
K 0.21
Mg 0.042
Na 6.22
S(6) 6.937
Si 4.08
-water 1 # kg

#SB i4 06/04/16

SOLUTION 8

temp 12
pH 9.61
pe -0.21
redox pe
units mg/l
density 1
Al 0.029
Alkalinity 13.89
Ca 4.09

Cl 4.17
F 6.097
Fe 0.001
K 0.045
Mg 0.006
Na 14.22
S(6) 4.715
Si 4.79
-water 1 # kg

#US i2 06/04/16

SOLUTION 9

temp 12
pH 9.03
pe 0.09
redox pe
units mg/l
density 1
Al 0.027
Alkalinity 16.72
Ca 6.91
Cl 0.276
F 4.763
Fe 0.01
K 0.24
Mg 0.03
Na 9.54
S(6) 6.535
Si 4.66
-water 1 # kg

#US i3

SOLUTION 10

temp 12
pH 8.7
pe 0.21
redox pe
units mg/l
density 1
Al 0.013
Alkalinity 18.69
Ca 7.78
Cl 0.261
F 4.348
Fe 0.001
K 0.16
Mg 0.026
Na 8.69
S(6) 6.592
Si 4.44
-water 1 # kg

#US i4

SOLUTION 11

temp 12
pH 8.87
pe 0.01
redox pe

units mg/l
density 1
Al 0.014
Alkalinity 16.89
Ca 7.39
Cl 0.251
F 4.419
Fe 0.001
K 0.09
Mg 0.021
Na 8.78
S(6) 6.367
Si 4.4
-water 1 # kg

#US i5
SOLUTION 12
temp 12
pH 8.68
pe 0.12
redox pe
units mg/l
density 1
Al 0.015
Alkalinity 16.23
Ca 7.59
Cl 0.237
F 4
Fe 0.001
K 0.24
Mg 0.017
Na 8.43
S(6) 7.253
Si 4.66
-water 1 # kg

#US i6
SOLUTION 13
temp 12
pH 8.56
pe 0.11
redox pe
units mg/l
density 1
Al 0.007
Alkalinity 16.23
Ca 6.73
Cl 0.322
F 5.041
Fe 0.001
K 0.14
Mg 0.0109
Na 10.3
S(6) 7.374
Si 4.67
-water 1 # kg

#VE i2 06/04/16

SOLUTION 14
temp 12
pH 9.39
pe -0.14
redox pe
units mg/l
density 1
Al 0.02
Alkalinity 16.39
Ca 5.31
Cl 1.405
F 4.231
Fe 0.001
K 0.41
Mg 0.018
Na 10.72
S(6) 5.49
Si 4.54
-water 1 # kg

#VE i3 06/04/16

SOLUTION 15
temp 12
pH 9.2
pe -0.03
redox pe
units mg/l
density 1
Al 0.027
Alkalinity 18.03
Ca 6.83
Cl 1.673
F 5.811
Fe 0.474
K 0.33
Mg 0.041
Na 11.26
S(6) 2.99
Si 3.18
-water 1 # kg

INVERSE_MODELING 1
-solutions 1 6
-uncertainty 0.5 0.05
-phases
Albite dis
Anorthite dis
Calcite
Quartz dis
K-Feldspar dis
Phlogopite dis
Fluorite dis
Clinochlore-14A dis
Kaolinite
Illite
Annite
Muscovite dis
Pyrite dis
Halite

```

CO2(g)
# Fe(OH)3      pre
  H2S(g)      pre
-range        1000
-tolerance    1e-15
-mineral_water false
-multiple_precision true
-mp_tolerance 1e-12
-censor_mp    1e-20

```

INVERSE_MODELING 2

```

-solutions 2 6
-uncertainty 0.5 0.05

```

```

-phases
  Albite      dis
  Anorthite   dis
  Calcite
  Quartz      dis
  K-Feldspar  dis
  Phlogopite  dis
  Fluorite    dis
  Clinocllore-14A dis
  Kaolinite
  Illite
  Annite
  Muscovite   dis
  Pyrite      dis
  Halite
  CO2(g)

```

```

# Fe(OH)3      pre
  H2S(g)      pre
-range        1000
-tolerance    1e-15
-mineral_water false
-multiple_precision true
-mp_tolerance 1e-12
-censor_mp    1e-20

```

INVERSE_MODELING 3

```

-solutions 3 6
-uncertainty 0.5 0.05

```

```

-phases
  Albite      dis
  Anorthite   dis
  Calcite
  Quartz      dis
  K-Feldspar  dis
  Phlogopite  dis
  Fluorite    dis
  Clinocllore-14A dis
  Kaolinite
  Illite
  Annite
  Muscovite   dis
  Pyrite      dis
  Halite
  CO2(g)

```

```

# Fe(OH)3      pre

```

```
H2S(g)      pre
-range      1000
-tolerance  1e-15
-mineral_water  false
-multiple_precision  true
-mp_tolerance 1e-12
-censor_mp 1e-20
```

INVERSE_MODELING 4

```
-solutions  4  6
-uncertainty 0.5      0.05
-phases
```

```
Albite      dis
Anorthite   dis
Calcite
Quartz      dis
K-Feldspar  dis
Phlogopite  dis
Fluorite    dis
Clinochlore-14A  dis
Kaolinite
Illite
Annite
Muscovite   dis
Pyrite      dis
Halite
CO2(g)
```

```
# Fe(OH)3    pre
H2S(g)      pre
-range      1000
-tolerance  1e-15
-mineral_water  false
-multiple_precision  true
-mp_tolerance 1e-12
-censor_mp 1e-20
```

END

Appendix II

Consists of the peak alignment tables output by R2DGC and is split into two tables one for the soil and sediment samples (3a, 3b, 4a, 4b, 5a, 5b, 6a, 6b) and another for the liquid samples (a-g and LW). Compound names are from mass spectra matches in ChromaTOF using the internal MS database with as match above 75%.

Compound	3a	3b	4a	4b	5a	5b	6a	6b
Toluene	4.81E+07	2.44E+07	4.19E+07	3.90E+07	4.09E+07	3.49E+07	4.16E+07	3.24E+07
Hexanal	1.04E+07	1.19E+07	8.39E+06	1.86E+07	8.30E+06	1.81E+07	1.49E+07	9.72E+06
Acetic.acid..butyl.ester	1.08E+07	1.17E+07	1.06E+07	1.76E+07	1.24E+07	2.00E+07	1.69E+07	1.75E+07
X2.Hexene..4.ethyl.2.3.dimethyl.	2.06E+06	2.94E+06	2.50E+06	5.80E+06	4.25E+06	3.09E+06	2.36E+06	3.95E+06
Butane..2.3.dimethyl.2.3.dinitro.	6.98E+06	3.55E+06	4.04E+06	6.03E+06	5.29E+06	4.93E+06	4.37E+06	4.78E+06
Butyl.tert.butyl.isopropoxyborane	1.29E+06	2.72E+06	2.49E+06	5.05E+06	2.41E+06	1.33E+05	0.00E+00	8.29E+05
X3.Penten.2.one..4.methyl.	1.90E+07	1.19E+07	1.42E+07	2.51E+07	2.26E+07	1.64E+07	1.76E+07	1.94E+07
Cyclotetrasiloxane..octamethyl.	2.11E+06	3.37E+06	3.34E+06	1.96E+07	7.18E+06	6.31E+05	6.09E+05	7.33E+05
X1.3.Dioxolane..2..1.methylethyl..	0.00E+00	1.17E+06	4.20E+05	1.78E+06	2.48E+06	4.37E+06	4.22E+06	4.22E+06
X4.Methyl.2.hexanol	3.51E+06	9.14E+05	2.58E+06	1.19E+06	2.92E+06	3.78E+06	5.81E+06	3.10E+06
X1.Hexene..4.5.dimethyl.	2.59E+06	2.80E+06	0.00E+00	1.79E+05	2.43E+06	4.87E+06	5.72E+06	6.45E+06
Propanoic.acid..2.methoxy.	9.99E+05	2.91E+06	4.91E+05	2.80E+06	2.87E+06	2.43E+05	8.72E+05	1.11E+06
X2.Heptanone	2.02E+05	7.22E+05	4.84E+05	4.89E+05	1.01E+06	7.12E+05	8.53E+05	9.14E+05
X1.Heptene..5.methyl.	5.73E+06	3.57E+06	5.81E+06	8.68E+06	4.88E+06	8.10E+06	8.70E+06	9.65E+06
Oxime...methoxy.phenyl._	6.33E+05	4.67E+05	3.80E+05	7.84E+05	1.28E+06	2.38E+06	8.07E+05	2.33E+06
Butanoic.acid	4.56E+06	3.79E+06	5.86E+06	7.25E+06	0.00E+00	3.56E+05	8.78E+05	5.03E+06
Unknown.19	5.29E+05	7.94E+05	4.90E+05	6.29E+05	2.18E+06	1.22E+06	2.50E+06	1.13E+06
Vanillin..tert.butyl.dimethylsilyl.ether	6.74E+05	2.47E+06	4.12E+05	4.68E+05	1.99E+05	2.86E+05	4.90E+06	2.53E+05
Diethylcyanamide	2.03E+06	5.03E+06	6.06E+05	8.87E+05	3.02E+06	1.79E+07	1.97E+07	2.27E+07
p.Xylene	8.36E+06	5.94E+06	5.82E+06	1.67E+07	6.06E+06	1.03E+07	1.03E+07	8.38E+06
X2.Pentanone..4.hydroxy.4.methyl.	1.92E+06	1.81E+06	1.55E+06	4.89E+06	3.61E+06	3.62E+06	3.31E+06	3.44E+06
Decane	1.02E+06	7.46E+05	7.90E+05	1.71E+06	7.83E+05	1.36E+06	1.16E+06	1.71E+06
X2.Pentanone..4.hydroxy.4.methyl..1	1.22E+05	2.34E+05	1.99E+05	1.05E+06	5.62E+04	2.54E+05	4.24E+05	1.94E+05

X2.Heptanone.1	9.40E+04	7.39E+05	1.82E+05	2.96E+05	4.01E+05	5.59E+05	1.57E+05	3.46E+05
p.Xylene.1	3.88E+06	2.74E+06	2.17E+06	4.93E+06	1.94E+06	3.45E+06	3.27E+06	3.26E+06
Ethanedioic.acid..dimethyl.ester	2.97E+06	3.84E+06	3.57E+06	9.88E+06	1.68E+06	8.05E+05	6.18E+05	1.63E+06
X1.3.5.7.Cyclooctatetraene	3.34E+05	1.01E+06	3.32E+05	5.56E+05	1.95E+05	6.03E+05	7.04E+05	6.47E+05
Octane..3.5.dimethyl.	1.01E+06	2.63E+05	8.18E+05	2.04E+06	8.53E+05	4.35E+05	1.92E+05	3.28E+05
X2.Heptanone..4.methyl.	9.92E+04	1.07E+05	1.14E+05	1.09E+05	1.08E+05	1.78E+05	2.55E+05	0.00E+00
X2.Butanone..3.4.epoxy.3.ethyl.	4.92E+05	4.61E+05	3.08E+05	5.54E+05	1.81E+05	3.69E+05	1.40E+05	3.00E+05
X2.Heptanone..6.methyl.	4.11E+05	4.60E+05	2.97E+05	2.56E+05	2.56E+05	5.22E+05	0.00E+00	1.57E+05
Benzene..propyl.	9.78E+05	1.10E+06	1.00E+06	7.05E+05	3.47E+05	1.73E+06	1.18E+06	9.27E+05
Pentanoic.acid	4.40E+06	4.30E+06	3.27E+06	7.86E+06	2.12E+06	5.15E+06	4.77E+06	8.01E+06
Benzene..1.ethyl.3.methyl.	2.06E+06	2.17E+06	1.95E+06	3.76E+06	1.56E+06	3.65E+06	3.47E+06	4.36E+06
X2.Butanone	2.01E+06	1.99E+06	6.59E+05	4.29E+06	3.98E+05	4.20E+05	1.33E+05	2.18E+05
Ethane..1.1.2.2.tetrachloro.	8.86E+05	2.80E+05	4.77E+05	1.23E+06	4.30E+05	2.08E+05	3.04E+05	3.59E+05
Benzene..1.2.3.trimethyl.	6.55E+05	4.81E+05	4.26E+05	9.43E+05	4.79E+05	8.34E+05	9.78E+05	1.17E+06
Octane..3.5.dimethyl..1	3.57E+05	2.02E+05	2.48E+05	5.27E+05	3.57E+05	3.97E+05	3.27E+05	4.76E+05
Undecane	1.57E+07	2.18E+07	1.63E+07	2.89E+07	1.48E+07	4.09E+07	3.92E+07	4.29E+07
Carbamoyl.chloride..phenyl.	2.48E+05	2.87E+04	1.87E+05	1.97E+05	2.20E+05	0.00E+00	0.00E+00	1.46E+05
Benzene..1.ethyl.4.methyl.	8.01E+05	8.39E+05	8.72E+05	1.25E+06	5.01E+05	1.31E+06	1.37E+06	1.49E+06
Benzaldehyde..2.5.bis..trimethylsilyl.oxy..	3.42E+04	1.54E+05	1.94E+05	4.87E+05	1.71E+05	4.54E+05	2.54E+05	2.76E+05
Benzene...2.methylpropyl..	9.01E+03	1.02E+05	7.99E+04	8.95E+04	7.77E+04	2.78E+05	1.88E+05	1.43E+05
Benzene..1.2.3.trimethyl..1	4.07E+06	3.45E+06	3.62E+06	6.93E+06	2.85E+06	5.99E+06	6.02E+06	7.70E+06
Propanoic.acid..2.hydroxy.2.methyl.	2.23E+05	2.10E+05	8.52E+04	7.30E+05	1.02E+05	3.42E+05	9.50E+04	1.41E+05
Cyclotrisiloxane..hexamethyl.	5.08E+04	3.83E+05	1.03E+05	9.02E+05	6.34E+05	9.60E+05	8.39E+04	1.01E+06
Benzeneacetaldehyde....methyl.	3.41E+05	2.78E+05	2.24E+05	1.19E+06	2.17E+05	7.65E+05	2.16E+05	9.11E+05

X1.Hexanol..2.ethyl.	6.56E+05	6.15E+05	0.00E+00	1.37E+06	4.69E+05	1.03E+06	3.87E+04	1.10E+06
Ethane..pentachloro.	2.84E+05	2.96E+05	3.34E+05	3.29E+05	1.71E+05	5.08E+05	6.89E+05	6.71E+05
Benzene..1.methyl.3..1.methylethyl..	3.64E+05	3.42E+05	1.96E+05	4.54E+05	2.02E+05	6.06E+05	4.62E+05	5.95E+05
Formamide..N.N.diethyl.	6.19E+05	2.31E+05	0.00E+00	8.56E+05	1.45E+05	3.53E+05	2.30E+05	4.38E+05
X2.5.Hexanedione	3.36E+05	2.21E+05	2.72E+05	2.70E+05	5.62E+04	3.53E+05	2.41E+05	3.96E+05
X4.7.Methano.1H.indene..3a.4.7.7a.tetra hydro.	2.23E+04	2.47E+04	3.27E+04	3.48E+04	2.33E+04	8.10E+04	8.33E+04	1.04E+05
Phenol	2.76E+06	1.98E+06	1.31E+06	3.79E+06	1.27E+06	3.85E+06	3.72E+06	4.69E+06
Benzene..1.2.3.trimethyl..2	1.00E+06	9.06E+05	5.64E+05	1.30E+06	5.05E+05	1.44E+06	1.41E+06	1.76E+06
Benzaldehyde	8.35E+06	9.75E+06	5.79E+06	1.22E+07	4.33E+06	9.21E+06	6.31E+06	6.65E+06
Benzene..1.methyl.3.propyl.	9.22E+05	4.45E+05	4.00E+05	6.61E+05	5.15E+05	9.76E+05	1.58E+06	1.85E+06
Heptanoic.acid	6.94E+06	5.59E+06	7.37E+06	1.30E+07	8.22E+03	3.65E+06	3.04E+06	4.27E+06
Benzene..butyl.	1.17E+06	8.22E+05	1.01E+06	1.80E+06	4.46E+05	3.93E+06	3.31E+06	4.17E+06
Butyrolactone	5.21E+05	7.89E+05	9.60E+05	1.60E+06	6.58E+05	2.91E+05	1.86E+05	1.58E+05
Benzene..1.methyl.4.propyl.	4.84E+05	3.16E+05	2.61E+05	7.86E+05	1.34E+05	4.43E+05	3.96E+05	5.83E+05
Indane	1.50E+06	4.35E+05	1.05E+06	1.95E+06	2.85E+05	7.16E+05	6.33E+05	6.94E+05
X2.Octenal...E..	1.50E+06	4.35E+05	1.05E+06	1.95E+06	2.85E+05	7.45E+05	5.97E+05	7.54E+05
X2.Octenal...E...1	1.50E+06	4.35E+05	1.05E+06	1.95E+06	2.85E+05	7.45E+05	5.97E+05	7.54E+05
Dodecane	1.58E+06	1.55E+06	1.36E+06	2.32E+06	1.06E+06	2.63E+06	2.64E+06	3.38E+06
X1.Hexene..4.5.dimethyl..1	4.75E+06	3.68E+06	4.38E+06	9.71E+06	2.75E+06	3.47E+06	1.54E+06	2.61E+06
Undecane..2.6.dimethyl.	2.24E+05	2.33E+05	2.57E+05	4.66E+05	3.71E+05	4.57E+05	3.47E+05	4.87E+05
X1.3.5.Cycloheptatriene..3.7.7.trimethyl.	0.00E+00	1.91E+06	1.94E+06	4.93E+06	9.57E+05	1.76E+06	6.68E+05	8.43E+05
X3.Dodecene...Z..	5.25E+05	7.46E+05	5.51E+05	1.21E+06	5.67E+05	1.32E+06	9.30E+05	1.42E+06
Benzene..1.methyl.2..1.methylethyl..	4.52E+05	5.49E+05	4.48E+05	7.05E+05	3.74E+05	1.04E+06	9.60E+05	1.17E+06
Nonanal	2.23E+06	1.45E+06	1.26E+06	2.43E+06	1.26E+06	2.52E+06	1.85E+06	2.76E+06

Phenol..2.methyl.	4.52E+05	3.14E+05	2.14E+05	9.25E+05	5.66E+05	4.62E+05	1.92E+05	3.82E+05
Benzyl.Alcohol	2.18E+06	3.01E+06	1.71E+06	4.52E+06	1.26E+06	3.76E+06	2.91E+06	2.30E+06
Benzene..4.ethyl.1.2.dimethyl.	2.13E+05	2.73E+05	1.11E+05	2.43E+05	1.35E+05	3.30E+05	3.87E+05	3.59E+05
Dodecane..2.6.11.trimethyl.	5.22E+05	5.12E+05	3.58E+05	7.70E+05	3.73E+05	7.86E+05	7.66E+05	8.51E+05
Unknown.85	3.56E+05	1.76E+05	2.02E+05	3.68E+05	1.37E+04	9.25E+04	9.67E+04	6.04E+04
Phenol..3.methyl.	5.80E+05	5.76E+05	9.26E+05	4.56E+06	7.36E+05	4.93E+05	4.83E+05	2.32E+05
Benzene..4.ethyl.1.2.dimethyl..1	1.73E+05	1.60E+05	1.80E+05	3.29E+05	1.80E+05	1.42E+05	2.54E+05	1.05E+05
Octanoic.Acid	2.38E+06	2.15E+06	1.06E+06	2.59E+06	6.54E+05	2.05E+06	3.23E+06	2.14E+06
X2.Heptanone..6.methyl..1	2.33E+05	2.30E+05	7.36E+04	3.26E+05	0.00E+00	8.40E+04	0.00E+00	1.35E+05
Benzaldehyde..2.methyl.	4.64E+05	1.72E+05	2.49E+05	1.28E+06	6.19E+04	7.06E+04	1.17E+05	2.08E+05
Acetophenone	4.53E+05	5.20E+05	3.64E+05	9.45E+05	3.93E+05	3.35E+05	6.48E+05	6.53E+05
X2.Nonenal...E..	6.19E+05	4.83E+05	2.96E+05	7.94E+05	1.06E+05	3.43E+05	0.00E+00	3.37E+05
Tridecane	9.73E+05	1.03E+06	1.14E+06	1.45E+06	8.88E+05	1.66E+06	1.98E+06	1.99E+06
X1.3.8.p.Menthatriene	1.29E+05	1.56E+05	3.20E+04	1.03E+05	1.60E+05	1.32E+05	1.79E+05	1.28E+05
Decane..2.3.5.8.tetramethyl.	2.34E+05	2.77E+05	2.41E+05	4.01E+05	2.69E+05	5.09E+05	4.30E+05	5.89E+05
X2.Decanone	2.10E+05	1.21E+05	8.56E+04	2.03E+05	7.11E+05	1.38E+06	2.22E+05	1.39E+05
Dodecane..4.6.dimethyl.	0.00E+00	6.58E+04	5.41E+04	7.64E+04	1.12E+04	6.81E+04	6.93E+04	1.05E+05
Decanal	7.91E+05	9.60E+05	5.58E+05	1.01E+06	3.15E+05	6.80E+05	5.26E+05	7.36E+05
Undecane..4.7.dimethyl.	0.00E+00	1.29E+05	2.41E+04	1.24E+05	1.97E+05	2.00E+05	9.68E+04	1.67E+05
X2.Pentanone..4.hydroxy.4.methyl..2	5.12E+05	5.31E+05	2.84E+05	4.76E+05	2.06E+05	3.53E+05	1.61E+05	1.92E+05
Dodecane..2.6.10.trimethyl.	2.39E+05	1.49E+05	8.07E+04	1.66E+05	6.14E+04	1.75E+05	1.19E+05	2.39E+05
Ethanol..2..2.butoxyethoxy..	1.11E+06	1.65E+06	0.00E+00	1.34E+06	2.30E+05	1.07E+06	9.11E+05	1.33E+06
Nonanoic.acid	4.53E+06	2.66E+06	1.01E+06	5.65E+06	1.04E+06	3.41E+06	1.68E+06	2.82E+06
X2.Decenal...Z..	1.94E+06	4.26E+05	8.74E+05	2.05E+06	4.84E+05	1.27E+06	8.15E+05	9.47E+05

Tetradecane	2.09E+06	2.16E+06	1.33E+06	2.27E+06	1.13E+06	3.31E+06	2.97E+06	3.36E+06
X2.3H..Furanone..dihydro.5.propyl.	3.47E+05	2.79E+05	1.07E+05	4.68E+05	9.64E+04	1.01E+05	1.53E+05	9.59E+04
X2.Undecanone	3.70E+05	4.76E+05	2.27E+05	5.57E+05	2.48E+05	5.39E+05	4.00E+05	5.14E+05
X3.Dodecene...Z...1	9.02E+05	1.14E+06	6.03E+05	1.32E+06	6.50E+05	1.96E+06	1.39E+06	1.75E+06
Naphthalene	1.25E+06	1.40E+06	5.56E+05	2.17E+06	5.01E+05	1.12E+06	9.09E+05	8.84E+05
Dodecane..2.6.10.trimethyl..1	6.86E+05	5.23E+05	3.68E+05	1.22E+06	2.03E+05	5.87E+05	3.40E+05	4.57E+05
Benzaldehyde..2.4.dimethyl.	4.22E+05	3.99E+05	2.62E+05	7.68E+05	2.43E+05	5.18E+05	6.04E+05	5.86E+05
X2.Hepten.3.ol..4.5.dimethyl.	3.16E+05	3.66E+05	1.58E+05	3.37E+05	6.30E+04	2.74E+05	2.33E+05	2.64E+05
X1.Iodo.2.methylundecane	2.65E+05	3.82E+05	2.42E+05	3.74E+05	1.53E+05	6.69E+05	3.78E+05	4.88E+05
Propanoic.acid..2.methyl...anhydride	1.48E+05	1.89E+05	1.43E+05	2.72E+05	9.18E+04	3.31E+05	1.83E+05	2.63E+05
X2.4.Decadienal	4.64E+05	1.50E+05	1.58E+05	3.32E+05	1.10E+05	4.89E+05	3.62E+05	3.06E+05
Formamide..N.N.dibutyl.	2.36E+05	8.79E+04	0.00E+00	1.36E+05	1.74E+04	1.89E+05	5.59E+04	1.25E+05
X2.2.4.Trimethyl.1.3.pentanediol.diisobut yrate	1.16E+06	1.91E+06	5.67E+05	1.92E+06	7.57E+05	2.46E+06	1.73E+06	2.78E+06
X2.Undecenal	6.76E+05	5.60E+05	4.87E+05	8.06E+05	6.25E+05	1.16E+06	9.61E+05	8.93E+05
Pentadecane	2.51E+05	2.83E+05	1.93E+05	3.66E+05	2.38E+05	4.63E+05	4.09E+05	3.59E+05
Benzothiazole	1.07E+06	1.22E+06	4.88E+05	2.80E+06	3.69E+05	1.24E+06	1.41E+06	1.46E+06
Propanoic.acid..2.methyl...3.hydroxy.2.4.4.trimethylpentyl.ester	1.76E+06	2.84E+06	9.19E+05	2.57E+06	1.07E+06	3.84E+06	3.23E+06	3.76E+06
Dodecanal	2.78E+05	3.66E+05	1.25E+05	3.43E+05	1.49E+05	3.90E+05	2.55E+05	3.61E+05
Naphthalene..1.methyl.	3.13E+05	1.98E+05	1.97E+05	9.91E+05	6.09E+04	1.60E+05	1.64E+05	1.64E+05
Undecane..5.7.dimethyl.	8.46E+04	2.08E+05	2.01E+05	1.60E+05	5.72E+04	1.19E+05	1.10E+05	2.00E+05
X2.4.7.9.Tetramethyl.5.decyn.4.7.diol	5.21E+05	1.08E+06	2.19E+05	9.11E+05	4.67E+05	1.16E+06	6.62E+05	9.08E+05
Hexanedinitrile	2.05E+05	2.68E+05	1.62E+05	5.13E+05	2.28E+05	6.54E+05	5.76E+05	8.02E+05
Undecane..3.methyl.	8.03E+04	1.09E+05	5.36E+04	7.95E+04	5.61E+04	2.66E+05	8.42E+04	7.29E+04
Caprolactam	4.00E+05	1.42E+06	5.38E+05	2.27E+06	3.10E+05	2.33E+06	1.76E+06	1.93E+06

Triacetin	1.30E+06	1.22E+06	5.04E+05	1.47E+06	5.72E+05	1.65E+06	1.29E+06	1.37E+06
X3.Hepten.2.one..4.methyl.	2.69E+05	2.08E+05	8.67E+04	3.68E+05	6.50E+04	2.63E+05	2.43E+05	1.77E+05
n.Nonylcyclohexane	0.00E+00	4.10E+04	3.49E+04	5.50E+04	2.70E+04	1.52E+05	2.14E+05	1.77E+05
Hexadecane	2.08E+06	3.15E+06	1.23E+06	2.26E+06	9.68E+05	3.86E+06	3.05E+06	3.76E+06
X2.Pentadecyn.1.ol	3.37E+05	3.18E+05	3.12E+05	5.78E+05	3.72E+05	6.73E+05	2.80E+05	4.79E+05
X1.Hexadecene	1.07E+06	1.72E+06	5.61E+05	1.40E+06	6.80E+05	3.10E+06	1.77E+06	2.89E+06
X2.Tridecanone	3.29E+05	2.12E+05	1.88E+05	4.79E+05	1.58E+05	9.75E+04	1.05E+05	8.08E+04
X2.3H..Furanone..dihydro.5.pentyl.	2.86E+05	2.62E+05	1.46E+05	7.65E+05	1.73E+05	1.60E+05	2.35E+05	1.95E+05
Furan..tetrahydro.2.2.4.4.tetramethyl.	6.64E+05	6.34E+05	3.10E+05	1.03E+06	2.27E+05	4.84E+05	3.99E+05	4.60E+05
Undecanal	4.64E+05	3.45E+05	1.95E+05	4.06E+05	1.22E+05	3.13E+05	2.34E+05	2.86E+05
Decane..2.5.9.trimethyl.	1.37E+05	1.70E+05	1.03E+05	2.38E+05	0.00E+00	3.44E+05	1.28E+05	1.54E+05
X2.5.Cyclohexadiene.1.4.dione..2.6.bis.1.1.dimethylethyl..	2.41E+05	1.80E+05	1.13E+05	4.07E+05	2.01E+05	3.45E+05	1.29E+05	2.20E+05
Tridecanoic.acid..methyl.ester	1.98E+05	2.97E+05	1.23E+05	2.16E+05	1.00E+05	2.16E+05	2.46E+05	2.06E+05
Biphenyl	4.68E+05	0.00E+00	1.61E+05	3.73E+05	1.08E+05	1.06E+05	1.83E+05	2.50E+05
X1.2.Benzenedicarboxylic.acid	1.11E+06	4.77E+05	1.73E+05	7.56E+05	1.62E+05	2.89E+05	1.14E+05	3.43E+05
Benzaldehyde..4.hydroxy.	1.35E+06	6.35E+05	4.66E+05	1.29E+06	1.71E+05	1.53E+05	4.76E+04	1.65E+05
Propanenitrile..3.3..oxybis.	6.44E+04	2.69E+04	0.00E+00	1.66E+04	1.42E+05	3.86E+04	4.85E+04	2.77E+04
Decane..2.3.5.8.tetramethyl..1	1.72E+05	2.20E+05	8.73E+04	1.81E+05	7.11E+04	2.46E+05	1.78E+05	3.07E+05
Heptadecane..2.6.dimethyl.	1.28E+05	1.79E+05	6.71E+04	1.59E+05	1.17E+05	3.18E+05	2.26E+05	4.09E+05
Butylated.Hydroxytoluene	1.48E+05	5.00E+05	7.24E+04	1.24E+05	7.12E+05	2.20E+06	4.23E+06	4.18E+06
Ethanone..1..3.methyloxiranyl..	2.05E+05	1.82E+05	7.67E+04	2.42E+05	1.61E+05	8.77E+04	6.22E+04	8.79E+04
Phenol..2.4.bis.1.1.dimethylethyl..	1.35E+05	2.26E+05	4.23E+04	1.26E+05	1.27E+05	2.31E+05	2.15E+05	1.83E+05
Cyclohexane...1.methylethyl..	9.55E+04	1.26E+05	1.24E+05	1.41E+05	8.23E+04	3.87E+05	2.97E+05	3.25E+05
Hexadecane.1	1.55E+05	2.73E+05	1.20E+05	2.71E+05	3.60E+04	2.99E+05	1.82E+05	2.35E+05

X2.Tetradecanone	7.66E+04	1.01E+05	3.92E+04	5.40E+04	6.86E+04	8.93E+04	1.09E+05	8.26E+04
Benzene...1.methylnonyl..	6.18E+03	2.21E+04	9.96E+04	3.31E+04	4.67E+04	1.51E+05	1.19E+05	2.80E+04
Propanoic.acid..2.methyl...1..1.1.dimethyl ethyl..2.methyl.1.3.propanediyl.ester	6.18E+06	1.06E+07	3.07E+06	9.92E+06	4.52E+06	1.32E+07	1.01E+07	1.19E+07
X2.3H..Furanone..5.hexyldihydro.	1.26E+06	1.67E+06	3.79E+04	1.16E+06	5.20E+04	1.19E+05	6.67E+04	1.07E+05
Hexadecanal	8.37E+05	9.89E+05	2.58E+05	6.03E+05	2.93E+05	4.89E+05	2.65E+05	3.76E+05
Benzene...1.pentylhexyl..	8.19E+04	1.28E+05	1.17E+04	1.00E+05	0.00E+00	9.56E+04	4.81E+04	6.48E+04
Benzene...1.butylheptyl..	1.15E+05	9.78E+04	6.61E+04	2.09E+05	7.20E+04	2.79E+05	1.78E+05	1.71E+05
Benzene...1.propyloctyl..	8.49E+04	2.18E+05	1.60E+05	1.46E+05	1.30E+05	2.34E+05	1.25E+05	1.37E+05
Ethanone..1.1...1.4.phenylene.bis.	5.52E+05	2.19E+05	7.76E+04	2.85E+05	4.55E+04	1.05E+05	1.16E+05	1.03E+05
X1.Iodo.2.methylundecane.1	3.50E+05	2.99E+05	1.89E+05	6.80E+04	9.84E+04	2.82E+05	3.20E+05	2.37E+05
X1.Cyclohexanone..2.methyl.2..3.methyl. 2.oxobutyl.	2.86E+04	3.32E+04	0.00E+00	6.73E+04	7.51E+03	3.39E+04	0.00E+00	4.28E+04
Dimethyl.phthalate	1.88E+05	1.31E+05	7.41E+04	1.49E+05	2.34E+04	7.64E+04	5.06E+04	5.85E+04
Ethanone..1..4..1.hydroxy.1.methylethyl. phenyl..	3.51E+05	2.61E+05	1.06E+05	2.51E+05	1.74E+05	3.24E+05	5.80E+05	7.28E+05
Acenaphthene	1.17E+05	1.77E+05	0.00E+00	2.02E+05	2.68E+04	7.25E+04	2.92E+04	4.65E+04
Nonadecane	1.06E+06	1.30E+06	5.26E+05	1.12E+06	4.15E+05	1.64E+06	1.36E+06	1.77E+06
Dodecyl.acrylate	9.97E+05	8.02E+05	3.29E+05	1.60E+06	2.36E+05	7.36E+05	5.59E+05	9.48E+05
Benzene..1.methyl.3..phenylmethyl..	2.08E+05	1.83E+05	5.48E+04	2.02E+05	1.07E+05	0.00E+00	2.02E+05	4.31E+04
X1.Hexadecene.1	8.11E+05	1.37E+06	2.53E+05	9.19E+05	2.48E+05	2.11E+06	1.24E+06	2.08E+06
Dibenzofuran	2.54E+05	1.31E+05	6.48E+04	3.43E+05	4.80E+04	1.30E+05	7.03E+04	1.15E+05
X2.Octanone	1.02E+05	1.84E+05	5.82E+04	1.25E+05	1.65E+05	8.36E+04	8.51E+04	4.74E+04
Methyl.n.hexyl.ketone.1.phenyl.1.2.ethan ediol.ketal.1	1.36E+05	1.91E+05	0.00E+00	2.13E+05	0.00E+00	1.38E+05	6.30E+04	5.32E+04
Benzene...1.methyldecyl..	4.01E+04	1.61E+05	3.88E+04	1.28E+05	6.45E+04	1.60E+05	1.35E+05	1.71E+05
Unknown.194	1.58E+05	2.65E+01	1.38E+05	2.07E+05	1.45E+05	1.95E+05	3.52E+04	1.18E+05

X2.3H..Furanone..5.hexyldihydro..1	4.19E+04	1.09E+05	0.00E+00	9.44E+04	0.00E+00	4.52E+04	3.38E+04	7.88E+04
Benzene...1.pentylheptyl..	9.17E+05	1.45E+06	6.16E+05	1.24E+06	3.54E+05	1.33E+06	8.40E+05	8.06E+05
Benzene...1.pentylheptyl...1	9.17E+05	1.45E+06	6.16E+05	1.24E+06	3.54E+05	1.33E+06	8.40E+05	8.06E+05
Benzene...1.butylloctyl..	7.65E+04	1.11E+05	6.09E+04	2.96E+05	3.63E+04	1.16E+05	6.06E+04	1.05E+05
Benzene...1.propylnonyl..	3.45E+05	2.84E+05	1.24E+05	1.82E+05	9.69E+04	4.67E+05	5.38E+05	3.71E+05
Tributyl.phosphate	3.34E+04	0.00E+00	3.21E+03	3.14E+04	3.85E+04	6.03E+04	3.95E+03	5.52E+04
Benzene...1.ethyldecyl..	3.33E+05	4.61E+05	1.67E+05	2.78E+05	0.00E+00	2.89E+05	3.52E+05	4.44E+05
n.Hexyl.salicylate	3.77E+04	1.56E+05	2.02E+04	4.85E+04	7.31E+04	1.13E+05	1.22E+05	1.61E+05
X1.6.Dioxacyclododecane.7.12.dione	6.83E+05	6.52E+05	2.97E+05	1.03E+06	4.68E+05	1.60E+06	1.53E+06	2.00E+06
Unknown.205	5.21E+04	3.50E+05	3.13E+04	1.29E+05	0.00E+00	4.18E+04	9.74E+03	8.81E+04
Nonadecane.1	3.54E+06	2.53E+05	2.89E+05	5.97E+05	1.67E+05	3.57E+05	3.03E+05	3.08E+05
Cyclopentaneacetic.acid..3.oxo.2.pentyl...methyl.ester	9.14E+04	0.00E+00	1.63E+04	1.15E+05	2.20E+04	2.24E+05	7.63E+04	1.08E+05
Diethyl.Phthalate	6.31E+05	9.80E+05	2.09E+05	1.14E+06	3.14E+05	1.04E+06	1.08E+06	1.28E+06
Fluorene	5.94E+05	3.01E+05	1.73E+04	3.84E+05	0.00E+00	6.24E+05	6.61E+05	1.28E+06
Isopropyl.Myristate	1.25E+05	1.70E+05	7.00E+04	2.46E+05	1.97E+05	4.90E+05	3.00E+05	5.25E+05
Cyclohexane..2.propenyl.	5.45E+05	3.63E+04	2.87E+05	1.05E+05	0.00E+00	2.25E+05	1.84E+05	1.47E+05
Nonadecane..2.methyl.	7.63E+04	2.49E+05	0.00E+00	1.18E+05	0.00E+00	9.16E+04	1.97E+05	1.25E+05
X2.Hexanone..4.methyl.	2.67E+04	2.19E+05	9.00E+04	3.40E+05	2.78E+04	7.49E+04	5.98E+04	9.49E+04
Benzene...1.methylundecyl..	1.12E+04	1.35E+05	1.77E+04	5.98E+04	4.61E+03	1.22E+05	1.17E+05	1.53E+05
Benzene...1.hexylheptyl..	1.42E+05	2.40E+05	5.28E+04	6.10E+05	8.27E+04	8.34E+04	2.51E+04	1.48E+05
X2.Pentadecanone..6.10.14.trimethyl.	2.96E+06	3.76E+06	1.52E+06	5.21E+06	4.36E+05	7.44E+05	3.99E+05	3.73E+05
Benzophenone	1.24E+05	8.90E+04	0.00E+00	1.83E+05	6.35E+04	1.49E+05	1.35E+05	1.33E+05
X1.Docosene	5.17E+05	1.81E+05	1.95E+05	2.22E+05	0.00E+00	5.57E+05	3.07E+05	3.18E+05
X2.Pentanone..4.hydroxy.4.methyl..3	3.20E+05	4.78E+05	2.00E+05	1.06E+06	1.68E+05	1.46E+05	1.42E+05	1.28E+05

Hexadecanoic.acid..methyl.ester	1.37E+06	1.19E+06	8.08E+05	1.74E+06	1.12E+06	1.44E+07	2.99E+07	2.11E+07
Butanedioic.acid..phenyl.	4.37E+05	2.71E+05	1.46E+05	2.61E+05	4.32E+04	2.13E+05	5.82E+04	1.14E+05
Heneicosane	4.63E+06	6.50E+05	1.29E+06	2.67E+06	2.90E+05	8.34E+05	2.29E+05	1.81E+05
X2.Propanol..1.chloro...phosphate..3.1.	4.77E+05	6.35E+05	4.03E+05	1.02E+06	4.34E+05	1.36E+06	8.84E+05	1.13E+06
X2.Propanol..1.chloro...phosphate..3.1..1	2.51E+05	2.63E+05	8.14E+04	1.51E+05	4.10E+04	2.79E+05	1.64E+05	2.04E+05
X1.2.Benzenedicarboxylic.acid..bis.2.methylpropyl..ester	5.48E+05	7.98E+05	3.47E+05	9.63E+05	6.45E+05	1.71E+06	1.41E+06	1.02E+06
Phenanthrene	4.01E+05	1.34E+05	1.61E+05	3.29E+05	1.61E+05	2.50E+05	1.57E+05	1.80E+05
Benzenesulfonamide..N.butyl.	5.45E+05	4.10E+05	1.41E+05	6.73E+05	1.42E+05	7.82E+05	5.50E+05	7.81E+05
Heneicosane.1	3.70E+06	7.77E+05	1.06E+06	2.38E+06	3.04E+05	6.47E+05	3.02E+05	1.76E+05
X7.9.Di.tert.butyl.1.oxaspiro.4.5.deca.6.9.diene.2.8.dione	9.54E+05	9.16E+05	4.16E+05	1.53E+06	5.53E+05	1.74E+06	2.08E+06	1.48E+06
X1.2.Benzenedicarboxylic.acid..butyl.2.methylpropyl.ester	3.04E+05	9.41E+04	7.11E+04	1.26E+05	6.22E+04	2.46E+05	7.24E+05	6.04E+05
Octadecanoic.acid..methyl.ester	8.16E+05	1.59E+06	1.23E+06	2.51E+06	1.58E+06	1.09E+08	8.31E+06	5.80E+06
X9.Octadecenoic.acid..Z.....methyl.ester	1.71E+06	1.01E+06	1.29E+06	2.01E+06	2.01E+06	1.35E+08	2.71E+08	2.07E+08
X9.Octadecenoic.acid..Z.....methyl.ester.1	2.19E+06	6.72E+05	8.93E+05	1.38E+06	9.18E+05	1.43E+07	0.00E+00	2.20E+06
Dibutyl.phthalate	5.30E+05	5.28E+05	2.75E+05	8.37E+05	1.15E+05	1.54E+06	2.80E+06	2.11E+06
Ethanone..2.2.dimethoxy.1.2.diphenyl.	2.43E+05	4.29E+04	1.22E+05	2.18E+05	1.60E+04	4.68E+05	1.12E+06	8.18E+05
Heneicosane.2	7.23E+06	2.25E+06	2.13E+06	4.81E+06	4.26E+05	9.62E+05	2.57E+05	0.00E+00
Octadecanoic.acid	4.64E+06	3.04E+06	1.36E+05	5.40E+06	0.00E+00	3.02E+07	7.85E+07	2.31E+07
Oleic.Acid	5.76E+06	0.00E+00	1.74E+06	1.80E+07	0.00E+00	3.78E+06	8.22E+08	3.79E+08
Nonadecane.2	3.49E+06	1.22E+06	1.15E+06	2.31E+06	2.28E+05	4.12E+05	1.22E+05	1.01E+05
Nonanamide	4.84E+05	3.70E+05	1.65E+05	7.86E+05	7.58E+04	5.62E+06	4.57E+06	3.46E+06
Heptacosane	9.88E+06	7.48E+06	3.23E+06	8.61E+06	5.15E+05	1.01E+06	2.58E+06	2.27E+06
Unknown.266	2.64E+05	2.99E+05	1.96E+05	2.39E+05	1.91E+05	2.16E+06	0.00E+00	2.81E+06

Pyrene	5.21E+05	2.34E+05	2.17E+05	7.31E+05	1.72E+05	3.45E+06	5.52E+06	4.24E+06
Heptacosane.1	3.62E+06	1.11E+06	1.16E+06	2.43E+06	2.58E+05	4.32E+05	3.48E+05	4.27E+05
Ethanone..2..formyloxy..1.phenyl.	0.00E+00	5.18E+04	0.00E+00	4.65E+05	2.89E+05	1.28E+06	2.13E+06	1.65E+06
Pyrene.1	2.10E+05	4.25E+04	6.91E+04	3.20E+05	7.01E+03	5.32E+04	2.65E+04	1.25E+05
Nonanamide.1	2.15E+05	4.08E+05	3.16E+05	8.79E+05	3.73E+05	1.17E+06	3.02E+06	3.96E+06
Heptacosane.2	1.38E+07	3.05E+06	3.52E+06	9.72E+06	1.43E+06	1.24E+06	1.30E+05	5.36E+04
Heptacosane.3	4.30E+06	1.82E+06	1.67E+06	3.87E+06	4.44E+05	3.89E+05	4.53E+05	6.21E+05
Heptacosane.4	1.64E+07	6.94E+06	7.85E+06	2.37E+07	1.53E+06	1.80E+06	2.95E+05	1.00E+05
Nonadecane..2.methyl..1	1.63E+06	1.12E+06	7.66E+05	2.07E+06	1.39E+05	4.54E+05	1.80E+06	0.00E+00
Heptacosane.5	1.26E+07	1.04E+07	5.40E+06	1.92E+07	1.71E+06	1.44E+06	1.00E+05	6.76E+04
X1.2.Benzenedicarboxylic.acid..diisodecyl. ester	1.57E+06	2.56E+06	1.76E+06	3.20E+06	1.61E+06	5.30E+06	5.60E+06	6.09E+06
X13.Docosenamide...Z..	2.94E+06	2.94E+06	1.47E+06	1.37E+06	1.51E+06	3.89E+06	5.02E+06	3.97E+06
Unknown.401	2.77E+06	3.00E+06	1.84E+06	1.09E+06	1.01E+06	4.41E+07	3.20E+06	8.41E+06
Unknown.510	2.34E+04	1.87E+05	5.84E+04	2.38E+05	3.43E+04	1.21E+05	1.80E+05	2.60E+05
Tetradecane.1	6.26E+05	4.47E+05	4.46E+05	5.19E+05	3.62E+05	1.03E+06	6.36E+05	5.98E+05
Hexadecane.2	3.21E+06	4.49E+05	3.58E+05	6.51E+05	2.64E+05	7.62E+05	5.10E+05	5.57E+05
Eicosane	1.60E+06	4.95E+05	3.68E+05	9.72E+05	2.92E+05	6.32E+05	5.75E+05	7.29E+05

Compound	a	b	c	d	e	f	g	LW
Toluene	1.38E+08	0.00E+00	0.00E+00	0.00E+00	1.56E+08	9.10E+06	1.78E+07	2.88E+07
Hexanal	1.73E+07	2.14E+05	0.00E+00	4.34E+06	2.75E+07	6.02E+06	8.61E+06	8.79E+06
Acetic.acid..butyl.ester	4.29E+06	3.35E+05	4.59E+05	2.59E+06	1.42E+07	5.06E+06	8.29E+06	7.66E+06
X2.Hexene..4.ethyl.2.3.dimethyl.	7.51E+05	0.00E+00	0.00E+00	5.41E+05	1.29E+06	3.70E+05	0.00E+00	0.00E+00
Butane..2.3.dimethyl.2.3.dinitro.	1.18E+06	1.28E+06	1.57E+06	8.14E+05	1.14E+06	7.73E+05	1.58E+05	3.44E+05
Butyl.tert.butyl.isopropoxyborane	2.53E+06	1.09E+05	0.00E+00	1.97E+06	2.24E+06	2.41E+06	6.60E+05	8.21E+05
X3.Penten.2.one..4.methyl.	8.32E+06	0.00E+00	0.00E+00	4.91E+06	2.03E+07	2.08E+06	5.75E+06	4.46E+06
Cyclotetrasiloxane..octamethyl.	2.61E+06	2.80E+05	2.76E+05	8.44E+05	9.37E+05	3.35E+05	6.65E+05	7.46E+05
X1.3.Dioxolane..2..1.methylethyl..	1.09E+06	8.16E+03	9.62E+04	4.07E+05	1.98E+05	1.06E+06	0.00E+00	3.16E+05
X4.Methyl.2.hexanol	1.29E+06	0.00E+00	0.00E+00	8.26E+05	7.29E+05	7.98E+05	3.17E+05	5.57E+05
X1.Hexene..4.5.dimethyl.	2.06E+06	1.55E+05	4.30E+05	1.56E+06	1.52E+06	1.22E+06	2.67E+05	5.06E+06
Propanoic.acid..2.methoxy.	6.18E+06	9.63E+04	1.47E+05	2.94E+06	5.36E+06	3.28E+06	2.08E+06	1.70E+06
X2.Heptanone	6.04E+05	0.00E+00	0.00E+00	6.99E+05	5.88E+05	3.73E+05	0.00E+00	2.13E+05
X1.Heptene..5.methyl.	4.06E+06	3.28E+05	3.48E+05	3.07E+06	3.07E+06	2.56E+06	6.53E+05	2.36E+06
Oxime...methoxy.phenyl._	8.69E+05	4.60E+05	4.02E+05	4.31E+06	5.48E+05	1.18E+06	3.93E+05	1.17E+06
Butanoic.acid	9.69E+05	0.00E+00	0.00E+00	2.01E+06	1.42E+06	2.04E+06	2.10E+05	0.00E+00
Unknown.19	2.19E+06	0.00E+00	0.00E+00	1.87E+05	3.03E+06	2.50E+05	6.95E+05	2.53E+05
Vanillin..tert.butyl(dimethyl)silyl.ether	9.27E+05	8.79E+05	7.50E+05	6.74E+05	1.68E+05	6.13E+05	9.28E+05	2.47E+06
Diethylcyanamide	4.30E+06	6.89E+05	7.28E+05	6.87E+06	6.85E+06	5.57E+06	2.06E+06	3.06E+06
p.Xylene	4.94E+06	0.00E+00	0.00E+00	1.03E+06	5.31E+06	1.24E+06	3.16E+06	1.83E+06
X2.Pentanone..4.hydroxy.4.methyl.	9.00E+06	0.00E+00	0.00E+00	8.02E+06	1.42E+07	9.02E+06	4.80E+06	4.42E+06
Decane	5.95E+05	1.10E+05	0.00E+00	1.34E+05	1.08E+06	1.09E+05	2.50E+05	2.50E+05

X2.Pentanone..4.hydroxy.4.methyl..1	3.99E+05	0.00E+00	0.00E+00	4.57E+05	1.27E+06	4.69E+05	6.37E+02	2.35E+05
X2.Heptanone.1	4.72E+05	0.00E+00	0.00E+00	4.84E+05	1.67E+06	0.00E+00	0.00E+00	5.22E+05
p.Xylene.1	3.03E+06	1.33E+05	0.00E+00	2.07E+06	5.26E+06	1.39E+06	1.11E+06	1.91E+06
Ethanedioic.acid..dimethyl.ester	1.51E+06	0.00E+00	0.00E+00	1.05E+06	2.03E+06	2.03E+06	1.49E+05	0.00E+00
X1.3.5.7.Cyclooctatetraene	6.61E+05	6.55E+04	1.16E+05	5.60E+05	1.23E+06	3.67E+05	8.37E+04	2.28E+05
Octane..3.5.dimethyl.	8.92E+05	0.00E+00	0.00E+00	0.00E+00	2.13E+06	0.00E+00	5.53E+05	1.61E+06
X2.Heptanone..4.methyl.	1.21E+05	0.00E+00	0.00E+00	3.77E+05	4.97E+05	2.41E+05	2.08E+05	2.65E+05
X2.Butanone..3.4.epoxy.3.ethyl.	1.39E+07	0.00E+00	0.00E+00	2.26E+07	4.39E+07	1.31E+07	9.19E+06	1.30E+07
X2.Heptanone..6.methyl.	2.41E+05	4.63E+04	7.21E+04	1.37E+05	3.53E+05	1.95E+05	0.00E+00	2.55E+05
Benzene..propyl.	8.94E+05	0.00E+00	0.00E+00	8.21E+05	1.56E+06	3.83E+05	1.34E+06	2.49E+05
Pentanoic.acid	5.51E+06	0.00E+00	0.00E+00	2.44E+07	9.18E+06	1.23E+07	3.47E+06	2.80E+06
Benzene..1.ethyl.3.methyl.	3.37E+06	1.10E+05	8.48E+04	2.03E+06	4.24E+06	2.32E+06	1.32E+06	8.74E+05
X2.Butanone	1.54E+06	0.00E+00	0.00E+00	9.51E+05	1.89E+06	4.05E+05	3.75E+06	7.09E+05
Ethane..1.1.2.2.tetrachloro.	1.48E+07	0.00E+00	0.00E+00	3.01E+07	5.28E+07	2.18E+07	2.25E+06	1.90E+05
Benzene..1.2.3.trimethyl.	2.49E+06	1.70E+04	3.42E+04	2.14E+06	4.57E+06	2.07E+06	1.13E+06	4.86E+05
Octane..3.5.dimethyl..1	1.11E+06	0.00E+00	0.00E+00	1.71E+05	9.55E+05	2.39E+05	3.19E+05	3.96E+06
Undecane	1.68E+06	0.00E+00	0.00E+00	3.14E+05	2.38E+06	4.88E+05	5.55E+05	1.23E+05
Carbamoyl.chloride..phenyl.	8.09E+05	0.00E+00	0.00E+00	8.83E+05	1.39E+06	1.20E+06	1.15E+06	3.05E+05
Benzene..1.ethyl.4.methyl.	7.77E+05	4.78E+04	1.10E+05	5.11E+05	1.21E+06	7.37E+05	2.44E+05	4.31E+05
Benzaldehyde..2.5.bis..trimethylsilyl.oxy..	2.41E+05	1.63E+05	3.23E+05	7.83E+04	3.09E+05	1.20E+05	8.40E+04	3.39E+05
Benzene...2.methylpropyl..	2.72E+05	0.00E+00	0.00E+00	0.00E+00	4.51E+05	0.00E+00	9.35E+04	1.08E+05
Benzene..1.2.3.trimethyl..1	4.82E+06	2.45E+05	3.46E+05	2.49E+06	7.66E+06	2.35E+06	1.37E+06	2.74E+06
Propanoic.acid..2.hydroxy.2.methyl.	2.40E+06	0.00E+00	0.00E+00	2.81E+06	5.36E+06	1.08E+06	3.30E+06	0.00E+00
Cyclotrisiloxane..hexamethyl.	8.58E+05	0.00E+00	2.99E+04	0.00E+00	0.00E+00	4.16E+05	0.00E+00	4.82E+05

Benzeneacetaldehyde....methyl.	4.95E+05	0.00E+00	0.00E+00	2.74E+05	6.41E+05	9.55E+05	0.00E+00	0.00E+00
X1.Hexanol..2.ethyl.	7.07E+05	0.00E+00	0.00E+00	5.16E+05	1.60E+06	9.55E+05	4.08E+05	4.48E+05
Ethane..pentachloro.	7.29E+05	0.00E+00	0.00E+00	8.11E+05	1.70E+06	2.98E+05	3.76E+05	0.00E+00
Benzene..1.methyl.3..1.methylethyl..	8.83E+05	0.00E+00	0.00E+00	4.99E+05	8.91E+05	1.11E+07	1.37E+06	2.94E+05
Formamide..N.N.diethyl.	3.95E+05	0.00E+00	0.00E+00	5.80E+05	1.74E+06	4.26E+05	2.05E+05	4.16E+05
X2.5.Hexanedione	1.55E+06	0.00E+00	0.00E+00	2.83E+06	4.96E+06	1.22E+06	1.24E+06	1.04E+06
X4.7.Methano.1H.indene..3a.4.7.7a.tetra hydro.	1.11E+05	0.00E+00	0.00E+00	5.44E+04	9.28E+04	1.80E+05	0.00E+00	0.00E+00
Phenol	1.60E+06	7.33E+04	1.63E+05	2.68E+06	2.93E+06	2.29E+06	1.65E+06	9.39E+05
Benzene..1.2.3.trimethyl..2	1.25E+06	1.21E+05	6.75E+04	7.11E+05	2.38E+06	7.64E+05	3.59E+05	4.36E+05
Benzaldehyde	5.61E+07	2.00E+05	6.92E+04	1.73E+07	6.36E+07	1.71E+07	1.12E+07	2.66E+07
Benzene..1.methyl.3.propyl.	4.91E+06	1.80E+04	1.80E+04	2.13E+06	4.17E+06	1.88E+06	7.23E+05	8.02E+05
Heptanoic.acid	7.57E+06	0.00E+00	0.00E+00	1.04E+07	1.85E+07	3.51E+06	3.46E+06	1.83E+05
Benzene..butyl.	5.41E+05	0.00E+00	0.00E+00	5.67E+05	0.00E+00	0.00E+00	1.95E+06	7.37E+04
Butyrolactone	8.96E+05	0.00E+00	0.00E+00	4.39E+05	1.12E+06	4.36E+05	0.00E+00	0.00E+00
Benzene..1.methyl.4.propyl.	3.87E+05	0.00E+00	0.00E+00	1.91E+05	6.48E+05	3.88E+06	5.00E+05	2.43E+05
Indane	1.26E+06	5.80E+04	0.00E+00	6.54E+05	3.64E+06	9.32E+05	7.61E+05	3.83E+05
X2.Octenal...E..	9.82E+05	5.80E+04	0.00E+00	6.54E+05	2.82E+06	9.32E+05	7.06E+05	3.83E+05
X2.Octenal...E...1	9.82E+05	5.80E+04	0.00E+00	6.54E+05	2.82E+06	9.32E+05	7.06E+05	3.83E+05
Dodecane	1.39E+06	0.00E+00	0.00E+00	4.05E+05	1.73E+06	6.37E+05	5.23E+05	3.31E+06
X1.Hexene..4.5.dimethyl..1	3.74E+05	0.00E+00	0.00E+00	2.41E+05	0.00E+00	4.58E+05	2.71E+05	1.48E+06
Undecane..2.6.dimethyl.	1.26E+05	0.00E+00	0.00E+00	8.51E+04	7.04E+04	0.00E+00	1.31E+06	6.54E+05
X1.3.5.Cycloheptatriene..3.7.7.trimethyl.	6.30E+06	0.00E+00	0.00E+00	1.30E+06	4.32E+07	4.65E+05	6.94E+05	1.03E+06
X3.Dodecene...Z..	2.18E+06	0.00E+00	0.00E+00	0.00E+00	3.68E+06	2.38E+06	7.21E+05	3.44E+07
Benzene..1.methyl.2..1.methylethyl..	1.37E+06	0.00E+00	0.00E+00	5.46E+05	9.66E+06	2.95E+05	7.58E+05	8.51E+05

Nonanal	3.15E+06	2.00E+05	2.70E+05	1.48E+06	4.62E+06	2.53E+06	2.59E+06	1.77E+07
Phenol..2.methyl.	7.21E+05	0.00E+00	0.00E+00	0.00E+00	1.43E+06	0.00E+00	3.78E+05	3.74E+05
Benzyl.Alcohol	9.68E+06	0.00E+00	0.00E+00	1.11E+07	3.59E+07	1.29E+07	5.53E+06	1.02E+07
Benzene..4.ethyl.1.2.dimethyl.	1.69E+06	0.00E+00	0.00E+00	1.32E+06	3.81E+06	8.49E+06	5.65E+05	1.03E+06
Dodecane..2.6.11.trimethyl.	1.34E+06	0.00E+00	0.00E+00	2.67E+05	6.71E+05	6.54E+05	2.24E+05	5.95E+06
Unknown.85	5.03E+06	0.00E+00	0.00E+00	2.24E+06	7.60E+06	5.99E+06	8.37E+06	1.52E+06
Phenol..3.methyl.	7.99E+05	0.00E+00	0.00E+00	7.06E+05	1.94E+06	8.97E+05	7.91E+05	8.24E+05
Benzene..4.ethyl.1.2.dimethyl..1	9.17E+05	0.00E+00	0.00E+00	6.95E+05	1.50E+06	4.87E+05	2.45E+05	4.16E+05
Octanoic.Acid	7.24E+06	0.00E+00	0.00E+00	4.87E+06	4.97E+06	1.67E+08	1.17E+07	2.64E+06
X2.Heptanone..6.methyl..1	1.60E+06	0.00E+00	0.00E+00	2.58E+06	4.96E+06	1.04E+06	1.26E+06	1.08E+06
Benzaldehyde..2.methyl.	1.01E+06	0.00E+00	2.22E+05	1.20E+06	2.21E+06	7.45E+05	2.23E+06	7.72E+05
Acetophenone	8.21E+05	0.00E+00	0.00E+00	7.66E+05	1.66E+06	1.23E+06	2.12E+05	5.29E+05
X2.Nonenal...E..	5.74E+05	0.00E+00	1.68E+05	6.67E+05	1.49E+06	0.00E+00	2.94E+05	7.33E+05
Tridecane	1.04E+06	1.89E+05	1.59E+05	4.86E+05	9.26E+05	3.70E+05	1.75E+05	6.09E+06
X1.3.8.p.Menthatriene	5.40E+05	0.00E+00	2.22E+05	0.00E+00	1.75E+06	7.33E+07	0.00E+00	3.82E+05
Decane..2.3.5.8.tetramethyl.	1.43E+06	0.00E+00	0.00E+00	3.58E+05	1.02E+06	9.10E+05	1.64E+05	5.02E+06
X2.Decanone	1.60E+06	0.00E+00	1.04E+04	1.60E+06	2.71E+06	2.39E+06	1.14E+06	6.37E+05
Dodecane..4.6.dimethyl.	6.70E+05	0.00E+00	0.00E+00	1.67E+05	5.19E+05	3.40E+05	6.92E+04	1.74E+06
Decanal	1.16E+06	0.00E+00	0.00E+00	3.67E+05	1.43E+06	1.59E+05	4.94E+05	2.38E+06
Undecane..4.7.dimethyl.	8.07E+05	0.00E+00	0.00E+00	2.93E+05	4.63E+05	4.82E+05	1.25E+05	2.61E+06
X2.Pentanone..4.hydroxy.4.methyl..2	3.04E+07	0.00E+00	0.00E+00	3.21E+07	6.90E+07	3.66E+07	1.49E+07	8.86E+06
Dodecane..2.6.10.trimethyl.	2.55E+05	1.03E+05	1.45E+05	6.14E+04	3.03E+05	2.56E+05	0.00E+00	7.00E+05
Ethanol..2..2.butoxyethoxy..	1.75E+06	0.00E+00	0.00E+00	0.00E+00	5.99E+06	1.73E+06	1.07E+06	1.15E+06
Nonanoic.acid	6.79E+06	0.00E+00	0.00E+00	7.56E+06	2.16E+07	5.36E+07	2.80E+06	7.88E+06

X2.Decenal...Z..	7.54E+05	0.00E+00	3.00E+05	7.83E+05	2.04E+06	4.26E+06	1.28E+06	1.50E+06
Tetradecane	1.79E+06	9.51E+04	1.21E+05	4.40E+05	2.02E+06	1.05E+06	5.24E+05	1.07E+07
X2.3H..Furanone..dihydro.5.propyl.	2.19E+06	0.00E+00	0.00E+00	2.00E+06	5.65E+06	0.00E+00	8.30E+05	1.00E+06
X2.Undecanone	1.33E+05	0.00E+00	0.00E+00	2.30E+04	1.73E+05	1.86E+06	7.76E+05	1.51E+05
X3.Dodecene...Z...1	9.27E+06	0.00E+00	0.00E+00	1.39E+05	1.19E+07	1.25E+07	4.12E+06	2.82E+07
Naphthalene	4.83E+06	3.46E+04	9.79E+04	1.81E+06	1.04E+07	3.97E+06	2.37E+06	1.85E+06
Dodecane..2.6.10.trimethyl..1	5.78E+05	7.07E+04	9.33E+04	1.13E+05	1.27E+06	8.97E+05	1.94E+05	1.78E+06
Benzaldehyde..2.4.dimethyl.	7.22E+06	6.09E+04	4.80E+05	1.70E+07	3.27E+07	1.17E+07	2.14E+06	5.33E+06
X2.Hepten.3.ol..4.5.dimethyl.	1.30E+05	0.00E+00	0.00E+00	0.00E+00	3.84E+05	1.12E+06	0.00E+00	8.36E+05
X1.Iodo.2.methylundecane	2.07E+06	6.98E+04	1.32E+05	6.95E+05	6.66E+06	4.60E+06	1.57E+06	5.63E+06
Propanoic.acid..2.methyl...anhydride	2.10E+05	0.00E+00	0.00E+00	1.75E+05	6.36E+05	1.75E+06	9.10E+04	4.28E+05
X2.4.Decadienal	2.26E+05	0.00E+00	0.00E+00	4.86E+05	5.17E+05	3.44E+05	8.94E+05	1.31E+05
Formamide..N.N.dibutyl.	1.19E+06	0.00E+00	0.00E+00	1.69E+06	2.19E+06	1.10E+07	1.99E+06	7.08E+05
X2.2.4.Trimethyl.1.3.pentanediol.diisobut yrate	1.56E+06	0.00E+00	0.00E+00	5.36E+05	5.63E+06	6.28E+06	1.02E+06	2.98E+06
X2.Undecenal	5.07E+05	5.31E+04	1.94E+05	1.49E+06	1.43E+06	4.06E+06	1.28E+06	8.68E+05
Pentadecane	2.16E+06	0.00E+00	0.00E+00	1.65E+06	7.67E+06	3.91E+06	1.41E+06	1.36E+07
Benzothiazole	9.15E+06	1.11E+05	1.16E+05	1.76E+06	5.64E+06	1.66E+07	2.72E+07	2.14E+06
Propanoic.acid..2.methyl...3.hydroxy.2.4. 4.trimethylpentyl.ester	1.80E+06	0.00E+00	0.00E+00	5.46E+05	8.45E+06	6.77E+06	1.63E+06	4.34E+06
Dodecanal	8.65E+05	0.00E+00	0.00E+00	3.88E+05	1.17E+06	6.93E+06	0.00E+00	1.40E+06
Naphthalene..1.methyl.	2.59E+06	0.00E+00	0.00E+00	6.03E+05	8.82E+06	3.11E+06	7.51E+05	1.04E+06
Undecane..5.7.dimethyl.	7.68E+05	0.00E+00	0.00E+00	7.98E+05	2.82E+06	1.21E+06	4.17E+05	1.01E+06
X2.4.7.9.Tetramethyl.5.decyn.4.7.diol	9.52E+05	0.00E+00	0.00E+00	9.29E+05	2.07E+06	7.11E+06	2.59E+06	4.15E+05
Hexanedinitrile	7.46E+05	0.00E+00	0.00E+00	3.23E+05	4.82E+05	2.91E+05	0.00E+00	6.15E+05
Undecane..3.methyl.	6.09E+05	0.00E+00	0.00E+00	5.20E+05	2.41E+06	1.07E+06	3.06E+05	1.80E+06

Caprolactam	4.18E+06	0.00E+00	0.00E+00	4.80E+05	9.36E+05	2.91E+06	3.57E+05	1.68E+06
Triacetin	1.07E+06	0.00E+00	0.00E+00	1.38E+06	7.69E+06	2.56E+06	1.60E+06	1.29E+06
X3.Hepten.2.one..4.methyl.	1.56E+06	0.00E+00	0.00E+00	2.28E+06	9.75E+06	2.36E+06	1.00E+06	1.33E+06
n.Nonylcyclohexane	1.70E+05	0.00E+00	0.00E+00	1.04E+05	6.04E+05	2.59E+05	1.51E+05	5.10E+05
Hexadecane	4.29E+06	6.80E+04	1.26E+05	5.61E+06	1.91E+07	6.46E+06	3.23E+06	3.49E+07
X2.Pentadecyn.1.ol	4.59E+06	0.00E+00	0.00E+00	7.24E+05	2.01E+06	1.03E+07	8.69E+06	1.09E+06
X1.Hexadecene	4.25E+06	0.00E+00	0.00E+00	3.51E+06	1.82E+07	5.47E+06	3.22E+06	9.17E+06
X2.Tridecanone	4.93E+05	0.00E+00	0.00E+00	6.16E+05	4.60E+05	4.54E+05	2.21E+05	2.63E+05
X2.3H..Furanone..dihydro.5.pentyl.	9.48E+05	0.00E+00	0.00E+00	5.91E+05	3.80E+06	3.74E+06	1.36E+06	2.26E+06
Furan..tetrahydro.2.2.4.4.tetramethyl.	9.61E+06	0.00E+00	0.00E+00	1.66E+07	4.09E+07	1.33E+07	7.57E+06	6.27E+06
Undecanal	3.05E+05	0.00E+00	0.00E+00	1.88E+05	6.56E+05	1.89E+06	1.47E+05	2.16E+06
Decane..2.5.9.trimethyl.	5.22E+06	0.00E+00	0.00E+00	3.14E+06	2.26E+07	4.49E+06	1.27E+06	8.58E+06
X2.5.Cyclohexadiene.1.4.dione..2.6.bis.1.1.dimethylethyl..	4.87E+06	0.00E+00	0.00E+00	7.55E+06	1.38E+07	9.21E+06	2.69E+06	5.63E+06
Tridecanoic.acid..methyl.ester	1.65E+05	0.00E+00	0.00E+00	2.88E+04	1.55E+06	7.33E+06	7.11E+04	1.51E+05
Biphenyl	1.93E+06	0.00E+00	0.00E+00	0.00E+00	5.75E+06	2.58E+06	1.50E+06	9.32E+05
X1.2.Benzenedicarboxylic.acid	7.28E+05	1.18E+05	1.49E+05	1.38E+06	1.11E+07	3.44E+07	7.45E+06	4.09E+05
Benzaldehyde..4.hydroxy.	5.38E+05	0.00E+00	0.00E+00	1.81E+05	3.96E+05	2.51E+06	1.85E+05	0.00E+00
Propanenitrile..3.3..oxybis.	1.56E+05	0.00E+00	0.00E+00	1.64E+05	8.04E+05	2.29E+05	5.91E+04	0.00E+00
Decane..2.3.5.8.tetramethyl..1	6.65E+06	0.00E+00	0.00E+00	1.04E+07	2.70E+07	1.03E+07	4.06E+06	5.66E+06
Heptadecane..2.6.dimethyl.	5.26E+06	0.00E+00	0.00E+00	8.79E+06	4.42E+06	7.20E+06	2.98E+06	4.44E+06
Butylated.Hydroxytoluene	8.06E+05	9.78E+04	9.08E+04	8.62E+05	9.71E+05	2.07E+06	0.00E+00	8.53E+05
Ethanone..1..3.methyloxiranyl..	1.08E+07	0.00E+00	0.00E+00	1.62E+07	3.55E+07	1.83E+07	8.00E+06	2.71E+06
Phenol..2.4.bis.1.1.dimethylethyl..	4.64E+06	1.91E+05	6.83E+05	1.38E+07	2.33E+07	1.26E+07	3.06E+06	3.07E+06
Cyclohexane...1.methylethyl..	7.79E+05	0.00E+00	0.00E+00	7.93E+05	2.79E+06	8.75E+05	1.26E+06	1.22E+06

Hexadecane.1	1.62E+07	0.00E+00	0.00E+00	3.22E+07	2.98E+07	2.32E+07	4.65E+06	1.05E+07
X2.Tetradecanone	3.19E+05	0.00E+00	0.00E+00	2.64E+05	4.35E+05	2.55E+05	1.64E+05	1.71E+05
Benzene...1.methylnonyl..	1.67E+05	0.00E+00	0.00E+00	2.05E+05	5.80E+05	9.75E+04	4.32E+03	2.87E+05
Propanoic.acid..2.methyl...1..1.1.dimethyl ethyl..2.methyl.1.3.propanediyl.ester	2.25E+07	7.31E+04	1.52E+05	2.69E+07	1.26E+08	6.03E+07	2.07E+07	3.65E+07
X2.3H..Furanone..5.hexyldihydro.	5.93E+05	0.00E+00	0.00E+00	8.66E+05	2.02E+06	5.74E+05	4.12E+05	5.40E+05
Hexadecanal	6.19E+05	1.35E+05	2.96E+05	2.85E+05	9.85E+05	1.42E+06	1.72E+06	1.75E+06
Benzene...1.pentylhexyl..	8.35E+04	0.00E+00	0.00E+00	1.42E+05	3.56E+05	1.55E+05	3.87E+04	3.42E+05
Benzene...1.butylheptyl..	1.22E+05	0.00E+00	0.00E+00	1.36E+05	5.01E+05	2.56E+05	9.88E+04	4.50E+05
Benzene...1.propyloctyl..	2.56E+05	0.00E+00	0.00E+00	8.09E+04	5.70E+05	2.72E+05	4.93E+04	3.21E+05
Ethanone..1.1...1.4.phenylene.bis.	2.34E+06	0.00E+00	0.00E+00	5.69E+06	1.06E+07	2.11E+06	1.19E+07	1.42E+06
X1.Iodo.2.methylundecane.1	2.71E+06	0.00E+00	0.00E+00	5.58E+06	1.31E+07	4.36E+06	1.55E+06	9.15E+06
X1.Cyclohexanone..2.methyl.2..3.methyl. 2.oxobutyl.	1.73E+06	0.00E+00	0.00E+00	8.37E+05	4.95E+06	6.77E+06	1.65E+06	6.70E+05
Dimethyl.phthalate	7.32E+05	0.00E+00	0.00E+00	1.61E+06	3.20E+06	3.70E+06	1.26E+06	5.52E+05
Ethanone..1..4..1.hydroxy.1.methylethyl. phenyl..	4.00E+06	0.00E+00	0.00E+00	1.66E+06	3.33E+06	1.81E+07	3.08E+06	8.89E+05
Acenaphthene	1.68E+06	0.00E+00	0.00E+00	0.00E+00	6.05E+06	4.32E+06	1.22E+06	1.21E+06
Nonadecane	7.60E+06	0.00E+00	1.05E+05	1.50E+07	5.27E+07	9.06E+06	4.40E+06	3.60E+07
Dodecyl.acrylate	3.12E+06	0.00E+00	0.00E+00	4.84E+06	1.13E+07	4.33E+06	1.54E+06	1.97E+06
Benzene..1.methyl.3..phenylmethyl..	1.33E+06	0.00E+00	0.00E+00	0.00E+00	3.95E+06	2.80E+06	3.80E+05	7.30E+05
X1.Hexadecene.1	9.40E+06	0.00E+00	0.00E+00	1.54E+07	5.85E+07	7.99E+06	2.26E+06	1.94E+07
Dibenzofuran	3.71E+06	0.00E+00	0.00E+00	2.41E+06	1.03E+07	4.18E+06	2.19E+06	6.29E+05
X2.Octanone	3.68E+05	0.00E+00	0.00E+00	3.64E+05	8.24E+05	2.97E+05	7.22E+04	8.50E+05
Methyl.n.hexyl.ketone.1.phenyl.1.2.etha nediol.ketal.1	1.27E+06	0.00E+00	0.00E+00	1.36E+06	2.23E+06	1.23E+06	8.13E+05	3.52E+05
Benzene...1.methyldecyl..	4.11E+05	0.00E+00	0.00E+00	4.09E+05	1.01E+06	9.76E+05	6.93E+05	5.94E+05

Unknown.194	9.95E+05	9.81E+04	5.91E+04	1.31E+06	2.61E+06	1.52E+07	1.41E+07	5.48E+05
X2.3H..Furanone..5.hexyldihydro..1	6.21E+05	0.00E+00	0.00E+00	1.35E+06	3.14E+06	3.09E+06	8.47E+05	1.41E+05
Benzene...1.pentylheptyl..	2.00E+06	0.00E+00	0.00E+00	2.48E+06	7.50E+06	2.73E+06	1.07E+06	5.10E+06
Benzene...1.pentylheptyl...1	2.00E+06	0.00E+00	0.00E+00	2.48E+06	7.50E+06	2.73E+06	1.07E+06	5.10E+06
Benzene...1.butylloctyl..	2.34E+05	0.00E+00	0.00E+00	3.51E+05	1.20E+06	1.99E+05	1.33E+05	1.65E+06
Benzene...1.propylnonyl..	3.32E+05	0.00E+00	0.00E+00	3.65E+05	8.27E+05	3.37E+05	6.01E+05	1.62E+06
Tributyl.phosphate	1.23E+06	0.00E+00	0.00E+00	1.14E+06	2.23E+06	3.40E+06	5.31E+05	9.54E+04
Benzene...1.ethyldecyl..	3.67E+05	0.00E+00	0.00E+00	3.93E+05	9.28E+05	4.42E+05	3.49E+05	2.76E+06
n.Hexyl.salicylate	5.33E+05	0.00E+00	0.00E+00	4.57E+05	1.27E+06	3.58E+06	8.45E+05	5.44E+05
X1.6.Dioxacyclododecane.7.12.dione	2.10E+06	0.00E+00	0.00E+00	2.00E+06	3.84E+06	3.22E+06	2.07E+06	1.55E+06
Unknown.205	1.98E+06	0.00E+00	0.00E+00	7.31E+05	6.68E+06	2.76E+06	1.09E+06	1.06E+06
Nonadecane.1	4.86E+06	1.97E+04	7.29E+04	9.57E+06	3.38E+07	8.00E+06	4.80E+06	3.10E+07
Cyclopentaneacetic.acid..3.oxo.2.pentyl...methyl.ester	1.05E+06	0.00E+00	0.00E+00	1.71E+06	4.47E+06	4.89E+06	1.53E+06	3.71E+05
Diethyl.Phthalate	1.43E+06	0.00E+00	0.00E+00	4.02E+06	1.09E+07	2.70E+06	2.10E+06	3.92E+05
Fluorene	1.43E+06	0.00E+00	0.00E+00	5.76E+05	5.02E+06	1.65E+06	1.54E+06	1.27E+06
Isopropyl.Myristate	1.90E+06	0.00E+00	0.00E+00	2.55E+06	6.38E+06	1.83E+06	1.02E+06	3.31E+06
Cyclohexane..2.propenyl.	1.26E+06	0.00E+00	0.00E+00	2.55E+06	5.66E+06	7.10E+05	8.86E+05	3.17E+06
Nonadecane..2.methyl.	1.25E+07	0.00E+00	0.00E+00	3.49E+07	7.18E+07	1.66E+07	7.12E+06	2.91E+07
X2.Hexanone..4.methyl.	1.12E+04	0.00E+00	0.00E+00	3.19E+05	5.28E+05	3.14E+05	7.39E+04	3.28E+05
Benzene...1.methylundecyl..	5.85E+05	0.00E+00	0.00E+00	7.30E+05	2.45E+06	1.16E+06	2.10E+05	6.15E+06
Benzene...1.hexylheptyl..	1.38E+06	0.00E+00	0.00E+00	1.12E+06	2.67E+06	8.72E+05	4.58E+05	1.08E+07
X2.Pentadecanone..6.10.14.trimethyl.	4.74E+05	3.74E+04	1.47E+05	6.53E+05	2.24E+06	3.69E+05	2.22E+05	7.95E+05
Benzophenone	1.78E+06	0.00E+00	0.00E+00	2.33E+06	3.94E+06	2.36E+06	2.26E+06	2.35E+05
X1.Docosene	3.99E+06	0.00E+00	0.00E+00	4.34E+06	4.13E+07	4.17E+06	1.22E+06	1.28E+07

X2.Pentanone..4.hydroxy.4.methyl..3	7.17E+05	0.00E+00	0.00E+00	9.51E+05	2.45E+06	9.31E+05	3.05E+05	2.88E+06
Hexadecanoic.acid..methyl.ester	1.54E+07	0.00E+00	0.00E+00	2.90E+07	6.16E+07	1.89E+07	9.83E+06	1.21E+07
Butanedioic.acid..phenyl.	1.39E+06	0.00E+00	0.00E+00	1.84E+06	3.82E+06	1.22E+06	1.35E+06	2.83E+05
Heneicosane	1.93E+06	1.65E+05	2.86E+05	3.06E+06	8.16E+06	1.89E+06	1.37E+06	6.08E+07
X2.Propanol..1.chloro...phosphate..3.1.	6.36E+06	2.09E+04	3.08E+04	6.92E+06	1.35E+07	7.04E+06	2.56E+06	3.71E+06
X2.Propanol..1.chloro...phosphate..3.1..1	2.07E+06	0.00E+00	0.00E+00	2.84E+06	5.15E+06	2.73E+06	7.75E+05	8.85E+05
X1.2.Benzenedicarboxylic.acid..bis.2.methylpropyl..ester	5.18E+06	0.00E+00	0.00E+00	8.94E+06	1.59E+07	6.91E+06	2.64E+06	2.81E+06
Phenanthrene	3.90E+06	0.00E+00	0.00E+00	3.67E+06	1.06E+07	4.11E+06	1.72E+06	1.71E+06
Benzenesulfonamide..N.butyl.	7.23E+06	0.00E+00	0.00E+00	1.61E+07	3.59E+07	1.14E+07	3.13E+07	2.41E+06
Heneicosane.1	1.40E+06	0.00E+00	1.11E+05	3.05E+06	6.85E+06	1.66E+06	7.99E+05	2.55E+07
X7.9.Di.tert.butyl.1.oxaspiro.4.5.deca.6.9.diene.2.8.dione	8.88E+06	0.00E+00	0.00E+00	2.72E+07	4.22E+07	4.21E+07	9.86E+06	3.25E+06
X1.2.Benzenedicarboxylic.acid..butyl.2.methylpropyl.ester	1.18E+06	0.00E+00	0.00E+00	4.06E+06	7.33E+06	6.88E+06	1.38E+06	3.69E+05
Octadecanoic.acid..methyl.ester	2.02E+07	0.00E+00	0.00E+00	4.49E+07	9.05E+07	2.83E+07	1.58E+07	1.41E+07
X9.Octadecenoic.acid..Z....methyl.ester	9.99E+06	0.00E+00	0.00E+00	5.97E+07	8.59E+07	2.81E+07	1.00E+07	1.07E+07
X9.Octadecenoic.acid..Z....methyl.ester.1	4.21E+06	0.00E+00	0.00E+00	1.25E+06	1.72E+07	3.25E+06	2.15E+06	1.80E+06
Dibutyl.phthalate	6.95E+06	0.00E+00	2.37E+04	1.38E+07	3.10E+07	1.49E+07	5.98E+06	5.71E+06
Ethanone..2.2.dimethoxy.1.2.diphenyl.	6.74E+05	0.00E+00	0.00E+00	1.14E+06	2.33E+06	2.72E+06	5.93E+06	0.00E+00
Heneicosane.2	1.75E+06	0.00E+00	0.00E+00	2.50E+06	5.07E+06	2.26E+06	6.98E+05	4.20E+07
Octadecanoic.acid	4.35E+07	0.00E+00	0.00E+00	4.87E+07	9.36E+07	1.39E+08	1.47E+08	7.43E+05
Oleic.Acid	4.97E+06	0.00E+00	0.00E+00	2.74E+06	4.14E+07	9.09E+06	7.07E+08	1.10E+07
Nonadecane.2	1.73E+06	0.00E+00	0.00E+00	2.88E+06	6.40E+06	1.89E+06	4.82E+05	1.30E+07
Nonanamide	1.74E+06	0.00E+00	0.00E+00	1.59E+06	3.55E+06	2.33E+06	0.00E+00	4.26E+05
Heptacosane	3.41E+06	0.00E+00	1.22E+05	2.47E+06	5.77E+06	1.61E+06	7.45E+05	2.43E+07

Unknown.266	9.92E+05	0.00E+00	0.00E+00	1.50E+06	2.79E+06	0.00E+00	4.05E+06	1.16E+06
Pyrene	1.22E+06	0.00E+00	0.00E+00	1.61E+06	3.50E+06	2.88E+06	6.02E+06	3.56E+05
Heptacosane.1	2.83E+06	0.00E+00	0.00E+00	1.59E+07	3.03E+07	5.79E+06	8.79E+05	8.92E+06
Ethanone..2..formyloxy..1.phenyl.	1.26E+06	0.00E+00	0.00E+00	3.17E+06	6.83E+06	2.20E+06	7.36E+05	8.63E+04
Pyrene.1	6.36E+05	0.00E+00	0.00E+00	9.23E+05	1.37E+06	6.71E+05	6.02E+05	6.37E+04
Nonanamide.1	2.28E+06	0.00E+00	1.03E+04	1.28E+06	4.00E+06	1.59E+06	1.65E+06	6.90E+05
Heptacosane.2	3.24E+06	0.00E+00	4.77E+04	4.87E+06	5.15E+06	2.13E+06	3.56E+05	2.35E+07
Heptacosane.3	1.09E+07	0.00E+00	0.00E+00	2.38E+07	2.60E+07	4.34E+06	1.05E+06	1.22E+07
Heptacosane.4	1.29E+06	6.65E+04	8.25E+04	7.07E+06	1.35E+07	2.52E+06	2.42E+05	2.53E+07
Nonadecane..2.methyl..1	3.31E+06	0.00E+00	0.00E+00	1.00E+07	2.36E+07	6.03E+06	2.17E+05	1.90E+07
Heptacosane.5	9.87E+05	0.00E+00	0.00E+00	3.92E+06	8.33E+06	1.25E+06	2.93E+05	2.30E+07
X1.2.Benzenedicarboxylic.acid..diisodecyl.ester	2.63E+07	1.30E+05	9.62E+05	2.67E+07	2.88E+07	3.73E+06	2.57E+06	3.93E+06
X13.Docosenamide...Z..	1.89E+07	7.73E+05	2.94E+06	1.45E+07	8.67E+06	5.59E+06	3.85E+06	2.44E+07
Unknown.401	2.03E+06	0.00E+00	2.13E+06	2.85E+06	3.33E+06	3.32E+06	7.72E+07	1.62E+07
Unknown.510	1.47E+07	0.00E+00	0.00E+00	2.42E+07	4.65E+07	1.57E+07	1.88E+06	1.09E+05
Tetradecane.1	1.87E+06	1.75E+05	1.57E+05	6.14E+05	4.28E+06	2.41E+06	1.29E+06	1.23E+07
Hexadecane.2	1.21E+07	6.92E+04	1.11E+05	1.47E+07	6.13E+07	1.00E+07	6.26E+06	3.73E+07
Eicosane	7.06E+06	7.40E+04	8.45E+04	6.71E+06	1.67E+07	7.68E+06	3.57E+06	1.51E+07

Appendix III

Consists of the time series of major ion geochemistry, and physio chemistry for all samples taken from the GTS borehole monitoring network.

Date	Borehole	Code	Al mg/l	Ca mg/l	Fe mg/l	K mg/l	Li mg/l	Mg mg/l	Mn mg/l	Na mg/l	Si mg/l	Sr mg/l
23/10/2014	BOHP98.007 i2	K	0.033	4.966	0.003	0.416	0.000	0.018	0.000	10.980	4.751	0.149
03/11/2014	BOHP98.007 i2	K	0.030	4.976	0.003	0.428	0.000	0.018	0.000	11.150	4.774	0.150
06/11/2014	BOHP98.007 i2	K	0.033	4.907	0.007	0.447	0.000	0.020	0.000	10.950	4.699	0.149
12/11/2014	BOHP98.007 i2	K	0.034	5.199	0.006	1.282	0.000	0.026	0.000	11.700	4.869	0.154
19/11/2014	BOHP98.007 i2	K	0.033	5.305	0.003	0.763	0.000	0.022	0.000	10.830	4.808	0.156
27/11/2014	BOHP98.007 i2	K	0.034	5.556	0.005	0.563	0.000	0.023	0.000	10.530	4.792	0.155
23/02/2015	BOHP98.007 i2	K	0.023	4.793	0.002	0.475	0.000	0.022	0.000	10.250	4.728	0.152
02/03/2015	BOHP98.007 i2	K	0.025	4.939	0.003	0.387	0.000	0.023	0.000	9.993	4.907	0.149
09/03/2015	BOHP98.007 i2	K	0.024	4.731	0.004	0.448	0.000	0.023	0.000	9.977	4.861	0.153
16/03/2015	BOHP98.007 i2	K	0.026	4.615	0.031	0.447	0.000	0.022	0.001	10.380	4.590	0.143
23/03/2015	BOHP98.007 i2	K	0.035	5.212	0.026	0.431	0.000	0.058	0.001	10.190	4.701	0.150
25/08/2015	BOHP98.007 i2	K	0.032	4.579	0.026	0.357	0.000	0.013	0.001	9.612	4.409	0.142
01/02/2016	BOHP98.007 i2	K	0.057	5.184	0.025	0.469	0.039	0.032	0.001	11.282	4.499	0.176
02/02/2016	BOHP98.007 i2	K	0.071	5.640	0.025	0.381	0.039	0.045	0.001	11.430	4.825	0.185
03/02/2016	BOHP98.007 i2	K	0.069	5.829	0.022	0.377	0.040	0.041	0.001	11.560	4.827	0.186
04/02/2016	BOHP98.007 i2	K	0.139	5.525	0.075	0.398	0.037	0.090	0.003	10.910	4.754	0.176
05/02/2016	BOHP98.007 i2	K	0.181	5.384	0.114	0.491	0.040	0.109	0.003	11.240	4.907	0.175
08/02/2016	BOHP98.007 i2	K	0.158	5.289	0.098	0.499	0.043	0.103	0.003	11.340	4.900	0.174
11/02/2016	BOHP98.007 i2	K	0.110	5.121	0.074	0.432	0.038	0.064	0.002	11.110	4.731	0.170
17/02/2016	BOHP98.007 i2	K	0.088	5.322	0.058	0.400	0.038	0.055	0.002	11.390	4.722	0.171
22/02/2016	BOHP98.007 i2	K	0.089	5.410	0.024	0.549	0.040	0.052	0.001	11.470	4.720	0.175
29/02/2016	BOHP98.007 i2	K	0.085	5.529	0.045	0.484	0.042	0.048	0.002	11.070	4.581	0.174
09/03/2016	BOHP98.007 i2	K	0.073	5.606	0.011	0.446	0.035	0.037	0.001	11.080	4.619	0.177

14/03/2016	BOHP98.007 i2	K	0.051	5.387	0.007	0.404	0.040	0.034	0.001	11.460	4.773	0.176
21/03/2016	BOHP98.007 i2	K	0.049	5.163	0.001	0.377	0.037	0.032	0.000	11.100	4.603	0.170
29/03/2016	BOHP98.007 i2	K	0.044	5.287	0.001	0.354	0.034	0.027	0.000	11.220	4.636	0.173
06/04/2016	BOHP98.007 i2	K	0.046	5.294	0.001	0.382	0.036	0.029	0.000	11.410	4.729	0.175
23/10/2014	BOHP98.007 i3	J	0.034	4.869	0.003	0.414	0.000	0.017	0.000	10.960	4.706	0.147
03/11/2014	BOHP98.007 i3	J	0.036	4.890	0.003	0.426	0.000	0.017	0.000	11.210	4.794	0.149
06/11/2014	BOHP98.007 i3	J	0.044	4.878	0.008	0.437	0.000	0.018	0.000	10.970	4.669	0.147
12/11/2014	BOHP98.007 i3	J	0.037	4.743	0.007	0.437	0.000	0.018	0.000	10.920	4.633	0.145
19/11/2014	BOHP98.007 i3	J	0.037	5.146	0.006	0.584	0.000	0.023	0.000	10.820	4.697	0.150
27/11/2014	BOHP98.007 i3	J	0.037	5.503	0.006	0.506	0.000	0.023	0.000	10.650	4.795	0.154
23/02/2015	BOHP98.007 i3	J	0.034	4.804	0.002	0.637	0.000	0.021	0.000	10.330	4.757	0.152
02/03/2015	BOHP98.007 i3	J	0.028	5.013	0.005	0.400	0.000	0.024	0.001	10.320	4.914	0.148
09/03/2015	BOHP98.007 i3	J	0.028	4.642	0.008	0.442	0.000	0.023	0.000	9.929	4.879	0.153
16/03/2015	BOHP98.007 i3	J	0.026	4.586	0.006	0.452	0.000	0.020	0.000	10.440	4.582	0.142
23/03/2015	BOHP98.007 i3	J	0.022	4.859	0.014	0.489	0.000	0.019	0.000	10.010	4.541	0.146
25/08/2015	BOHP98.007 i3	J	0.039	4.540	0.028	0.364	0.000	0.013	0.001	9.706	4.434	0.142
23/10/2014	BOSB80.001	G	0.034	8.494	0.000	0.188	0.000	0.038	0.000	6.096	4.214	0.143
31/10/2014	BOSB80.001	G	0.034	8.298	0.000	0.187	0.000	0.038	0.001	6.063	4.185	0.142
06/11/2014	BOSB80.001	G	0.037	8.456	0.002	0.332	0.000	0.039	0.001	6.133	4.212	0.143
12/11/2014	BOSB80.001	G	0.037	8.322	0.003	0.278	0.000	0.039	0.001	6.146	4.221	0.143
19/11/2014	BOSB80.001	G	0.040	8.401	0.003	0.989	0.000	0.046	0.001	6.663	4.178	0.142
27/11/2014	BOSB80.001	G	0.039	9.224	0.009	0.363	0.000	0.049	0.000	5.899	4.202	0.147
23/02/2015	BOSB80.001	G	0.025	8.418	0.004	0.232	0.000	0.045	0.001	5.845	4.283	0.147
02/03/2015	BOSB80.001	G	0.025	7.906	0.003	0.205	0.000	0.045	0.001	5.323	4.148	0.141

09/03/2015	BOSB80.001	G	0.030	8.196	0.007	0.278	0.000	0.049	0.001	5.587	4.348	0.146
16/03/2015	BOSB80.001	G	0.019	7.887	0.003	0.219	0.000	0.043	0.001	5.524	4.031	0.136
23/03/2015	BOSB80.001	G	0.029	8.287	0.025	0.213	0.000	0.044	0.001	5.523	4.069	0.140
25/08/2015	BOSB80.001	G	0.039	7.691	0.022	0.067	0.000	0.035	0.001	5.063	3.892	0.134
01/02/2016	BOSB80.001	G	0.048	8.936	0.013	0.255	0.011	0.047	0.001	6.360	4.122	0.162
02/02/2016	BOSB80.001	G	0.059	9.220	0.014	0.196	0.013	0.056	0.002	6.220	4.136	0.162
03/02/2016	BOSB80.001	G	0.027	9.210	0.001	0.167	0.009	0.052	0.001	6.327	4.120	0.163
04/02/2016	BOSB80.001	G	0.055	9.314	0.003	0.177	0.010	0.054	0.001	6.234	4.165	0.164
05/02/2016	BOSB80.001	G	0.056	8.823	0.016	0.360	0.013	0.051	0.001	6.265	4.159	0.157
08/02/2016	BOSB80.001	G	0.054	8.813	0.008	0.173	0.010	0.053	0.001	6.000	4.037	0.158
11/02/2016	BOSB80.001	G	0.049	8.564	0.014	0.212	0.011	0.048	0.001	6.185	4.076	0.155
17/02/2016	BOSB80.001	G	0.062	8.952	0.028	0.154	0.011	0.054	0.002	6.351	4.141	0.160
22/02/2016	BOSB80.001	G	0.039	8.701	0.001	0.178	0.009	0.042	0.001	6.363	4.087	0.157
29/02/2016	BOSB80.001	G	0.046	9.465	0.001	0.251	0.009	0.041	0.001	6.346	4.123	0.165
09/03/2016	BOSB80.001	G	0.052	9.412	0.001	0.227	0.011	0.041	0.001	6.244	4.064	0.163
14/03/2016	BOSB80.001	G	0.044	9.030	0.001	0.225	0.012	0.046	0.001	6.353	4.214	0.163
21/03/2016	BOSB80.001	G	0.042	8.889	0.001	0.177	0.008	0.043	0.001	6.338	4.154	0.161
29/03/2016	BOSB80.001	G	0.037	8.695	0.001	0.191	0.006	0.043	0.001	6.172	4.084	0.159
06/04/2016	BOSB80.001	G	0.040	8.726	0.001	0.212	0.007	0.042	0.001	6.216	4.077	0.159
07/11/2014	BOSB80.003 i4	I	0.022	3.924	0.006	0.152	0.000	0.010	0.003	14.210	4.441	0.099
12/11/2014	BOSB80.003 i4	I	0.026	3.739	0.004	0.411	0.000	0.008	0.001	14.600	4.481	0.099
19/11/2014	BOSB80.003 i4	I	0.026	4.098	0.006	0.570	0.000	0.015	0.002	14.000	4.586	0.103
27/11/2014	BOSB80.003 i4	I	0.024	4.265	0.008	0.210	0.000	0.012	0.000	13.760	4.718	0.106
23/02/2015	BOSB80.003 i4	I	0.021	3.399	0.000	0.766	0.000	0.009	0.000	13.550	4.296	0.095

02/03/2015	BOSB80.003 i4	I	0.017	3.901	0.009	0.181	0.000	0.013	0.001	13.190	5.035	0.104
09/03/2015	BOSB80.003 i4	I	0.015	3.760	0.005	0.083	0.000	0.010	0.000	12.950	4.977	0.107
16/03/2015	BOSB80.003 i4	I	0.011	3.585	0.005	0.163	0.000	0.008	0.001	13.290	4.793	0.101
25/08/2015	BOSB80.003 i4	I	0.035	3.234	0.026	0.035	0.000	0.000	0.001	12.510	4.194	0.092
01/02/2016	BOSB80.003 i4	I	0.067	3.813	0.049	0.207	0.085	0.025	0.002	14.910	4.614	0.110
02/02/2016	BOSB80.003 i4	I	0.061	4.155	0.018	0.084	0.078	0.015	0.001	15.160	4.856	0.120
03/02/2016	BOSB80.003 i4	I	0.075	4.161	0.038	0.121	0.075	0.031	0.002	14.550	4.773	0.117
04/02/2016	BOSB80.003 i4	I	0.045	4.083	0.016	0.056	0.073	0.016	0.001	14.270	4.705	0.117
05/02/2016	BOSB80.003 i4	I	0.043	3.880	0.025	0.113	0.079	0.014	0.001	14.530	4.761	0.114
08/02/2016	BOSB80.003 i4	I	0.036	3.847	0.011	0.119	0.079	0.013	0.000	14.390	4.751	0.114
17/02/2016	BOSB80.003 i4	I	0.041	4.013	0.014	0.055	0.079	0.012	0.001	15.230	4.831	0.116
22/02/2016	BOSB80.003 i4	I	0.027	4.072	0.001	0.130	0.074	0.008	0.000	14.520	4.699	0.117
29/02/2016	BOSB80.003 i4	I	0.032	4.194	0.001	0.091	0.074	0.006	0.000	14.400	4.700	0.120
09/03/2016	BOSB80.003 i4	I	0.036	4.346	0.001	0.135	0.076	0.007	0.000	14.600	4.800	0.123
14/03/2016	BOSB80.003 i4	I	0.045	4.360	0.017	0.107	0.079	0.017	0.001	15.030	4.989	0.123
21/03/2016	BOSB80.003 i4	I	0.024	4.188	0.001	0.052	0.076	0.006	0.000	14.870	5.012	0.124
29/03/2016	BOSB80.003 i4	I	0.024	4.245	0.001	0.042	0.075	0.006	0.000	14.800	5.055	0.128
06/04/2016	BOSB80.003 i4	I	0.029	4.092	0.001	0.045	0.070	0.006	0.000	14.220	4.790	0.122
23/10/2014	BOUS 85.002 i2	F	0.019	6.607	0.001	0.342	0.000	0.023	0.000	9.267	5.020	0.168
31/10/2014	BOUS 85.002 i2	F	0.020	6.719	0.001	0.448	0.000	0.025	0.002	9.559	5.106	0.170
06/11/2014	BOUS 85.002 i2	F	0.023	6.812	0.004	0.326	0.000	0.024	0.002	9.490	4.833	0.178
12/11/2014	BOUS 85.002 i2	F	0.021	6.672	0.002	0.324	0.000	0.022	0.001	9.448	4.900	0.173
19/11/2014	BOUS 85.002 i2	F	0.025	6.632	0.003	0.373	0.000	0.023	0.001	9.450	4.841	0.173
27/11/2014	BOUS 85.002 i2	F	0.033	7.353	0.017	0.413	0.000	0.033	0.002	8.845	4.784	0.178

23/02/2015	BOUS 85.002 i2	F	0.020	6.504	0.014	0.295	0.000	0.031	0.002	8.689	4.717	0.184
02/03/2015	BOUS 85.002 i2	F	0.018	6.481	0.013	0.348	0.000	0.030	0.001	8.450	4.929	0.176
09/03/2015	BOUS 85.002 i2	F	0.015	6.302	0.004	0.323	0.000	0.029	0.001	8.255	4.879	0.175
16/03/2015	BOUS 85.002 i2	F	0.024	6.449	0.037	0.437	0.000	0.035	0.002	8.816	4.736	0.172
23/03/2015	BOUS 85.002 i2	F	0.022	6.610	0.032	0.300	0.000	0.030	0.002	8.512	4.656	0.172
25/08/2015	BOUS 85.002 i2	F	0.027	6.513	0.031	0.349	0.000	0.024	0.002	8.673	4.835	0.167
01/02/2016	BOUS 85.002 i2	F	0.041	6.896	0.029	0.458	0.013	0.032	0.002	9.660	4.792	0.195
02/02/2016	BOUS 85.002 i2	F	0.036	7.047	0.009	0.360	0.012	0.031	0.002	9.754	4.913	0.200
03/02/2016	BOUS 85.002 i2	F	0.044	7.549	0.016	0.302	0.012	0.036	0.002	9.983	5.025	0.209
04/02/2016	BOUS 85.002 i2	F	0.044	7.378	0.016	0.280	0.009	0.036	0.002	9.747	4.876	0.205
05/02/2016	BOUS 85.002 i2	F	0.040	7.278	0.009	0.259	0.008	0.035	0.002	9.606	4.797	0.202
08/02/2016	BOUS 85.002 i2	F	0.036	6.874	0.001	0.317	0.011	0.030	0.001	9.755	4.772	0.195
11/02/2016	BOUS 85.002 i2	F	0.038	6.516	0.014	0.325	0.011	0.031	0.001	9.242	4.545	0.187
17/02/2016	BOUS 85.002 i2	F	0.041	6.960	0.018	0.313	0.014	0.033	0.002	9.710	4.729	0.197
22/02/2016	BOUS 85.002 i2	F	0.027	6.896	0.001	0.286	0.008	0.026	0.001	9.918	4.771	0.195
29/02/2016	BOUS 85.002 i2	F	0.032	7.169	0.001	0.344	0.011	0.025	0.001	9.591	4.660	0.198
09/03/2016	BOUS 85.002 i2	F	0.030	7.338	0.001	0.315	0.009	0.024	0.001	9.556	4.689	0.202
14/03/2016	BOUS 85.002 i2	F	0.043	7.094	0.001	0.450	0.028	0.033	0.002	9.890	4.860	0.206
21/03/2016	BOUS 85.002 i2	F	0.030	7.122	0.001	0.349	0.013	0.027	0.001	9.635	4.785	0.201
29/03/2016	BOUS 85.002 i2	F	0.027	7.079	0.001	0.291	0.006	0.026	0.001	9.883	4.852	0.205
06/04/2016	BOUS 85.002 i2	F	0.027	6.914	0.001	0.241	0.004	0.025	0.001	9.541	4.656	0.201
23/10/2014	BOUS 85.002 i3	E	0.008	7.671	0.001	0.140	0.000	0.022	0.001	8.579	4.635	0.197
31/10/2014	BOUS 85.002 i3	E	0.009	7.474	0.002	0.141	0.000	0.022	0.001	8.536	4.581	0.194
06/11/2014	BOUS 85.002 i3	E	0.010	7.668	0.002	0.230	0.000	0.024	0.003	8.805	4.665	0.198

12/11/2014	BOUS 85.002 i3	E	0.010	7.464	0.004	0.214	0.000	0.022	0.002	8.569	4.549	0.193
19/11/2014	BOUS 85.002 i3	E	0.011	7.399	0.004	0.308	0.000	0.023	0.002	8.614	4.553	0.193
27/11/2014	BOUS 85.002 i3	E	0.011	8.193	0.007	0.339	0.000	0.029	0.001	8.196	4.577	0.200
23/02/2015	BOUS 85.002 i3	E	0.011	7.767	0.016	0.190	0.000	0.032	0.002	8.369	4.821	0.208
02/03/2015	BOUS 85.002 i3	E	0.000	7.303	0.000	0.644	0.000	0.027	0.001	7.816	4.676	0.199
09/03/2015	BOUS 85.002 i3	E	0.000	7.295	0.005	0.205	0.000	0.028	0.002	7.736	4.701	0.199
16/03/2015	BOUS 85.002 i3	E	0.006	7.219	0.022	0.197	0.000	0.030	0.002	8.000	4.508	0.191
23/03/2015	BOUS 85.002 i3	E	0.000	7.312	0.000	0.163	0.000	0.024	0.002	7.842	4.450	0.192
25/08/2015	BOUS 85.002 i3	E	0.013	7.384	0.032	0.183	0.000	0.020	0.002	7.860	4.435	0.189
01/02/2016	BOUS 85.002 i3	E	0.159	8.023	0.313	0.275	0.012	0.120	0.004	8.862	4.794	0.228
02/02/2016	BOUS 85.002 i3	E	0.025	8.270	0.010	0.170	0.011	0.032	0.002	8.958	4.592	0.230
03/02/2016	BOUS 85.002 i3	E	0.033	8.451	0.011	0.139	0.009	0.036	0.002	8.905	4.650	0.235
04/02/2016	BOUS 85.002 i3	E	0.031	8.465	0.015	0.125	0.009	0.038	0.002	8.823	4.570	0.231
05/02/2016	BOUS 85.002 i3	E	0.030	7.951	0.027	0.594	0.015	0.036	0.002	8.980	4.593	0.224
08/02/2016	BOUS 85.002 i3	E	0.024	7.922	0.001	0.232	0.009	0.039	0.001	9.009	4.558	0.223
11/02/2016	BOUS 85.002 i3	E	0.022	7.553	0.015	0.167	0.011	0.031	0.002	8.560	4.393	0.216
17/02/2016	BOUS 85.002 i3	E	0.029	7.821	0.025	0.174	0.013	0.034	0.002	8.687	4.467	0.221
22/02/2016	BOUS 85.002 i3	E	0.012	8.067	0.001	0.090	0.007	0.026	0.001	9.228	4.656	0.227
29/02/2016	BOUS 85.002 i3	E	0.016	8.151	0.001	0.203	0.010	0.026	0.002	8.660	4.395	0.226
09/03/2016	BOUS 85.002 i3	E	0.025	8.606	0.001	0.151	0.006	0.026	0.002	8.856	4.469	0.231
14/03/2016	BOUS 85.002 i3	E	0.018	8.087	0.001	0.251	0.017	0.030	0.002	9.012	4.602	0.230
21/03/2016	BOUS 85.002 i3	E	0.014	7.933	0.001	0.144	0.011	0.026	0.002	8.820	4.613	0.227
29/03/2016	BOUS 85.002 i3	E	0.021	7.933	0.001	0.179	0.014	0.026	0.002	8.726	4.468	0.224
06/04/2016	BOUS 85.002 i3	E	0.013	7.783	0.001	0.161	0.005	0.026	0.002	8.692	4.440	0.222

23/10/2014	BOUS 85.002 i4	D	0.010	7.414	0.000	0.122	0.000	0.020	0.000	8.662	4.725	0.210
31/10/2014	BOUS 85.002 i4	D	0.013	7.242	0.001	0.175	0.000	0.021	0.003	8.651	4.694	0.207
06/11/2014	BOUS 85.002 i4	D	0.010	7.193	0.000	0.126	0.000	0.019	0.001	8.754	4.682	0.208
12/11/2014	BOUS 85.002 i4	D	0.012	7.243	0.003	0.181	0.000	0.021	0.002	8.769	4.659	0.208
19/11/2014	BOUS 85.002 i4	D	0.016	6.954	0.005	0.172	0.000	0.019	0.000	8.548	4.508	0.201
27/11/2014	BOUS 85.002 i4	D	0.019	7.836	0.010	0.270	0.000	0.026	0.001	8.416	4.650	0.213
23/02/2015	BOUS 85.002 i4	D	0.011	7.100	0.013	0.196	0.000	0.026	0.001	8.188	4.690	0.212
02/03/2015	BOUS 85.002 i4	D	0.012	6.884	0.013	0.329	0.000	0.027	0.001	7.787	4.637	0.209
09/03/2015	BOUS 85.002 i4	D	0.024	6.923	0.010	0.147	0.000	0.025	0.002	7.819	4.685	0.209
16/03/2015	BOUS 85.002 i4	D	0.000	6.731	0.000	0.145	0.000	0.020	0.001	7.918	4.371	0.198
23/03/2015	BOUS 85.002 i4	D	0.013	6.526	0.034	0.172	0.000	0.028	0.002	7.968	4.457	0.197
25/08/2015	BOUS 85.002 i4	D	0.015	6.901	0.036	0.178	0.000	0.017	0.002	7.690	4.395	0.196
01/02/2016	BOUS 85.002 i4	D	0.030	7.456	0.018	0.236	0.014	0.027	0.001	8.790	4.402	0.232
02/02/2016	BOUS 85.002 i4	D	0.030	7.819	0.009	0.161	0.012	0.029	0.001	8.915	4.611	0.241
03/02/2016	BOUS 85.002 i4	D	0.044	7.912	0.009	0.099	0.012	0.031	0.002	8.822	4.553	0.241
04/02/2016	BOUS 85.002 i4	D	0.032	7.707	0.012	0.130	0.012	0.030	0.002	8.606	4.427	0.236
05/02/2016	BOUS 85.002 i4	D	0.024	7.510	0.007	0.312	0.013	0.025	0.001	8.938	4.526	0.234
08/02/2016	BOUS 85.002 i4	D	0.022	7.297	0.003	0.134	0.010	0.026	0.001	8.709	4.383	0.228
11/02/2016	BOUS 85.002 i4	D	0.025	7.303	0.018	0.133	0.010	0.030	0.002	8.775	4.458	0.229
17/02/2016	BOUS 85.002 i4	D	0.027	7.393	0.021	0.146	0.010	0.030	0.002	8.799	4.438	0.230
22/02/2016	BOUS 85.002 i4	D	0.018	7.402	0.001	0.032	0.006	0.022	0.001	8.933	4.473	0.229
29/02/2016	BOUS 85.002 i4	D	0.015	7.790	0.001	0.162	0.008	0.021	0.001	8.834	4.413	0.237
09/03/2016	BOUS 85.002 i4	D	0.021	8.068	0.001	0.140	0.006	0.024	0.001	8.820	4.428	0.240
14/03/2016	BOUS 85.002 i4	D	0.018	7.567	0.001	0.187	0.014	0.024	0.001	8.877	4.469	0.234

21/03/2016	BOUS 85.002 i4	D	0.022	7.763	0.001	0.239	0.010	0.028	0.002	9.064	4.585	0.238
29/03/2016	BOUS 85.002 i4	D	0.014	7.377	0.001	0.129	0.009	0.021	0.001	8.812	4.420	0.232
06/04/2016	BOUS 85.002 i4	D	0.014	7.385	0.001	0.093	0.006	0.021	0.001	8.780	4.402	0.232
23/10/2014	BOUS 85.002 i5	C	0.003	7.258	0.003	0.241	0.000	0.015	0.000	8.058	4.571	0.174
31/10/2014	BOUS 85.002 i5	C	0.007	7.345	0.005	0.436	0.000	0.017	0.004	8.286	4.621	0.175
06/11/2014	BOUS 85.002 i5	C	0.004	7.209	0.002	0.267	0.000	0.015	0.003	8.181	4.659	0.175
12/11/2014	BOUS 85.002 i5	C	0.007	7.196	0.002	0.235	0.000	0.014	0.001	8.106	4.619	0.174
19/11/2014	BOUS 85.002 i5	C	0.008	7.155	0.006	0.273	0.000	0.015	0.000	8.219	4.597	0.173
27/11/2014	BOUS 85.002 i5	C	0.009	7.739	0.005	0.282	0.000	0.018	0.001	7.770	4.585	0.177
23/02/2015	BOUS 85.002 i5	C	0.000	7.292	0.011	0.277	0.000	0.020	0.002	7.845	4.645	0.179
02/03/2015	BOUS 85.002 i5	C	0.000	7.007	0.003	0.257	0.000	0.019	0.001	7.356	4.703	0.179
09/03/2015	BOUS 85.002 i5	C	0.000	7.174	0.008	0.433	0.000	0.020	0.001	7.445	4.792	0.179
16/03/2015	BOUS 85.002 i5	C	0.000	8.229	0.052	0.406	0.000	0.028	0.004	10.190	4.996	0.209
23/03/2015	BOUS 85.002 i5	C	0.000	6.463	0.023	0.245	0.000	0.019	0.001	7.317	4.402	0.164
25/08/2015	BOUS 85.002 i5	C	0.013	7.079	0.040	0.289	0.000	0.016	0.002	7.416	4.452	0.166
01/02/2016	BOUS 85.002 i5	C	0.022	7.544	0.017	0.289	0.010	0.022	0.001	8.400	4.511	0.201
02/02/2016	BOUS 85.002 i5	C	0.019	7.758	0.013	0.223	0.009	0.023	0.003	8.252	4.514	0.200
03/02/2016	BOUS 85.002 i5	C	0.021	8.090	0.007	0.200	0.011	0.024	0.002	8.324	4.598	0.206
04/02/2016	BOUS 85.002 i5	C	0.034	7.905	0.018	0.204	0.009	0.030	0.002	8.112	4.512	0.201
05/02/2016	BOUS 85.002 i5	C	0.019	7.453	0.012	0.301	0.011	0.022	0.001	8.196	4.538	0.197
08/02/2016	BOUS 85.002 i5	C	0.018	7.397	0.001	0.243	0.010	0.021	0.001	8.244	4.504	0.195
11/02/2016	BOUS 85.002 i5	C	0.020	7.418	0.017	0.211	0.008	0.025	0.001	8.307	4.573	0.197
17/02/2016	BOUS 85.002 i5	C	0.027	7.461	0.020	0.174	0.010	0.026	0.002	8.172	4.417	0.195
22/02/2016	BOUS 85.002 i5	C	0.011	7.381	0.001	0.143	0.010	0.017	0.001	8.383	4.494	0.194

29/02/2016	BOUS 85.002 i5	C	0.012	7.937	0.001	0.246	0.009	0.017	0.002	8.275	4.457	0.202
09/03/2016	BOUS 85.002 i5	C	0.013	7.967	0.001	0.215	0.006	0.018	0.001	8.167	4.422	0.201
14/03/2016	BOUS 85.002 i5	C	0.020	7.844	0.001	0.233	0.015	0.021	0.001	8.537	4.690	0.204
21/03/2016	BOUS 85.002 i5	C	0.009	7.652	0.001	0.210	0.009	0.017	0.001	8.450	4.676	0.203
29/03/2016	BOUS 85.002 i5	C	0.007	7.490	0.001	0.292	0.008	0.019	0.001	8.252	4.504	0.197
06/04/2016	BOUS 85.002 i5	C	0.015	7.588	0.001	0.242	0.012	0.017	0.001	8.430	4.664	0.204
23/10/2014	BOUS 85.002 i6	B	0.012	6.991	0.000	0.112	0.000	0.010	0.000	9.336	4.582	0.154
31/10/2014	BOUS 85.002 i6	B	0.013	6.936	0.000	0.117	0.000	0.010	0.000	9.397	4.562	0.154
06/11/2014	BOUS 85.002 i6	B	0.015	6.878	0.000	0.132	0.000	0.010	0.000	9.442	4.562	0.154
12/11/2014	BOUS 85.002 i6	B	0.015	6.865	0.067	0.150	0.000	0.010	0.001	9.393	4.520	0.152
19/11/2014	BOUS 85.002 i6	B	0.018	6.857	0.002	0.215	0.000	0.011	0.000	9.560	4.548	0.152
27/11/2014	BOUS 85.002 i6	B	0.016	7.189	0.002	0.240	0.000	0.012	0.000	8.942	4.420	0.152
23/02/2015	BOUS 85.002 i6	B	0.010	6.729	0.002	0.000	0.000	0.014	0.001	9.332	4.739	0.157
02/03/2015	BOUS 85.002 i6	B	0.012	6.860	0.029	6.045	0.000	0.019	0.002	9.400	4.808	0.157
09/03/2015	BOUS 85.002 i6	B	0.012	6.686	0.012	0.438	0.000	0.016	0.001	9.023	4.772	0.153
16/03/2015	BOUS 85.002 i6	B	0.036	6.337	0.058	0.369	0.000	0.032	0.002	8.695	4.828	0.153
23/03/2015	BOUS 85.002 i6	B	0.010	6.214	0.025	0.260	0.000	0.014	0.001	9.165	4.611	0.146
25/08/2015	BOUS 85.002 i6	B	0.045	6.414	0.038	0.242	0.000	0.024	0.002	9.173	4.637	0.140
01/02/2016	BOUS 85.002 i6	B	0.045	6.873	0.063	0.201	0.017	0.020	0.001	10.352	4.628	0.169
02/02/2016	BOUS 85.002 i6	B	0.032	7.082	0.006	0.123	0.015	0.017	0.001	10.240	4.693	0.172
03/02/2016	BOUS 85.002 i6	B	0.033	7.358	0.008	0.113	0.015	0.019	0.001	10.400	4.757	0.176
04/02/2016	BOUS 85.002 i6	B	0.076	7.128	0.204	0.142	0.013	0.040	0.002	9.924	4.676	0.168
05/02/2016	BOUS 85.002 i6	B	0.032	6.574	0.012	0.254	0.021	0.018	0.000	10.010	4.582	0.162
08/02/2016	BOUS 85.002 i6	B	0.024	6.702	0.001	0.146	0.013	0.015	0.000	10.170	4.616	0.165

11/02/2016	BOUS 85.002 i6	B	0.031	6.590	0.013	0.154	0.016	0.018	0.000	10.210	4.636	0.164
17/02/2016	BOUS 85.002 i6	B	0.033	6.847	0.017	0.137	0.015	0.020	0.001	10.410	4.679	0.167
22/02/2016	BOUS 85.002 i6	B	0.018	6.778	0.001	0.102	0.014	0.011	0.000	10.610	4.739	0.167
29/02/2016	BOUS 85.002 i6	B	0.023	7.126	0.001	0.181	0.012	0.013	0.000	10.240	4.594	0.170
09/03/2016	BOUS 85.002 i6	B	0.036	7.419	0.001	0.224	0.019	0.018	0.001	10.040	4.538	0.169
14/03/2016	BOUS 85.002 i6	B	0.022	6.862	0.001	0.157	0.019	0.015	0.000	10.400	4.760	0.171
21/03/2016	BOUS 85.002 i6	B	0.019	6.804	0.001	0.111	0.013	0.012	0.000	10.310	4.629	0.167
29/03/2016	BOUS 85.002 i6	B	0.018	7.056	0.001	0.123	0.013	0.015	0.000	10.380	4.702	0.170
06/04/2016	BOUS 85.002 i6	B	0.007	6.732	0.001	0.142	0.015	0.011	0.000	10.340	4.669	0.168
31/10/2014	BOUS85.003	H	0.021	8.030	0.003	0.300	0.000	0.022	0.000	9.170	4.570	0.150
06/11/2014	BOUS85.003	H	0.022	7.486	0.002	0.252	0.000	0.020	0.000	8.668	4.507	0.132
12/11/2014	BOUS85.003	H	0.020	7.471	0.003	0.281	0.000	0.020	0.000	8.331	4.472	0.130
19/11/2014	BOUS85.003	H	0.019	7.380	0.000	0.224	0.000	0.025	0.001	7.947	4.282	0.126
23/02/2015	BOUS85.003	H	0.008	7.593	0.000	0.228	0.000	0.024	0.000	8.560	4.566	0.138
02/03/2015	BOUS85.003	H	0.011	7.251	0.005	0.244	0.000	0.027	0.001	7.685	4.487	0.131
09/03/2015	BOUS85.003	H	0.011	7.152	0.003	0.220	0.000	0.025	0.001	7.598	4.537	0.133
16/03/2015	BOUS85.003	H	0.000	7.215	0.005	0.229	0.000	0.024	0.001	7.881	4.360	0.127
23/03/2015	BOUS85.003	H	0.012	7.497	0.015	0.222	0.000	0.023	0.001	7.689	4.365	0.129
25/08/2015	BOUS85.003	H	0.021	7.869	0.034	0.142	0.000	0.022	0.001	6.766	4.160	0.108
01/02/2016	BOUS85.003	H	0.039	8.511	0.014	0.281	0.020	0.031	0.001	9.104	4.461	0.153
02/02/2016	BOUS85.003	H	0.037	8.811	0.008	0.192	0.016	0.034	0.001	8.941	4.463	0.153
03/02/2016	BOUS85.003	H	0.038	8.761	0.006	0.188	0.018	0.033	0.001	8.922	4.434	0.152
04/02/2016	BOUS85.003	H	0.048	8.450	0.026	0.178	0.018	0.038	0.001	8.654	4.352	0.146
05/02/2016	BOUS85.003	H	0.026	7.975	0.001	0.279	0.020	0.027	0.000	8.821	4.372	0.143

08/02/2016	BOUS85.003	H	0.032	7.937	0.014	0.231	0.018	0.030	0.001	8.777	4.305	0.141
11/02/2016	BOUS85.003	H	0.033	7.825	0.011	0.209	0.016	0.030	0.001	8.826	4.440	0.145
17/02/2016	BOUS85.003	H	0.036	8.196	0.020	0.178	0.017	0.032	0.001	9.068	4.424	0.147
22/02/2016	BOUS85.003	H	0.029	8.169	0.001	0.350	0.022	0.026	0.001	8.801	4.279	0.148
29/02/2016	BOUS85.003	H	0.025	8.861	0.001	0.221	0.017	0.025	0.000	8.990	4.353	0.155
09/03/2016	BOUS85.003	H	0.027	8.878	0.001	0.227	0.018	0.023	0.000	8.751	4.290	0.156
14/03/2016	BOUS85.003	H	0.026	8.381	0.001	0.220	0.020	0.027	0.001	9.102	4.509	0.155
21/03/2016	BOUS85.003	H	0.028	8.620	0.001	0.191	0.016	0.027	0.001	9.256	4.582	0.160
29/03/2016	BOUS85.003	H	0.021	8.269	0.001	0.190	0.016	0.024	0.000	8.949	4.400	0.156
06/04/2016	BOUS85.003	H	0.022	8.442	0.001	0.215	0.015	0.025	0.000	8.941	4.389	0.157
23/10/2014	BOVE88.003 i2	M	0.016	5.429	0.000	0.458	0.000	0.016	0.000	10.600	4.798	0.166
31/10/2014	BOVE88.003 i2	M	0.021	5.182	0.000	0.454	0.000	0.016	0.000	10.720	4.865	0.156
06/11/2014	BOVE88.003 i2	M	0.022	5.252	0.003	0.505	0.000	0.018	0.001	10.630	4.593	0.153
12/11/2014	BOVE88.003 i2	M	0.028	5.219	0.006	0.563	0.000	0.019	0.000	10.650	4.767	0.157
19/11/2014	BOVE88.003 i2	M	0.015	5.407	0.000	0.584	0.000	0.021	0.000	10.410	4.772	0.156
27/11/2014	BOVE88.003 i2	M	0.021	5.667	0.002	0.539	0.000	0.020	0.000	10.130	4.840	0.156
23/02/2015	BOVE88.003 i2	M	0.010	5.351	0.000	0.478	0.000	0.021	0.000	10.100	4.894	0.166
02/03/2015	BOVE88.003 i2	M	0.012	4.882	0.001	0.500	0.000	0.021	0.000	9.641	4.974	0.149
09/03/2015	BOVE88.003 i2	M	0.014	4.909	0.002	0.433	0.000	0.022	0.000	9.665	4.921	0.154
16/03/2015	BOVE88.003 i2	M	0.009	4.701	0.002	0.610	0.000	0.019	0.000	9.888	4.603	0.142
23/03/2015	BOVE88.003 i2	M	0.012	5.180	0.014	0.448	0.000	0.020	0.001	9.723	4.671	0.152
25/08/2015	BOVE88.003 i2	M	0.000	5.789	0.035	0.438	0.000	0.017	0.001	9.621	4.326	0.182
01/02/2016	BOVE88.003 i2	M	0.029	5.257	0.011	0.488	0.036	0.021	0.000	10.856	4.585	0.176
02/02/2016	BOVE88.003 i2	M	0.042	5.550	0.010	0.445	0.034	0.027	0.001	10.960	4.793	0.174

03/02/2016	BOVE88.003 i2	M	0.039	5.347	0.016	0.426	0.032	0.026	0.001	10.510	4.554	0.165
04/02/2016	BOVE88.003 i2	M	0.033	5.417	0.001	0.421	0.032	0.025	0.001	10.710	4.680	0.169
05/02/2016	BOVE88.003 i2	M	0.035	5.214	0.011	0.482	0.038	0.024	0.000	10.880	4.730	0.166
08/02/2016	BOVE88.003 i2	M	0.034	5.068	0.008	0.467	0.036	0.024	0.000	10.570	4.571	0.164
11/02/2016	BOVE88.003 i2	M	0.036	5.071	0.017	0.453	0.033	0.026	0.001	10.550	4.567	0.162
17/02/2016	BOVE88.003 i2	M	0.035	5.226	0.013	0.374	0.034	0.029	0.001	10.770	4.521	0.165
22/02/2016	BOVE88.003 i2	M	0.023	5.369	0.001	0.498	0.035	0.019	0.000	10.720	4.481	0.170
29/02/2016	BOVE88.003 i2	M	0.024	5.653	0.001	0.465	0.034	0.020	0.000	10.620	4.446	0.175
09/03/2016	BOVE88.003 i2	M	0.023	5.896	0.001	0.468	0.030	0.021	0.000	10.700	4.432	0.181
14/03/2016	BOVE88.003 i2	M	0.034	5.368	0.001	0.415	0.032	0.023	0.000	10.920	4.715	0.171
21/03/2016	BOVE88.003 i2	M	0.024	5.285	0.001	0.403	0.032	0.018	0.000	10.780	4.673	0.171
29/03/2016	BOVE88.003 i2	M	0.024	5.377	0.001	0.412	0.029	0.019	0.000	10.800	4.536	0.173
06/04/2016	BOVE88.003 i2	M	0.020	5.307	0.001	0.407	0.029	0.018	0.000	10.720	4.536	0.172
23/10/2014	BOVE88.003 i3	L	0.023	6.594	0.006	0.381	0.000	0.043	0.002	10.600	2.981	0.180
31/10/2014	BOVE88.003 i3	L	0.018	6.351	0.005	0.438	0.000	0.035	0.004	10.610	3.012	0.172
06/11/2014	BOVE88.003 i3	L	0.020	6.238	0.018	0.357	0.000	0.035	0.006	10.540	3.007	0.166
12/11/2014	BOVE88.003 i3	L	0.025	6.148	0.013	0.625	0.000	0.037	0.005	10.730	3.088	0.165
19/11/2014	BOVE88.003 i3	L	0.023	6.493	0.015	0.905	0.000	0.056	0.008	10.870	3.198	0.169
27/11/2014	BOVE88.003 i3	L	0.014	6.561	0.015	0.463	0.000	0.043	0.008	10.150	3.241	0.163
23/02/2015	BOVE88.003 i3	L	0.013	5.890	0.048	0.339	0.000	0.044	0.007	10.190	3.506	0.159
02/03/2015	BOVE88.003 i3	L	0.040	6.012	0.059	0.367	0.000	0.046	0.004	9.791	3.029	0.159
09/03/2015	BOVE88.003 i3	L	0.032	5.802	0.076	0.319	0.000	0.042	0.002	9.815	3.262	0.162
16/03/2015	BOVE88.003 i3	L	0.026	5.531	0.082	0.576	0.000	0.043	0.003	10.130	3.199	0.146
23/03/2015	BOVE88.003 i3	L	0.019	5.545	0.081	0.326	0.000	0.034	0.002	9.791	3.188	0.146

25/08/2015	BOVE88.003 i3	L	0.000	5.286	0.035	0.235	0.000	0.025	0.003	9.733	3.063	0.141
01/02/2016	BOVE88.003 i3	L	0.048	6.057	0.026	0.511	0.045	0.038	0.003	11.440	3.056	0.169
02/02/2016	BOVE88.003 i3	L	0.048	6.607	0.017	0.312	0.035	0.042	0.003	11.410	3.219	0.179
03/02/2016	BOVE88.003 i3	L	0.062	6.642	0.025	0.298	0.032	0.049	0.004	11.100	3.132	0.176
04/02/2016	BOVE88.003 i3	L	0.047	6.700	0.013	0.315	0.031	0.044	0.004	11.230	3.157	0.178
05/02/2016	BOVE88.003 i3	L	0.047	6.444	0.038	0.393	0.036	0.042	0.004	11.420	3.207	0.176
08/02/2016	BOVE88.003 i3	L	0.042	6.369	0.024	0.395	0.036	0.041	0.004	11.190	3.084	0.175
11/02/2016	BOVE88.003 i3	L	0.046	6.463	0.043	0.368	0.034	0.045	0.004	11.180	3.197	0.181
17/02/2016	BOVE88.003 i3	L	0.052	7.096	0.098	0.360	0.036	0.056	0.005	11.910	3.240	0.189
22/02/2016	BOVE88.003 i3	L	0.033	7.210	0.092	0.434	0.036	0.042	0.004	11.360	2.998	0.193
29/02/2016	BOVE88.003 i3	L	0.031	7.122	0.109	0.386	0.033	0.039	0.004	10.970	2.975	0.185
09/03/2016	BOVE88.003 i3	L	0.058	7.552	0.079	0.463	0.038	0.050	0.004	11.300	3.202	0.190
14/03/2016	BOVE88.003 i3	L	0.012	6.776	0.042	0.357	0.035	0.039	0.003	11.610	3.342	0.187
21/03/2016	BOVE88.003 i3	L	0.033	6.972	0.226	0.339	0.031	0.040	0.005	11.430	3.263	0.185
29/03/2016	BOVE88.003 i3	L	0.030	7.007	0.370	0.348	0.032	0.044	0.006	11.380	3.224	0.187
06/04/2016	BOVE88.003 i3	L	0.027	6.832	0.474	0.329	0.032	0.041	0.006	11.260	3.176	0.185

Date	Borehole	Code	EC uS/cm	pH	Eh mV	F mg/l	Cl mg/l	SO4 mg/l	CO3 mg/l	HCO3 mg/l
23/10/2014	BOHP98.007 i2	K	90.000	9.660	207.600	3.960	1.633	4.452	3.300	13.000
03/11/2014	BOHP98.007 i2	K	92.900	9.630	244.500	3.646	1.651	4.001	0.000	19.000
06/11/2014	BOHP98.007 i2	K	91.700	8.510	214.100	4.111	1.660	5.035	0.000	19.000
12/11/2014	BOHP98.007 i2	K	83.600	8.830	209.500	3.351	29.777	3.783	0.000	19.000
19/11/2014	BOHP98.007 i2	K	84.200	9.640	221.800	4.025	1.543	4.823	0.000	19.000
27/11/2014	BOHP98.007 i2	K	81.800	9.280	226.900	4.223	1.960	4.941	0.000	18.000
23/02/2015	BOHP98.007 i2	K	67.600	9.380	487.100	4.054	1.814	5.024	0.000	21.296
02/03/2015	BOHP98.007 i2	K	85.500	9.580	486.100	4.091	1.805	4.742	0.000	17.037
09/03/2015	BOHP98.007 i2	K	87.900	9.700	399.100	3.941	1.770	4.202	0.000	17.963
16/03/2015	BOHP98.007 i2	K	87.900	9.720	399.100	4.726	1.988	4.394	0.000	18.200
23/03/2015	BOHP98.007 i2	K	81.800	9.720	376.100	3.661	1.891	4.830	0.000	18.400
25/08/2015	BOHP98.007 i2	K	80.700	9.590	221.900	3.451	1.640	4.624	0.000	17.800
01/02/2016	BOHP98.007 i2	K	74.000	9.660	119.200	4.663	1.979	5.029	0.000	19.000
02/02/2016	BOHP98.007 i2	K	76.200	9.460	97.400	4.595	1.906	5.052	0.000	19.200
03/02/2016	BOHP98.007 i2	K	76.000	9.420	96.500	4.781	1.903	5.067	0.000	19.200
04/02/2016	BOHP98.007 i2	K	75.400	9.360	105.000	4.753	1.899	5.083	4.000	14.400
05/02/2016	BOHP98.007 i2	K	76.600	9.400	118.400	4.790	1.877	5.098	4.800	11.800
08/02/2016	BOHP98.007 i2	K	1.400	8.160	160.200	4.696	1.825	4.962	6.400	10.400
11/02/2016	BOHP98.007 i2	K	76.200	9.410	81.300	4.173	1.385	5.318	1.200	18.200
17/02/2016	BOHP98.007 i2	K	76.000	9.250	94.200	4.584	1.812	5.287	0.800	18.600
22/02/2016	BOHP98.007 i2	K	76.000	9.440	87.300	4.514	1.800	5.282	0.400	12.800
29/02/2016	BOHP98.007 i2	K	74.400	9.410	87.800	4.534	1.803	5.310	0.800	18.000

09/03/2016	BOHP98.007 i2	K	74.400	9.390	111.200	4.763	1.818	4.954	0.000	19.600
14/03/2016	BOHP98.007 i2	K	74.500	8.930	169.000	4.729	1.820	4.948	0.000	19.000
21/03/2016	BOHP98.007 i2	K	74.300	9.480	56.500	4.713	1.815	4.969	2.800	15.600
29/03/2016	BOHP98.007 i2	K	74.000	9.440	2.300	4.707	1.824	4.967	4.000	13.400
06/04/2016	BOHP98.007 i2	K	75.700	9.340	8.400	4.727	1.824	4.971	0.000	19.600
23/10/2014	BOHP98.007 i3	J	90.900	9.590	196.800	4.034	1.759	4.381	0.000	19.000
03/11/2014	BOHP98.007 i3	J	93.000	8.500	269.100	3.751	1.881	3.778	0.000	19.000
06/11/2014	BOHP98.007 i3	J	92.000	8.780	216.900	4.207	1.744	5.526	0.000	19.000
12/11/2014	BOHP98.007 i3	J	84.400	9.680	218.500	3.659	1.908	3.511	0.000	19.000
19/11/2014	BOHP98.007 i3	J	84.200	9.450	219.300	4.245	2.035	5.677	0.000	18.000
27/11/2014	BOHP98.007 i3	J	82.000	8.820	220.500	4.284	1.739	5.079	0.000	20.000
23/02/2015	BOHP98.007 i3	J	64.200	9.630	442.100	3.280	0.525	1.458	0.000	12.407
02/03/2015	BOHP98.007 i3	J	85.900	9.700	458.100	4.200	2.371	5.441	0.000	17.407
09/03/2015	BOHP98.007 i3	J	90.500	9.730	387.100	4.031	3.608	3.516	0.000	17.593
16/03/2015	BOHP98.007 i3	J	90.500	9.730	387.100	4.015	2.059	4.516	0.000	18.600
23/03/2015	BOHP98.007 i3	J	91.300	9.610	373.100	2.453	0.478	1.448	0.000	19.000
25/08/2015	BOHP98.007 i3	J	81.000	9.660	198.800	3.425	1.594	4.654	0.000	18.800
23/10/2014	BOSB80.001	G	79.600	9.280	274.900	3.763	0.215	5.177	0.000	21.000
31/10/2014	BOSB80.001	G	76.100	9.100	302.000	3.348	0.139	5.563	0.000	20.000
06/11/2014	BOSB80.001	G	82.900	8.700	253.300	3.070	0.191	4.973	0.000	20.000
12/11/2014	BOSB80.001	G	65.700	9.360	319.500	3.323	0.211	6.172	0.000	19.000
19/11/2014	BOSB80.001	G	71.600	8.920	290.400	3.457	0.831	5.590	0.000	19.000
27/11/2014	BOSB80.001	G	76.100	8.950	266.900	3.270	0.334	5.748	0.000	19.000
23/02/2015	BOSB80.001	G	58.300	9.150	477.100	3.362	0.217	6.945	0.000	16.667

02/03/2015	BOSB80.001	G	72.500	9.360	497.100	3.176	0.158	6.448	0.000	17.037
09/03/2015	BOSB80.001	G	70.000	9.300	414.100	3.415	0.227	6.985	0.000	17.778
16/03/2015	BOSB80.001	G	70.000	9.300	414.100	3.091	0.084	6.047	0.000	18.800
23/03/2015	BOSB80.001	G	86.800	9.310	387.100	1.091	0.111	3.320	0.000	19.600
25/08/2015	BOSB80.001	G	77.600	9.150	304.400	2.935	0.141	6.266	0.000	18.200
01/02/2016	BOSB80.001	G	68.200	8.990	79.300	3.699	0.193	6.890	0.000	19.600
02/02/2016	BOSB80.001	G	69.700	8.750	292.300	4.835	0.759	7.175	0.000	19.600
03/02/2016	BOSB80.001	G	69.300	8.830	134.900	3.806	0.182	6.894	0.000	0.000
04/02/2016	BOSB80.001	G	68.500	8.980	148.600	3.756	0.195	6.896	0.000	20.000
05/02/2016	BOSB80.001	G	69.000	9.060	126.300	3.771	0.179	6.869	0.000	20.200
08/02/2016	BOSB80.001	G	67.400	8.830	156.000	3.788	0.185	6.867	0.000	19.800
11/02/2016	BOSB80.001	G	69.700	8.990	116.100	3.772	0.174	6.924	0.000	19.000
17/02/2016	BOSB80.001	G	69.500	8.880	166.600	3.714	0.174	6.851	0.000	19.200
22/02/2016	BOSB80.001	G	69.700	8.740	154.300	3.606	0.172	7.248	0.000	12.800
29/02/2016	BOSB80.001	G	67.900	8.740	143.600	3.627	0.169	7.275	0.000	20.000
09/03/2016	BOSB80.001	G	67.900	8.840	135.600	3.748	0.173	6.919	0.000	19.000
14/03/2016	BOSB80.001	G	68.200	8.850	182.100	3.816	0.175	6.975	0.000	19.800
21/03/2016	BOSB80.001	G	1.000	7.800	338.600	3.742	0.171	6.925	0.000	20.000
29/03/2016	BOSB80.001	G	68.200	8.880	92.600	3.757	0.171	6.948	0.000	19.400
06/04/2016	BOSB80.001	G	69.300	8.890	40.300	3.731	0.195	6.937	0.000	20.000
07/11/2014	BOSB80.003 i4	I	99.800		220.500	5.435	4.128	3.569	0.000	17.000
12/11/2014	BOSB80.003 i4	I	93.500	8.900	190.400	3.373	4.600	3.688	0.000	16.000
19/11/2014	BOSB80.003 i4	I	93.500	8.770	216.300	6.542	4.223	3.812	0.000	16.000
27/11/2014	BOSB80.003 i4	I	90.000	6.770	244.400	5.399	4.697	4.348	0.000	17.000

23/02/2015	BOSB80.003 i4	I	73.600	9.310	411.100	5.348	4.033	4.325	0.000	15.741
02/03/2015	BOSB80.003 i4	I	90.300	9.600	483.100	5.132	2.797	4.091	0.000	16.111
09/03/2015	BOSB80.003 i4	I	99.900	9.660	379.100	5.176	3.825	4.495	0.000	16.111
16/03/2015	BOSB80.003 i4	I	99.900	9.820	379.100	5.091	3.852	4.554	0.000	19.000
25/08/2015	BOSB80.003 i4	I	88.300	9.790	201.300	4.367	3.659	3.170	0.000	16.400
01/02/2016	BOSB80.003 i4	I	81.900	9.790	97.400	5.983	4.473	4.053	0.000	20.600
02/02/2016	BOSB80.003 i4	I	84.900	9.790	137.500	5.957	4.466	4.175	0.000	16.400
03/02/2016	BOSB80.003 i4	I	85.200	9.580	84.700	6.145	4.450	4.365	0.000	21.200
04/02/2016	BOSB80.003 i4	I	63.800	9.580	130.300	6.143	4.462	4.427	4.000	10.800
05/02/2016	BOSB80.003 i4	I	85.400	9.570	110.700	6.167	4.424	4.470	5.200	9.400
08/02/2016	BOSB80.003 i4	I	83.200	9.450	171.500	6.147	4.378	4.364	5.600	9.400
17/02/2016	BOSB80.003 i4	I	85.900	9.550	107.900	6.171	4.389	4.264	0.000	11.000
22/02/2016	BOSB80.003 i4	I	86.400	9.470	82.300	5.842	4.367	4.523	0.000	17.800
29/02/2016	BOSB80.003 i4	I	84.700	9.530	84.300	5.841	4.334	4.569	0.000	17.400
09/03/2016	BOSB80.003 i4	I	1.400	5.860	386.400	6.090	4.368	4.508	0.000	17.400
14/03/2016	BOSB80.003 i4	I	85.400	9.510	136.500	6.105	4.328	4.484	1.600	15.600
21/03/2016	BOSB80.003 i4	I	85.100	9.550	63.100	6.085	4.262	4.637	4.800	10.600
29/03/2016	BOSB80.003 i4	I	85.500	9.650	1.500	6.070	4.187	4.646	7.600	6.400
06/04/2016	BOSB80.003 i4	I	87.400	9.610	-12.800	6.087	4.170	4.715	5.200	10.600
23/10/2014	BOUS 85.002 i2	F	10.000	9.150	449.300	4.194	0.227	5.493	0.000	22.000
31/10/2014	BOUS 85.002 i2	F	90.400	9.380	189.900	4.260	0.257	5.005	0.000	21.000
06/11/2014	BOUS 85.002 i2	F	85.000	8.890	164.700	3.960	0.191	5.069	0.000	20.000
12/11/2014	BOUS 85.002 i2	F	81.600	8.950	195.600	4.509	0.173	5.979	0.000	20.000
19/11/2014	BOUS 85.002 i2	F	80.400	9.040	219.900	3.758	0.183	4.545	0.000	20.000

27/11/2014	BOUS 85.002 i2	F	81.600	8.930	183.600	3.750	0.413	5.667	0.000	21.000
23/02/2015	BOUS 85.002 i2	F	66.400	9.110	342.100	4.322	0.295	6.512	0.000	16.852
02/03/2015	BOUS 85.002 i2	F	82.100	9.360	466.100	4.149	0.396	6.357	0.000	18.889
09/03/2015	BOUS 85.002 i2	F	117.000	9.320	384.100	4.366	0.697	7.100	0.000	19.074
16/03/2015	BOUS 85.002 i2	F	117.000	9.320	384.100	3.850	0.332	5.951	0.000	22.800
23/03/2015	BOUS 85.002 i2	F	81.000	9.350	335.100	3.904	0.481	6.464	0.000	20.800
25/08/2015	BOUS 85.002 i2	F	82.400	9.320	11.300	3.522	0.232	5.617	0.000	19.400
01/02/2016	BOUS 85.002 i2	F	72.400	9.030	251.000	4.961	0.287	6.162	0.000	19.800
02/02/2016	BOUS 85.002 i2	F	74.600	9.030	22.800	4.832	0.332	6.332	0.000	19.400
03/02/2016	BOUS 85.002 i2	F	74.400	9.110	136.800	4.998	0.285	6.117	0.000	20.200
04/02/2016	BOUS 85.002 i2	F	73.600	9.170	161.300	4.934	0.285	6.231	0.000	19.800
05/02/2016	BOUS 85.002 i2	F	74.200	9.160	165.300	4.947	0.280	6.153	0.000	20.400
08/02/2016	BOUS 85.002 i2	F	72.600	9.150	151.400	4.916	0.279	6.199	0.000	20.800
11/02/2016	BOUS 85.002 i2	F	74.800	9.150	118.700	4.884	0.273	6.233	0.000	20.200
17/02/2016	BOUS 85.002 i2	F	74.300	8.900	119.300	4.933	0.271	6.276	0.000	20.800
22/02/2016	BOUS 85.002 i2	F	74.300	9.000	74.700	4.856	0.272	6.182	0.000	13.400
29/02/2016	BOUS 85.002 i2	F	72.700	8.860	121.600	4.632	0.263	6.382	0.000	20.200
09/03/2016	BOUS 85.002 i2	F	72.800	9.170	97.400	4.663	0.272	6.740	0.000	19.800
14/03/2016	BOUS 85.002 i2	F	72.800	9.120	105.400	4.819	0.272	6.410	0.000	20.000
21/03/2016	BOUS 85.002 i2	F	72.600	8.980	50.800	4.814	0.270	6.402	0.000	19.800
29/03/2016	BOUS 85.002 i2	F	72.600	9.010	19.800	4.782	0.278	6.413	0.000	21.600
06/04/2016	BOUS 85.002 i2	F	74.200	9.030	5.300	4.763	0.276	6.535	0.000	20.400
23/10/2014	BOUS 85.002 i3	E	89.600	9.150	169.200	3.874	0.195	5.899	0.000	22.000
31/10/2014	BOUS 85.002 i3	E	91.000	8.860	197.100	3.988	0.241	5.924	0.000	21.000

06/11/2014	BOUS 85.002 i3	E	88.300	8.940	186.400	3.411	0.198	5.066	0.000	21.000
12/11/2014	BOUS 85.002 i3	E	82.900	8.910	202.300	4.176	0.193	6.123	0.000	21.000
19/11/2014	BOUS 85.002 i3	E	83.000	8.960	202.400	3.940	0.394	3.396	0.000	21.000
27/11/2014	BOUS 85.002 i3	E	83.300	8.890	200.100	3.659	0.372	5.913	0.000	20.000
23/02/2015	BOUS 85.002 i3	E	65.000	9.040	342.100	3.989	0.498	6.459	0.000	19.815
02/03/2015	BOUS 85.002 i3	E	91.000	9.270	473.100	3.965	0.771	6.316	0.000	18.519
09/03/2015	BOUS 85.002 i3	E	85.500	9.180	405.100	2.901	0.307	5.973	0.000	19.259
16/03/2015	BOUS 85.002 i3	E	85.500	9.180	405.100	3.709	0.284	6.246	0.000	21.000
23/03/2015	BOUS 85.002 i3	E	112.100	9.220	342.100	3.750	0.209	5.921	0.000	20.800
25/08/2015	BOUS 85.002 i3	E	83.000	9.030	-35.900	3.272	0.134	5.801	0.000	20.800
01/02/2016	BOUS 85.002 i3	E	72.900	8.220	226.600	4.396	0.249	6.558	0.000	20.600
02/02/2016	BOUS 85.002 i3	E	73.600	8.320	81.600	4.375	0.242	6.637	0.000	21.000
03/02/2016	BOUS 85.002 i3	E	74.700	9.060	167.600	4.469	0.240	6.659	0.000	21.600
04/02/2016	BOUS 85.002 i3	E	73.900	9.020	173.300	4.464	0.241	6.639	0.000	20.200
05/02/2016	BOUS 85.002 i3	E	74.500	9.050	198.900	4.470	0.248	6.678	0.000	21.600
08/02/2016	BOUS 85.002 i3	E	72.500	8.940	160.600	4.437	0.235	6.548	0.000	21.800
11/02/2016	BOUS 85.002 i3	E	74.600	8.870	106.500	4.402	0.240	6.528	0.000	21.000
17/02/2016	BOUS 85.002 i3	E	74.200	8.300	130.300	4.519	0.229	6.451	0.000	21.600
22/02/2016	BOUS 85.002 i3	E	74.400	8.770	82.900	4.359	0.228	6.449	0.000	13.800
29/02/2016	BOUS 85.002 i3	E	73.000	7.930	101.000	4.206	0.236	6.816	0.000	21.000
09/03/2016	BOUS 85.002 i3	E	72.700	8.470	101.900	4.174	0.228	6.653	0.000	22.000
14/03/2016	BOUS 85.002 i3	E	72.900	8.700	136.500	4.366	0.230	6.567	0.000	20.600
21/03/2016	BOUS 85.002 i3	E	73.000	8.860	38.100	4.344	0.229	6.450	0.000	21.200
29/03/2016	BOUS 85.002 i3	E	72.500	8.790	-5.200	4.330	0.228	6.517	0.000	21.800

06/04/2016	BOUS 85.002 i3	E	74.000	8.700	12.400	4.348	0.261	6.592	0.000	22.800
23/10/2014	BOUS 85.002 i4	D	86.000	9.200	135.000	3.767	0.213	5.628	0.000	21.000
31/10/2014	BOUS 85.002 i4	D	89.500	8.950	146.400	4.006	0.304	5.948	0.000	20.000
06/11/2014	BOUS 85.002 i4	D	87.600	8.970	170.900	3.400	0.206	4.885	0.000	19.000
12/11/2014	BOUS 85.002 i4	D	81.300	8.980	202.400	4.524	0.344	6.391	0.000	19.000
19/11/2014	BOUS 85.002 i4	D	81.900	8.960	186.500	3.407	0.290	4.906	0.000	20.000
27/11/2014	BOUS 85.002 i4	D	83.100	8.940	188.600	3.858	0.412	6.716	0.000	19.000
23/02/2015	BOUS 85.002 i4	D	81.200	9.050	239.100	4.008	0.274	6.513	0.000	18.148
02/03/2015	BOUS 85.002 i4	D	250.000	9.140	435.100	3.730	0.298	6.513	0.000	17.407
09/03/2015	BOUS 85.002 i4	D	84.000	9.340	387.100	3.835	0.270	6.269	0.000	18.704
16/03/2015	BOUS 85.002 i4	D	84.000	9.340	387.100	3.718	0.246	5.946	0.000	20.000
23/03/2015	BOUS 85.002 i4	D	82.300	9.320	313.100	1.879	0.053	2.340	0.000	20.000
25/08/2015	BOUS 85.002 i4	D	82.100	9.220	122.200	3.275	0.172	5.554	0.000	20.000
01/02/2016	BOUS 85.002 i4	D	71.700	9.020	178.500	4.390	0.272	6.803	0.000	17.000
02/02/2016	BOUS 85.002 i4	D	73.700	9.140	54.700	4.356	0.269	6.877	0.000	20.000
03/02/2016	BOUS 85.002 i4	D	73.600	9.060	207.000	4.461	0.267	6.690	0.000	17.400
04/02/2016	BOUS 85.002 i4	D	72.700	9.110	199.900	4.514	0.270	6.863	0.000	19.800
05/02/2016	BOUS 85.002 i4	D	73.300	9.040	194.500	4.506	0.268	6.870	0.000	21.200
08/02/2016	BOUS 85.002 i4	D	71.400	9.030	184.600	4.436	0.260	6.823	0.000	21.400
11/02/2016	BOUS 85.002 i4	D	73.600	9.020	104.300	4.424	0.261	6.874	0.000	20.800
17/02/2016	BOUS 85.002 i4	D	73.400	8.970	148.400	4.382	0.257	6.445	0.000	21.000
22/02/2016	BOUS 85.002 i4	D	73.600	8.990	84.500	4.394	0.257	6.546	0.000	13.200
29/02/2016	BOUS 85.002 i4	D	71.400	8.670	122.200	4.237	0.251	6.147	0.000	20.000
09/03/2016	BOUS 85.002 i4	D	71.500	8.660	90.300	4.200	0.252	5.638	0.000	20.600

14/03/2016	BOUS 85.002 i4	D	71.800	8.960	133.300	4.379	0.255	6.761	0.000	20.000
21/03/2016	BOUS 85.002 i4	D	72.100	9.020	39.200	4.350	0.257	6.498	0.000	20.000
29/03/2016	BOUS 85.002 i4	D	71.500	8.950	-4.300	4.380	0.256	6.436	0.000	21.000
06/04/2016	BOUS 85.002 i4	D	73.200	8.870	0.600	4.419	0.251	6.367	0.000	20.600
23/10/2014	BOUS 85.002 i5	C	65.000	9.200	193.800	3.609	0.343	3.654	0.000	22.000
31/10/2014	BOUS 85.002 i5	C	87.100	9.170	218.800	3.512	0.224	5.792	0.000	19.000
06/11/2014	BOUS 85.002 i5	C	86.500	8.380	199.700	3.001	0.277	5.046	0.000	20.000
12/11/2014	BOUS 85.002 i5	C	79.300	8.950	235.900	3.643	0.357	6.584	0.000	19.000
19/11/2014	BOUS 85.002 i5	C	79.700	8.800	220.900	3.567	0.311	4.806	0.000	19.000
27/11/2014	BOUS 85.002 i5	C	82.300	8.930	213.100	3.606	0.209	6.535	0.000	19.000
23/02/2015	BOUS 85.002 i5	C	62.200	8.990	404.100	3.564	0.395	6.920	0.000	17.222
02/03/2015	BOUS 85.002 i5	C	160.200	9.290	498.100	3.420	0.271	6.843	0.000	18.148
09/03/2015	BOUS 85.002 i5	C	75.300	9.560	445.100	3.185	0.374	6.853	0.000	18.519
16/03/2015	BOUS 85.002 i5	C	75.300	9.560	445.100	3.127	0.185	5.695	0.000	19.400
23/03/2015	BOUS 85.002 i5	C	76.400	9.230	381.100	3.437	0.273	7.145	0.000	19.400
25/08/2015	BOUS 85.002 i5	C	80.000	9.250	126.500	3.014	0.102	6.010	0.000	19.600
01/02/2016	BOUS 85.002 i5	C	69.500	8.770	134.800	3.958	0.230	6.593	0.000	20.200
02/02/2016	BOUS 85.002 i5	C	71.100	8.900	61.600	3.910	0.231	6.641	0.000	19.800
03/02/2016	BOUS 85.002 i5	C	71.200	9.000	224.000	4.093	0.231	6.819	0.000	20.200
04/02/2016	BOUS 85.002 i5	C	70.600	9.060	230.900	4.042	0.244	6.882	0.000	20.000
05/02/2016	BOUS 85.002 i5	C	74.300	9.000	238.700	4.129	0.232	7.073	0.000	20.200
08/02/2016	BOUS 85.002 i5	C	69.200	8.870	215.700	4.035	0.223	7.011	0.000	21.200
11/02/2016	BOUS 85.002 i5	C	71.800	8.950	136.500	3.987	0.219	7.058	0.000	20.000
17/02/2016	BOUS 85.002 i5	C	71.400	8.840	177.800	3.991	0.219	7.076	0.000	20.200

22/02/2016	BOUS 85.002 i5	C	71.600	8.850	111.200	3.807	0.212	7.419	0.000	13.400
29/02/2016	BOUS 85.002 i5	C	70.300	8.930	121.100	3.810	0.215	7.513	0.000	19.200
09/03/2016	BOUS 85.002 i5	C	69.600	8.520	123.800	3.768	0.213	7.468	0.000	19.400
14/03/2016	BOUS 85.002 i5	C	69.900	8.740	146.700	3.995	0.220	7.323	0.000	19.800
21/03/2016	BOUS 85.002 i5	C	69.800	8.270	48.200	4.014	0.216	7.250	0.000	18.800
29/03/2016	BOUS 85.002 i5	C	69.600	8.790	58.300	3.990	0.225	7.241	0.000	20.400
06/04/2016	BOUS 85.002 i5	C	71.300	8.680	7.100	4.001	0.237	7.253	0.000	19.800
23/10/2014	BOUS 85.002 i6	B	86.100	9.200	193.800	4.436	0.304	6.955	0.000	21.000
31/10/2014	BOUS 85.002 i6	B	92.700	9.360	175.800	4.347	0.227	6.759	0.000	19.000
06/11/2014	BOUS 85.002 i6	B	92.400	9.050	172.400	3.636	0.255	5.723	0.000	20.000
12/11/2014	BOUS 85.002 i6	B	84.300	8.950	240.100	4.443	0.384	7.100	0.000	19.000
19/11/2014	BOUS 85.002 i6	B	84.900	9.120	184.100	4.113	0.535	5.653	0.000	19.000
27/11/2014	BOUS 85.002 i6	B	87.600	9.150	185.300	4.994	0.346	7.294	0.000	18.000
23/02/2015	BOUS 85.002 i6	B	68.500	9.200	300.100	4.572	0.386	7.563	0.000	17.222
02/03/2015	BOUS 85.002 i6	B	82.800	9.480	487.100	4.994	0.628	7.528	0.000	18.148
09/03/2015	BOUS 85.002 i6	B	137.700	9.450	448.100	3.616	0.101	3.821	0.000	18.148
16/03/2015	BOUS 85.002 i6	B	137.700	9.450	448.100	4.285	0.410	7.160	0.000	19.200
23/03/2015	BOUS 85.002 i6	B	98.100	9.410	356.100	4.819	0.531	7.831	0.000	19.200
25/08/2015	BOUS 85.002 i6	B	85.000	9.370	-20.500	3.817	0.219	6.611	0.000	20.000
01/02/2016	BOUS 85.002 i6	B	74.400	8.800	111.300	4.869	0.324	7.348	0.000	19.200
02/02/2016	BOUS 85.002 i6	B	76.900	9.160	55.000	4.955	0.320	7.412	0.000	19.600
03/02/2016	BOUS 85.002 i6	B	76.600	9.130	247.900	5.079	0.319	7.399	0.000	19.600
04/02/2016	BOUS 85.002 i6	B	75.700	9.120	247.300	5.043	0.318	7.357	0.000	19.600
05/02/2016	BOUS 85.002 i6	B	76.300	8.900	245.600	5.072	0.340	7.399	0.000	19.800

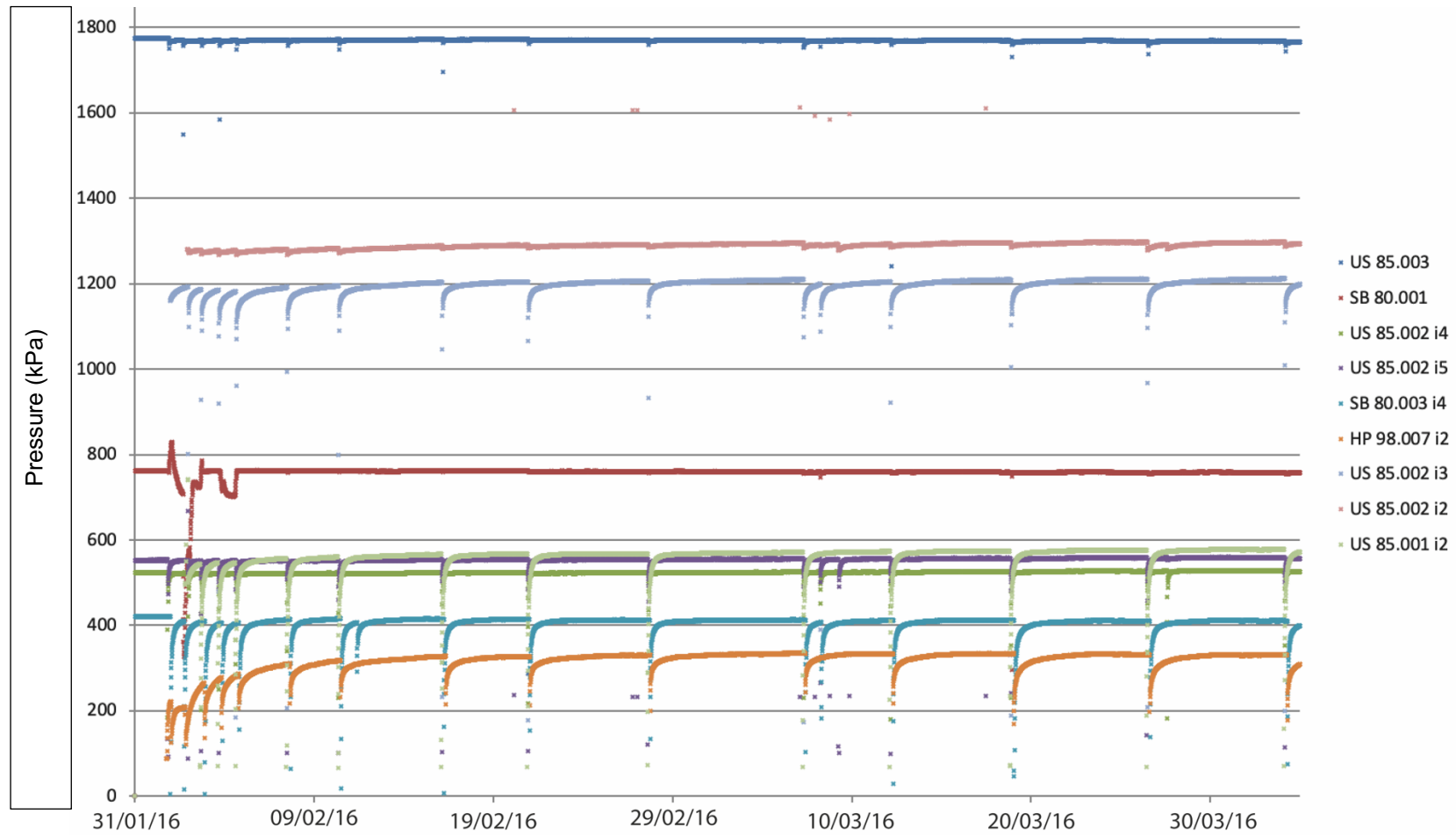
08/02/2016	BOUS 85.002 i6	B	74.200	8.900	218.500	5.042	0.315	7.329	0.000	20.000
11/02/2016	BOUS 85.002 i6	B	76.500	8.600	160.400	5.006	0.312	7.331	0.000	19.600
17/02/2016	BOUS 85.002 i6	B	76.500	8.640	224.900	5.001	0.321	7.364	0.000	19.600
22/02/2016	BOUS 85.002 i6	B	76.500	8.740	119.000	4.833	0.303	7.476	0.000	13.600
29/02/2016	BOUS 85.002 i6	B	74.600	8.690	105.800	4.851	0.325	7.515	0.000	19.600
09/03/2016	BOUS 85.002 i6	B	74.600	8.270	131.800	5.023	0.311	7.353	0.000	18.600
14/03/2016	BOUS 85.002 i6	B	74.700	8.630	157.000	5.002	0.310	7.365	0.000	18.800
21/03/2016	BOUS 85.002 i6	B	74.600	8.470	33.700	5.033	0.310	7.444	0.000	20.000
29/03/2016	BOUS 85.002 i6	B	74.700	8.650	48.400	4.958	0.335	7.403	0.000	19.600
06/04/2016	BOUS 85.002 i6	B	75.800	8.560	6.400	5.041	0.322	7.374	0.000	19.800
31/10/2014	BOUS85.003	H	94.300	9.310	351.900	3.710	0.800	5.690	0.000	20.000
06/11/2014	BOUS85.003	H	89.600	6.850	235.800	3.836	0.679	4.823	0.000	19.000
12/11/2014	BOUS85.003	H	80.300	9.270	247.700	3.843	0.787	5.890	0.000	18.000
19/11/2014	BOUS85.003	H	83.100	9.420	268.200	3.933	0.876	6.498	0.000	19.000
23/02/2015	BOUS85.003	H	68.600	9.180	487.100	3.434	0.207	2.041	0.000	16.481
02/03/2015	BOUS85.003	H	86.600	9.130	498.100	4.054	0.654	6.723	0.000	17.778
09/03/2015	BOUS85.003	H	86.100	9.250	445.100	3.244	0.050	1.302	0.000	17.037
16/03/2015	BOUS85.003	H	86.100	9.500	445.100	4.064	0.730	6.044	0.000	20.000
23/03/2015	BOUS85.003	H	183.500	9.500	387.100	3.674	0.701	6.510	0.000	18.800
25/08/2015	BOUS85.003	H	82.600	9.500	410.900	3.284	0.530	6.850	0.000	20.000
01/02/2016	BOUS85.003	H	77.900	9.390	56.900	4.861	0.773	7.276	0.000	20.200
02/02/2016	BOUS85.003	H	79.600	9.180	260.200	3.725	0.191	6.897	0.000	19.800
03/02/2016	BOUS85.003	H	78.500	9.350	86.900	4.937	0.747	7.094	0.000	20.200
04/02/2016	BOUS85.003	H	77.300	9.230	167.300	4.942	0.784	7.096	0.000	20.400

05/02/2016	BOUS85.003	H	77.400	9.370	130.400	4.860	0.745	7.030	1.200	17.600
08/02/2016	BOUS85.003	H	75.900	9.310	90.400	4.878	0.730	7.030	1.600	17.800
11/02/2016	BOUS85.003	H	78.100	9.350	140.100	4.961	0.729	7.013	0.000	20.200
17/02/2016	BOUS85.003	H	78.400	9.250	125.000	4.930	0.733	7.071	0.000	19.800
22/02/2016	BOUS85.003	H	79.000	9.270	80.100	4.733	0.733	7.516	0.000	13.000
29/02/2016	BOUS85.003	H	77.600	9.290	130.800	4.826	0.747	7.605	0.000	20.800
09/03/2016	BOUS85.003	H	78.200	9.270	125.800	5.064	0.756	7.390	0.000	20.000
14/03/2016	BOUS85.003	H	77.700	9.330	201.000	4.994	0.749	7.206	0.000	20.000
21/03/2016	BOUS85.003	H	77.800	9.320	133.700	4.946	0.741	7.263	0.000	20.000
29/03/2016	BOUS85.003	H	77.200	9.320	104.100	5.106	0.735	7.225	0.000	20.800
06/04/2016	BOUS85.003	H	78.900	9.310	56.500	4.959	0.717	7.325	0.000	20.600
23/10/2014	BOVE88.003 i2	M	88.800	9.580	190.300	3.795	1.216	4.934	0.000	21.000
31/10/2014	BOVE88.003 i2	M	90.500	9.600	208.600	3.323	1.200	4.279	0.000	20.000
06/11/2014	BOVE88.003 i2	M	89.000	8.980	202.900	5.795	1.689	0.978	0.000	19.000
12/11/2014	BOVE88.003 i2	M	81.600	8.980	208.700	4.584	2.761	0.917	0.000	19.000
19/11/2014	BOVE88.003 i2	M	81.400	9.540	225.100	4.010	1.756	4.912	0.000	19.000
27/11/2014	BOVE88.003 i2	M	79.400	9.320	214.300	3.797	2.019	5.208	0.000	19.000
23/02/2015	BOVE88.003 i2	M	67.300	9.460	461.100	3.809	1.417	5.750	0.000	17.593
02/03/2015	BOVE88.003 i2	M	91.000	9.530	473.100	3.623	1.447	5.194	0.000	18.889
09/03/2015	BOVE88.003 i2	M	67.800	9.530	387.100	3.495	1.251	5.603	0.000	18.148
16/03/2015	BOVE88.003 i2	M	67.800	9.450	387.100	3.562	1.448	4.930	0.000	20.800
23/03/2015	BOVE88.003 i2	M	82.400	9.450	333.100	3.243	1.317	5.321	0.000	19.200
25/08/2015	BOVE88.003 i2	M	81.400	9.570	208.500	3.182	1.242	5.608	0.000	20.400
01/02/2016	BOVE88.003 i2	M	71.400	9.240	90.100	4.099	1.469	5.383	0.000	19.200

02/02/2016	BOVE88.003 i2	M	72.800	9.260	198.600	4.131	1.457	5.351	0.000	19.200
03/02/2016	BOVE88.003 i2	M	72.200	9.320	87.100	4.256	1.448	5.342	0.000	19.400
04/02/2016	BOVE88.003 i2	M	71.500	9.330	105.100	4.190	1.450	5.342	2.800	15.400
05/02/2016	BOVE88.003 i2	M	72.000	9.330	192.500	4.287	1.424	5.415	2.400	15.400
08/02/2016	BOVE88.003 i2	M	71.200	9.320	113.700	4.217	1.384	5.307	2.800	15.600
11/02/2016	BOVE88.003 i2	M	72.700	9.340	79.900	5.816	1.659	3.448	0.000	20.400
17/02/2016	BOVE88.003 i2	M	73.000	9.310	110.200	4.217	1.390	5.389	0.000	20.400
22/02/2016	BOVE88.003 i2	M	73.200	9.300	79.400	4.016	1.374	5.684	0.000	13.600
29/02/2016	BOVE88.003 i2	M	72.000	9.380	99.500	4.059	1.388	5.814	0.000	19.600
09/03/2016	BOVE88.003 i2	M	71.800	9.400	109.500	4.246	1.411	5.611	0.000	18.800
14/03/2016	BOVE88.003 i2	M	71.900	9.390	133.800	4.231	1.372	5.329	0.000	18.600
21/03/2016	BOVE88.003 i2	M	72.700	9.350	41.000	4.217	1.394	5.318	0.800	17.600
29/03/2016	BOVE88.003 i2	M	71.400	9.410	-6.900	4.255	1.413	5.564	2.800	15.200
06/04/2016	BOVE88.003 i2	M	73.000	9.390	-8.500	4.231	1.405	5.490	0.000	20.000
23/10/2014	BOVE88.003 i3	L	93.100	9.280	153.700	5.440	1.553	5.072	0.000	24.000
31/10/2014	BOVE88.003 i3	L	94.100	9.190	172.900	4.449	1.463	0.679	0.000	22.000
06/11/2014	BOVE88.003 i3	L	92.900	8.020	185.700	4.973	1.733	0.962	0.000	21.000
12/11/2014	BOVE88.003 i3	L	84.200	9.000	163.100	4.831	2.981	0.990	0.000	21.000
19/11/2014	BOVE88.003 i3	L	83.800	9.030	166.200	4.956	2.015	1.435	0.000	21.000
27/11/2014	BOVE88.003 i3	L	81.400	8.730	180.100	5.259	1.977	1.354	0.000	19.000
23/02/2015	BOVE88.003 i3	L	69.000	9.570	305.100	3.834	0.535	0.559	0.000	18.889
02/03/2015	BOVE88.003 i3	L	80.200	8.800	498.100	4.862	1.459	2.034	0.000	19.259
09/03/2015	BOVE88.003 i3	L	83.300	9.410	321.100	5.316	1.733	3.581	0.000	19.074
16/03/2015	BOVE88.003 i3	L	83.300	9.230	321.100	6.692	2.500	2.714	0.000	20.400

23/03/2015	BOVE88.003 i3	L	86.900	9.230	301.100	1.523	1.312	2.231	0.000	19.200
25/08/2015	BOVE88.003 i3	L	82.200	9.230	197.400	4.288	1.584	2.083	0.000	19.000
01/02/2016	BOVE88.003 i3	L	76.100	9.140	103.100	5.887	1.881	2.453	0.000	21.400
02/02/2016	BOVE88.003 i3	L	78.100	9.120	232.200	5.838	1.851	2.599	0.000	20.200
03/02/2016	BOVE88.003 i3	L	78.500	9.210	143.900	6.000	1.823	2.707	0.000	20.200
04/02/2016	BOVE88.003 i3	L	77.700	9.230	161.900	5.912	1.822	2.915	0.000	21.400
05/02/2016	BOVE88.003 i3	L	78.600	9.180	181.800	5.797	1.736	3.374	0.000	22.000
08/02/2016	BOVE88.003 i3	L	78.000	9.230	163.300	5.793	1.709	3.271	0.000	22.400
11/02/2016	BOVE88.003 i3	L	81.100	9.210	137.100	6.094	4.393	4.463	0.000	21.600
17/02/2016	BOVE88.003 i3	L	82.200	9.200	131.500	5.806	1.620	3.846	0.000	14.400
22/02/2016	BOVE88.003 i3	L	83.000	9.230	102.300	5.588	1.597	4.275	0.000	15.200
29/02/2016	BOVE88.003 i3	L	80.200	9.130	100.100	5.565	1.556	4.172	0.000	21.800
09/03/2016	BOVE88.003 i3	L	79.600	9.220	119.200	5.707	1.522	3.641	0.000	21.600
14/03/2016	BOVE88.003 i3	L	79.500	9.260	145.000	5.957	1.557	3.446	0.000	0.000
21/03/2016	BOVE88.003 i3	L	79.000	9.200	46.100	5.765	1.568	3.331	0.000	22.200
29/03/2016	BOVE88.003 i3	L	78.400	9.230	-2.100	5.811	1.641	3.143	0.800	1.400
06/04/2016	BOVE88.003 i3	L	79.900	9.200	-1.900	5.811	1.673	2.991	0.000	22.000

Appendix IV Available pressure data from NAGRA LASMO monitored boreholes during the periods of sampling in 2016.



*Each drop in pressure corresponds with a groundwater sampling event. Pressure recovers to a steady state in all cases. Boreholes SB 80.001 has fluctuations due to drilling works, HP increasing pressure in Feb 2016 was a result of reinstallation of the borehole pressure monitoring system.